Lecture Notes in Civil Engineering

Xianbin Liu *Editor*

Proceedings of 2021 China-Europe International Conference on Pipelines and Trenchless Technology

Springer

Lecture Notes in Civil Engineering

Volume 212

Lecture Notes in Civil Engineering (LNCE) publishes the latest developments in Civil Engineering—quickly, informally and in top quality. Though original research reported in proceedings and post-proceedings represents the core of LNCE, edited volumes of exceptionally high quality and interest may also be considered for publication. Volumes published in LNCE embrace all aspects and subfields of, as well as new challenges in, Civil Engineering. Topics in the series include:

- Construction and Structural Mechanics
- Building Materials
- Concrete, Steel and Timber Structures
- Geotechnical Engineering
- Earthquake Engineering
- Coastal Engineering
- Ocean and Offshore Engineering; Ships and Floating Structures
- Hydraulics, Hydrology and Water Resources Engineering
- Environmental Engineering and Sustainability
- Structural Health and Monitoring
- Surveying and Geographical Information Systems
- Indoor Environments
- Transportation and Traffic
- Risk Analysis
- Safety and Security

To submit a proposal or request further information, please contact the appropriate Springer Editor:

– Pierpaolo Riva at pierpaolo.riva@springer.com (Europe and Americas);
– Swati Meherishi at swati.meherishi@springer.com (Asia–except China, Australia, and New Zealand);
– Wayne Hu at wayne.hu@springer.com (China).

All books in the series now indexed by Scopus and EI Compendex database!

Xianbin Liu
Editor

Proceedings of 2021 China-Europe International Conference on Pipelines and Trenchless Technology

Springer

Editor
Xianbin Liu
College of Marine and Environmental
Sciences
Tianjin University of Science
and Technology
Tianjin, China

ISSN 2366-2557 ISSN 2366-2565 (electronic)
Lecture Notes in Civil Engineering
ISBN 978-981-19-4066-8 ISBN 978-981-19-4067-5 (eBook)
https://doi.org/10.1007/978-981-19-4067-5

This Springer imprint is published by the registered company Springer Nature Singapore Pte Ltd.
The registered company address is: 152 Beach Road, #21-01/04 Gateway East, Singapore 189721, Singapore

Contents

Trenchless Restoration Technology and Environmental Restoration

Application of Trenchless Directional Drilling Technology in Sewage Pipeline Construction

Jianbao Fu, Lihao Cheng, Haihui Fan, and Longyang Xu

Abstract To solve the problems of pipeline construction in dense building spacing, difficult road occupation, under crossing railways, highways, rivers and other areas where excavation is not allowed, trenchless directional drilling technology is introduced for pipeline laying. This technology is not affected by the buried depth of pipelines, ground restrictions, groundwater, etc., and has the advantages of high construction speed, high efficiency and low comprehensive cost. It can skillfully solve a series of problems that cannot be solved by excavating buried pipelines and fully demonstrate its superiority. Based on the sewage pipeline laying in Guangming District, Shenzhen, this paper briefly expounds the construction principle, advantages and disadvantages of trenchless directional drilling technology, systematically sums up its main processes, and analyzes the quality control under each operation process.

Keywords Pipeline laying · Trenchless directional drilling technology · Urban sewage pipeline · Gravity pipeline laying technology

1 Introduction

Trenchless directional drilling technology is not affected by ground structures, buried depth of pipelines and environmental protection, with short construction time, high efficiency and low comprehensive cost. It can solve a series of problems encountered

J. Fu (✉)
Key Laboratory of Port Geotechnical Engineering, Ministry of Communications, PRC, Key Laboratory of Tianjin Port Geotechnical Engineering, Tianjin Port Engineering Institute Co., Ltd. of CCCC First Harbor Engineering Co., Ltd., Tianjin, China
e-mail: 276339170@qq.com

J. Fu · L. Cheng · H. Fan · L. Xu
CCCC First Harbor Engineering Company Ltd., Tianjin, China

L. Cheng · H. Fan · L. Xu
No. 5 Engineering Co. Ltd. of CCCC First Harbor Engineering Co. Ltd., Qinhuangdao, China

X. Liu (ed.), *Proceedings of 2021 China-Europe International Conference on Pipelines and Trenchless Technology*, Lecture Notes in Civil Engineering 212,
https://doi.org/10.1007/978-981-19-4067-5_1

in the excavation of buried pipes, and can give full play to its superiority and scientificity when pipeline construction is carried out in densely populated areas, densely spaced buildings and other areas where excavation is not allowed.

This study is based on the laying of sewage pipe network in Guangming District, Shenzhen. Influenced by topography, surface structures, roads, etc., there are a large number of plots that do not have the conditions for excavation and construction. At the same time, the sewage pipe network belongs to gravity flow pipeline, and the requirements for elevation are extremely strict. Considering the construction difficulties comprehensively, trenchless directional drilling technology was adopted to lay gravity flow pipelines, reduce the surface interference and control the elevation to improve the efficiency.

Trenchless directional drilling technology is a construction method in which a directional drilling rig is erected on the ground, the drill bit is drilled along the design direction through a guiding system without a large amount of soil excavation, and after the hole is formed, the pipe is reamed several times, and the pipe is pulled back into place according to the pipe to complete the pipe laying. Generally, it is a construction method after the pipe is welded and formed once [1].

2 Project Overview

A paper mill was built near a river, and rainwater and sewage mixed into the river channel all the time, which brought great negative influence to the local river treatment. In order to solve the problem of sewage flowing into the river, a new factory sewage pipeline was needed. The new sewage pipeline will be introduced into the municipal sewage pipe network, with a total length of 560 m and 21 inspection wells. Because the access section from the factory to the municipal pipe network is 120 m in total, its road is narrow, both sides are mostly old residential areas, and the soil is hard and buried deeply, so it is impossible to adopt the traditional steel sheet pile supporting excavation construction. Due to the influence of the construction site, geology, traffic and other reasons, in order to reduce the influence on the surrounding buildings, reduce the road traffic pressure and speed up the construction progress, the trenchless directional drilling construction technology will be adopted in this section. The buried depth of this section is 3–5 m, and the pipe material is PE pipe with a diameter of 400 mm [2].

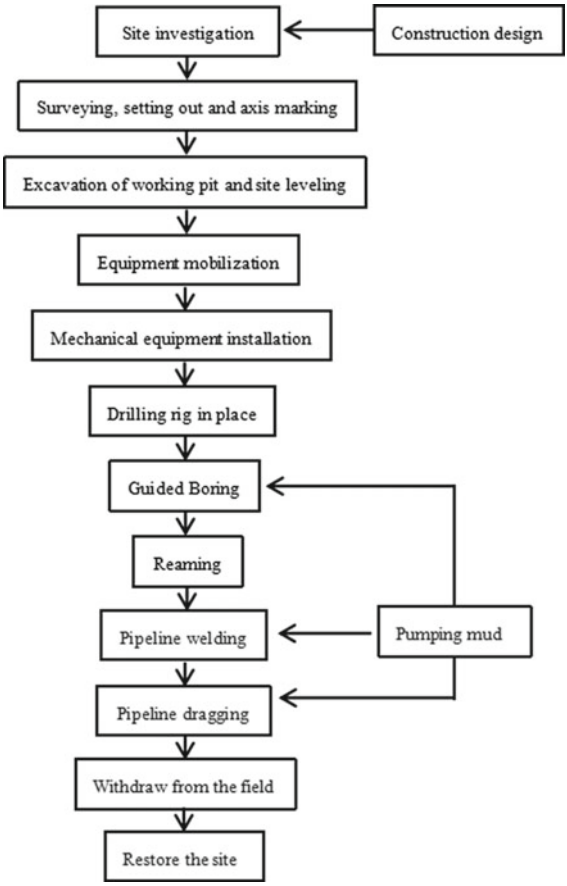

Fig. 1 Construction process flow chart of trenchless directional drilling

3 Construction Technology

3.1 Construction Process Flow

The construction process flow chart of trenchless directional drilling is shown in Fig. 1.

3.2 Construction Preparation

Before construction, firstly, make clear the soil quality and geophysical survey of the pipeline position, which directly affects whether trenchless directional drilling can be carried out normally, and determine the laying track [1], equipment used and mud

Table 1 Construction preparation list

Serial number	Type	Preparation
1	Geology	Highly weathered argillaceous siltstone
2	Geophysical prospecting	There is no underground cable, and there is no conflict between existing rainwater pipes and newly-built pipelines
3	Trajectory	The burial angle is 10 °C, the unearthed angle is 20 °C, the radius of curvature is 60 m, and the length of straight line section is 120 m
4	Drilling rig	Xugong XZ180: The maximum pulling (feeding) force is 180(180)kN, the generator power is 97 kW, the working weight is 850 kg, the maximum pipe diameter is 600 mm, and the maximum length is 150 m
5	Mud configuration	20% bentonite, 1% zhuanyebao, 75% water and 2% caustic soda by weight of bentonite

configuration according to geological conditions, pipe diameter and single laying length. The preparatory work was shown in Table 1.

3.3 Construction Preparation

Before construction, firstly, make clear the soil quality and geophysical survey of the pipeline position, which directly affects whether trenchless directional drilling can be carried out normally, and determine the laying track [1], equipment used and mud configuration according to geological conditions, pipe diameter and single laying length. The preparatory work was shown in Table 1.

3.4 Working Pit Setting

The length direction of the working pit was consistent with the design axis direction. Keep the slope around the working pit stable and the soil solid. The excavation of the working pit was long, and the direction should be consistent with the guide axis. The surrounding soil should be firm and the slope should be stable to ensure that the guide rod can be drilled normally.

3.5 Guided Boring

The construction of pilot hole is the key part of directional drilling pipeline laying technology, which determines the final direction of pipeline laying, especially the elevation control of gravity flow sewage pipeline is very strict. During the construction, the selection shall be made according to the friction. Firstly, the working pit shall be set at the two positions of soil entry and excavation, and the size shall be 2–4 m long, 1.5 m wide and 1.5–2 m deep. The excavation of the working pit is long, the direction should be consistent with the guide axis, the surrounding soil shall be firm, and channel steel shall be used for support to ensure the stability of the slope and the normal drilling of the guide rod.

After the equipment is in place, drill according to the axis trajectory determined by the design scheme. Drifting requires light pressure and slow rotation to ensure that the guide rod is stressed evenly and can be drilled normally. After entering the straight section, adjust it to light pressure and fast rotation, so as to enhance the guidance and stability of the drill bit and drill pipe. During the guided drilling process, the trajectory parameters measured by the receiver are compared with the design parameters, and the deviation should be adjusted in time. During the adjustment process, it is advisable to gradually and gently correct the deviation.

3.6 Back Reaming

After the drill bit is drilled into the receiving work pit, the construction part of the pilot hole is completed. Dismantle the starting drill pipe and pilot bit, and replace it with reaming bit to pull back reaming along the original track. The geology of the dragging section is strongly weathered argillaceous siltstone, and the scraper reamer is used for back reaming. According to the specification requirements, the general aperture should be expanded to 1.2–1.5 times of the pipe diameter of the laid pipeline, and the pipe diameter of this project is 400 mm, that is, the aperture to be reamed is 400 mm $\times$ 1.5 = 600 mm. Reaming should be carried out step by step according to the specifications of 150, 300, 400 and 600 (see Fig. 2), and reaming must not be carried out over the steps, so as to avoid mud imbalance and pore diameter collapse, and subsequent processes cannot be completed.

3.7 Pipeline Back Dragging

After multi-stage reaming to meet the design requirements, pipeline installation can be started. The pipe is welded and formed at the position of receiving the working pit. Install rotary joint (universal joint) at the tail of reamer. The other end of rotary joint is connecte with the welded pipeline, so as to carry out the pipeline back-dragging

Fig. 2 Back reaming bit

installation. The use of rotary joint can not only transfer the pulling force, but also prevent the pipe from rotating with the reamer, so as to ensure the normal operation of the pipe pulling back. During the dragging process, unless special circumstances are encountered, it should be continuously completed until the reamer and finished product pipeline are exposed from the working pit. According to the construction experience, the pulling speed should be controlled within 2 m/min [3].

3.8 Inspection Well Installation

Because the sewage pipeline is pressureless, the elevation control from upstream to downstream is extremely strict. After the pipeline dragging construction is completed, it is necessary to carry out the pipeline inspection well construction to verify whether the elevation of the dragging pipe meets the design requirements and whether there is the phenomenon of inverted slope water storage. According to the specification and design requirements, the spacing of inspection wells shall be 40 m. According to the depth of the well, ordinary excavator or telescopic boom shall be used for excavation, and the reverse method, open caisson or pile driving shall be used to support and install the shaft.

3.9 Key Points of Operation

(1) Strictly control the axis positioning measurement and correct it in time. When the pilot hole is constructed, the directional drilling rig is used for horizontal drilling. On the ground of trenchless area, the direction and depth of the drill bit

are controlled by navigation equipment such as direction indicator, so that the guide hole forms the laying center line strictly according to the designed axis.
(2) With the construction of drilling engineering, adjust drilling parameters at any time to avoid damage to equipment caused by drilling in different strata.
(3) Closely monitor the construction process, and pay attention to whether there are geological emergencies, such as mud leakage, sudden change of WOB, etc.
(4) After the pilot hole drilling construction is completed, it is necessary to check the elevation and orientation of the working surface of the soil inlet of the working tunnel and the unearthed outlet of the receiving pit to ensure that the pilot hole is consistent with the design axis.
(5) According to the design drawings and actual points, after the construction check of the axis of the pilot hole is completed, replace the pilot bit with the back expansion bit, and carry out the construction back expansion with the pilot hole as the axis.
(6) After reaming is completed, the completed reaming must be checked according to the design drawings to confirm that its depth and direction accuracy can meet the requirements of pipeline construction.

3.10 Construction Efficiency Comparison

By using trenchless directional drilling construction, since the equipment comes into play, the sharing time is 7 days. Compared with traditional excavation construction, it saves 15 days on the premise of overcoming the influence of surrounding buildings. At the same time, personnel investment is less than traditional excavation (Table 2).

4 Process Comparison

Compared with the traditional excavation construction technology, the trenchless directional drilling construction technology has the following advantages:

(1) Compared with traditional excavation construction, trenchless directional drilling construction technology can reduce pavement breaking, earthwork excavation and foundation trench support by 95% in areas with dense structures on the ground. As the excavation amount of foundation trench is greatly reduced, the potential safety hazards and safety risks caused by trench support are correspondingly reduced.
(2) Compared with the traditional excavation construction, the trenchless directional drilling construction technology only needs to occupy roads in two places, which reduces the occupation by more than 80%, thus reducing the costs of occupation, enclosure and guidance, and at the same time reducing the traffic pressure and safety risks of vehicles and pedestrians.

Table 2 Construction efficiency comparison table

Serial number			Traditional excavation technology		
Construction content	Cost input	Remarks	Construction content	Cost input	Remarks
Working well excavation/d	0.5		Steel sheet pile driving/d	6	Hard soil, traffic influence
Rig in place installation/d	0.5		Excavation and pipe burying/d	10	Traffic influence
Guided drilling/d	1		Steel sheet pile extraction/d	2	
Reaming (150–600 mm)/d	3	Reaming 4 times	Pavement restoration/d	3	Segmented recovery
Pipe pullback and installation/d	1		Personnel input/person	7	
Pavement restoration/d	1				
Personnel input/person	4				

(3) In the areas with dense structures on the ground, excavators and other equipment can't be used for excavation in most locations, but only manual trenching is used, which leads to low construction efficiency and many potential safety hazards. The trenchless directional drilling construction technology effectively avoids this kind of problems, reduces personnel investment, reduces safety risks and shortens the construction period.
(4) Using trenchless directional drilling construction technology, it is not necessary to break the pavement in large quantities, thus reducing the time occupied by pavement restoration and saving the construction period by 40% as a whole.

5 Conclusion

In the process of pipeline laying, it is inevitable to be affected by surface structures and cannot be implemented by traditional excavation technology. During the implementation of the project, the old structures cannot be driven with steel sheet piles. During the implementation of this project, steel sheet piles can't be driven in old structures. Due to narrow roads, large flow of people and inability to excavate in a large area, trenchless directional drilling technology was finally adopted to smoothly connect the sewage pipelines and municipal pipe network. Based on the laying of sewage pipes, this paper focuses on the difficulties and difficulties in the construction process, as well as the comparison with traditional excavation technology. Combined with practical cases, it is concluded that trenchless directional drilling technology

can shorten the construction period, save investment and achieve good economic and social benefits under specific conditions.

With the acceleration of urban rhythm, a large number of municipal pipe networks need to be newly built and repaired. Trenchless drilling technology, because of its high speed, high efficiency, low pollution and other characteristics, has given a new direction for pipeline installation, and will certainly be more widely used. This paper introduces engineering examples to provide reference for similar sewage pipeline installation projects.

References

1. Technical specification for pipeline crossing by horizontal directional drilling CECS 382:2014
2. Ye Y (2007) Research on trenchless construction technology of urban sewage pipeline. Today's Sci Technol 4:41–43
3. Xuan B, Hu Y, Li J, et al (2008) Construction of buried trenchless (directional drilling) polyethylene pipe in sewage engineering. J Changzhou Inst Technol 21(S1):309–313
4. Chen Z, Yu S (2009) Trenchless technology of directional drill tugger for laying of large caliber pipeline applied to urban water supply pipeline. Build Constr 33(2):116–118
5. Hong J, Ren G, Zhang L (2012) Discussion on problems of trenchless towing tubes in operation and maintenance of cables in Hangzhou grid. Zhejiang Electr Power (1):22–24

Numerical Study of the Effect of Dynamic Capillary Pressure on Oil–Water Flow in Tight Reservoirs

Limin Yang

Abstract Due to the fact that capillary pressure is one of the central key elements defining the oil–water flow behavior in porous media with low permeability, it's of significance to take the dynamic capillarity (e.g., dynamic capillary pressure, i.e., DCP) into account during water flooding process in formations with extremely low permeability. This article studies the effect of DCP on oil–water flow in low permeable formations by performing reservoir simulation based on a new mathematical model included DCP. In addition, taking four different kinds of well patterns (diamond shaped inverted 9-spot well network, rectangular inverted 9-spot well network, 7-spot well pattern and 5-spot well pattern) for examples, the influence of DCP on displacement characteristics of these well patterns is analyzed. The primary results show that, under a given saturation, DCP is greater than quasi-static capillary pressure, thus, for low permeable formations, DCP was too significant to be neglected. In addition, significant effect of DCP on oil–water flow characterization (e.g., the pressure drop loss, degree of oil recovery) is observed. Specifically, DCP causes pressure drop loss to become larger. The faster the production rate is, the greater the amplitude of pressure drop loss will be. The pressure drop loss range from large to small is the diamond shaped inverted 9-spot well pattern > the rectangular inverted 9-spot well pattern > the 7-spot well pattern > the 5-spot well pattern. Meanwhile, a larger capillary dynamic coefficient leads to a lower degree of oil recovery rate and a lower output per well. As a result, the main objective of this research is to give an alternative perspective to study oil–water flow in low permeability reservoirs.

Keywords Low permeability reservoirs · Dynamic capillary pressure · Pressure drop loss · Degree of oil recovery

L. Yang (✉)
Faculty of Science and Arts, China University of Petroleum-Beijing at Karamay, Karamay 834000, China
e-mail: ylm@cup.edu.cn

X. Liu (ed.), *Proceedings of 2021 China-Europe International Conference on Pipelines and Trenchless Technology*, Lecture Notes in Civil Engineering 212,
https://doi.org/10.1007/978-981-19-4067-5_2

1 Introduction

After primary oil recovery, water injection has been widely used to maintain formation pressure, displace the crude oil and improve oil recovery in tight reservoirs with low permeable [1–3]. Thus, to improve the efficiency of water displacement, it's of significance to perform simulation on oil–water two-phase flow. In general, oil–water two-phase flow behavior in porous media is delineated by capillary pressure and other factors (e.g., permeability, relative permeability, viscosity, etc.) [4, 5]. In this study, oil–water flow behavior in low permeability reservoirs is characterized mainly by capillary pressure.

Generally, capillary pressure is described based on the assumption that the time derivative of fluid saturation is zero (i.e., steady condition) [5, 6]. However, essentially speaking, the capillary pressure corresponding to steady condition is quasi-static capillary pressure (QSCP), which is suitable for steady displacement process and may be not suitable for characterizing dynamical conditions [5, 7–9]. As an alternative model, dynamic capillary pressure (DCP), the capillary pressure defined under transient flow condition during displacement, has proven to be more reasonable for tight reservoirs with low permeability [5, 7–10]. As the areal patterns (e.g., the 5-spot well pattern, the 7-spot well pattern, the diamond shaped inverted 9-spot well pattern and the rectangular inverted 9-spot well pattern) have been applied more and more widely in the development of tight reserves with low permeability, it is necessary to analyze the effect of DCP on oil–water flow in different well pattern units. Thus, in this study, we will develop a new transient seepage flow model considering the DCP, and study the effect of DCP on oil–water flow in different well pattern units of tight reservoirs.

2 Mathematical Model Development

2.1 Model Hypothesis

Supposed that a rectangular closed stratum is horizontal, homogeneity, uniform thickness. In addition, only Newtonian fluids (water phase fluid and oil phase fluid) flow in this low permeable stratum, during which gravity and buoyancy can be ignored. In addition, the two-phase flow is two-dimensional isothermal flow, which ignores the variation of temperature.

2.2 Mathematical Model

For oil–water flow in the reservoirs, based on the model hypothesis and mass conservation, we have

$$\frac{\partial}{\partial x}\left(\frac{k_{\mathrm{o}}}{B_{\mathrm{o}}\mu_{\mathrm{o}}}\frac{\partial p_{\mathrm{o}}}{\partial x}\right)+\frac{\partial}{\partial y}\left(\frac{k_{\mathrm{o}}}{B_{\mathrm{o}}\mu_{\mathrm{o}}}\frac{\partial p_{\mathrm{o}}}{\partial y}\right)+q_{\mathrm{o}} = \frac{1000}{86.4}\frac{\partial}{\partial t}\left(\frac{\varphi S_{\mathrm{o}}}{B_{\mathrm{o}}}\right), \tag{1}$$

$$\frac{\partial}{\partial x}\left(\frac{k_{\mathrm{w}}}{B_{\mathrm{w}}\mu_{\mathrm{w}}}\frac{\partial p_{\mathrm{w}}}{\partial x}\right)+\frac{\partial}{\partial y}\left(\frac{k_{\mathrm{w}}}{B_{\mathrm{w}}\mu_{\mathrm{w}}}\frac{\partial p_{\mathrm{w}}}{\partial y}\right)+q_{\mathrm{w}} = \frac{1000}{86.4}\frac{\partial}{\partial t}\left(\frac{\varphi S_{\mathrm{w}}}{B_{\mathrm{w}}}\right), \tag{2}$$

where p is the pressure, MPa; k is the permeability, 10^{-3} μm^2; B is the volume ratio, m^3/m^3; μ is viscosity, mPa·s; φ is the porosity, %; S is the saturation, %; t is the production time, d; q is the source sink term, 1/d; the subscript o represents oil phase; and the subscript w represents water phase.

To characterize the DCP, a common model can be utilized, which is [5, 8–10]

$$p_{\mathrm{c,dyn}} = p_{\mathrm{o}} - p_{\mathrm{w}} = p_{\mathrm{c,stat}}(S_{\mathrm{w}}) + \frac{10^{-9}}{86.4}\tau\frac{\partial S_{\mathrm{w}}}{\partial t}, \tag{3}$$

where $p_{\mathrm{c,dyn}}$ denotes the dynamic capillary pressure (DCP), MPa; $p_{\mathrm{c,stat}}$ denotes the quasi-static capillary pressure (QSCP), MPa; and τ denotes the capillary dynamic coefficient, kg/(m·s). Physically speaking, parameter τ is related to pore structure of porous media and water saturation, which can be determined by using experiments [5] and micro-scale simulation [7]. In this paper, for the sake of simplification, τ is assigned as 1.0×10^6 kg/(m·s) to perform the simulation. In future study, we will combine the experiments and simulation to low the uncertainty.

The following equation for the initial condition and outer close boundary condition is

$$\begin{cases} p|_{t=0} = p_{\mathrm{e}}, \\ \frac{\partial p_{\mathrm{o}}}{\partial \vec{n}}\Big|_{x,y\in\Gamma_{\mathrm{out}}} = 0, \\ \frac{\partial p_{\mathrm{w}}}{\partial \vec{n}}\Big|_{x,y\in\Gamma_{\mathrm{out}}} = 0, \end{cases} \tag{4}$$

where p_{e} denotes the initial formation pressure, MPa; $\vec{n}$ denotes the outward normal direction; and Γ_{out} denotes the outer boundary. In addition, for the inner boundary, the injection wells and oil wells are at constant pressure. That is, oil producers and water injectors are under the fixed bottom hole pressure to produce.

2.3 Numerical Solution

In this study, we adopt grid block center in space to split the stratum. Specifically, in the x direction, the grid is recorded as i, the total number of grid node is N and the step size is Δx. In addition, in the y direction, the grid is recorded as j, the total number of grid node is M and the step size is Δy. According to pressure drop change rule, in this study, the changing time size method is used to perform the simulation, which is

$$\Delta t_n = \min\left(\Delta t_0 \cdot \alpha^n, \Delta t_{\max}\right), \tag{5}$$

where Δt_n is the time step of step n, d; Δt_0 is the initial time step, d; α is the time step change series, which is taken as 1.5 in this study; $\Delta t_{\max}$ is the largest time step allowed, d.

Based on the grids in space and time step, the mathematical equations can be discrete. Moreover, to make the equations more concise, hereinafter, p_o is represented as p, and S_w is represented as S. Thus, based on the equation $p_{i,j}^{n+1} = p_{i,j}^n + \delta p_{i,j}$, for a given mesh point (i, j) in the $n + 1$ time step, if source sink term is separately considered in the constant pressure condition, we have

$$\begin{cases} a_{oi,j}\delta p_{i-1,j} + b_{oi,j}\delta p_{i+1,j} + c_{oi,j}\delta p_{i,j} \\ +d_{oi,j}\delta p_{i,j-1} + e_{oi,j}\delta p_{i,j+1} = f_{oi,j} - \frac{V}{\Delta t_n}\frac{\varphi}{B_o}\delta S_{i,j}, \\ a_{wi,j}\delta p_{i-1,j} + b_{wi,j}\delta p_{i+1,j} + c_{wi,j}\delta p_{i,j} \\ +d_{wi,j}\delta p_{i,j-1} + e_{wi,j}\delta p_{i,j+1} \\ = sa_{i,j}\delta S_{i-1,j} + sb_{i,j}\delta S_{i+1,j} + sc_{i,j}\delta S_{i,j} \\ +sd_{i,j}\delta S_{i,j-1} + se_{i,j}\delta S_{i,j+1} + f_{wi,j}, \end{cases} \tag{6}$$

where the definitions of relevant parameters in Eq. (6) can be found in the Appendix.

If we ignore the skin effect and the effect of wellbore storage, the discrete results of source sink terms can be obtained as

$$\begin{cases} q_{wi_{inj},j_{inj}} = \dfrac{0.0864\left(p_{iwf} - p_{i_{inj},j_{inj}}\right)}{\frac{\mu_w \Delta x \Delta y}{2\pi k_{wi_{inj},j_{inj}}} \ln \frac{0.14\sqrt{\Delta x^2+\Delta y^2}}{r_w}}, \\ q_{oi_{pro},j_{pro}} = \dfrac{0.0864\left(p_{i_{pro},j_{pro}} - p_{wf}\right)}{\frac{\mu_o \Delta x \Delta y}{2\pi k_{oi_{pro},j_{pro}}} \ln \frac{0.14\sqrt{\Delta x^2+\Delta y^2}}{r_w}}, \\ q_{wi_{pro},j_{pro}} = \dfrac{0.0864\left(p_{i_{pro},j_{pro}} - p_{wf}\right)}{\frac{\mu_w \Delta x \Delta y}{2\pi k_{wi_{pro},j_{pro}}} \ln \frac{0.14\sqrt{\Delta x^2+\Delta y^2}}{r_w}}, \end{cases} \tag{7}$$

where q is the flow rate, m^3/d; p_{wf} is the bottom hole pressure of the production wells, MPa; p_{iwf} is the bottom hole pressure of the injection wells, MPa; r_w is the

well radius, cm; subscript i_{pro} is the nodes of producing wells in x direction; j_{pro} is the nodes of producing wells in y direction; i_{inj} is the nodes of injection wells in x direction; j_{inj} is the nodes of injection wells in y direction.

By IMPES (the implicit pressure and explicit saturation) method, the discrete equations can be sequentially solved with Matlab. Specifically, the pressure can be solved firstly, then, the saturation and DCP will be solved. Finally, by using the iteration algorithm, the production behavior can be analyzed.

3 Results and Discussions

3.1 The Effect of DCP on Pressure Distribution

For a reservoir with the following parameters: $p_{iwf} = 25$ MPa, $p_{wf} = 5$ MPa, $p_e = 20$ MPa, $k = 1.0 \times 10^{-3}$ μm^2, $h = 10$ m, $\varphi = 0.20$, $\mu_o = 10$ mPa·s, $\mu_w = 1.0$ mPa·s, $B_o = 1.051$ m^3/m^3, $B_w = 1.0$ m^3/m^3, $C_f = 2 \times 10^{-5}$ MPa^{-1}, $r_w = 0.12$ m, $L_x = 400$ m, $L_y = 400$ m. In addition, τ is assigned as 1.0×10^6 kg/(m·s). Based on the numerical solution in this study, oil–water two-phase flow in low permeable formations with various well patterns (e.g., the 5-spot well pattern, the 7-spot well pattern, the diamond shaped inverted 9-spot well pattern, and the rectangular inverted 9-spot well pattern) can be analyzed.

Figure 1 shows the the effect of the DCP on the formation pressure distribution of the low permeability reservoir with various well patterns. Specifically, Figs. 1a and b are for the 5-spot well pattern, Figs. 1c and d are for the 7-spot well pattern, Figs. 1e and f are for the diamond-shape inverted 9-spot well pattern, and Figs. 1g and h are for the rectangular-shape inverted 9-spot well pattern. As depicted in Fig. 1, due to DCP, the stratum pressure drop will increase for different well patterns. For example, by comparing Fig. 1a and b, we can see that, due to DCP, the formation pressure decreases. In other words, affected by DCP, the formation pressure drop will increase. The main reason may be that, DCP will result in the increasing of water flooding seepage resistance, leading to the increasing of stratum pressure drop. In addition, results (Fig. 1) suggest that, the effect of DCP on the formation pressure drop varies with the well patterns, which is anticipated. In this study, due to DCP, the range of pressure drop in descending order is: the diamond-shape inverted 9-spot well pattern > the rectangle-shape inverted 9-spot well pattern > the 7-spot well pattern > the 5-spot well pattern. The main reason may be that, the recovery rate of the diamond-shape inverted 9-spot well pattern is higher than others, thus, the rate of change in water saturation is greater. As a result, the DCP for the diamond-shape inverted 9-spot well pattern is relative higher than others, the effect of DCP is more obvious, and the water flooding seepage resistance is larger. Consequently, the formation pressure drop for the diamond-shape inverted 9-spot well pattern is larger than that for other well patterns.

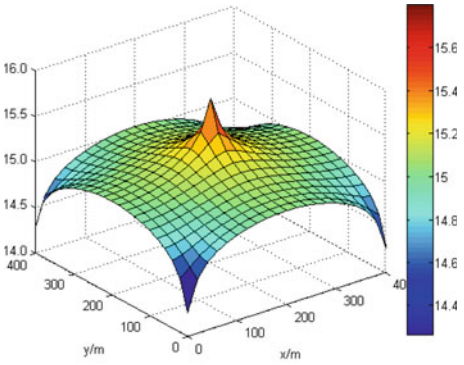

(a) QSCP of the 5-spot well pattern

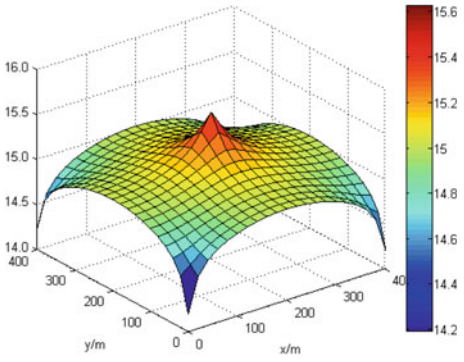

(b) DCP of the 5-spot well pattern

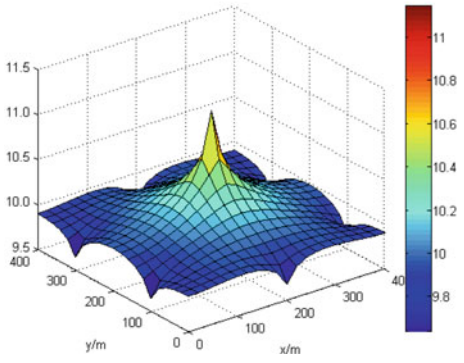

(c) QSCP of the 7-spot well pattern

Fig. 1 The comparison of pressure distribution between QSCP and DCP for different well patterns

Fig. 1 (continued)

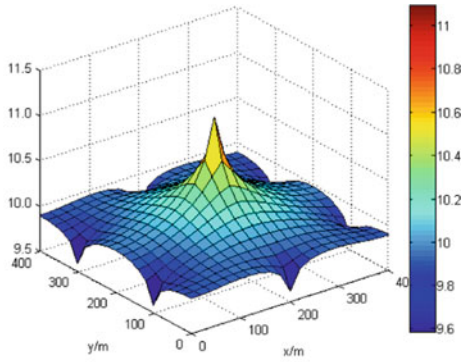

(d) DCP of the 7-spot well pattern

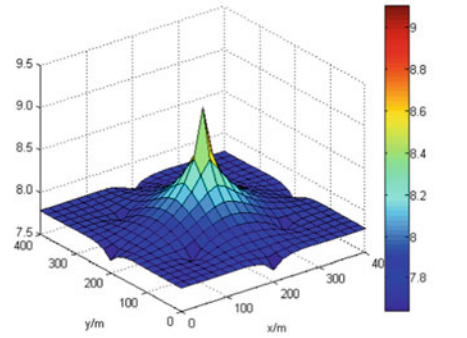

(e) QSCP of the diamond-shape inverted 9-spot well pattern

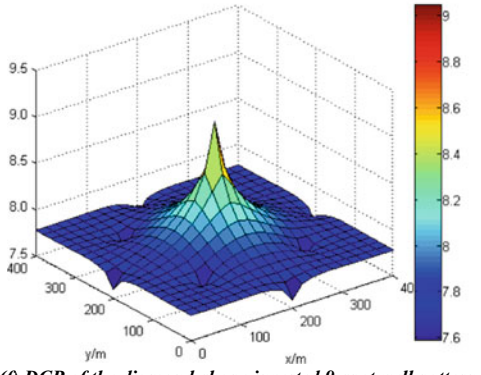

(f) DCP of the diamond-shape inverted 9-spot well pattern

Fig. 1 (continued)

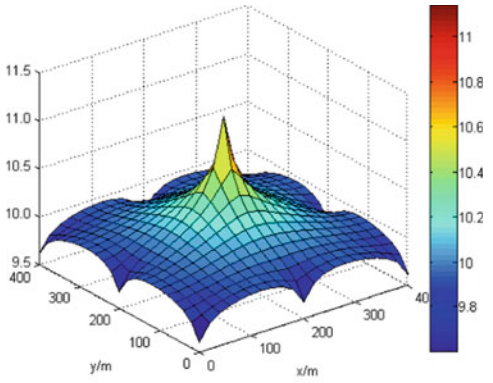

(g) QSCP of the rectangular-shape inverted 9-spot well pattern

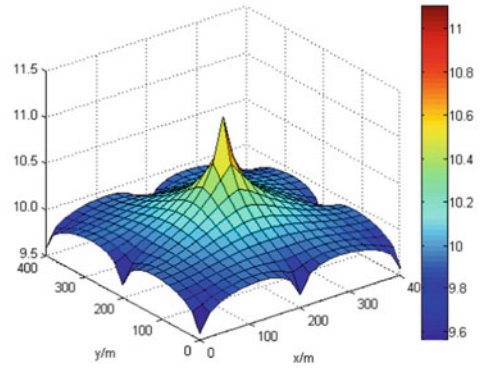

(h) DCP of the rectangular-shape inverted 9-spot well pattern

3.2 The Effect of DCP on Degree of Oil Recovery

To further study the effect of DCP on oil–water flow in low permeability reservoirs, Figs. 2 and 3 show the average residual oil saturation (Sor) versus DCP for different well patterns and the production per well (q) versus DCP for different well patterns, respectively. As demonstrated in Figs. 2 and 3, for each well pattern, with the increasing of DCP, the average remaining oil of the stratum will increases and the oil production will decrease. That is, the DCP will lead to the low degree of oil

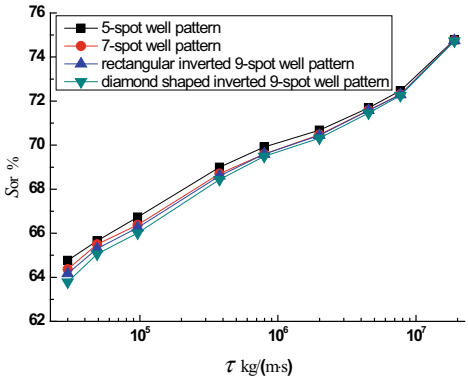

Fig. 2 The average residual oil saturation versus DCP for different well patterns

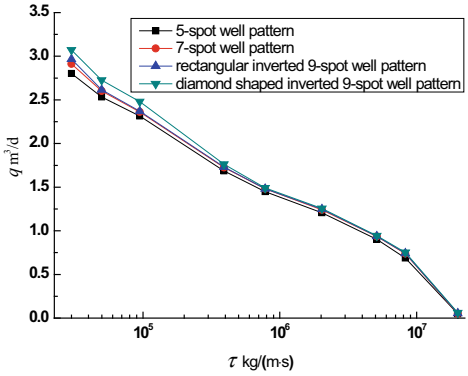

Fig. 3 The output per well versus DCP for different well patterns

recovery and low production rate. In addition, due to DCP, the range of the decrease of oil production in descending order is the diamond-shape inverted 9-spot well pattern > the rectangle-shape inverted 9-spot well pattern > the 7-spot well pattern > the 5-spot well pattern. Moreover, Fig. 3 reveals that, when DCP increases up to a certain value, the oil production will reduce to zero. Thus, the more obvious capillary dynamic effect is, the greater the water drive oil resistance is. Thus, to some extent, if DCP is ignored during the simulation, the well production of the reservoir will be overestimated.

4 Conclusion

Based on the results and discussions presented above, the conclusions are obtained as below:

(1) It is shown that, the effect of dynamic capillary pressure (DCP) on oil–water flow in low permeability reservoirs is significant. During the oil production in low permeable formations, if we ignore the DCP, the well production of the reservoir will be overestimated.
(2) During the water flooding in low permeable reservoirs, DCP acts as the displacement resistance, making the oilfield difficult to establish effective hydrodynamic system. For a given capillary dynamic coefficient, the range of pressure drop in descending order is the diamond-shape inverted 9-spot well pattern > the rectangle-shape inverted 9-spot well pattern > the 7-spot well pattern > the 5-spot well pattern.
(3) It is concluded that, due to DCP, the remaining oil will increase and oil production rate will decrease. Thus, the recovery rate for low permeability reservoirs should be optimized.

Acknowledgements This work was financially supported by the Natural Science Foundation of Xinjiang Uygur Autonomous Region (XQZX20210022).

Appendix

The relevant parameters in Eq. (6) can be summarized, as follows:

$$
\begin{cases}
F_1 = \frac{\Delta y}{\Delta x};\ F_2 = \frac{\Delta x}{\Delta y};\ V = \frac{1000\Delta x\Delta y}{86.4};\\
i = 2, 3, \cdots, N-1;\ j = 2, 3, \cdots, M-1;\\
\lambda_{\mathrm{o}i+\frac{1}{2},j} = \left(\frac{k_\mathrm{o}}{B_\mathrm{o}\mu_\mathrm{o}}\right)_{i+\frac{1}{2},j};\ \lambda_{\mathrm{o}i-\frac{1}{2},j} = \left(\frac{k_\mathrm{o}}{B_\mathrm{o}\mu_\mathrm{o}}\right)_{i-\frac{1}{2},j};\\
\lambda_{\mathrm{o}i,j+\frac{1}{2}} = \left(\frac{k_\mathrm{o}}{B_\mathrm{o}\mu_\mathrm{o}}\right)_{i,j+\frac{1}{2}};\ \lambda_{\mathrm{o}i,j-\frac{1}{2}} = \left(\frac{k_\mathrm{o}}{B_\mathrm{o}\mu_\mathrm{o}}\right)_{i,j-\frac{1}{2}};\\
\lambda_{\mathrm{w}i+\frac{1}{2},j} = \left(\frac{k_\mathrm{w}}{B_\mathrm{w}\mu_\mathrm{w}}\right)_{i+\frac{1}{2},j};\ \lambda_{\mathrm{w}i-\frac{1}{2},j} = \left(\frac{k_\mathrm{w}}{B_\mathrm{w}\mu_\mathrm{w}}\right)_{i-\frac{1}{2},j};\\
\lambda_{\mathrm{w}i,j+\frac{1}{2}} = \left(\frac{k_\mathrm{w}}{B_\mathrm{w}\mu_\mathrm{w}}\right)_{i,j+\frac{1}{2}};\ \lambda_{\mathrm{w}i,j-\frac{1}{2}} = \left(\frac{k_\mathrm{w}}{B_\mathrm{w}\mu_\mathrm{w}}\right)_{i,j-\frac{1}{2}};\\
a_{\mathrm{w}i,j} = F_1\lambda_{\mathrm{w}i-\frac{1}{2},j};\ b_{\mathrm{w}i,j} = F_1\lambda_{\mathrm{w}i+\frac{1}{2},j};\\
d_{\mathrm{w}i,j} = F_2\lambda_{\mathrm{w}i,j-\frac{1}{2}};\ e_{\mathrm{w}i,j} = F_2\lambda_{\mathrm{w}i,j+\frac{1}{2}};\\
sa_{i,j} = \frac{10^{-9}}{86.4}\frac{a_{wi,j}}{\Delta t_n}\tau;\ sb_{i,j} = \frac{10^{-9}}{86.4}\frac{b_{\mathrm{w}i,j}}{\Delta t_n}\tau;\\
sd_{i,j} = \frac{10^{-9}}{86.4}\frac{d_{\mathrm{w}i,j}}{\Delta t_n}\tau;\ se_{i,j} = \frac{10^{-9}}{86.4}\frac{e_{\mathrm{w}i,j}}{\Delta t_n}\tau;\\
a_{\mathrm{o}i,j} = F_1\lambda_{\mathrm{o}i-\frac{1}{2},j};\ b_{\mathrm{o}i,j} = F_1\lambda_{\mathrm{o}i+\frac{1}{2},j};\\
d_{\mathrm{o}i,j} = F_2\lambda_{\mathrm{o}i,j-\frac{1}{2}};\ e_{\mathrm{o}i,j} = F_2\lambda_{\mathrm{o}i,j+\frac{1}{2}};\\
c_{\mathrm{w}i,j} = -\left(\begin{array}{l} F_1\lambda_{\mathrm{w}i+\frac{1}{2},j} + F_1\lambda_{\mathrm{w}i-\frac{1}{2},j} + F_2\lambda_{\mathrm{w}i,j-\frac{1}{2}}\\ +F_2\lambda_{\mathrm{w}i,j+\frac{1}{2}} + \frac{V}{\Delta t_n}\frac{S^n_{i,j}}{B_\mathrm{w}}C_\mathrm{f}\end{array}\right);\\
sc_{i,j} = \frac{V}{\Delta t_n}\frac{\varphi}{B_\mathrm{w}} - \frac{10^{-9}}{86.4}\frac{(a_{wi,j}+b_{\mathrm{w}i,j}+d_{\mathrm{w}i,j}+e_{\mathrm{w}i,j})\tau}{\Delta t_n};\\
c_{\mathrm{o}i,j} = -\left(\begin{array}{l} \frac{V}{\Delta t_n}\frac{1-S^n_{i,j}}{B_o}C_\mathrm{f} + F_1\lambda_{\mathrm{o}i+\frac{1}{2},j}\\ +F_1\lambda_{\mathrm{o}i-\frac{1}{2},j} + F_2\lambda_{\mathrm{o}i,j+\frac{1}{2}} + F_2\lambda_{\mathrm{o}i,j-\frac{1}{2}}\end{array}\right);\\
f_{\mathrm{w}i,j} = a_{\mathrm{w}i,j}\left(p^n_{i,j} - p^n_{\mathrm{c,stat}i,j} - p^n_{i-1,j} + p^n_{\mathrm{c,stat}i-1,j}\right)\\
-b_{\mathrm{w}i,j}\left(p^n_{i+1,j} - p^n_{\mathrm{c,stat}i+1,j} - p^n_{i,j} + p^n_{\mathrm{c,stat}i,j}\right)\\
+d_{\mathrm{w}i,j}\left(p^n_{i,j} - p^n_{\mathrm{c,stat}i,j} - p^n_{i,j-1} - \delta p_{\mathrm{c,stat}i,j-1}\right)\\
-e_{\mathrm{w}i,j}\left(p^n_{i,j+1} - p^n_{\mathrm{c,stat}i,j+1} - p^n_{i,j} + p^n_{\mathrm{c,stat}i,j}\right);\\
f_{oi,j} = a_{\mathrm{o}i,j}\left(p^n_{i,j} - p^n_{i-1,j}\right) - b_{\mathrm{o}i,j}\left(p^n_{i+1,j} - p^n_{i,j}\right)\\
-e_{\mathrm{o}i,j}\left(p^n_{i,j+1} - p^n_{i,j}\right) + d_{\mathrm{o}i,j}\left(p^n_{i,j} - p^n_{i,j-1}\right)
\end{cases}
$$

References

1. Hughes RV, Pfister RJ (1947) Advantages of brines in secondary recovery of petroleum by water-flooding. Trans AIME 170(01):187–201
2. Wang D, Niu D, Li HA (2017) Predicting waterflooding performance in low-permeability reservoirs with linear dynamical systems. SPE J 22(05):1596–1608
3. Mohammad RS, Tareen MYK, Mengel A et al (2020) Simulation study of relative permeability and the dynamic capillarity of waterflooding in tight oil reservoirs. J Pet Explor Prod Technol 10(5):1891–1896
4. Zhang H, He S, Jiao C et al (2015) Investigation of dynamic effect of capillary pressure in ultra-low permeability sandstones. Indian Geotech J 45(1):79–88

5. Tian SB, Lei G, He SL et al (2012) Dynamic effect of capillary pressure in low permeability reservoirs. Pet Explor Dev 39(3):405–411
6. Baldwin BA, Spinler EA (1998) A direct method for simultaneously determining positive and negative capillary pressure curves in reservoir rock. J Petrol Sci Eng 20(3–4):161–165
7. Tang M, Zhan H, Ma H et al (2019) Upscaling of dynamic capillary pressure of two-phase flow in sandstone. Water Resour Res 55(1):426–443
8. Gray WG, Hassanizadeh SM (1991) Unsaturated flow theory including interfacial phenomena. Water Resour Res 27(8):1855–1863
9. Hassanizadeh SM, Celia MA, Dahle HK (2002) Dynamic effect in the capillary pressure-saturation relationship and its impact on unsaturated flow. Vadose Zone J 1(1):38–57
10. Abbasi J, Ghaedi M, Riazi M (2018) A new numerical approach for investigation of the effects of dynamic capillary pressure in imbibition process. J Petrol Sci Eng 162:44–54

Study of Impact of Urban Nonpoint Source Pollution on River Water Quality Based on Integrated Simulation and Discussion on Corresponding Prevention Measures

Ningrui Zhao

Abstract Not only is the Dian Lake a water source for the people of Kunming, but also it receives the point and nonpoint source pollution load in its basin. With the control over point source pollution and the development of urbanization in recent years, nonpoint sources have become important pollution sources in the Dian Lake Basin. Therefore, this study used the InfoWorks Integrated Catchment Modeling (ICM) model to obtain the basic urban information and the parameters of urban nonpoint source pollution discharge to calculate urban nonpoint source pollution load in Kunming. The study found that the nonpoint source pollution load is linearly correlated with precipitation, and the pollution load of chemical oxygen demand (COD) is the most serious while that of total phosphorus (TP) is the lightest in Kunming. In addition, this study used a QUAL2K one-dimensional water quality model to simulate the change of pollutant concentration in the river before and after precipitation, and it was found that the pollutant concentration in the water increased by up to 8.1 times after precipitation. Based on the calculation result and the urban nonpoint pollution characteristics of Kunming, four measures were proposed to reduce urban nonpoint source pollution load, including adopting green roofs and adding drainage outlet treatment device.

Keywords Urban nonpoint source pollution · InfoWorks ICM model · Pollution load estimation · QUAL2K model · Prevention and control measures · Green roofs · Permeable paving · Drainage outlet treatment device

1 Introduction

The Dian Lake is located in Kunming City of Yunnan Province in China. The Dian Lake is the drainage receiving waterbody of the entire basin, and its water environment is vital to the socio-economic development of the Dian Lake Basin area. Since the 1970s, due to rapid industrialization, urbanization and the campaign to reclaim

N. Zhao (✉)
College of Environmental Science and Engineering, Beijing Forestry University, Beijing, China
e-mail: nz2362@columbia.edu

X. Liu (ed.), *Proceedings of 2021 China-Europe International Conference on Pipelines and Trenchless Technology*, Lecture Notes in Civil Engineering 212,
https://doi.org/10.1007/978-981-19-4067-5_3

land from lakes, the water quality of the Dian Lake has become worse and worse. Over the past 20 years, the water quality of the Dian Lake has been moderately improved by a series of control measures. However, the water quality of some into-lake rivers remains classified as Inferior Grade V, and urban and agricultural nonpoint source pollution control remains an important task in improving the quality of the water environment in the Dian Lake Basin. This study aims to analyze the characteristics of urban nonpoint source pollution load in the Dian Lake Basin and propose measures to prevent and control nonpoint source pollution in the Dian Lake Basin, thus providing guidance on improving the water eco-environment of the Dian Lake. The methods and conclusions applied in this study can also be applied to other cities with serious nonpoint source pollution and old pipeline networks with missing data, so they are of theoretical and practical significance for pollution prevention and control of urban nonpoint source pollution.

2 Background of the Study

2.1 Uncertainty Analysis

Uncertainty analysis has become an important approach for scientific research [1]. In evaluation, planning, prediction, and other types of research problems based on models, uncertainty can even decisively impact the study findings and their explanations. Uncertainty arises from limitations to the past, present, or future knowledge. Depending on the size of limitations, researchers divide uncertainties into five grades [2]. Specifically, the uncertainties in the first three grades can be accurately described via sensitivity analysis, probability distribution, or ordering. The uncertainties in the 4th grade list all scenarios that are likely to take place going forward, but the likelihoods for their occurrences cannot be ordered or compared. The uncertainties in the 5th grade represent complete unknowns, (i.e., things may develop in any direction) [3]. This study provided diverse and flexible pollution prevention measures under different assumptions based on uncertainty analysis, and we adjusted the pollution prevention strategies according to the development of the system [4].

2.2 Mechanism Model of the Basin

The water environment system of the basin has been evolving for a long time, and so has people's understanding about the system. Over recent years, researchers have proposed many new terms and concepts for the water environment system, such as Low Impact Development (LID), Sustainable Urban Drainage System (SUDS) [5], Water Sensitive Urban Design (WSUD) [6], and Integrated Urban Water Management (IUWM), etc.

Combined with the integrated model of the urban drainage system and the water quality model of the receiving waterbody, integrated simulation can be conducted on the process for the generation, influx, and discharge of pollutants in the water environment system of the basin, as well as the process for water quality response of the receiving waterbody. The mechanism model can be used to precisely depict and simulate various components and processes of the system, considering multiple factors including hydrology, hydraulics, and water quality through an integrated approach. However, this type of models tends to have heavy demand for data, high requirements for data quality, and significant calculating intensity. As a result, even a single simulation can be time-consuming. In addition, high levels of model integration can add uncertainty into the model.

2.3 Material Flow Analysis

The material flow analysis method was first applied in the field of economic research, and around 1970, the material flow analysis method was introduced into the field of resource conservation and environmental management, with two main research directions: one is urban metabolism. For example, Wang et al. built an calculation framework for urban material flow analysis and explained two types of material flow analysis indicators, scale indicators and evaluation indicators, showing the important source industries of material consumption [7]. The other one is the pollutant transport pathway analysis of watersheds, cities or regions. For example, Pivnenko et al. combined static material flow analysis with dynamic material and substance flow modeling to provide methods for assessing pollutant levels in the material cycle [8]. As the field of material flow analysis research expanded, urban water practitioners had gradually introduced the method to the field of urban water systems. The material flow analysis method can be applied to a variety of scenarios, and its application has expanded from material balance analysis to other research subjects including the analysis of pollutant discharge structures, the evaluation of environmental impacts and environmental carrying capacities and the development of supporting tool for circular economy policies.

3 Methods

3.1 Analysis of Social, Economical, and Natural Environment of the Dian Lake Basin

We gathered data on land use, digital elevation, water system, and geographic information of the studied area, and used remote sensing interpretation, GIS data

processing and spatial analysis to systematically identify the physiographic characteristics of the Dian Lake Basin, focusing on the spatial distribution and changes of the underlying surface. Parameters considered include digital elevation, land use, soil type, reservoir and river conditions, and meteorological conditions.

We analyzed the social and economic development and pollution discharge characteristics of Dian Lake Basin by analyzing data from socio-economic statistical yearbooks and bulletins. Based on long-term water quality monitoring data of rivers and lakes entering the lake, we analyzed the current situation of water quality in Dian Lake Basin and its spatial and temporal changes.

3.2 Characteristics Identification and Accounting of Urban Nonpoint Source Pollution Load

Controlling over urban nonpoint source pollution represents one of the key elements in controlling the pollution in the Dian Lake. This study computed urban nonpoint source pollution load surrounding the studied area and examined the characteristics of the generation, influx, and discharge of urban nonpoint source pollution, by establishing a method for estimating and analyzing pollution load based on existing data and supplementary monitoring results.

Building a Model for the Estimation of Urban Nonpoint Source Pollution Load
Following the principles of equal emphasis on rainwater and sewage and coordinating the simulation and the actual measurement, this study estimated and analyzed urban nonpoint source pollution load within the built-up areas in the Dian Lake Basin. We adopted the InfoWorks Integrated Catchment Modeling (ICM) model for the drainage system of the Dian Lake Basin provided by Kunming as the foundation, collected missing data and conducted necessary monitoring. The basic data needed for the study were socio-economic data, drainage system data, data on pollution sources and water environment quality, hydrologic data, data on urban planning and construction, and meteorological data. Table 1 shows the requirements for the precision and range of various data.

Estimation of Urban Noon-Point Source Pollution Load
Based on the calculated parameters extracted from the model, we selected some typical precipitation events to carry out the simulation of the generation, influx, and discharge process of pollution load, to determine the generated urban nonpoint source pollutants under a certain selected precipitation condition.

Table 1 Requirements for important basic data

Item	Precision requirements	Time range
Demographic data	Detailed to blocks/streets	Status-quo
Land use type	CAD/vector data	Status-quo
Data on the drainage pipeline network	Attributes such as pipe diameter, pipe length, elevation, and burial depth Attributes of ancillary facilities of the pipeline network including pump station, storage pond, overflow facility, and diversion gate	Status-quo
Sewage treatment production statement	Volume of water inlet and outlet, water quality [indicators such as chemical oxygen demand (COD), suspended solids (SS), total nitrogen (TN), total phosphorus (TP), and ammonia nitrogen (NH_3-N)]	Status-quo, year-round, day by day
Digital elevation/topographic data	Entire studied area, vector data	Status-quo
Precipitation data	Entire studied area	Year-round, rain by rain

3.3 Simulation of the Impact of Urban Nonpoint Source Pollution Loads on Water Quality

We used the QUAL2K model, a one-dimensional comprehensive river water quality model, to simulate and calculate the water quality changes due to urban nonpoint source pollution after precipitation.

4 Nonpoint Source Pollution Load Calculation Results and Discussion

4.1 Estimation of Urban Nonpoint Source Pollution Load

Taking western urban areas of Kunming City as an instance, the calculation result based on collected basic data and site survey provided data for pollution prevention

and control measures. All the data and information used in the paper are provided by Kunming City.

Parameter Selection

From the InfoWorks ICM model for the drainage system of the Dian Lake Basin provided by Kunming, we extracted demographic and area information, and underlying surface information, and obtained the runoff coefficients of five types of underlying including greenbelt, roof, road, water area and others as Table 2 shows.

Calculation of Nonpoint Source Pollution Load

Take the western urban areas of Kunming as an instance. The western urban areas occupy an area of 66.47 km^2, with the areas of the greenbelt, commercial land, public land, industrial land, residential land, roads, squares, water areas, and undeveloped land being respectively 4.60, 4.65, 8.35, 8.77, 17.35, 6.38, 0.22, 1.33, and 8.25 (unit: km^2). Commercial land, public land, industrial land, and residential land were calculated as roof underlying surface; roads and squares were calculated as road underlying surface; and undeveloped land was calculated as other underlying surface.

As shown by the precipitation data of Kunming, the city had precipitation every month and the precipitation peaked at 73.1 mm in 2018. Characteristic precipitations of 1.0, 15.0, and 50 mm were selected to calculate nonpoint source pollution load. The calculation of urban nonpoint source pollution load in a single precipitation is shown in Eq. (1), and the selected values for a_i and b_j are shown in Table 3. The calculation results are shown in Table 3.

Table 2 Information on runoff production of various types of underlying surfaces in the Dian Lake Basin

Type of underlying surface	Runoff production coefficient	COD ($mg\text{-}L^{-1}$)	TN ($mg\text{-}L^{-1}$)	TP ($mg\text{-}L^{-1}$)	NH_3-N ($mg\text{-}L^{-1}$)
Greenbelt	0.25	55.00	2.80	0.38	2.73
Roof	0.80	58.00	2.72	0.39	1.65
Road	0.80	175.00	3.21	0.59	2.36
Water area	0.00	0.00	0.00	0.00	0.00
Others	0.35	175.00	3.21	0.59	2.36

Table 3 Comparison of pollution load results from different typical precipitation nonpoint sources in western urban areas of Kunming

Pollutant type	COD (g)	TN (g)	TP (g)	NH_3-N (g)
Precipitation capacity of 1 mm	3 307 813.14	114 573.64	17 462.64	74 059.36
Precipitation capacity of 15 mm	49 617 197.08	1 718 604.65	261 939.56	1 110 890.36
Precipitation capacity of 50 mm	165 390 656.92	5 728 682.17	873 131.86	3 702 967.85

$$W_{ij} = a_i \times b_j \times S_i \times p/1000 \quad (1)$$

where:

W_{ij}—Load of the j^{th} kind of pollutant generated by the i^{th} type of underlying surface in a certain precipitation, unit: g;
a_i—Runoff coefficient of the i^{th} type of underlying surface;
b_j—Runoff production concentration of the j^{th} kind of pollutant, unit: mg/L;
Si—Area of the i^{th} type of underlying surface, unit: m^2;
P—Precipitation capacity, unit: mm;

The pollutant loads of COD, TN, TP, and NH_3-N are linearly correlated with the level of precipitation with a positive correlation. The pollutant loads were plotted against the level of precipitation in Figs. 1 and 2. The positive correlation coefficient is highest for COD load and smallest for TP load, and the correlation coefficient for TN load is smaller than that for COD load but larger that those for TP and NH_3-N.

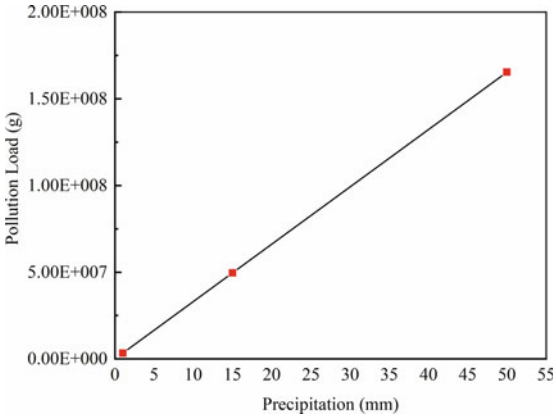

Fig. 1 The relationship between COD pollutant concentration and precipitation

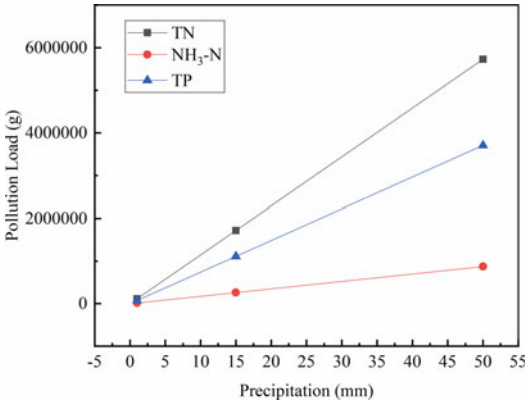

Fig. 2 The relationship between three pollutants concentration and precipitation

With the same level of precipitation, the COD load is the highest, and the TP load is the lowest. With strengthened control over point source pollution and constant urban development in recent years, the area occupied by roads keeps expanding. Consequently, urban nonpoint source pollution has become more an more significant in the Dian Lake Basin. Given frequent extreme weathers and uncontrollable precipitations, measures must be taken to control urban nonpoint source pollution.

4.2 Discussion on Prevention and Control Measures for Urban Nonpoint Source Pollution

Based on the actual pollution characteristics of the studied Dian Lake Basin, we proposed four types of prevention and control measures suitable for different functional zones of Kunming City.

According to the runoff production information of various underlying surfaces in the Dian Lake Basin, it is evident that hard surfaces such as roads and roofs tend to have higher runoff production coefficients. Too much hard paving can result in reduced infiltration efficiency of the surface and increased rainwater runoff discharge. Without initial pollution interception treatment of rainwater, a considerable level of pollution load can be generated through infiltration or direct discharge. To reduce the pollution load and protect the water environment, we recommend strategies such as reduced roads and roofs and increased greenbelts.

Green Roofs

Table 4 shows the areas and proportions of different types of underlying surfaces in the western urban areas of Kunming. Among these types of surfaces, roof takes the largest share, as Fig. 3 shows. If some measures could be taken to the roof to reduce its runoff production concentration, the overall pollution load can be substantially lowered.

Roof greening can control the nonpoint source pollution arising from precipitation runoffs falling onto the roofs of urban buildings, reducing the overly high proportion of hard paving in the city [9]. The shift from hard paving to natural land and plants can expand the area of urban greenbelt. In times of precipitation, rainwater infiltrates into the prepared soil or enters collection facilities, reducing runoff during precipitations.

Table 4 Areas and proportions of different types of underlying surfaces in western urban areas of Kunming

Type of underlying surface	Total	Water system	Greenbelt	Undeveloped	Road	Roof	Unknowns
Area (m^2)	66 474 295	1 331 174	4 600 580	8 250 157	6 598 195	39 126 848	6 567 341
Proportion	100%	2.00%	6.92%	12.41%	9.93%	58.86%	9.88%

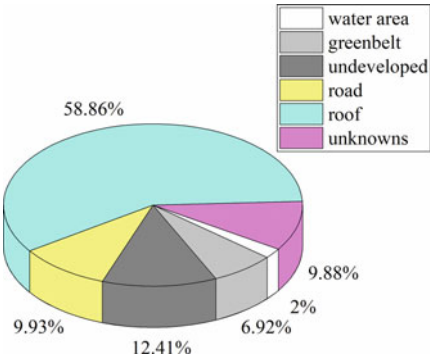

Fig. 3 Proportion of different underlying surface area

The collected rainwater will be discharged later or will be recycled in the storage and purification system installed on the roofs [10]. The application of roof greening technology can be of great significance to improving the ecological condition of Kunming.

Taking the 15 mm precipitation capacity as an instance, the calculation result is shown in Table 5.

According to Table 5, if all the current roofs in the western urban areas of Kunming were changed into green roof, and the runoff production coefficients and runoff production concentrations are the same as those of greenbelt, the nonpoint source pollution load would be drastically reduced, and the degrees of reduction of all pollutants would be above 30%, with TP even reduced by over 50%.

Roads

In addition to roofs that take a big share, roads also represent a type of underlying surfaces with a high runoff production coefficient and a large area. Roads, despite accounting for a mere 9.93% of the total area, if reconstructed, would still remarkably reduce the overall pollution load.

A high runoff production coefficient of the roads points to a high impermeability rate. If the runoff production coefficient is to be lowered, measures should be taken to improve road permeability. As for the paving of permeable road surface, the structure typically falls into the permeable tile course, permeable leveling course, permeable base course, and soil matrix [11]. Permeable roads have a large porosity, making

Table 5 Comparison of nonpoint source pollution load before and after use of green roofs in western urban areas of Kunming

Pollutant type	COD (g)	TN (g)	TP (g)	NH_3-N (g)
Status-quo	49 617 197.08	1 718 604.65	261 939.56	1 110 890.36
Green roof	30 454 823.27	852 336.24	134 581.67	736 739.87
Reduction volume	19 162 373.81	866 268.41	127 357.89	374 150.48
Reduction proportion	38.62%	50.41%	48.62%	33.68%

it easy for rainwater to infiltrate and therefore making it difficult to generate direct surface runoff. As the runoff during the precipitation decreased, the burden on the urban drainage pipeline network will be lessened [12], thus easing the urban waterlogging. Meanwhile, various structures using permeable paving generally feature a simple rainwater purification treatment function, playing throttling, adsorption, and purification roles successively at the physical, chemical, and biological levels. Rainwater infiltrates through the permeable concrete and restores into underground water, increasing soil moisture and resuming the living environment of soil microbe in an eco-friendly way. While ensuring the basic functionality of the road surfaces, permeable paving plays two roles of reducing runoff and simply purifying rainwater.

Reducing runoff production concentrations can also contribute to mitigated pollution load. To some extent, the cleaner the roads are, the lower the runoff production concentrations are. The easiest and most effective way to keep the roads clean and tidy is sweeping them, including artificial sweeping by cleaners and mechanical dust collection by watering carts, road sweepers and other equipment. Normally, the removal rate of surface dust varies directly with the sweeping frequency of streets. According to the study by Sutherland et al. [13] on the relationship between the sweeping frequency and dust removal coefficient, if sweepers are used to sweep the roads, when the sweeping frequency is low, increased sweeping frequency could significantly boost the dust removal rate. Therefore, in terms of reducing urban surface source pollution load, it is advisable that Kunming moderately raise its daily frequency of road sweeping.

5 Water Quality Simulation

Water pollution prevention and control measures for the Dian Lake Basin are generally divided into two parts: pollutant emission reduction and water quality improvement. In practice, the water quality targets are set based on surface water environmental quality standards, and the target is typically one or two levels higher than the current water quality situation. The emission reduction targets are then calculated on the basis of the water quality targets. The previous part of this study explained the static simulation of nonpoint source pollution load, but the relationship between water quality change and the nonpoint source pollution remains unclear. Therefore, in this section, a water quality model is established to simulate the spatial and temporal impact of a precipitation.

5.1 QUAL2K Model

The QUAL2K model is a one-dimensional model in which pollutants migrate in the direction of water flow, and the effects of turbulence and diffusion occur in the mainstream direction, which is consistent with the concentration gradient. Each

river section was assumed to have constant hydraulic properties. It was assumed that pollutants were uniformly mixed in each unit of water. The biotransformation reactions and sedimentation processes in each unit of water are in accordance with the first-order reaction kinetic equations [14].

In this study, we focused on the water quality changes associated with urban nonpoint source pollution runoff entering the pipelines with the mix of rainwater and sewage and then discharged into the river through the overflow of sewage plants. Because the width and water depth of the studied river (the Laoyunliang River), which flows through the western urban area of Kunming, are much smaller than its length, the change in pollutant concentration across the river width and water depth is small compared to that across the river length and therefore can be neglected. Thus, the river can be approximated as one-dimensional and the model was used for water quality simulation studies in the Dian Lake Basin.

5.2 Water Quality Change Simulation

The pollutant concentration data from the upstream monitoring points of the Old Canal River channel were input data to the QUAL2K model, in which the geographic information of the river section was obtained through BIGEMAP. Due to the limited amount of data available regarding the current water quality along the studied river, there were difficulties in parameter calibration, so for parameters including velocity, hydrolysis rate, etc., we adopted values recommended by the book QUAL2K River Water Quality Simulation Model Theoretical Methods and Application Guide [15].

In this study, all the runoff from the catchment area of the third water quality purification plant in Kunming due to precipitation was assumed to enter the pipelines with the mix of sewage and rainwater, and then a part of the mixed sewage overflow was directly discharged into the river before entering the water plant. The discharge to the river was point discharge, but the source of sewage is urban nonpoint pollution. The catchment area included in the model was assumed to have only one overflow discharge point and produce no nonpoint source discharge.

The process of running the model is shown in Fig. 4 along with the pollutant concentration profile along the river.

In this study, June 26, 2016 was selected as an example for calculation. The upstream water quality of the Laoyunliang River was 249 mg/L COD, 2.52 mg/L TP, 21.5 mg/L TN, and 17.6 mg/L NH_3-N. The precipitation on that day was 11.2 mm, and the overflow was 10%. The water volume of the third water quality purification plant in Kunming on that day was 21.35 m^3, and the pollutant concentrations in the mix of rainwater and domestic sewage water before entering the plant were 83.6 mg/L BOD_5, 233 mg/L COD, 72 mg/L SS, 30.1 mg/L TN, 3.16 mg/L TP, and 25.5 mg/L NH_3-N.

The simulation results showed that the water quality at about 7 km upstream from the Old Canal was 151.05 mg/L COD, 1.36 mg/L TP, 19.78 mg/L TN, and 10.2 mg/L NH_3-N. As the pollutants migrated downstream, the diffusion and self-purification

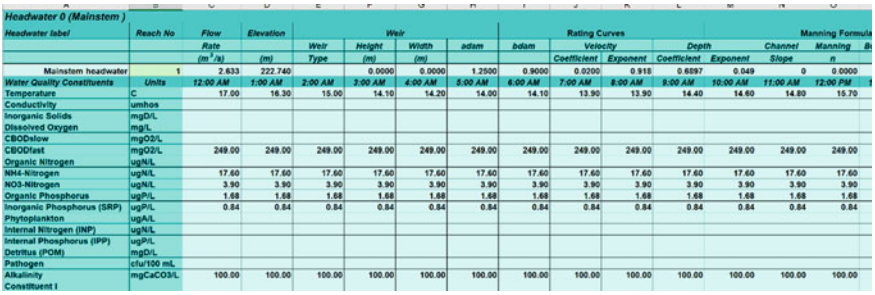

Headwater 0 (Mainstem)																	
Headwater label	Reach No	Flow	Elevation	Weir					Rating Curves						Manning Formula		
		Rate		Weir	Height	Width	adam	bdam	Velocity		Depth		Channel	Manning	B
		(m^3/s)	(m)	Type	(m)	(m)			Coefficient	Exponent	Coefficient	Exponent	Slope	n	
Mainstem headwater	1	2.633	222.740		0.0000	0.0000	1.2500	0.9000	0.0200	0.918	0.6897	0.049	0	0.0000	
Water Quality Constituents	Units	12:00 AM	1:00 AM	2:00 AM	3:00 AM	4:00 AM	5:00 AM	6:00 AM	7:00 AM	8:00 AM	9:00 AM	10:00 AM	11:00 AM	12:00 PM			
Temperature	C	17.00	16.30	15.00	14.10	14.20	14.00	14.10	13.90	13.90	14.40	14.60	14.80	15.70			
Conductivity	umhos																
Inorganic Solids	mgD/L																
Dissolved Oxygen	mg/L																
CBODslow	mgO2/L																
CBODfast	mgO2/L	249.00	249.00	249.00	249.00	249.00	249.00	249.00	249.00	249.00	249.00	249.00	249.00	249.00			
Organic Nitrogen	ugN/L																
NH4-Nitrogen	ugN/L	17.60	17.60	17.60	17.60	17.60	17.60	17.60	17.60	17.60	17.60	17.60	17.60	17.60			
NO3-Nitrogen	ugN/L	3.90	3.90	3.90	3.90	3.90	3.90	3.90	3.90	3.90	3.90	3.90	3.90	3.90			
Organic Phosphorus	ugP/L	1.68	1.68	1.68	1.68	1.68	1.68	1.68	1.68	1.68	1.68	1.68	1.68	1.68			
Inorganic Phosphorus (SRP)	ugP/L	0.84	0.84	0.84	0.84	0.84	0.84	0.84	0.84	0.84	0.84	0.84	0.84	0.84			
Phytoplankton	ugA/L																
Internal Nitrogen (INP)	ugN/L																
Internal Phosphorus (IPP)	ugP/L																
Detritus (POM)	mgD/L																
Pathogen	cfu/100 mL																
Alkalinity	mgCaCO3/L	100.00	100.00	100.00	100.00	100.00	100.00	100.00	100.00	100.00	100.00	100.00	100.00	100.00			
Constituent I																	

Fig. 4 QUAL2K model runs

of the water body led to a decrease in the concentration of all pollutants, with the TP concentration decreased the most (by 46%).

Compared with the water quality on June 16, 2016 (i.e. COD 18.69 mg/L, TP 0.32 mg/L, TN 15.21 mg/L, and NH3-N 3.19 mg/L) without precipitation, the pollutant concentrations in the river after precipitation were 8.1, 4.3, 1.3, and 3.2 times higher than the no-rain-day concentrations. All pollutants increased significantly during precipitation, except for TN, which changed only moderately. The urban nonpoint source pollution problem caused by precipitation had a significant impact on the water quality of the Laoyunliang River and increased the pollutant load, so it is indispensable to solve the problem of nonpoint source pollution.

5.3 Discussion on Prevention and Control Measures for Urban Nonpoint Source Pollution

Due to the late construction of urban pipe network in Kunming, some sewage network outfalls overflow during rainfalls, and the overflow sewage is directly discharged into rivers without treatment, which can pollute the river water and cause eutrophication and odor in rivers. Therefore, based on the simulation result illustrated in this section, we recommend introducing a simple treatment device for overflow sewage at the outlet of precipitation sewage pipes [16].

Li et al. found that microbial bacteria and bio-composite enzymes added into the outfall can effectively and stably remove COD, NH_3-N, TN and TP from the river outfall, reducing the pollution load into the river, with average removal rates of respectively 48.7%, 36.7%, 20.1% and 32.5% [17].

For cities with frequent and heavy rainfall and old pipe networks like Kunming, it is recommended to install sewage treatment devices at the outlets of the overflowing sewage to reduce the concentration of pollutants entering the river and thus reduce the pollution load.

6 Conclusion

(1) Profiles of main pollutions along the studied river during rainfalls were generated using the QUAL2K model, and the calculation results indicate that concentrations of main pollutants can increase significantly during precipitation.
(2) Four preventive measures were proposed to alleviate the problem of nonpoint source pollution: a) adopting green roofs; b) utilizing permeable road paving; c) increasing road sweeping frequency and d) adding overflow treatment devices at sewage plants.

References

1. Xie L, de Souza Carlos E (1992) Robust H/sub infinity/control for linear systems with norm-bounded time-varying uncertainty. IEEE Trans Autom Control 37(8):1188–1191
2. Kwakkel JH, Walker WE, Marchau VA (2010) Classifying and communicating uncertainties in model-based policy analysis. Int J Technol Policy Manage 10(4):299–315
3. Walker WE, Harremoës P, Rotmans J, Van Der Sluijs JP, Van Asselt MB, Janssen P, Krayer von Krauss MP (2003) Defining uncertainty: a conceptual basis for uncertainty management in model-based decision support. Integr Assess 4(1):5–17
4. Beh EH, Maier HR, Dandy GC (2015) Scenario driven optimal sequencing under deep uncertainty. Environ Model Softw 68:181–195
5. Yang W, Zhang J (2021) Assessing the performance of gray and green strategies for sustainable urban drainage system development: a multi-criteria decision-making analysis. J Clean Prod 293:126191
6. Jamei E, Tapper N (2019) Wsud and urban heat island effect mitigation. In: Approaches to water sensitive urban design. Woodhead Publishing, pp 381–407
7. Wang X, Li Y, Liu N, Zhang Y (2020) An urban material flow analysis framework and measurement method from the perspective of urban metabolism. J Clean Prod 257:120564
8. Pivnenko K, Laner D, Astrup TF (2016) Material cycles and chemicals: dynamic material flow analysis of contaminants in paper recycling. Environ Sci Technol 50(22):12302–12311
9. Kasmin H, Musa S (2012) Green roof as a potential Sustainable structure for runoff reduction. In: 2012 IEEE symposium on business, engineering and industrial applications. IEEE, pp 889–893
10. Chow M, Bakar M (2016) A review on the development and challenges of green roof systems in Malaysia. World Academy of Science, Engineering and Technology, Open Science Index 109. Int J Archit Environ Eng 10(1):16–20
11. Bateni N, Lai SH, Putuhena F, Mah YS, Mannan A (2018) A rainfall simulator used for testing of hydrological performances of micro-detention permeable pavement. Int J Eng Technol 7:44–48
12. Liu Y, Li T, Peng H (2018) A new structure of permeable pavement for mitigating urban heat island. Sci Total Environ 634:1119–1125
13. Sutherland RC, Jelen SL (1997) Contrary to conventional wisdom, street sweeping can be an effective BMP. Adv Model Manage Stormwater Impacts 5:179–190
14. Boustani F, Gohargani E (2015) Use QUAL2K model for water quality simulation in the Beshar river
15. Zhao Y, Chen Y, Wu Y (2015) QUAL2K river water quality simulation model theoretical methods and application guide

16. Ward S, Butler D (2009) Compliance with the urban waste water treatment directive: European Union city responses in relation to combined sewer overflow discharges
17. Li Y, Li C, Wang S, Chen J, Shi H, Liang W (2018) Application of composite microbial bacterial agents in the enhanced treatment of river outfall pollution. J Water Supply Drainage 54(S2):95–99

Temperature Alternation Stress Analysis of Tee Pipe Weld Structure Based on Submodel Method

Xiaolei Wang, Jiang Ma, Jianguo Chen, Xiaoyan Chen, Zhaoming Zhou, and Jia Zhang

Abstract In pipeline design, the position of the pipe connection is one of the weakest links because the wall of the pipe is weakened by opening and the continuity of the original structure is destroyed. Besides, the forces and torques applied by pipes through nozzles can produce high stresses in local areas of nozzles. This paper is based on transient thermo-mechanical theory, submodel method is adopted to establish the tee weld structure model. The stress distribution in key weld positions of tee pipe under temperature alternating load is analyzed. At the same time, the stress in the local discontinuous area where the stress changes rapidly at the connection between the nozzle and the shell is analyzed accurately. Finally, the strength of the weld is evaluated. The results show that the maximum stress is concentrated at the weld seam, the maximum stress is 226.03 MPa, and the maximum stress gradually spreads around the branch pipe. The maximum stress calculated by the submodel method is 238.65 MP. The stress linearization of the maximum stress concentration position of the weld was evaluated. The conclusion has an important guiding role in reducing the operation failure risk, structural stress failure risk, and production medium leakage risk of tee pipes under complex temperature alternating conditions.

Keywords Submodel method · Temperature alternation · Tee pipe · Stress analysis · Strength assessment

X. Wang · J. Ma · J. Chen · X. Chen
The First Gas Production Plant of Xinjiang Oilfield Company, Xinjiang, Karamay 834000, China

Z. Zhou
School of Mechatronic Engineering, Southwest Petroleum University, Chengdu 610500, China

J. Zhang (✉)
State Key Laboratory of Oil and Gas Reservoir Geology and Exploration, Southwest Petroleum University, Chengdu 610500, China
e-mail: zhangjiaswpu@163.com

X. Liu (ed.), *Proceedings of 2021 China-Europe International Conference on Pipelines and Trenchless Technology*, Lecture Notes in Civil Engineering 212,
https://doi.org/10.1007/978-981-19-4067-5_4

1 Introduction

Tee pipe is a very common equipment in the natural gas processing plant and other industrial production fields. Among them, tee pipe welding is one of the weak parts of the pipe. Due to the specific mating structure, there is obvious stress concentration. Under the action of various loads such as temperature fluctuation, vibration, and impact, there is a great risk of fatigue failure at the weld, which may induce pipeline leakage or even explosion and other serious consequences [1, 2]. However, there is no calculation standard or specification for weld fatigue strength, related research reports are also very limited. Therefore, it is necessary to adopt an effective method to comprehensively evaluate the structural strength of tee pipes. Correct evaluation of the harmfulness of tee structure is directly related to the problem of the whole pipeline system security and economy.

Currently, most scholars use the finite element method (FEM) to solve the stress distribution under different parameters of pipes. Du [3] carried out numerical simulation and theoretical calculation of thermal stress of single pipe crack under steady-state conditions, and the results showed that the maximum stress-causing plastic deformation occurred on the outer wall. Sun [4] calculated the temperature field and stress field of the reactor pressure vessel by using FEM and determined the crack propagation path in different directions and the corresponding stress distribution by using the extended finite element method (XFEM). Si [5] carried out creep-fatigue crack tests on improved X12Cr rotor steel under 600 loads using C(T) sample. Chen [6] studied the fracture mechanics of confined thermal shock in nuclear reactor pressure vessels (RPV). The results show that the location of the deepest crack front and the crack surface should be considered. Kandil [7] analyzed the stress distribution of pressure vessels under steady-state action and obtained the relationship between average stress and stress amplitude under different working conditions. Barsoum [8] obtained the plastic and failure model constants of autoclaves through the uniaxial tensile test and notched ring test. Chen [9] discussed the inducement of the low-temperature working condition of liquid ethane pipeline and simulated the low-temperature stress of liquid ethane pipeline under special phase transformation working conditions.

Scholars have done a lot of research on the stress analysis of pipelines, but all of them ignore the stress and strength analysis of pressure pipelines under complex loads, which has great limitations. In this paper, a three-way pipeline in a natural gas processing plant is studied. The three-dimensional physical model of tee pipe and weld was established, and the submodel calculation method was introduced to study the temperature field and stress field changes of pipe nozzles under service conditions.

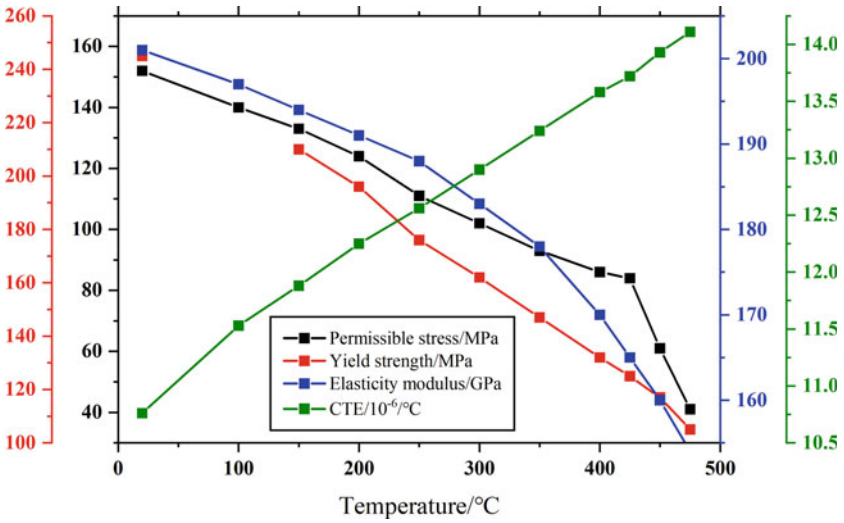

Fig. 1 20G material performance (wall thickness ≤100 mm)

2 Design Parameters and Numerical Model Analysis

2.1 Design Parameter

The pipeline is industrial in use for a natural gas processing plant. The pipe tee connection is welded, and the welding coefficient is 0.85. Tee pipe and bend material are ASME standard SA-182F11 CL2, the material is 20G, the pipe diameter is 100 mm, the wall thickness is 10 mm, design pressure is 10 MPa, design temperature is 320 °C, working pressure is 7.2 Mpa, working temperature is 290 °C. The thermal expansion coefficient, elastic modulus, thermal conductivity, Poisson's ratio, density, and other characteristic parameters of pipe fitting materials are selected according to the material characteristics in ASME-SECTION II PART-D, as shown in Fig. 1.

2.2 FE Model

In this work, the stress distribution of the weld at the tee is mainly studied. Therefore, only the tee part of the pipeline is selected for numerical analysis. The physical model of tee and weld shall be established according to the size of the design drawing, as shown in Fig. 2. The weld model of tee pipe includes base material and weld zone, which includes welding zone, fusion zone, and heat-affected zone. The base material and weld zone are heat-treated low carbon steel. It is assumed that face A is subjected to full displacement without DOF constraints, and face B is subjected to z-direction

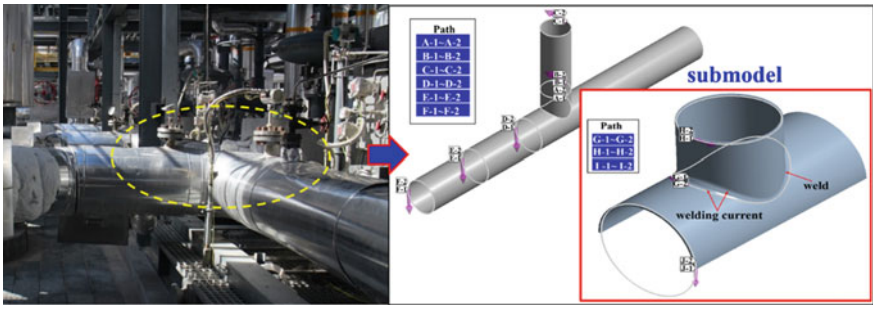

Fig. 2 FE model

Fig. 3 Grid division

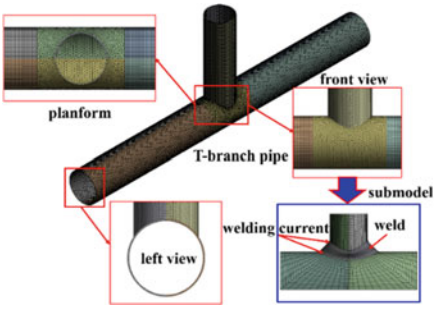

free displacement constraints. The internal pressure of 7.2 MPa perpendicular to the surface direction was applied on the inner surface of pipe C, and the pull force (support reaction force) facing the vertical end of pipe D was applied for the Shell-Solid element submodel analysis.

Considering the complexity and precision of the solution, the effect of grid independence is eliminated. The model is divided into unstructured grids, and the overall grid quality is above 0.8, the meshing is shown in Fig. 3.

3 Result Analysis

3.1 Temperature Field Analysis

Figure 4 shows the temperature variation trend in the tee pipe (40–290). It can be seen that the temperature increases linearly along the wall thickness direction during the calculation time. Figure 5 shows the temperature distribution of tee pipes under operating conditions. It can be seen from the figure that the highest temperature of the inner wall of the pipe is 290 °C, the lowest temperature of the outer wall of the pipe is 40 °C, and the temperature difference between the inside and outside of the

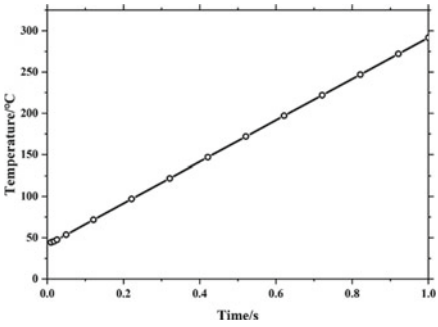

Fig. 4 Temperature loading

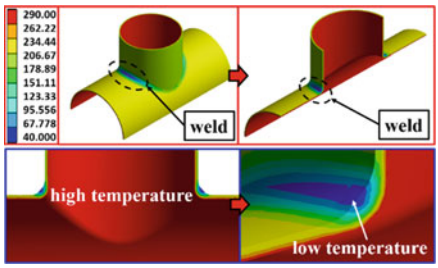

Fig. 5 Temperature field distribution

pipe is 250 °C. The lowest temperature occurs outside of the tee connection (straight pipe section). The outer wall temperature of the branch pipe is lower than that of the straight pipe. The temperature distribution in other positions of tee pipes is more uniform.

3.2 Analysis of Stress Field

Figure 6 shows the stress distribution of the pipe at operating temperature. It can be seen from the Figure that the maximum stress of the tee pipe is 226.03 Mpa, and the maximum stress point appears on the inner surface of the tee pipe connection. The stress in other positions of the tee pipe is less than 100 MPa, which is less than the maximum allowable stress of the pipeline. Compared with other positions of the tee pipe, the stress level at the weld is significantly higher, and the stress difference is 125.19 Mpa. Take the path stress changes at different positions of tee pipes, and the paths are shown in Fig. 2 (Path A–Path F). Figure 7 shows the stress distribution along different paths.

It can be seen from the changes of the path stress that the stress in the radial direction of path A-1–A-2 (at the weld) is larger at the pipe position, and the maximum stress is 226.03 Mpa. The stress in the vertical direction of paths B-1–B-2 is large, with a maximum of 26.219 Mpa. The stress in the radial direction of path C-1–C-2 is large, the maximum is 35.203 Mpa, and the stress is very small compared with other

Fig. 6 Stress distribution

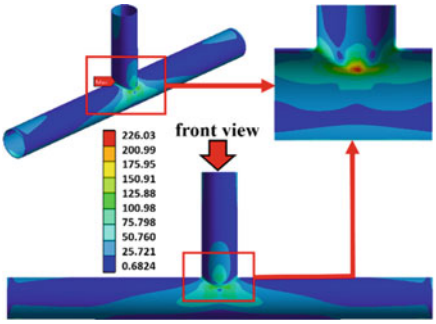

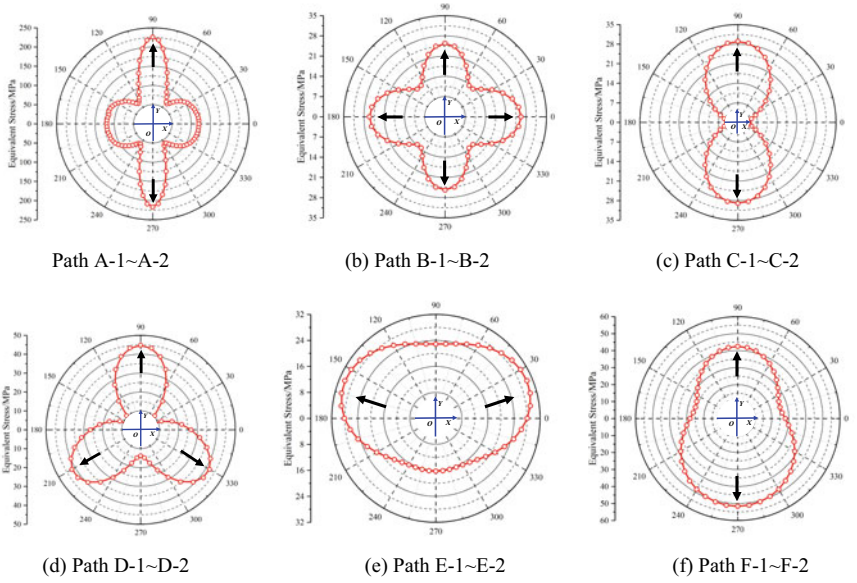

Path A-1~A-2 (b) Path B-1~B-2 (c) Path C-1~C-2

(d) Path D-1~D-2 (e) Path E-1~E-2 (f) Path F-1~F-2

Fig. 7 Stress distribution at different paths

positions of the weld. In the straight pipe position, path D-1–D-2 every 120° position stress is larger, the maximum is 44.843 MPa. The stress in the vertical direction of paths E-1–E-2 is large, with a maximum of 30.287 Mpa. The stress in the radial direction of path F-1–F-2 is large, the maximum is 51.677 Mpa, and the stress is very small compared with other positions of the weld. It can be concluded that the stress variation at the weld is complex and much greater than that at other positions of the tee pipe.

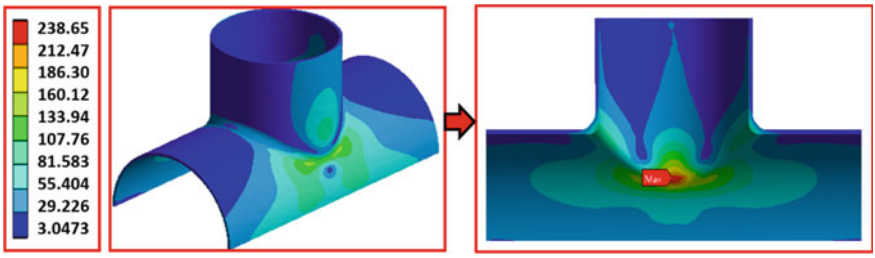

Fig. 8 Stress distribution of submodel

3.3 Stress Analysis of Submodel

The submodel method is also called the cutting boundary displacement method or specific boundary displacement method. The cut boundary refers to the boundary separated by the submodel from the whole model divided by the rough mesh. And the boundary condition of the submodel is the calculated displacement of the cutting boundary position after the whole model is calculated and analyzed. The submodel is based on Saint Venant's principle. Therefore, if the location of the sub-model is far from the stress concentration location, it is considered that more accurate solution results can be obtained. In this section, the submodel method is adopted to realize the perfect mesh division of the local area of the nozzles, and the stress in the local discontinuous area and the area with sharp stress change at the connection between the nozzles and the shell is analyzed precisely. From the calculation results of the full-size model in Sect. 3.2, it can be seen that stress concentration occurs at the weld joint position of the tee pipe, so stress changes at this position should be focused on. The chamfering operation was performed on the weld value to reduce the stress distortion caused by the sharp element, and the calculation results are shown in Fig. 8. Figure 9 shows the stress distribution along different paths.

It can be seen from the calculation results of the submodel that the maximum stress position is still at the weld, and the maximum stress is 238.65 MP (the maximum stress of the full-size model is 226.03 Mpa). Due to the sub-model technology, the mesh of the local area of the nozzles is perfectly divided, and the stress of the local discontinuous area and the area with a sharp change of stress at the connection between the nozzles and the shell is precisely analyzed. Therefore, the accuracy of finite element analysis is improved, the calculation is simplified and the time is saved by using the sub-model analysis method.

The strength evaluation of the stress concentration of the weld joint of the tee pipe was carried out. The evaluation is based on the evaluation strategy for elastic stress analysis in JB4732-1995 (Confirmed in 2005) "Steel Pressure Vessels-Analysis and Design Standards". The stress at the stress concentration is classified and evaluated by the linearization principle. First, a linearized path is set along with the minimum distance of wall thickness through the maximum stress node; Secondly, the tee joint weld due to geometric discontinuity. Therefore, the film stress obtained from the

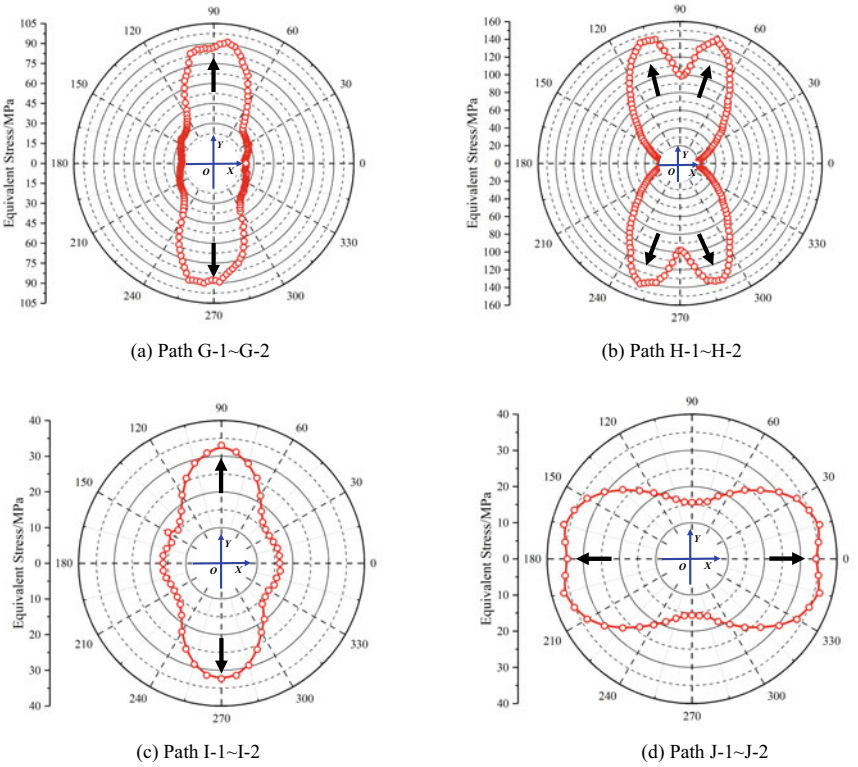

(a) Path G-1~G-2

(b) Path H-1~H-2

(c) Path I-1~I-2

(d) Path J-1~J-2

Fig. 9 Stress distribution at different paths

cross-section at the intersection is the primary local film stress P_L, corresponding to the primary local film stress intensity S_{II}. The bending stress in the discontinuous area of the overall pipeline structure should be classified into the category of secondary stress. To meet the requirements of JB4732-1995 (confirmed in 2005) "Steel Pressure Vessels—Analysis and Design Standards" for each stress intensity successively assessed. The film stress plus bending stress plus secondary stress is treated according to S_{IV}. Consequently, the stress intensity requirement of the weld seam was satisfied under operating conditions and the result was qualified. However, with the extension of the service time of the pipeline, the weld of the tee pipe may crack and other failure situations, which is easy to cause human and property losses. Therefore, in the service process of the three-way pipeline, it is necessary to increase the insulation layer at the nozzle position (reduce the heat exchange between the temperature in the pipe and the ambient temperature, and reduce the stress change caused by the temperature difference).

4 Conclusion

Based on the elastic analysis method, the stress intensity in high-stress zone of pipeline and weld was evaluated. The temperature distribution and stress distribution of the pipe and weld were analyzed by using the submodel method. The results show that the temperature along the wall thickness increases with the increase of time under operating conditions. Stress concentration exists at the weld joint of the tee pipe. And stress distribution can be obtained by stress analysis of the pipe and weld. Due to the discontinuity of the pipeline weld, there is stress concentration at the weld, and the maximum stress is 226.03 Mpa. By using the submodel analysis method, the accuracy of finite element analysis is improved, the calculation is simplified and the time is saved. The linear strength assessment was carried out in the heating process of the pipe weld, and the stress strength assessment of the weld was qualified to meet the strength requirements.

Acknowledgements This work is supported by the key research and development projects of sichuan province (2020YFG0180), national natural science foundation of China (51974271), and Xinjiang oilfield company project of PetroChina (Safety risk analysis and countermeasure study of natural gas cryogenic temperature alternating condition).

References

1. Wang C, Wang Z, Zhang J, et al (2021) Study on acoustic source characteristics of distributed optical fiber acoustic wave monitoring buried natural gas pipeline leakage. In: E3S web of conferences, vol 252. EDP Sciences, p 03043
2. Wang C, Feng X, Yang X, et al (2021) Analysis of thermal-force coupling stress field under the temperature of alternating of molecular sieve adsorption tower. In: E3S web of conferences. EDP Sciences, p 261
3. Du BC, He YL, Zheng ZJ et al (2016) Analysis of thermal stress and fatigue fracture for the solar tower molten salt receiver. Appl Thermal Eng 99:741–750
4. Sun X, Chai G, Bao Y (2017) Ultimate bearing capacity analysis of a reactor pressure vessel subjected to pressurized thermal shock with XFEM. Eng Failure Anal S1350630716301327
5. Si J, Yan ZR, Luo XM et al (2015) Low cycle fatigue crack growth behavior of modified rotor steel under high-temperature. Procedia Eng 130:1066–1074
6. Chen M, Lu F, Wang R et al (2014) Structural integrity assessment of the reactor pressure vessel under the pressurized thermal shock loading. Nucl Eng Des 272:84–91
7. Kandil A (1996) Analysis of thick-walled cylindrical pressure vessels under the effect of cyclic internal pressure and cyclic temperature. Int J Mech Sci 38(12):1319–1332
8. Barsoum I, Lawal SA, Simmons RJ et al (2018) Failure analysis of a pressure vessel subjected to an internal blast LOAD. Eng Fail Anal 91:354–369
9. Chen J, Guo Y, Lu G et al (2017) Low temperature characteristics of liquid ethane pipeline under phase transition. Nat Gas Oil 35(05):45–50

Main Technical Analysis of Sewage Treatment in Environmental Engineering

Zhen Ling

Abstract Water is the most dependent natural resource for the survival and development of animals and plants on the earth. The protection of water resources is a topic of widespread concern all over the world. In recent years, with the continuous improvement of China's industrialization and urbanization level, China's social demand for water resources is also increasing. At the same time, the random discharge of industrial production and domestic sewage has also caused serious pollution to the water resources in the natural environment, which has a great impact on people's drinking water safety and ecological environment protection. Therefore, it is very necessary to strengthen the scientific treatment of sewage. In view of this, this paper first analyzes the harm caused by water pollution, and then studies the importance and technical measures of water pollution treatment.

Keywords Environmental engineering · Sewage disposal · Main technology

1 Introduction

Water resources are important resources for human survival. Therefore, China must have more strict standards and effective technologies for the treatment of water resources. Urban environmental engineering construction is closely related to economy and people's life, and has attracted extensive attention with the acceleration of urban construction. In the process of implementing urban environmental engineering construction, only by earnestly implementing the fundamental requirements of the scientific outlook on development, taking the construction of an energy-saving society as the main goal, and better coordinating the relationship between urban residents and the environment, can we realize the mutual integration of urban construction and environmental protection [1].

According to the latest environmental bulletin released by China's Ministry of Ecology and Environment, the discharge of major environmental indicators in

Z. Ling (✉)
Hohai University, Nanjing 210003, China
e-mail: 1140891302@qq.com

X. Liu (ed.), *Proceedings of 2021 China-Europe International Conference on Pipelines and Trenchless Technology*, Lecture Notes in Civil Engineering 212,
https://doi.org/10.1007/978-981-19-4067-5_5

China's wastewater decreased year by year from 2016 to 2019 and the specific emissions of pollutants are shown in Table 1 [2]. The emissions of chemical oxygen demand, ammonia nitrogen, total nitrogen, total phosphorus, heavy metals, petroleum, volatile phenol and cyanide decreased by 13.8%, 18.5%, 4.8%, 34.0%, 28.0%, 45.7%, 46.0% and 34.0%, respectively.

At present, water resource shortage and water environmental pollution have become important factors restricting the sustainable development of urban society, economy and ecological environment in China. The treatment of urban sewage will be related to the living environment and health level of urban residents. In modern society, with the increasing awareness of environmental protection by the public and the government, Wastewater recovery and reuse is considered to be the best strategy to meet current and future water needs.

Table 1 Main indicators of Water environment statistics in China from 2016 to 2019

Index	Source	2016	2017	2018	2019
COD	Total	658.1	608.9	584.2	567.1
	Industrial production	122.8	91	81.4	77.2
	Agriculture	57.1	31.8	24.5	18.6
	Domestic activities	473.5	483.8	476.8	469.9
	Centralized pollution control and treatment	4.6	2.3	1.5	1.4
NH_4^+-N	Total	56.8	50.9	49.4	46.3
	Industrial production	6.5	4.4	4	3.5
	Agriculture	1.3	0.7	0.5	0.4
	Domestic activities	48.4	45.4	44.7	42.1
	Centralized pollution control and treatment	0.7	0.3	0.2	0.3
TN	Total	123.6	120.3	120.2	117.6
	Industrial production	18.4	15.6	14.4	13.4
	Agriculture	4.1	2.3	1.8	1.3
	Domestic activities	100.2	101.9	103.6	102.4
	Centralized pollution control and treatment	0.8	0.5	0.4	0.4
TP	Total	9	7	6.4	5.9
	Industrial production	1.7	0.8	0.7	0.8
	Agriculture	0.6	0.3	0.2	0.2
	Domestic activities	6.7	5.8	5.4	5
	Centralized pollution control and treatment	0	0	0	0

2 Significance of Sewage Treatment Technologies

2.1 Reduce Environmental Pollution

The main purpose of environmental engineering is to protect the local environment, reasonably solve the pollution problem, and allow pollutants to be discharged without polluting the natural environment. Environmental engineering is to carry out scientific and reasonable supervision in the process of pollutant discharge to ensure that the pollutant discharge reaches the discharge standard, so as to effectively reduce the environmental pollution caused by human activities, ensure the virtuous cycle of ecosystem and the balance of ecosystem. At present, the discharge of sewage in cities is large, which is one of the important factors causing environmental pollution. If the discharge of urban sewage is allowed, it will cause extremely serious damage to the earth's natural environment. At present, what we need to do is to strictly control the discharge of urban pollutants, do a good job in pollutant treatment, and gradually improve the environmental engineering system.

2.2 Improve the Utilization Efficiency of Water Resources

China has a vast territory and a large gap between regions. In some areas, water resources are relatively scarce. Due to the lack of water resources, the development of some cities has been greatly affected. Therefore, in some cities, we must do a good job in water resources management, reduce the pollution of urban sewage to water resources, reduce the pollution rate of water resources and improve the utilization rate of water resources, effectively alleviate the problem of lack of urban water resources as well. In the process of actual urban development, we must consider sewage treatment, improve the utilization rate of water resources and promote urban development.

2.3 Promoting the Sustainable Development of Enterprises and Cities

Advanced environmental sewage treatment technology has been adopted by urban environmental protection system, which not only greatly protects people's living environment, but also improves the utilization rate of water resources, promotes the recycling of water resources, and promotes the implementation of enterprise and urban sustainable development strategy.

With the development of technology, the role of sewage treatment plants has changed from nitrogen (N), phosphorus (P) and organic matter removal to integrated resource recovery, pollution control and carbon emission control measures. The main

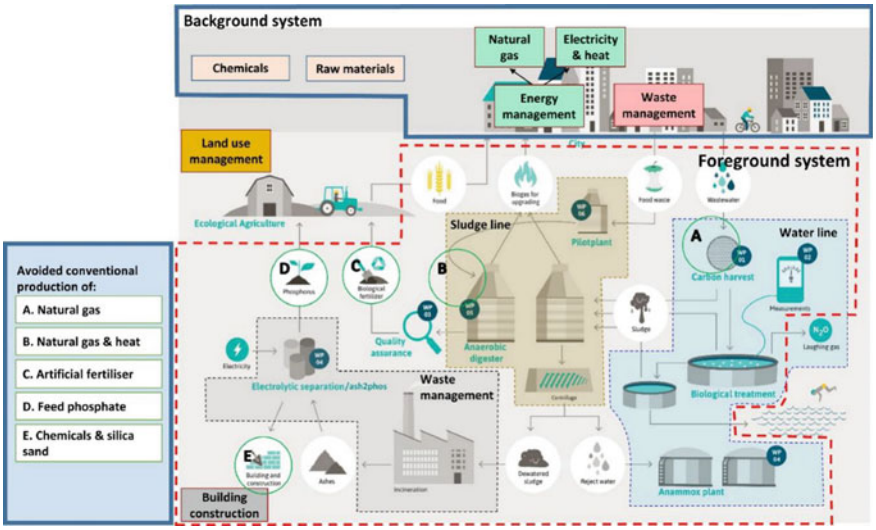

Fig. 1 Main system components/boundaries of the full-scale water resource recovery facility

system components of a comprehensive water recovery facility are shown in Fig. 1 [3]. In this paper, the goals, challenges and processes of sewage treatment in China are considered, and measures for sewage treatment development are proposed based on technological development, hoping to provide reference for the future development of sewage treatment measures.

3 Problems in Urban Sewage Treatment

3.1 Weak Sewage Treatment Capacity

At present, China's sewage discharge remains high, but the development of sewage treatment technology lags behind. The current sewage treatment technology can't solve the problem of daily sewage discharge. The management level has not reached the corresponding technical standards. This leads to the increasing accumulation of sewage and imperfect treatment technology. The sewage problem can't be treated timely and effectively, resulting in environmental pollution and great pressure on environmental engineering. In particular, China's modernization started later than developed countries, and there are still great differences between China's treatment technology and developed countries. It can't solve the serious problem of sewage discharge and treatment. In 2019, China's Ministry of Ecology and Environment surveyed and counted 9,322 urban sewage treatment plants with a designed treatment capacity of 250 million tons per day, treating a total of 74.27 billion tons of

wastewater, but as China develops, the amount of sewage that needs to be treated is increasing year by year.

3.2 Insufficient Rainwater Treatment and Utilization

Natural wealth includes many, such as rain. If rainwater can be fully utilized in life, it can greatly alleviate the problem of water shortage in cities. Therefore, in the process of urban sewage treatment, effective measures should be taken to turn rainwater into effective resources. In reality, people often ignore the treatment and utilization of rainwater resources and directly absorb rainwater resources from urban pipe network, which not only wastes a lot of water resources, but also easily causes pollution in rainy season.

3.3 Less Government Investment

In order to conduct centralized and effective treatment of sewage, it is necessary to make full use of sewage discharge system and sewage treatment plant. In the whole link, sewage treatment plant is the key core part. Most of the sewage treatment plants are invested and constructed by the local government. Therefore, the financial support of the government determines the working efficiency of the sewage treatment plant and the sewage treatment efficiency. However, in real life, the government does not pay much attention to the development of the project, so the capital investment is relatively small. Therefore, these sewage treatment plants are not enough to maintain efficient and stable urban sewage treatment.

4 Sewage Treatment Upgrading Measures

4.1 Establish a Perfect Sewage Treatment Mechanism

Urban environmental builders should be guided by the concept of green environmental protection, encourage more energy-saving and environmental protection technologies to participate in the construction, and formulate a perfect treatment mechanism to provide reference basis for various work. In terms of urban sewage and wastewater treatment, centralized treatment and decentralized treatment can be adopted. The two methods can be used reasonably in engineering construction to promote the recycling of water resources. For the wastewater with less serious pollution in life, it can be simply treated for urban greening and irrigation to enhance the utilization efficiency of water resources. For industrial wastewater and urban

construction wastewater, a unified treatment system and standard can be established to ensure the effective treatment of pollutants and reduce the impact of wastewater on the environment.

4.2 Cultivate Relevant Professionals

First, strengthen the training of technical talents, skilled personnel can better apply sludge treatment technology. Therefore, while focusing on the introduction of technical talents, we should also strengthen the cultivation of technical operation ability of such professionals. Secondly, strengthen the training of management talents. Sewage treatment depends not only on technicians, but also on managers. In order to ensure the orderly progress of each process, managers must make reasonable work arrangements. Therefore, the training of professional managers is very important. During the training, we should pay attention to improving their professional ability and management ability, properly manage various work contents, and then improve the efficiency of sewage treatment and realize the optimal allocation of resources in all aspects.

4.3 Improve Financing Channels and Solve the Problem of Pipeline Funds

Environmental protection is what everyone should do. When cities carry out environmental engineering construction, they often encounter the problem of shortage of funds, which seriously affects the normal and orderly development of environmental engineering. The state should establish an appropriate urban sewage treatment management system, make overall arrangements for urban sewage treatment by relevant departments, train more urban sewage treatment technical personnel, and strive to make more people realize the importance and urgency of urban sewage treatment.

5 Main Processing Technology

Sewage treatment plants mainly receive domestic sewage using similar treatment processes: primary (mechanical) treatment, secondary biological treatment and disinfection. Different treatment processes and sampling points of four sewage treatment plants are shown in Fig. 2 [4].

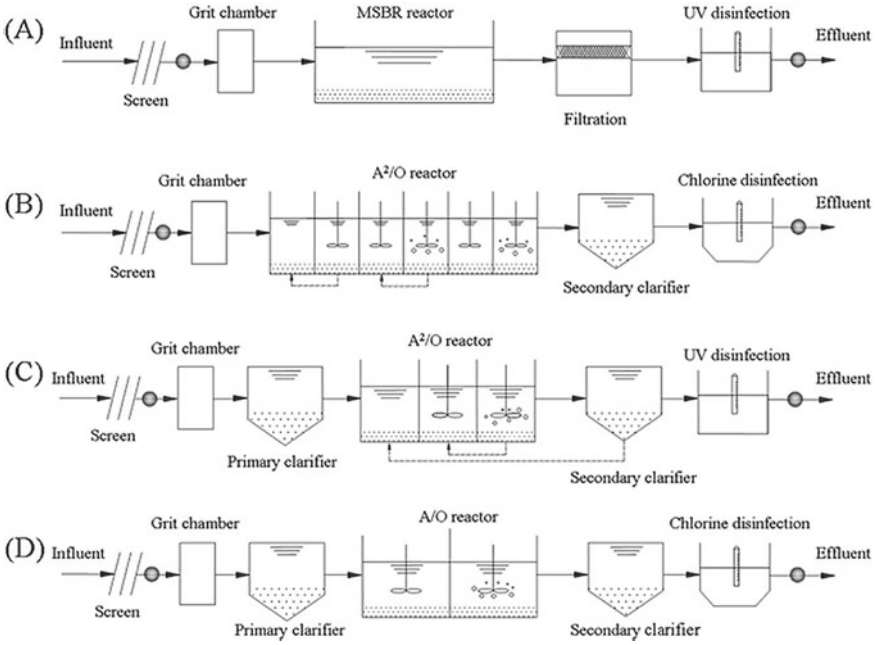

Fig. 2 Schematic diagram of the treatment processes in the four WWTPs. MSBR modified sequencing batch reactor; A^2/O anaerobic/anoxic/oxic process; A/O anoxic/oxic process

5.1 Physical Technology

Physical technology can treat specific pollutants in sewage and treat their impurities to improve the effect of environmental engineering sewage treatment. When using physical technology, the particles in the sewage can be removed by sedimentation method, or the oil substances in the sewage can be removed by filtration method and air flotation method, so as to ensure good treatment effect. However, its economy needs to be comprehensively considered, and the ability of physical technology in organic pollutant treatment is relatively poor. Therefore, physical technology is only the pretreatment stage, which can provide relatively convenient conditions for the follow-up work [5].

5.2 Aeration Biological Tank Technology

When using aeration biological tank for environmental engineering sewage teatment, it needs to be carried out from the following aspects. (1) Biological aerated tank mainly uses biological filter as the main carrier in environmental engineering

wastewater treatment, and appropriate fillers need to be added to it. After the completion of this aspect, it is necessary to use the way of oxygen supply to ensure that a large number of microorganisms can grow on the filler, and use microorganisms for sewage treatment, so as to improve the effect of sewage treatment of environmental engineering. (2) The biological aeration tank is relatively convenient in the treatment process, and the layout of various treatment devices is relatively close, which will not occupy a large space, and the treatment cycle is relatively short. In addition, during the treatment, the impurities contained in the sewage can be limited, which reduces the load consumption of the sewage purification process, so as to avoid the phenomenon of secondary pollution, achieve good treatment effect and ensure the balance of the ecological environment [6].

5.3 MSBR Technology

MSBR technology is relatively convenient and the cost is relatively low. At the same time, MSBR technology is generally developed from the following aspects. (1) After the sewage treatment process, it needs to be mixed with the reflux. Under anoxic conditions, the denitrifying bacteria used will use organic carbon as carbon source to complete anaerobic respiration and metabolism and treat the impurities contained in the sewage. At the same time, after the original sewage is interrupted, the sewage can be directly introduced into the main aeration grid, so that the organic carbon in the sewage can be explained, so as to effectively improve its treatment effect, and also provide relatively convenient conditions for subsequent environmental engineering sewage treatment. (2) During the treatment of MSBR technology, plasma can be used to treat environmental engineering wastewater, mainly under the condition of low temperature. It is mainly because the plasma has relatively strong adaptability and can degrade and precipitate the pollutants in the wastewater under the condition of low temperature, so as to achieve a good treatment effect of MSBR technology [7].

5.4 Activated Sludge Technology

Activated sludge technology needs to be done from the following aspects. (1) Activated sludge technology can adsorb the suspended solids in sewage during treatment, so as to improve the effect of environmental engineering sewage treatment. Generally, oxygenation is carried out manually, so that microorganisms and sewage can be mixed cultured, and the organic pollutants in sewage can be removed, decomposed and separated by using the adsorption, coagulation and oxidation of activated carbon, so as to ensure the effect of environmental engineering sewage treatment. (2) When using activated sludge technology, other technologies need to be used for cooperation, so as to achieve good results and avoid secondary pollution.

6 Conclusion

To sum up, sewage treatment is a very important work in the process of urban development, which must be highly valued by relevant personnel. Therefore, reasonable and effective methods and means shall be adopted to analyze and solve the existing problems with pertinence and purpose, so as to ensure that the quality of urban sewage treatment and discharge meets the standard and strengthen the protection of water resources.

References

1. Zhao H, Jiang X, Dong Y, Chen W, Cui J (2015) Geographic information system-based optimization of sewage treatment facilities by evaluating pollution effects and governance demands. J Water Reuse Desalin 5:104–118
2. Faragò M, Damgaard A, Madsen JA, Andersen JK, Thornberg D, Andersen MH, Rygaard M (2021) From wastewater treatment to water resource recovery: environmental and economic impacts of full-scale implementation. Water Res 204:117554
3. Song J, Cui S, Han Q, Li P, Zhang Q, Li M, Jiang C (2019) Biochemical treatment of municipal sewage in Northeast China in winter. IOP Conf Ser Earth Environ Sci 237
4. Sui Q, Wang D, Zhao W, Huang J, Yu G, Cao X, Qiu Z, Lu S (2015) Pharmaceuticals and consumer products in four wastewater treatment plants in urban and suburb areas of Shanghai. Environ Sci Pollut Res 22:6086–6094
5. Zhang J (2019) Main technical analysis of sewage treatment in environmental engineering. Jiangxi Build Mater (12):211–212
6. Zou D (2019) Main technologies of sewage treatment in environmental engineering. Reg Gov (7):96–97
7. Gao X (2019) Analysis of urban sewage treatment in environmental engineering. Constr Des Project (2):158–159

Study on the Application of Seismic-Based Casing Deformation Prediction Technology in Xinjiang Oil Field

Yunfeng Zhao, Jinling Du, Zhihong Tian, Aliyaha, Wenli Xu, Jingjing Deng, and Guangyao Han

Abstract With the application of horizontal well and hydraulic fracturing technology in the shale oil development of Xinjiang Oil Field, there are more and more casing deformation phenomena occurred, which may cause huge economic loss, no normal fracturing construction, well segment missing and low well yield, etc. In this paper, it analyzes geophysical response characteristics of the parts with casing deformation and establishes related model, thus casing deformation prediction can be conducted by using 3D seismic attributes before horizontal well fracturing, with the purposes of optimizing fracturing scheme, giving early warning to casing deformation by combining with micro-seismic monitoring results during hydraulic fracturing, reducing casing deformation to the greatest extent, improving reservoir stimulation effect, and enhancing well yield.

Keywords Microseismic monitoring · Casing deformation · Seismic attributes

1 Introduction

Along with the continuous development of exploration and development technology, shale oil exploration and development has gradually become a hot spot, breakthroughs have been made in Sichuan Basin, Songliao Basin, Ordos Basin, Junggar Basin, Qaidam Basin and other basins of our country with rich resource reserve, and the fastest shale oil exploration and development has made in Xinjiang Jimusar Basin with large-scale development formed. Jimusar Sag is a relatively independent half-graben spanning about 60 km from east to west, about 50 km from north to south, and covering an area of about 1,300 km^2. Lucaogou formatiom is mainly composed of saline seim-deep and deep lake faces with fine particles deposition. The dominant lithology of "upper sweet spot" is laminated arenaceous dolomite,

Y. Zhao (✉) · Z. Tian · Aliyaha · G. Han
Xinjiang Oilfield Company, PetroChina, Karamay City, China
e-mail: zhaoyf2@petrochina.com.cn

J. Du · W. Xu · J. Deng
BGP, CNPC, Beijing, China

X. Liu (ed.), *Proceedings of 2021 China-Europe International Conference on Pipelines and Trenchless Technology*, Lecture Notes in Civil Engineering 212,
https://doi.org/10.1007/978-981-19-4067-5_6

laminated debris feldspar sillty sandstone, and laminated calcareous sandstone; the dominant lithology of "lower sweet spot" is laminated dolomitic siltstone. The shale oil "sweet spot" reservoir space of Lucaogou formatiom in Jimusar Sag is mainly composed of remaining intergranular pores, intergranular dissolution pores, intragranular dissolved pore, intercrystalline pores, microfractures and organic matter pores, among which secondary dissolution pores are dominant, accounting for more than 70%.

In Jimusar Sag, shale oil has established the horizontal well and subdivision cut volume fracturing process and begun large-scale experimental production since the horizontal well fracturing development program has been confirmed. Along with the increase of horizontal wells, the horizontal well segments become longer, the fracturing well segments increase, and the occurrence of casing deformation in horizontal segments is also increasing. Casing deformation refers to a form of damage in which a part of the casing has great plastic deformation but without break. Casing deformation occurring in horizontal well segment means suspension of the fracturing construction, which will affect the progress of project, and loss of well segment will have direct influence on the output. Scholars have begun to study the causes of casing deformation. Zhou [1] and Lu [2] believe that the large-size natural fracture development area that intersects the wellhole at a large angle is not only apt to induce fracturing inter-well interference, but also easy to induce casing deformation. Chen [3] et al. believe that the development of faults and stratification is the internal cause of casing shear deformation. Xi [4–6] believes that the lithological interface in the reservoir is also an important factor that causes the casing deformation during the multistage fracturing of horizontal wells. Liao [7] and Gao [8] believes that the mechanical properties of the horizontal reservoir vary greatly along the wellhole direction, and the casing is prone to deform during the hydraulic fracturing process. In this paper, it analyzes the geophysical characteristics of the stratum based on various factors that affect the casing deformation, uses 3D seismic data to inverse the physical property and elastic parameters of the stratum, selects the sensitive geophysical parameters, and then predicts the well segments having casing deformation.

2 Methodology

According to previous research results, it is believed that factors affecting casing deformation can be divided into internal and external causes. The internal cause is geological conditions of the rock stratum that cause casing deformation; the external cause is that the casing deformation is caused by changes in rock stratum in the process of reservoir stimulation. In the course of this study, the technology was proposed which based on 3D seismic to predict casing deformation. Starting from internal and external factors, 3D seismic data was utilized to obtain parameters that can represent stratum properties, seismic attributes closely related to casing deformation were selected, and then well segments that have casing deformation were predicted combining the engineering parameters during the process of construction

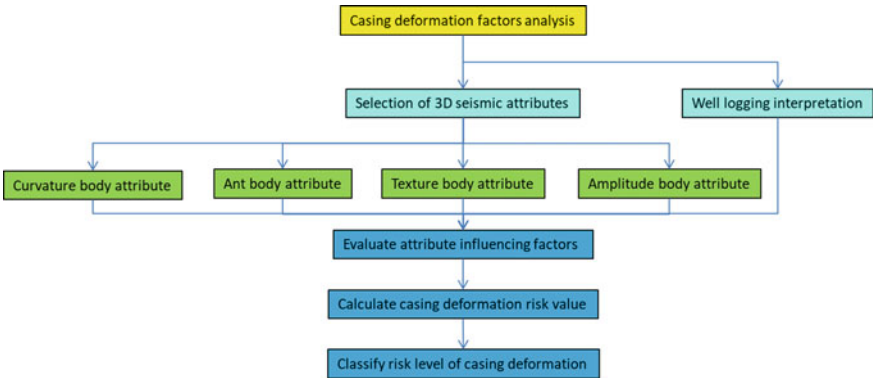

Fig. 1 Seismic-based casing deformation prediction technology process

of reservoir stimulation. The casing deformation prediction technology flow based on 3D seismic is shown in Fig. 1.

3 Casing Deformation Prediction Methods

It is found through the comprehensive analysis of well segments where the casing deformation and casing damages occur that casing deformation is mainly shear deformation, and it is often related to faults, bedding and natural fractures. Therefore, analyzing the existence of natural factures is an important link in predication of casing deformation. And utilization of seismic data can predict the natural fracture network in three-dimensional space. The coherence attribute is to calculate the correlation coefficient between the central trace and the neighboring traces in a certain time window. When there are fractures in the stratum, the correlation between the traces becomes worse, and the seismic attributes show a low coherence value. The coherence attribute currently used is the third-generation eigenvalue coherence attribute. This method can improve the transverse resolution of faults while ensuring the anti-noise capacity. As shown in Fig. 2, the position indicated by the arrow has a low coherence value, which is believed to be a natural fracture development area according to study. Curvature in three-dimensional space is a plane tangent a curved surface, forming a curve on the cutting surface. Its curvature value can be calculated at any point on the curve. Therefore, there are many curvature values. The most commonly used curvatures are average curvature, Gaussian curvature, maximum curvature and minimum curvature, most positive curvature and most negative curvature. The curvature value at any point in the three-dimensional space can be obtained by fitting the spatial curved surface equation with the apparent dip values of adjacent traces and sample points. Figure 3 shows the curvature attributes of the plane. The red part is the area where natural fractures develop. Ant body attribute is a method developed in recent

years to predict micro-fractures in the stratum. Using the ant tracking method for fault identification can reveal the micro-fractures hidden in seismic attributes, so it is widely used in micro-fracture prediction. Figure 4 is a profile of the ant body along the well trajectory. It can be clearly seen from the figure that 3 natural micro-fractures have developed. The above is the utilization of seismic attributes to predict natural fractures. These existing natural fractures are prone to have abnormal construction and casing deformation during the reservoir stimulation at the later stage.

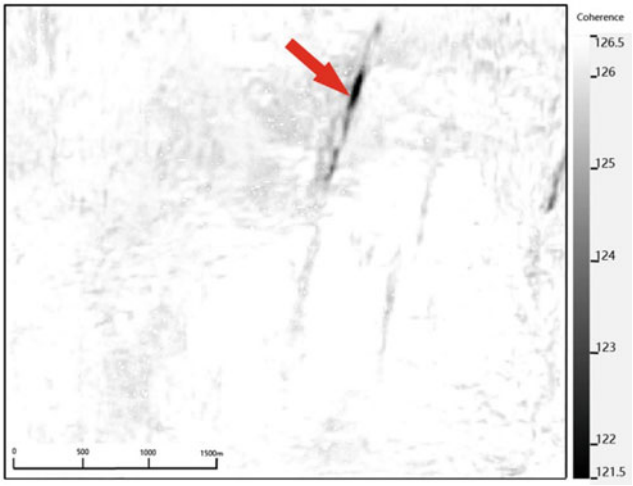

Fig. 2 Coherence attribute plan

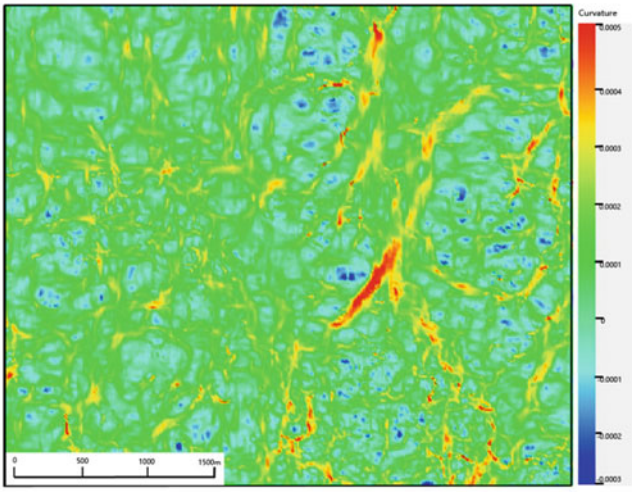

Fig. 3 Curvature attribute plan

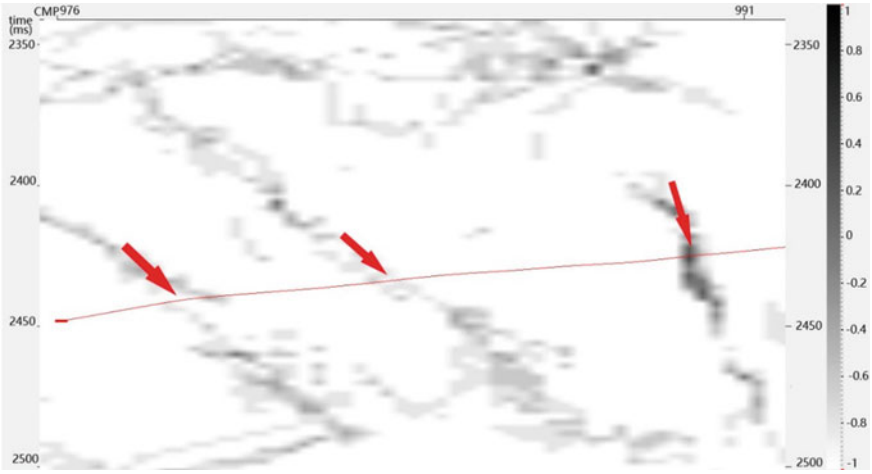

Fig. 4 Ant body attributes profile passing Well041

Another internal cause of casing deformation and casing damage is the difference in lithology and physical properties of the stratum that the well trajectory passes through. In the process of reservoir stimulation, these positions with difference are prone to unevenly distributed stress, which will cause engineering risks. Using 3D seismic data can also predict the stratum lithology and physical properties through attribute analysis and reservoir inversion. The seismic amplitude attribute is the comprehensive response of stratum lithology, internal fluid, physical properties, and changes in sequence. The difference in seismic amplitude is used to identify the difference in stratum features, and targeted measures are taken during the reservoir fracturing process at the later stage to avoid engineering risk. Figure 5 is an amplitude profile along the well trajectory of Well044. It can be seen that there are obvious anomalies in two seismic amplitudes. Therefore, the casing deformation at this place is related to the difference in stratum properties. The seismic texture attribute is a pattern recognition method, which can effectively identify the lateral variation of lithology by evaluating the change of data energy. The currently used method is to conduct grey level reformation of seismic data to produce grey level adjoint matrix, then extract characteristic value from the grey level adjoint matrix, and finally perform clustering. Figure 6 shows the texture body attributes profile along the well trajectory. The position indicated by the arrow in the figure has casing deformation during the fracturing process. This position is also where the texture attributes changes, which indicates that the lateral characteristics of the stratum here have changed, and that changes in lithology are the internal factors causing casing deformation.

The 3D seismic data can be used to predict stratum lithology, physical properties and characteristics of fracture, and make predictions in advance before hydraulic fracturing. At the same time, it is also possible to carry out early warning of casing deformation at the reservoir stimulation site via the results of micro-seismic monitoring. Figure 7 shows the fusion map of micro-seismic monitoring results and seismic

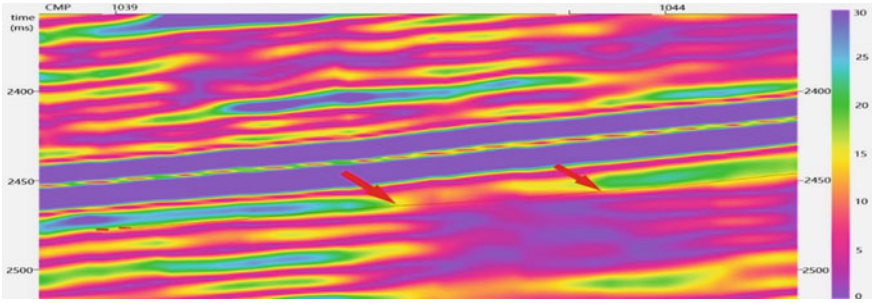

Fig. 5 Amplitude body attributes profile passing Well044

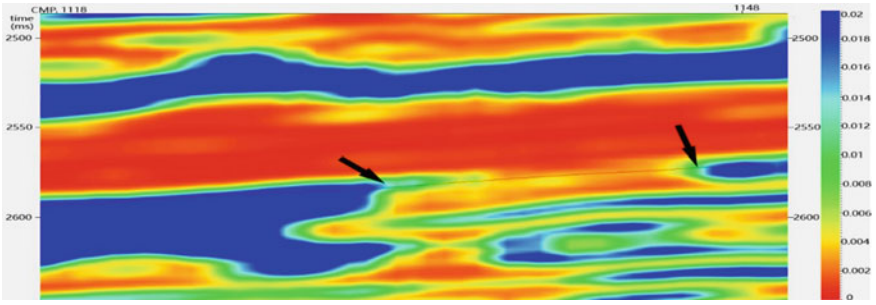

Fig. 6 Texture body attributes profile passing Well179

curvature attributes of Well421. During the fracturing process of Well421 from the 17th to the 21st segment, a great number of micro-seismic events with strong energy occur at the position of the 25th segment of the adjacent Well422. Besides, this position shows a high value in curvature attribute. It is predicted that the position is a natural fracture development area. Therefore, this position is the well segment with risk of casing deformation. In later stage, the Well422 downhole perforating gun encountered resistance at this position, which is caused by casing deformation according to analysis. When abnormality occurs in construction pressure during the fracturing process, it is often an early warning signal of casing deformation. Figure 8 shows the fracturing curves of the 23th segment (left) and 25th segment (right) of Well422. It can be seen from the figure that pressure of the 25th segment is obviously higher than that of the 23th segment during the process of reservoir stimulation. At the fracturing site, casing deformation also occurs in the 25th segment, affecting normal construction.

There are many factors that affect casing deformation, and multiple seismic attributes can be used for prediction. Therefore, in this study, the maximum value of each weight is set to 1, the difference of each attribute uses the value range of its own attribute as standard. The variation of each well segment with risk is taken as the weight. In this study, six seismic attributes were selected for casing deformation

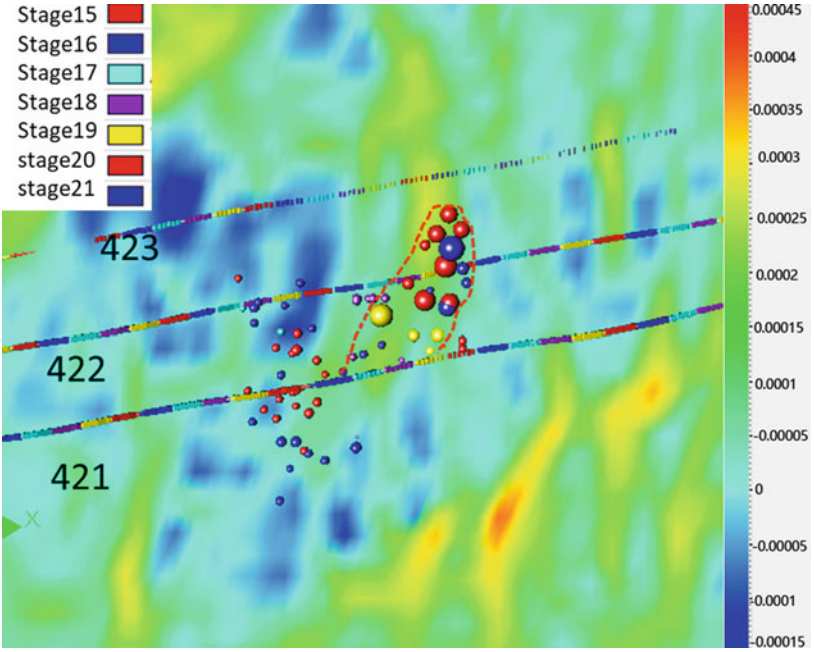

Fig. 7 Fusion map of microseismic monitoring results and seismic curvature attributes of Well421

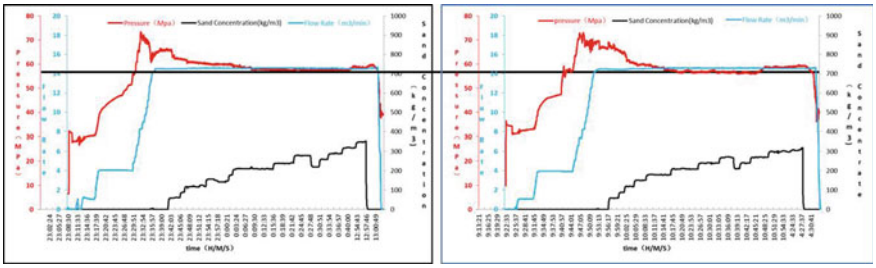

Fig. 8 Construction curves of segment 23 (left) and segment 25 (right) of Well422

risk prediction. Therefore, the maximum weight in this study is 6 and the minimum is 0.

Based on above, before performing hydraulic fracturing, use 3D seismic data to conduct a complete analysis of characteristics of changes of lithological and physical properties of the target layer and the distribution of fractures, predict where casing deformation is likely to occur in advance, refer to relevant cognition during fracturing design and optimize the construction design; make use of the micro-seismic monitoring results during the fracturing process, combining with fracturing curves to give engineering risk warning of the risky well segments, and adjust the hydraulic

fracturing parameters at any time to avoid casing deformation and other engineering risks to the greatest extent.

4 Application Example

In Jimusar sag, 58 platform was undergoing reservoir stimulation, and the probability of casing deformation in the horizontal well of the platform was predicted before hydraulic fracturing. Figure 9 shows the multiple attributes profiles of Well11 along the well trajectory. Seen from Fig.a-the coherence attribute profile, there are five low-value coherence locations along the well trajectory, which are considered locations where casing deformation is likely to occur. Seen from Fig.b-the curvature attribute profile, there are three high-value coherence locations along the well trajectory, which are considered to be locations where casing deformation is likely to occur. According to the ant body attribute profile in Fig.c, there are six high-value locations along the well trajectory, which are considered to be locations where casing deformation is likely to occur. According to the well logging interpretation profile in Fig.d, there are four coherent lithological difference interfaces along the well trajectory, which are considered to be locations where casing deformation is prone to occur. According to the texture body attribute profile in Fig.e, there are three positions with texture attribute difference along the well trajectory, which are considered to be locations where the lithology changes and casing deformation is likely to occur. According to the amplitude attribute profile in Fig.f, there are three positions with amplitude difference along the well trajectory, which are considered to be changes in physical properties or lithology and also positions where casing deformation is likely to occur. Based on the above detailed analysis of each single attribute, and then calculate the weight of each risky well segment according to the aforesaid weight method, and finally divide risky well segments into three risk levels (refer to Table 1) according to the value of weight, among which fracturing optimization design is required for Level-1 risk well segments during the design stage of fracturing, and importance should be laid to early warning during the process of fracturing. The Level 2 and Level 3 risky well segments require close attention and early warning during the fracturing construction process. Therefore, engineering designers fully considered the prediction results and optimized the fracturing design when designing reservoir stimulation. At the fracturing site, the micro-seismic monitoring results showed that there was no abnormal event point occurred in the well, and no early risk warning was given. No casing deformation or damage occurred in the entire well segment, and the fracturing construction was successfully completed through optimizing the fracturing construction and micro-seismic monitoring early risk warning.

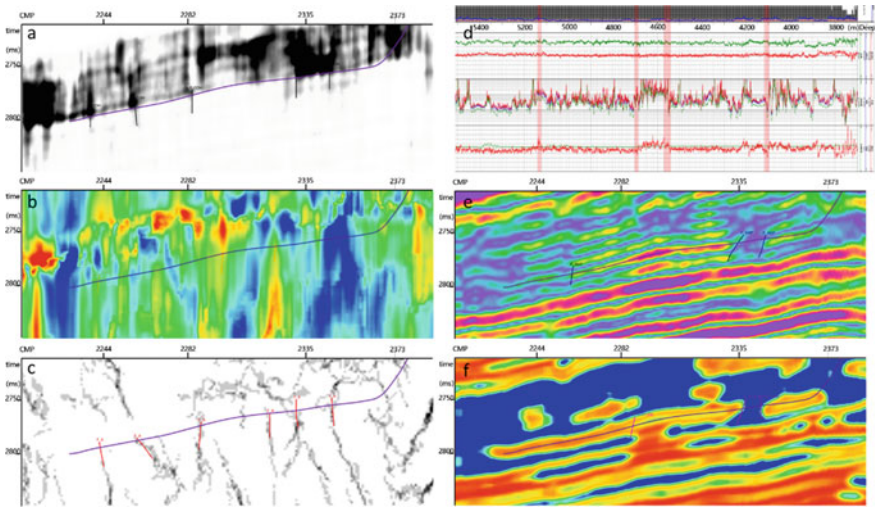

Fig. 9 Multiple attributes profile along the well trajectory of Well11

Table 1 Casing deformation risk levels of each well segment of Well11

Casing deformation predicted risk segment (m)	Casing deformation risk level
3930-4000	Level 1 risk segment
4050-4150	Level 1 risk segment
4250-4320	Level 3 risk segment
4550-4600	Level 3 risk segment
4690-4760	Level 3 risk segment
5050-5100	Level 2 risk segment
5120-5150	Level 3 risk segment
5250-5320	Level 2 risk segment

5 Cognition and Conclusion

It can be learned from this study and analysis that:

3D seismic attributes can predict the distribution of fractures and changes in lithology and physical properties of the target layer, and sensitive seismic attributes can be selected through seismic attribute analysis of the casing deformation position. Utilization of seismic attributes can predict the position of casing deformation. Comprehensive micro-seismic monitoring results can provide early warning of casing deformation position. Method proposed in this paper for prediction of casing

deformation using 3D seismic and micro-seismic monitoring results can ensure the completion of fracturing engineering.

References

1. Zhou XJ, Yong R, Fan Y et al (2020) Influence of natural fractures on fracturing of horizontal shale gas wells and process adjustment. J China Pet Explor 6:94–104
2. Lu QL, Liu Z, Guo JC et al (2021) Mechanisms of hydraulic fracturing induced casing shear deformation and a calculation model of casing deformation. J Pet Explor Dev 2:1–8
3. Chen CW, Shi L, Xiang DG et al (2016) Mechanism of casing deformation in Changning-Weiyuan shale gas demonstration area and countermeasures. J Nat Gas Ind 11:70–75
4. Xi Y, Li J, Liu GH et al (2016) Research on sensitivity of shale reservoir anisotropy's influence on casing stress. J Spec Oil Gas Reserv 6:128–133
5. Xi Y, Li J, Liu GH et al (2019) Overview of study on casing deformation during the process of multistage fracturing of shale gas horizontal wells. J Spec Oil Gas Reserv 1:1–6
6. Xi Y, Li J (2018) Mei Bowen effect of lithology interface on casing stress during stimulated reservoir volume fracturing. J China Pet Mach 5:115–121
7. Liao SM, Sang Y, Song Y et al (2017) Research on staged fracturing technology for casing deformation affected section of horizontal shale gas well and field test. J Nat Gas Ind 7:40–45
8. Gao LJ, Liu ZL, Qiao L et al (2017) Study on casing damage mechanism of hydraulic fracturing of shale gas and its numerical modeling. J China Pet Mach 1:75–80

Design of Automatic Manufacturing System for CIPP Pipe Hose

Mingtao Liu, Yibo Feng, Gang Chen, Jian Dong, Jingguo Cao, and Edmund Luksch

Abstract In recent years, trenchless pipeline repair technology has developed rapidly because of its advantages such as no impact on traffic, fast repair speed, high efficiency, no environmental damage, and no impact on people's normal life. Therefore, it is crucial to gain deep insight into the development of automatic pipeline production-line. In order to improve the production efficiency and quality of the bushing hose, this paper reformed on the original basis and designed an upgraded plan. The CAD model of automatic production line is established, and an intelligent manufacturing scheme is put forward. The solution improves the automatic production rate and preparation process of lined hose.

Keywords Trenchless equipment · Lined hose · Automation · Intelligent manufacturing

M. Liu · Y. Feng · G. Chen (✉) · J. Dong
College of Mechanical Engineering, Tianjin University of Science and Technology, Tianjin 300457, China
e-mail: chengang2020@tust.edu.cn

M. Liu
e-mail: liumingtao@tust.edu.cn

J. Dong
e-mail: skywoan@tust.edu.cn

J. Cao
College of Chemical Engineering and Materials Science, Tianjin University of Science and Technology, Tianjin 300457, China
e-mail: cjg@tust.edu.cn

E. Luksch
RTi ASIA-PACIFIC PTY LTD, 1/29 Rundle Street, 5067 Kent Town, SA, Austria
e-mail: edmund.luksch@rti.eu

X. Liu (ed.), *Proceedings of 2021 China-Europe International Conference on Pipelines and Trenchless Technology*, Lecture Notes in Civil Engineering 212,
https://doi.org/10.1007/978-981-19-4067-5_7

1 Introductions

With the increase of urban underground pipe network service time and urban sewage discharge, a large number of aging and damage problems have emerged in the early laid pipes. The traditional methods of excavation restoration are widely applied, but they have obvious disadvantages: it may affect the ground transportation, and even destroy the gas and electricity pipelines. The production technology of the lining hose is an indispensable part of the trenchless technology chain [1–4].

In order to achieve the continuous production of hoses, hot air welding is used in the joint process. The tensile strength of the inner and outer joints of the hose is higher than 5.0 MPa, and the joints of the hose can meet the requirements of use and can withstand the tensile stress and thermal stress of the curing process [2]. Combining the other approaches, it introduces the smart factory planning of melt blown fabric spinning and melt blown composite material (SMS) unit production line, and expounds the advantages and disadvantages of related process engineering and key components [5]. In addition, the integration of 2D and 3D data into a software platform will help automate the production process [6]. According to practical experience, the robot structure of industrial automation production line is designed. The PLC design of integrated control system is discussed from the aspects of control principle, hardware design and software development [7–9].

This paper focuses on the problems such as the low degree in automation of hose preparation equipment in Cured-In-Place Pipe (CIPP) technology of pipeline, the original production equipment is upgraded, an automatic production scheme for repair lining hoses is developed, and an intelligent production transformation plan, which will improve the production quality and efficiency of hoses.

2 Inner Hose and Its Production Process

2.1 Mechanical Properties of Inner Hose

The properties and performance of the base material play a crucial role in the quality of the inner hose. The inner hose adopts 800 g/m^2 staple fibre needle-punched non-woven composite material, and thermoplastic polyurethane elastomer (TPU) as impermeable film. The viscosity temperature is 167 °C. And the tensile strength is higher than 5.0 MPa. The test results of material properties are shown in Table 1, and the relevant properties are shown in Table 2.

Table 1 Material properties of 800 g/m^2 film-covered non-woven fabric [2]

Materials	Non-woven fabric	Film-covered (PU) non-woven fabric
Transverse strain/ε	8.08	5.1
Longitudinal strain/ε	17.54	18.48
Poisson's ratio/ν	0.46	0.28
Modulus of elasticity/E_t (MPa)	5.560	18.18

Table 2 Mechanical properties of 800 g/m^2 film-covered non-woven fabric [2]

Detection name		Test results
Breaking strength (dry)	Horizontal	1718 N
	Longitudinal	1752 N
Elongation at break (dry)	Horizontal	100%
	Longitudinal	102%
Tensile strength (dry)	Horizontal	7.16 MPa
	Longitudinal	7.3 MPa
Tear strength	Horizontal	690 N
	Longitudinal	770 N
CBR top breaking strength		3980 N
Puncture force		840 N

2.2 Production Process of Inner Hose

The proposed equipment is shown in Fig. 1, which is mainly composed of seven modules with different functions: (1) Conveyor (2) Lifting roller (3) Laser interferometer (4) Additional folding machine (5) Internal welding mechanism (6) External welding mechanism and (7) Seaming device.

The non-woven fabric tiling is implemented by the active roller, and then transported to the lifting rollers 2 by the conveyor 1. Then, the printer prints the relevant parameters on it. Under the action of laser interferometer 3 and seaming device 7, the fabric remains symmetrical and accurately enters the internal welding mechanism 5 and external welding mechanism 6. Meanwhile, to ensure product quality, the tension on the raw material is controlled to eliminate its deformation. Finally, additional folding machine 4 completes the hose into a shape that facilitates transport (Fig. 1).

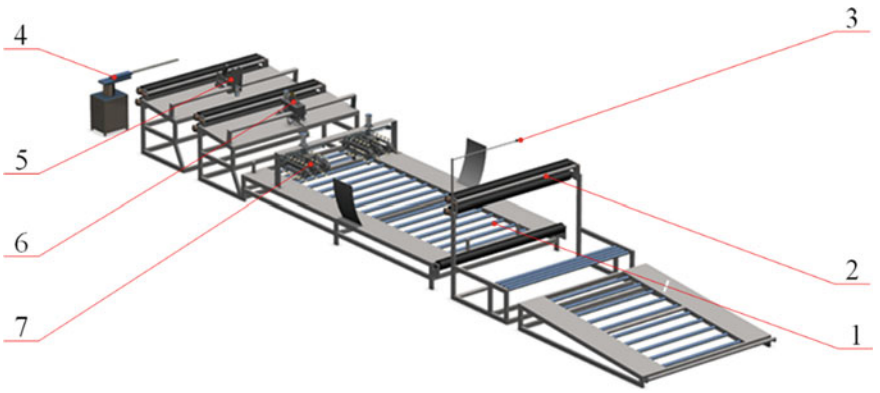

Fig. 1 CAD model of the CIPP pipe production equipment

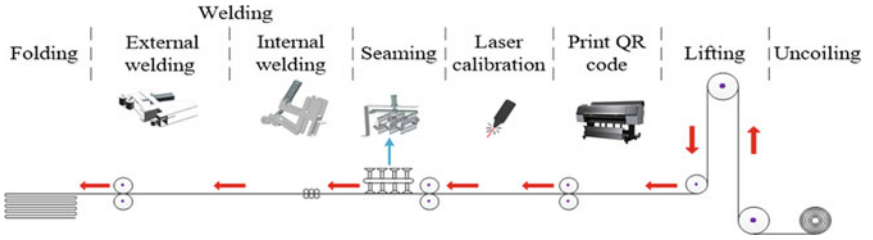

Fig. 2 Flow chart of production process

3 Key Equipments

3.1 Seaming Device

The CAD model of the seaming device is established as shown in Fig. 3, including suction cup, crawler, ball screw, servo-motor and pneumatic component. The suction cup grips the coated non-woven fabric. Under the guidance of laser interferometer, the deviation is adjusted and corrected to ensure the state of non-woven fabrics. The proposed equipment can align two types of non-woven fabrics, which greatly reduces the labor cost and rise the degree of automation.

The control system is completed by PLC, and an Adlink-Tech industrial computer with six independent RS232 interfaces, a RJ45-100 M network interface, and a PIO-3232 in/output interface card. The communication between computer and PLC adopts RJ45Fins-UDP protocol, which can ensure the real-time and fast communication; the laser interferometer adopts RS232 communication with a speed rate of 115,200 bit/s [10, 11].

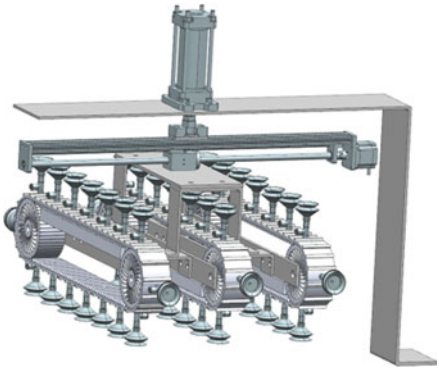

Fig. 3 Seaming device

(a) Internal welding (b) External welding

Fig. 4 Welding mechanism

3.2 Welding Mechanism

The mechanism adopts the asynchronous thermal composite welding method, which can guarantee the production quality of the lining hose without affecting its production efficiency. This process is mainly composed of the internal and external welding mechanism, as shown in Fig. 4(a), (b).

The working principle of the welding mechanism is as follows: the active roller pulls the inner sealing strip and the coated non-woven fabric into the hot air welding mechanism together. After that, the fan and temperature control box are opened in turn, and the welding torch is heated to a predetermined temperature. The internal seal strip and the outer layer of non-woven fabric are melted, and they are bonded to form a hose internal seal under the action of the pressure roller. The hose completing the internal welding will be pulled into the external welding mechanism, and the external welding principle is same as the internal welding principle.

4 Intelligent Production Line Planning of Inner Hose

A reasonable intelligent production scheme of repair lining hose is developed with the PLC and sensor data collection and transmission. And large data digital twin technology is used to trace and reproduce the product parameters. [12, 13] Meanwhile, HMI industrial touch screen is added at the key stations, and technicians modify production parameters at corresponding stations through the screen, so as to adjust the overall operation state. The intelligent production process flow of the above lined hose is shown in Fig. 5.

The figure shows an industrial camera with CMOS sensor based on mobile net-v2 defect detection algorithm is arranged on the production line. After the fabric is uncoiled and flattened, the defects of raw materials are warned by visual detection. [14, 15] Then, the QR coder is used to record the information of raw materials on the non-woven fabric, such as manufacturer, weight, width, length, etc., and upload them to the production management system.

The joint and welding process are carried out according to the given data such as temperature, pressure and speed. The computer and camera is used to detect of raw material defects and welding sealing effect in real time, and the process was recorded and uploaded together with QR code information and other production information.

Three levels of on-site, control and decision-making management are realized to construct the production management system as shown in Fig. 6. Different authorization is provided for different user groups to achieve hierarchical control. Relying on PLC controller and database management system, the field-level data is uploaded layer by layer to show the real-time production situation, and it is also provided for the decision-making level as real-time sales. As a result, the flexible production can be achieved, and the specific management structure is shown in Fig. 7.

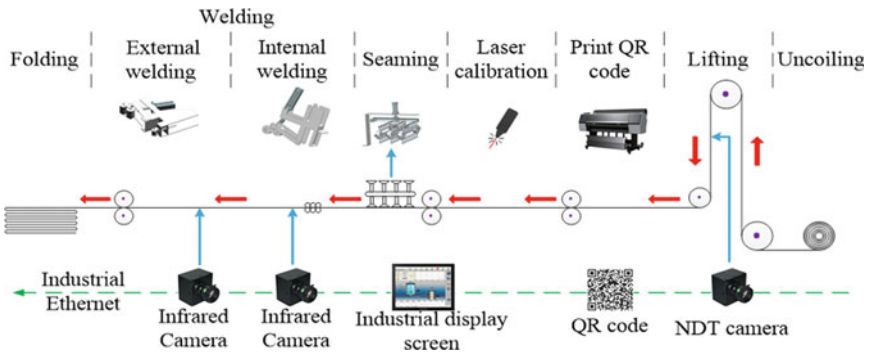

Fig. 5 Intelligent production process

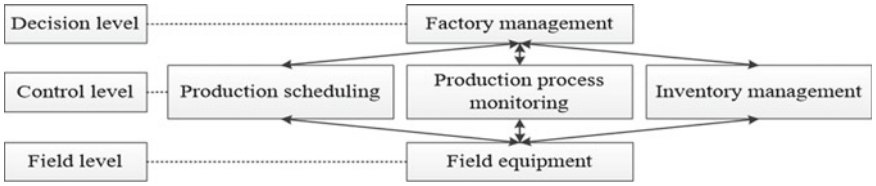

Fig. 6 Production management layer diagram

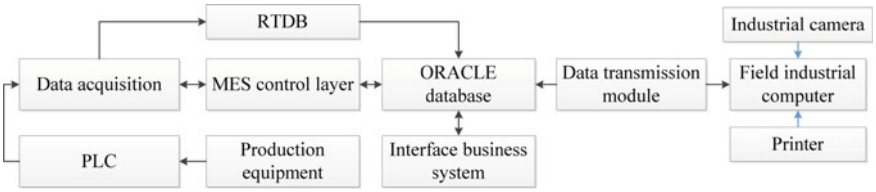

Fig. 7 Production management architecture diagram

5 Conclusion

According to the actual demand of lining hose preparation by trenchless technology, this paper analyzes the relevant performance of coated non-woven fabric, establishes the CAD model of the equipment, and formulates the upgrading scheme of lining hose production equipment. Some conclusions are drawn as follows:

(1) Relying on mechanical–electrical integration, PLC, industrial camera and other technical methods, this paper upgrades the original facility with low degree of automation, and puts forward a complete set of automation solution for lined hose production facility.
(2) An intelligent production scheme based on lined hose production is proposed. The industrial network platform is planned and constructed by using the technologies of database management, machine learning and machine vision.
(3) It is planned to realize the whole process management of production parameters, introduce digital twin technology, integrate and analyze on-site production parameters and relevant data, and realize the whole process management of product line.

References

1. Cao JG, Shi DY, Dong ZZ, Zhang DQ, Zhang J (2021) Overturned in situ curing (CIPP) technology for urban drainage pipeline repair. China Water Supply Drainage 37(06):128–133
2. Shi DY (2020) Study on preparation and application of lining hose for in-situ repair of drainage pipeline. Tianjin University of Science and Technology, Tianjin

3. Zhang WN (2019) Study on preparation and performance of non-woven lined hose for in-situ repair of drainage pipeline. Tianjin University of Science and Technology, Tianjin
4. Kong XL, Wen T, Fan X, Zhou YC (2020) Application of trenchless pipeline repair technology in urban water environment treatment. Constr Technol 49(18):73–75
5. Zhang S, Rao JH, Wu MG, Guo LL, Kang Z (2020) A construction scheme and case of non-woven intelligent workshop. Manuf Autom 42(10):134–136
6. Zhu S (2021) Integrating vision system scheme to effectively improve the efficiency of automatic production line. Sensor World 27(03):30–32
7. Li C (2021) Robot PLC control technology in automatic production line. Electron Technol 50(04):96–97
8. Zhang LG (2021) Design of industrial automation production line under PLC control. Electr World 05:184–185
9. Deng LL, Shen K, Zheng CQ (2021) Research on the application of sensors in electromechanical automation control. Internal Combust Engines Access 15:216–217
10. Xiao GL, Gong ZP, Wu G (2021) Design of automatic production equipment for Daxin packaging and sorting. Electromech Eng Technol 50(07):87–89
11. Xu G (2021) Design and implementation of a new fully automatic production line for face masks. Electromech Eng Technol 50(08):66–69
12. Ying LB (2011) Research on transmission control of non-woven production line. Sci Technol Commun 10:36+49
13. Wang J (2021) Research and analysis of automatic production line based on industrial robot. Internal Combust Engine Access 06:164–165
14. An M (2021) Design and implementation of fabric intelligent detection vision system for garment flexible production line. University of Chinese Academy of Sciences, Shenyang
15. Zhang B (2013) Research on on-line defect detection technology of non-woven fabrics based on machine vision. Huazhong University of Science and Technology, Wuhan

Formation Mechanism and Migration Law of Cuttings Bed in Horizontal Directional Drilling

Kai Zhang, ZongSheng Zhao, and YuXiang Huo

Abstract In this paper, FLUENT is used for iterative calculation of fluids to simulate the solid–liquid mixing into the annulus pipeline. Through simulation, the migration distance of debris particles at different positions under different flow rates, the variation law of volume fraction of debris at the fixed point of the pipeline and the change of sedimentary shape of debris at the bottom of the borehole are studied to explore the influence of the change of dip angle on the migration of debris particles during horizontal directional drilling. The experimental scheme shows that between 0 and 10°, each interval of 2° is set as a group. With the increase of inclination angle, the cuttings in the cross section of the borehole change. At the bottom of the cross section, a large number of cuttings deposit first occurs, and the volume of cuttings at the top decreases. The dip angle continues to increase, and the debris particles at the bottom slightly decrease, which are evenly distributed on both sides, and the volume of debris at the top gradually increases. With the increase of the angle, the cuttings at the bottom of the hole first increase and then decrease, reaching the maximum at 4°. At the same time, the sedimentary shape of the cuttings bed gradually changes from "javelin" to "tadpole" with the change of the angle.

Keywords Cuttings transport · Cuttings bed · Horizontal directional drilling

1 Introduction

With the increase of pipeline lines in China, trenchless technology as a new pipeline construction method is developing rapidly, which has made great contributions to the pipeline construction in the fields of water supply and drainage, oil and gas transportation and communication. Non-excavation refers to the use of various drilling

K. Zhang (✉) · Y. Huo
College of Environment and Civil Engineering, Chengdu University of Technology, Chengdu 610059, China
e-mail: 2414959279@qq.com

Z. Zhao
Qianxi Nanzhou Diligence School, Guizhou 562499, China

X. Liu (ed.), *Proceedings of 2021 China-Europe International Conference on Pipelines and Trenchless Technology*, Lecture Notes in Civil Engineering 212,
https://doi.org/10.1007/978-981-19-4067-5_8

equipment and technology, in the way of directional drilling, excavation of small area holes on the ground, laying, replacement and repair of underground pipelines, minimizing the interference to the surrounding environment, life and traffic. Horizontal directional drilling, as a trenchless construction technology, has been widely used in recent years. With the development and construction of cities and the continuous increase in energy demand, the construction application of horizontal directional drilling has also been widely increased, and the resulting engineering accidents have also increased. Through the analysis of a number of engineering accidents, it is found that the most important influencing factor in horizontal directional drilling construction is the cuttings bed generated by cuttings migration, which leads to the increase or even destruction of drill pipe torque and the blockage of drilling holes.

In this regard, in order to reduce the engineering losses caused by cuttings blockage, there has been a more in-depth study on cuttings migration in horizontal drilling in China. Wang Haige et al. [1]. used eight kinds of fluid as rock-carrying medium and considered a series of influencing factors on cuttings migration. It is considered that the drilling speed has a great influence on the formation of cuttings bed in the drilling process. With the increase of drilling speed, the area of cuttings bed on the annulus section becomes larger. Xiang et al. [2]. independently designed a large displacement horizontal cuttings migration device through cuttings migration law, and established a cuttings migration model. The study found that with the increase of well inclination angle, there was an inflection point in the range of 50–90°, and the inflection point was about 65°. At the inflection point, the thickness of cuttings bed was the largest. With the increase of inclination angle, the thickness of cuttings bed gradually decreased.

Zhixiang Cheng [3] studied the cuttings migration law under the conditions of inclination angles of 30, 50 and 70° by establishing the hexahedral structured network model and giving the boundary conditions. It was found that the smaller the inclination angle was, the faster the cuttings migration speed on the annulus section was. The influence of the inclination angle on the cuttings migration speed was small at the front of the well, but the influence of the inclination angle gradually increased with the increase of the well depth.

The above studies on cuttings migration and cuttings bed are mostly based on the large-displacement horizontal well section. Due to the long horizontal distance of large-displacement horizontal drilling, the drill pipe is more likely to sink at the bottom of the borehole, hindering the migration of cuttings and accelerating the formation of cuttings bed. There is little research on the law of cuttings migration and formation of cuttings bed under the condition of small angle inclination. This paper studies the mechanism of cuttings particle migration and formation of cuttings bed by FLUENT simulation of solid–liquid two-phase fluid in 0–10° borehole inclination angle.

2 Mathematical Model of Cuttings Movement Law

In the actual horizontal directional drilling process, due to the existence of drilling fluid and debris particles generated in the drilling process, the Eulerian two-fluid model is used to simulate the environment of debris particles in the drilling process. Since the fluid in the annulus section is turbulent, the Euler model alone cannot well restore the migration of cuttings, and the fluid motion mode needs to be considered. Therefore, this paper uses the Euler two-fluid model and the turbulence model to simulate the migration of cuttings.

2.1 Eulerian Model

In the annular section, in order to ensure the accuracy of the simulation and ensure that the cuttings migration process is not affected by other conditions except the change of angle inclination conditions, assuming that there is no exchange of material and energy in the solid–liquid two-phase in the two-fluid model, that is, the conservation of mass and momentum, which ensures the continuity of the solid–liquid two-phase, it can be simplified as the following equation [4–6]:

The liquid phase continuity equation contained in the mass conservation equation is shown in (1), where ε_l is the liquid phase concentration, ρ_l is the liquid phase density, and v_l is the liquid phase velocity.

$$\frac{\partial}{\partial t}(\varepsilon_l \rho_l) + \nabla \times (\varepsilon_l \rho_l v_l) = 0 \tag{1}$$

In the solid phase continuity Eq. (2), ε_s is solid concentration, ρ_s is solid density, v_s is solid velocity.

$$\frac{\partial}{\partial t}(\varepsilon_s \rho_s) + \nabla \times (\varepsilon_s \rho_s v_s) = 0 \tag{2}$$

The liquid momentum Eq. (3) included in the momentum conservation equation is as follows:

$$\frac{\partial}{\partial t}(\varepsilon_l \rho_l v_l) + \nabla \times (\varepsilon_l \rho_l v_l) = \varepsilon_l \nabla \tau_l + \varepsilon_l \rho_l g - \varepsilon_l \nabla p + \beta(v_l - v_s) \tag{3}$$

The stress tensor of the liquid phase * is expressed as (4):

$$\tau_l = u_l\left[\nabla v_l + (\nabla v_l)^T\right] - \frac{2}{3}u_l(\nabla v_l)I \tag{4}$$

g for gravity acceleration, 9.81 m/s^2. p is liquid pressure. β is the drag coefficient between liquid phase and solid phase. τ_l is the stress tensor of liquid phase.

In the solid phase momentum Eq. (5) and the corresponding solid force tensor τ_s (6), p_s is the solid phase pressure. ξ_s is solid dynamic viscosity. u_s is solid shear viscosity. $\vec{I}$ is unit vector.

$$\frac{\partial}{\partial t}\left(\varepsilon_s \rho_s \overrightarrow{v_s}\right) + \nabla \times \left(\varepsilon_s \rho_s \overrightarrow{v_s}\right) = \varepsilon_s \nabla \tau_s + \varepsilon_s \rho_s \vec{g} - \varepsilon_l \nabla p - \beta(v_l - v_s) \tag{5}$$

$$\tau_s = (-p_s + \xi_s \nabla v_s)\vec{I} + u_s \left\{ \left[\nabla v_s + (\nabla v_s)^T \right] - \frac{2}{3}(\nabla v_s)\vec{I} \right\} \tag{6}$$

2.2 Turbulent Flow Model

The k-e turbulence model of mixed phase in Eulerian two-phase flow is extended from the k-e turbulence model of single-phase fluid [7], so the turbulence model used in this paper is the k-e two-equation model. The k equation of turbulent kinetic energy and the e equation of dissipation rate in this model are expressed as (7) (8).

$$\rho \frac{\partial k}{\partial t} + \rho \nabla (v_1 k) = \nabla \left(\frac{u_1}{\sigma_k} \right) + G_k - \rho \varepsilon \tag{7}$$

$$\rho \frac{\partial \varepsilon}{\partial t} + \rho \nabla (v_1 \varepsilon) = \nabla \left(\frac{u_1}{\sigma_\varepsilon} \right) + c_1 G_k \frac{\varepsilon}{k} - \rho c_2 \frac{\varepsilon^2}{k} \tag{8}$$

$$G_k = u_t \left[\left(\frac{\partial u_t}{\partial y} + \frac{\partial u_l}{\partial x} \right)^2 + 2\left(\frac{\partial u_l}{\partial x} \right)^2 + 2\left(\frac{\partial v_l}{\partial y} \right)^2 \right] \tag{9}$$

$$u_l = c_u \rho k^2 / \varepsilon$$

x is axial length unit m, u, v is axial and radial velocity respectively, m/s, u_t is turbulent viscosity coefficient, G_k (9) is turbulent kinetic energy increment caused by average velocity gradient, ρ is fluid density, kg/m^3, k is turbulent kinetic energy per mass, m^2/s^2, ε is energy dissipation rate per mass, m^2/s^2, the values of constants in the equation are $c_u = 0.09$, $c_1 = 1.44$, $c_2 = 1.92$, $\sigma_k = 1.0$, $\sigma_\varepsilon = 1.33$.

3 Force Analysis of Cuttings Particles

In order to obtain the migration mechanism of debris particles, it is necessary to consider the force of debris particles on the annulus section and the relationship between debris particles and drilling fluid drill pipe. According to Fig. 1, the force analysis of suspended particles on the horizontal annulus section is carried out [8].

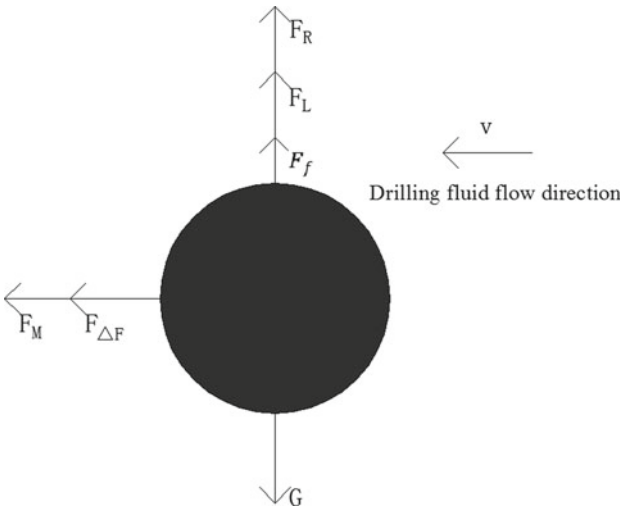

Fig. 1 Schematic diagram of force of debris particles

1. Gravity (G): The direction of debris particles is perpendicular to the surface by its own gravity, which is the main force of debris particles deposited into debris bed.

$$G = \rho g \frac{\pi d^3}{6} \tag{10}$$

2. Buoyancy (F_f): The upward buoyancy of cuttings particles by drilling fluid is opposite to the direction of gravity, which is an important reason for cuttings particles to suspend in horizontal wells.

$$F_f = \rho_l g \frac{\pi d^3}{6} \tag{11}$$

3. Towing force (F_D): The flow of drilling fluid will promote the force of particles to flow direction, which is the main reason for the migration of debris particles.

$$F_D = C_D \frac{\pi \rho_l \upsilon^2 d^2}{8} \tag{12}$$

4. Lifting force (F_L): When drilling fluid flows through the top and bottom of particles, the velocity of annulus section is not the same due to the influence of debris particles before the well section, and because debris is mostly deposited at the bottom of the section, the velocity of the lower part is larger than that of the upper part of the particles, so there is an axial pressure gradient difference between the top and bottom of the particles, thus generating upward lifting force.

$$F_L = C_L \frac{\pi \rho_l \upsilon^2 d^2}{8} \tag{13}$$

$$C_L = max\left\{0.09, 5.82\sqrt{\frac{\alpha_p}{Re_p}}\right\} \tag{14}$$

5. Rotary lifting force (F_R): When the drill pipe rotates, the drilling fluid moves along the rotation direction of the drill pipe, resulting in the difference of flow velocity on the cross section, and the pressure gradient is generated in the axial direction, resulting in upward lifting force.

$$F_R = C_R \frac{\pi \rho_l \upsilon_R^2 d^2}{8} \tag{15}$$

6. Pressure gradient force ($F_{\triangle P}$): force produced by pressure gradient changes during drilling fluid circulation.

$$F_{\triangle P} = \frac{\pi d^3}{6} G_{dp} \tag{16}$$

As shown in Fig. 2, when the drill pipe does not rotate, the cuttings are affected by gravity G and drilling fluid buoyancy F_f, and the cuttings particles are approximately uniformly distributed on the annulus section. With the rotation of the drill pipe and the flow of the drilling fluid, the cuttings are subjected to the combined action of F_D, F_L and F_R. As shown in Fig. 3, the cuttings particles rotate in the direction of the drill pipe movement on the annulus section, and move forward with the drilling fluid. After flowing through a certain distance, they are deposited at the bottom of the channel to form a cuttings bed. In the process of cuttings migration, the stress state of cuttings particles is complex, and the relevant motion Eqs. (17) and (18) are established.

$$(\rho - \rho_l) g \frac{\pi d^3}{6} - C_L \frac{\pi \rho_l \upsilon_z^2 d^2}{8} - C_R \frac{\pi \rho_l \upsilon_R^2 d^2}{8} + \sum F_y = \rho \frac{\pi d^3}{6} \frac{\partial v_y}{\partial t} \tag{17}$$

$$C_D \frac{\pi \rho_l \upsilon^2 d^2}{8} + \frac{\pi d^3}{6} G_{dp} + \sum F_z = \rho \frac{\pi d^3}{6} \frac{\partial v_z}{\partial t} \tag{18}$$

where v_z and v_y are the average velocity in the direction perpendicular to the drill pipe and the average velocity in the direction along the drill pipe, respectively. $\sum F_y$ and $\sum F_z$ represent the force acting on the direction perpendicular to the drill pipe and the force acting on the direction along the drill pipe, mainly including the interparticle force, the additional mass force, the Barcelona force and the Magnus effect force. The effects of these forces are relatively weak, so they are usually ignored in the actual calculation process.

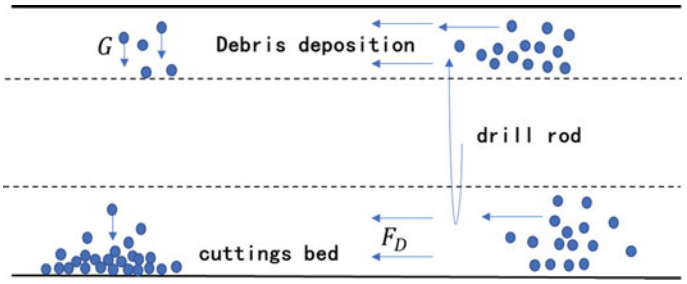

Fig. 2 Migration process of debris particles

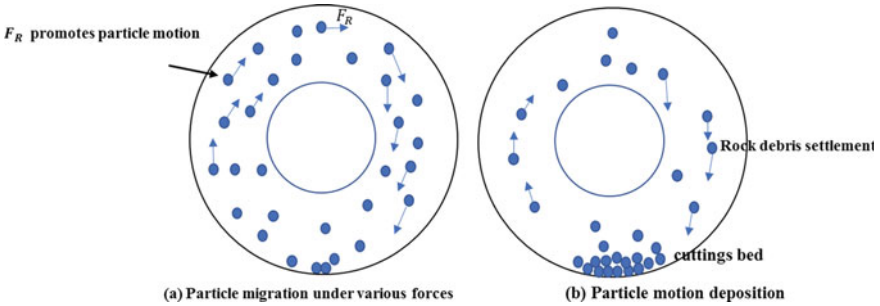

Fig. 3 Migration of debris particles in horizontal annulus

4 Validation of Numerical Simulation Analysis

The construction key points of horizontal directional drilling are mainly guiding hole drilling, expanding guiding hole and pulling into pipeline laying. The entry point and the unearthed point of the guide hole, the inclination angle of the inclined section and the straight section are also important factors affecting the construction. Through the establishment of the geometric model as shown in the figure, the cuttings particle migration law at each point under six working conditions was simulated between 0 and 10°, with each 2° as the interval of soil entry angle. At the same time, the volume fraction data of annulus section at 0.4 and 1.2 m from the bottom of the hole under different working conditions were collected, and then the cuttings migration law and the formation of cuttings bed under different inclination conditions were analysed.

For different dip angles, the volume distribution of debris at 0.4 m away from the bottom of the hole is shown in Fig. 4 With the increase of inclination angle, the debris at the top decreases first and then increases, and the debris at the bottom increases first to a peak and then decreases gradually. In the whole migration channel, with the increase of inclination angle, the cuttings gradually show uniform distribution, but the accumulation of cuttings at the bottom is much larger than that at other parts, and the cuttings bed is formed at the bottom of the cuttings accumulation. At 1.2 m, the cuttings migration law is similar to that at 0.4 m, as shown in Fig. 5.

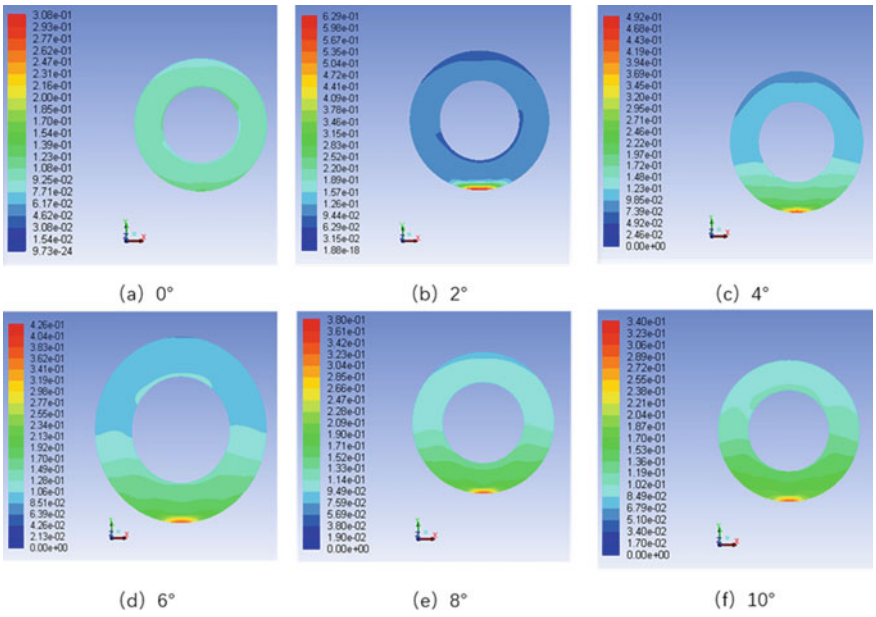

Fig. 4 Volume distribution of cuttings at different dip angles at 0.4 m

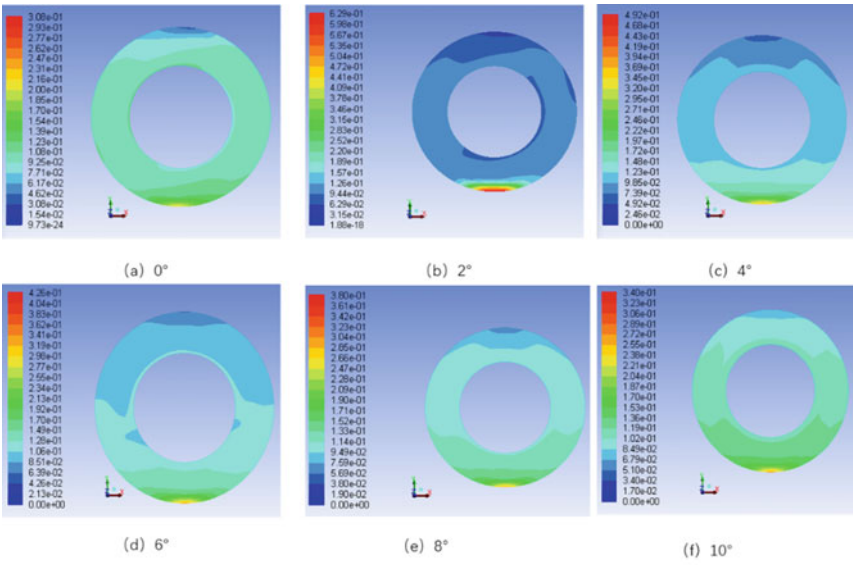

Fig. 5 Volume distribution of cuttings at different dip angles at 1.2 m

The volume fraction distribution of cuttings at each point on the cross section is mainly due to the fact that the cuttings migrate with the rotation of the drill pipe, so that the cuttings have along the rotation direction of the drill pipe.

Through the influence of the angles at 0.4 and 1.2 m on the volume distribution of cuttings, it can be found that when the inclination angle in the pipeline is 0°, the cuttings are more likely to accumulate at the bottom of the pipeline to form a cuttings bed. With the increase of the inclination angle, the cuttings gradually migrate to other parts of the pipeline, and show good uniformity on both sides. When the inclination angle is the same, with the deepening of the pipeline, the volume of cuttings at the bottom of the pipeline is more, indicating that the cuttings gradually tend to be evenly distributed with the increase of the pipeline distance, but the overall distribution is still shown as that the accumulated cuttings at the bottom are far greater than those at other parts of the pipeline. The distribution of debris on both sides of the pipeline is very close and uniform.

The main reason for this phenomenon is the force of cuttings in the pipeline. The cuttings accumulate at the bottom of the pipeline under the action of gravity to form a cuttings bed. The drilling fluid flow driven by the operation of the drill pipe changes the stress conditions of the cuttings. At this time, the cuttings are subjected to their own gravity, the drilling fluid buoyancy and the uplift force on the bottom cuttings brought by the drilling fluid flow. This uplift force only points to the position of the central axis of the pipeline, and also explains that the cuttings volume on both sides of the pipeline is always larger than that on the top.

5 Mechanism of Cuttings Migration and Formation of Cuttings Bed

According to the statistics of volume fraction integral values of cuttings under different working conditions, the results are shown in Table 1. The drilling inclination angle is divided into six groups according to the interval of every 2°. At the same time, the data statistics of the pipeline at every 0.2 m from the bottom of the hole are carried out to study the cuttings migration status in different pipeline distances at different inclination angles. The specific cuttings migration is shown in Fig. 6. It can be seen from the figure that the farther away from the bottom of the hole, the overall volume fraction of cuttings shows a downward trend. The dip angle of 0° shows a sudden drop after 2.2 m, and the dip angle of 2° and above shows a sudden drop after 2.4 m. At the same time, with the increase of dip angle, the volume fraction of cuttings at the orifice shows a good linear increase. The volume fraction of cuttings at the bottom of the hole increases with the increase of inclination angle, reaching the maximum at 4°. The inclination angle continues to increase, and the volume fraction of cuttings at the bottom of the hole decreases slightly and tends to be flat.

In order to more intuitively display the main sedimentary area of cuttings, the main sedimentary shape of cuttings and the maximum sedimentary thickness under a

Table 1 Statistical table of volume fraction of cuttings at bottom of annular cross section

Dip angle distance	0°	2°	4°	6°	8°	10°
0.2	0.003173	0.003178	0.003979	0.003864	0.003826	0.003806
0.4	0.003174	0.003447	0.004154	0.004018	0.003966	0.003947
0.6	0.003175	0.003487	0.003992	0.003885	0.003854	0.003852
0.8	0.003176	0.003503	0.003856	0.003742	0.003731	0.003746
1	0.003177	0.003491	0.003772	0.003644	0.003633	0.003659
1.2	0.003178	0.003466	0.003716	0.003583	0.003566	0.003596
1.4	0.003179	0.00343	0.003658	0.003523	0.003501	0.003534
1.6	0.00318	0.00339	0.003602	0.003466	0.003443	0.003479
1.8	0.00318	0.003358	0.003555	0.00342	0.003396	0.003433
2	0.003175	0.003326	0.0035	0.00337	0.003347	0.003382
2.2	0.003136	0.003282	0.003444	0.003325	0.003303	0.003334
2.4	0.002902	0.003219	0.003383	0.003282	0.003264	0.003293
2.6	0.002264	0.002945	0.003269	0.003208	0.003203	0.003233
2.8	0.001782	0.002021	0.002717	0.002954	0.00304	0.003098
3	0.001316	0.001296	0.001396	0.0015	0.001613	0.001752

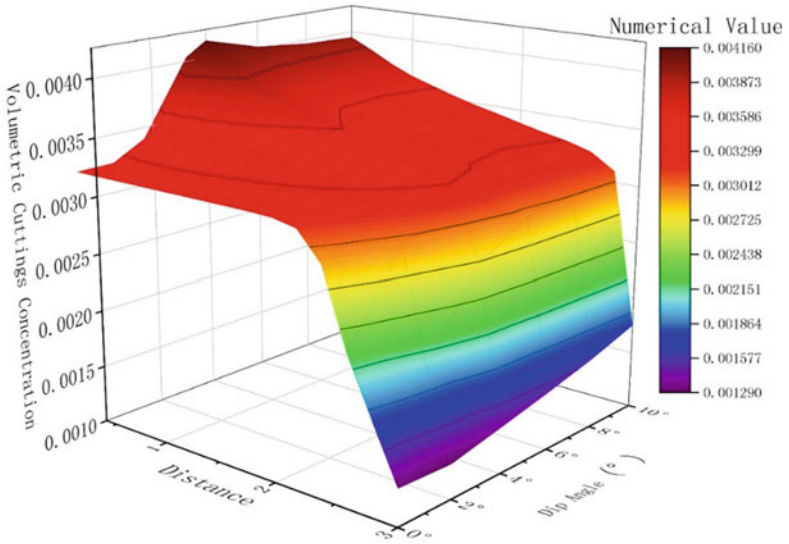

Fig. 6 Volume fraction variation of cuttings under different working conditions

Table 2 Statistics of negative maximum value of y axis

dip angle of hole	0°	2°	4°	6°	8°	10°
Y axis negative	−0.114	−0.107	−0.0900	−0.0963	−0.0999	−0.103

certain volume fraction of cuttings, this section uses Tecplot post-processing software to post-process each working condition. Since the smaller volume fraction of cuttings cannot intuitively reflect the volume change of cuttings, only the equivalent surface with volume fraction of 0.2 in the annulus computational flow field is analyzed. Table 2 shows the statistical table of the maximum values of the equivalent surface with the volume fraction of debris of 0.2 in the negative direction of y axis under different working conditions. Since the model coordinate axis is at the center of the annulus, the lower part of the annulus is in the negative direction of y axis, so the smaller the value in the table is, the thicker the debris deposition is. It can be found that the inclination angle increases gradually from 0 to 4°, and the thickness of debris deposition reaches the maximum at 4°, and then decreases gradually.

In order to further analyze the migration and deposition of cuttings in the borehole, the horizontal projection of the deposition shape of the equivalent surface at the bottom of the borehole with the volume fraction of 0.2 in Fig. 7.

It can be seen from Fig. 7 that the debris deposition shape at 0° is "javelin-shaped", with two tips and large middle, and the main deposition area is 1.1 m away from the

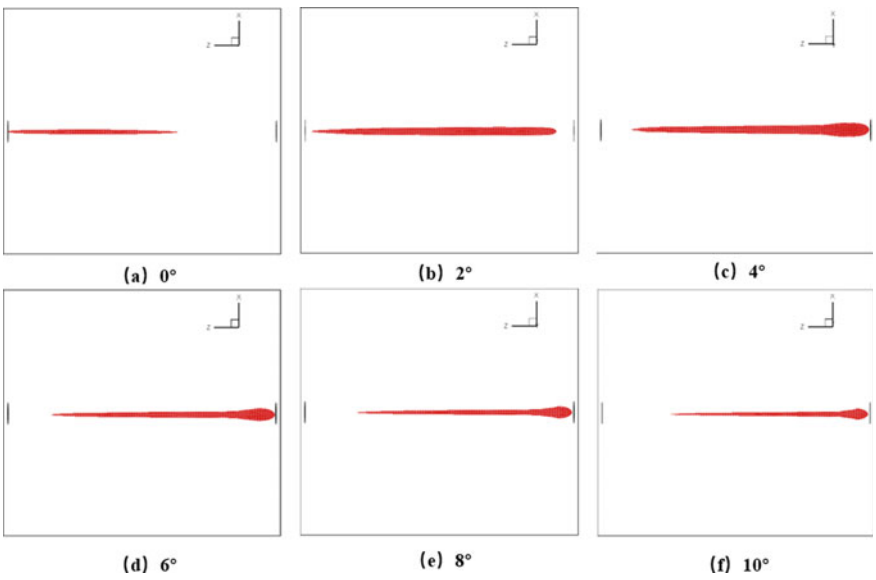

Fig. 7 Projection of sedimentary shape at bottom of borehole on the isosurface of cuttings volume fraction 0.2

bottom of the hole. At 2°, the sedimentary shape of cuttings is similar to "needle-like", showing a sharp end and a thick end. The main sedimentary area extends to the position of 2.9 m away from the bottom of the hole after 0.19 m away from the bottom of the hole. The debris deposition is the most serious at 4°. From 4 to 10°, the debris deposition is similar to "tadpole", with head and tail. At this time, the debris is deposited more at the bottom of the hole. At 4°, the main sedimentary area of debris starts from 0.018 m away from the bottom of the hole to 2.6 m away from the bottom of the hole. At 6°, the main sedimentary area of debris starts from about 0.015 m away from the bottom of the hole to about 2.5 m away from the bottom of the hole. At 8°, the main sedimentary area of debris starts from about 0.017 m away from the bottom of the hole to about 2.4 m away from the bottom of the hole. At 10°, the main sedimentary area of debris starts from about 0.02 m away from the bottom of the hole to about 2.23 m away from the bottom of the hole.

With the occurrence of dip angle, debris particles are hindered by the partial force of gravity G on the inclined plane, which shortens the migration distance of debris, makes debris deposition closer to the bottom of the hole and accumulates into clusters at the bottom of the hole. At the same time, the accumulation of cuttings at the bottom of the hole leads to the decrease of the cross section area at the bottom of the annular plane, which accelerates the flow rate and increases the rock carrying effect of the drilling fluid. Therefore, there is still cuttings deposition near the orifice, but the deposition thickness is small.

6 Discussions

Horizontal directional drilling as a new trenchless technology has brought great convenience in pipeline construction, but the formation of cuttings bed in the drilling process will greatly hinder the construction. Based on the research in this paper, some suggestions are put forward, hoping to help the practical engineering application. In the process of guiding hole drilling, the amount of pump can be appropriately increased, the flow rate of drilling fluid can be increased, and a certain amount of viscosifier can be added to strengthen the efficiency of drilling fluid carrying rock when drilling has a certain angle. Through the drilling of this section quickly, the influence of cuttings deposition on drilling can be reduced when the angle is inclined, and the main deposition site of cuttings can be determined, which can increase the efficiency of stopping drilling and cleaning, and ensure that there are no accidents such as poor pump and sticking.

7 Conclusion

Based on the above research results, the following conclusions are obtained:

(1) In the process of horizontal directional drilling, the stress state of cuttings particles is complex. When the inclination angle is 0°, the cuttings are subjected to gravity, drilling fluid buoyancy, and the drag force, lift force, rotary lift force and pressure gradient force of drilling fluid cuttings when the drill pipe is driven. Under complex stress conditions, it migrates to the direction of drilling fluid flow, and deposits form cuttings bed after flowing through a distance.
(2) The change of small angle dip angle on cuttings migration and formation of cuttings bed is mainly reflected in the sedimentary position of cuttings bed and the change of cuttings migration distance. When the well inclination angle is 0°, the cuttings are deposited as "javelin" when the drilling fluid flows to the side near the orifice, and the cuttings at the top migrate to the bottom to bond with other cuttings. At this time, the increase of the bond force between cuttings is no longer migrated with the drilling fluid, and the cuttings are deposited to form a cuttings bed. When the well inclination angle is 2°, the force of debris particles in the channel is gradually changed, and the effect of debris gravity is relatively weak, and the debris deposition is gradually close to the bottom of the hole in the form of needle. When the well inclination angle is 4–10°, the stress condition of cuttings particles changes at this time, and it will be affected by a gravity component that hinders the movement of cuttings with drilling fluid, so that the movement distance of cuttings particles in each part of the annulus section becomes shorter with drilling fluid. The cuttings bed deposited near the bottom of the hole is "tadpole". With the increase of the angle, the main formation position of the cuttings bed is closer to the bottom of the hole.
(3) The dip angle leads to the deposition of cuttings by gravity at the bottom of the hole, which leads to the decrease of the bottom section area of the bottom annular plane, and the increase of the flow rate of the drilling fluid, which increases the rock carrying effect of the drilling fluid to a certain extent. Therefore, the settlement of cuttings is smaller near the hole.

Acknowledgements This research was supported by the State Key Laboratory of Geohazard Prevention and Geoenvironment Protection Independent Research Project (SKLGP2017Z007), Demonstration of Key Technologies for Monitoring and Early Warning of Major Landslides in Qinghai Province (2021ZY014).

References

1. Xiang H, Sun B, Li H, Niu H (2014) Experimental research on cuttings transport in extended-reach horizontal well. Oil Drilling Prod Technol 36(3):1–6
2. Wang H, Liu X, Li H, Ding G (1995) An experimental study of transport of drilling cutting in a horizontal well. Acta Petrolei Sinica 4:125–132
3. Cheng Z (2016) Study on the cuttings migration rule in large displacement well under different deviation angle. Energy Energy Conserv 3:189–190
4. Sun X, Yan T, Wang K, Jiao J, Zhang Y (2013) Research progress of hole cleaning in complex structure well. Fault-Block Oil Gas Field 20(01):1–5

5. Lu C (2008) Numerical calculation of cuttings transportation in inclined borehole and flow field calculation of cuttings removing tool. China University of Petroleum
6. Wang Z, Zhang ZA (2004) model for two-layer cutting transport in horizontal wells. J China Univ Pet (Edn Nat Sci) (04):63–66
7. Ofei TN, Irawan S, Pao W (2014) CFD method for predicting annular pressure losses and cuttings concentration in eccentric horizontal wells. J Pet Eng (1):1–16
8. Wei S (2013) Study on cuttings migration law in horizontal section. Southwest Petroleum University, Chengdu, pp 43–46

Research on Dispersion and Distribution of Trenchless Underground Pipeline Location Based on Classification Statistics and Electromagnetic Method

Sitong Lu, Xinrong Mao, Jiayu Yuan, Min Chen, and Tianku Zhao

Abstract The emergence and development of underground trenchless pipeline detection with the emergence and development of cities is an eternal task. This is related to the vital interests of every resident, and it is also related to the sustainable development of the city. This paper analyzes several cases and studies the spatial distribution of trenchless pipelines. It is concluded that the same working well and porous pipelines have the characteristics of distribution and divergence. Through classified statistics of trenchless underground pipeline divergent probability distribution range. Assist related engineering and technical personnel in the service of owner's quotation and geophysical prospecting.

Keywords Trenchless · Underground pipeline · Guide instrument · Geophysical survey

1 Introduction

Trenchless technology has been in use as early as the end of the 19th century. The pipeline laying technology has been vigorously promoted in the country for several years. The biggest advantage of this method is that it does not damage the road surface, and only one working pit and one receiving pit can be used for pipeline construction. The target pipelines to be laid include communication pipeline, aviation fuel pipe, metal pipe, national defense optical cable, etc. [1].

Scholars have done some meaningful work for trenchless testing. For example, Zhang H.C. [2] et al. analyzed and studied the electromagnetic field characteristics of ultra-deep underground pipelines and found the effectiveness of magnetic exploration; Si Y.F. [3] Excavation of deep buried underground pipelines is difficult to detect. Small diameter trenchless deep buried underground pipelines are studied, and a detection method based on the principle of attitude measurement

S. Lu (✉) · X. Mao · J. Yuan · M. Chen · T. Zhao
Shanghai Geotechnical Engineering Detecting Centre Co., Ltd, Huanzhen South Road 522, Baoshan District, Shanghai 200436, People's Republic of China
e-mail: lust@sigee.com.cn

X. Liu (ed.), *Proceedings of 2021 China-Europe International Conference on Pipelines and Trenchless Technology*, Lecture Notes in Civil Engineering 212,
https://doi.org/10.1007/978-981-19-4067-5_9

is proposed; Mercer [4] et al. elaborated on the horizontal directional drilling positioning system. Provide a theoretical basis for the majority of engineering practitioners. This article found in several engineering cases that due to the porous nature of trenchless pipelines, there are often horizontal and vertical distributions during the underground laying process, which has a great impact on fine detection in cities. This article summarizes several cases, to study its plane distribution to obtain distribution statistical probability, to provide help for related engineering and technical personnel in the later period.

2 Technical Background

Trenchless underground pipeline detection is by analyzing the material of the underground pipeline, using the difference in physical properties between the underground pipeline and its surrounding medium (soil layer) in terms of electrical, magnetic, density, and thermal conductivity, as well as the underground pipeline and its surrounding soil. The layer has differences in electrical conductivity, magnetic permeability, dielectric constant, wave impedance and other physical parameters. Appropriate geophysical methods are selected to measure the characteristics of various physical field distributions to determine the existence and location of underground pipelines. The core problem of pipeline detection is to accurately locate and fix the depth of underground pipelines. In fact, the basic methods of underground pipeline detection are all due to the technical guarantee for the positioning and depth accuracy of underground pipelines. Commonly used comprehensive geophysical methods include ground penetrating radar method [5], high-density electrical method [6], electromagnetic induction method [7], artificial source shallow seismic method [8] and high-precision magnetic survey [9].

3 Trenchless Detection Test

3.1 The Guide Instrument Detects the Trenchless Setting

The data used in this paper is the application of the guidance instrument to detect the target area. The trenchless pipeline is a signal source inserted into the unthreaded hole in a bunch of trenchless pipelines, and the signal is received by the ground pipeline instrument to determine the depth and position of the pipeline (signal source) (Fig. 1).

Trenchless pipeline detection is mainly to determine the well position of the trenchless pipeline first, and after opening, extend the guide rod into the hollow hole in the underground trenchless pipeline, and combine the advancement of the guide rod and pipeline instrument detection to determine the pipeline horizontal position

Fig. 1 Construction drawing of the test site

and spatial position, and determine the recording point on the spot, and finally use the total station to measure the recording point to collect the coordinates.

3.2 Data Analysis of Test Results of a Project

A sewage pipe needs to be buried at the intersection of Zhangdong Road and Jidian Road in Zhangjiang area, Shanghai. Due to the influence of other pipelines nearby and the work well, the sewage pipe must be about 0.3 m below a power drain pipe that crosses the collector circuit. Pass, and the working well on the side of the power pipe cannot be moved. The power pipe has 16 holes in total, and each hole has a cable. The detection of 10 holes is smooth when the detection method is conducted on the

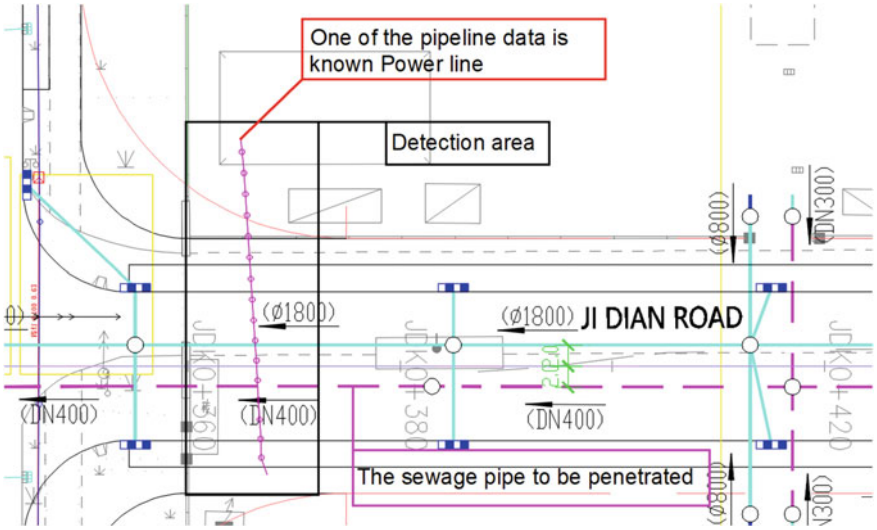

Fig. 2 Plan view of detection area

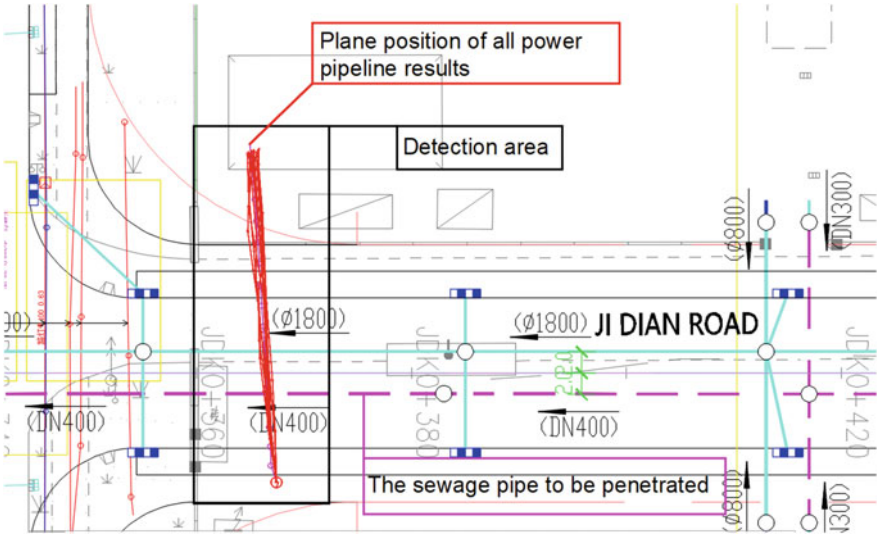

Fig. 3 Plan of detection result

spot. The other 6-hole detection instrument cannot enter the power hole smoothly, so the other 6 holes cannot be detected. Perform precise positioning (Fig. 2).

After data collation and drawings, Fig. 3 is a plan view of the detection result. Due to the long and slender pipelines in the tested area, the pipeline separation site of trenchless pipeline detection cannot be expressed through the plan. The horizontal relative position of the tested pipeline results and the time of detection 3D image is drawn at the elevation of, and the place where the pipeline separation position is relatively large is selected for example.

Due to different construction methods and regional soil quality of trenchless underground pipelines, pipeline deviations will occur in actual projects. The scope and extent of deviations are not convenient for inspection because they are buried in the ground, as shown in Figs. 4, 5, and 6. The green and orange pipelines are not connected in a straight line, but are offset within a certain range. The deviation from the drilling inspection position is a maximum of 0.85 m, and the randomly selected detection pipeline has an overall divergence range width of 1.45 m. The vertical offset is 0.4 m.

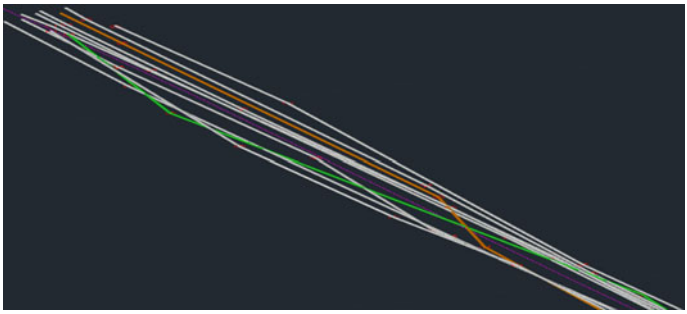

Fig. 4. 3D top view of detection results

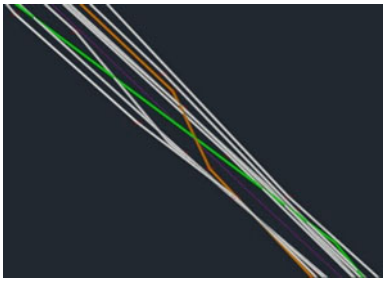

Fig. 5. 3D partial map of detection result

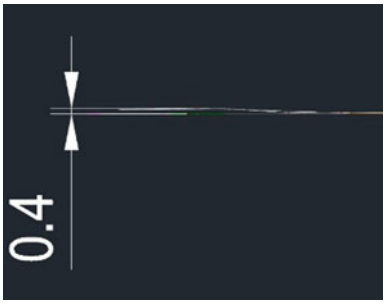

Fig. 6. 3D left side view of detection result (m)

As shown in Fig. 7, the pink color in the figure is the pipe position data provided by the pipeline owner, and the red color is the actual measured position of the different casing holes. The difference between the two can be clearly seen from the figure. If you rely on the data of the pipeline owner to carry out the pre-construction design of the project, it will cause a large deviation. In some fine detection requirements, it cannot be completed by relying on only one pipeline data. Design Basis.

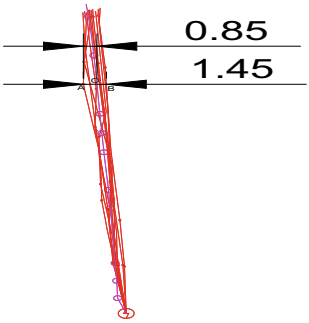

Fig. 7 Plan view of pipeline detection result (m)

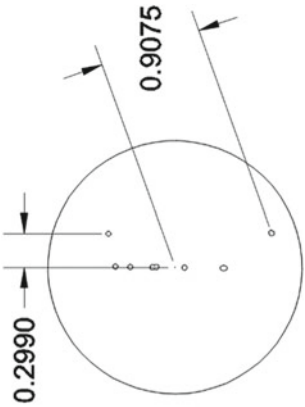

Fig. 8 Cross-section figure (m)

In view of the uneven distribution of pipelines underground, draw the following pipeline detection cross-sectional view. The inner small ring represents the pipeline, and its distribution is drawn from the actual detection data through CAD to draw a cross-sectional view.

It can be clearly seen from Fig. 8 that the pipeline farthest from the actual center is 0.907 m. The maximum height difference is 0.299 m. Compared with the normal distribution of pipelines (Fig. 9), there is a big difference.

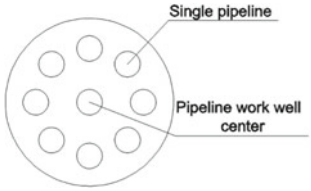

Fig. 9 Idealized distribution model

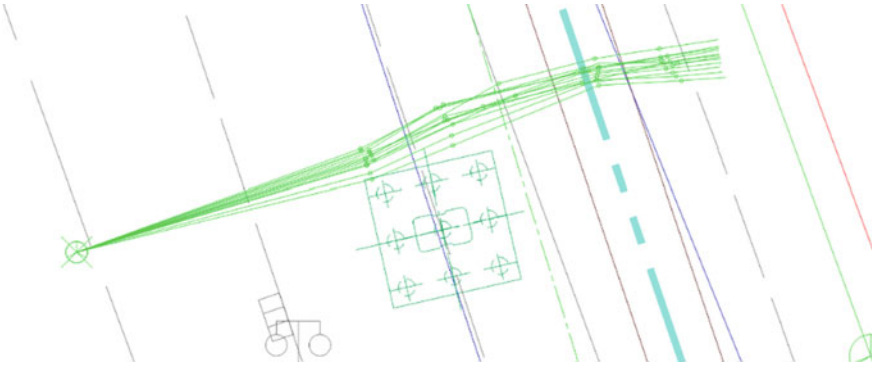

Fig. 10 Luoshan Road detection result

3.3 Data Analysis of Luoshan Road Test Results

The Luoshan Road plan requires the construction of a pile foundation on Luoshan Road, and a bundle of trenchless pipelines may be under the designed pile foundation. After detecting the entire bundle of trenchless underground information pipelines, all twelve lines are carried out. For detection, the detection depth is about 8 m, and the detection is carried out by the guiding instrument method. The data sorting and drawing are as follows, where Fig. 10 is the result of Luoshan Road detection.

It can be seen from Fig. 10 that by detecting different holes with certain differences in their positions, it can be seen that the pipeline has divergence, not extending along the fixed way, and the position has also changed. If only one pipeline is selected for detection, if the pipeline close to the pile foundation is not selected for detection, it will have a great negative impact on the project, and it is very likely to cause damage to the underground pipeline during the piling process.

3.4 Excavation Pipeline Detection Statistics

A statistical analysis of the company's trenchless pipeline detection projects is carried out. The specific data are shown in the following table (Table 1) (Fig. 11):

Table 1 Dispersion statistics of pipeline detection for trenchless pipelines

Item number	Pipeline type	Material	number of holes	Number of measured holes	Maximum plane distance (m)	Spacing differentiation (m)
Project 1	Electricity	PVC	16	10	1.45	1.0–1.5
Project 2	Information	PE	16	12	1.86	>1.5
Project 3	Information	PE	24	17	1.97	>1.5
Project 4	Information	PE	12	6	1.24	1.0–1.5
Project 5	Electricity	PVC	14	4	0.71	0.5–1.0
Project 6	Electricity	PVC	20	3	1.13	1.0–1.5
Project 7	Electricity	PVC	12	10	1.44	1.0–1.5
Project 8	Information	PE	8	3	1.23	1.0–1.5
Project 9	Unicom	PE	8	4	1.09	1.0–1.5
Project 10	Telecom	PE	21	7	1.12	1.0–1.5
Project 11	Mobile	PE	5	3	0.86	0.5–1.0
Project 12	Juntong	PE	12	3	1.19	1.0–1.5
Project 13	Unicom	PE	8	3	0.62	0.5–1.0
Project 14	Netcom	PE	8	4	0.84	0.5–1.0
Project 15	Mobile	PE	5	2	0.46	<0.5
Project 16	Cable TV	PE	6	3	0.48	<0.5
Project 17	Juntong	PE	12	5	0.92	0.5–1.0
Project 18	Telecom	PE	14	4	1.08	1.0–1.5
Project 19	Unicom	PE	21	7	1.67	>1.5
Project 20	Mobile	PE	14	7	1.41	1.0–1.5

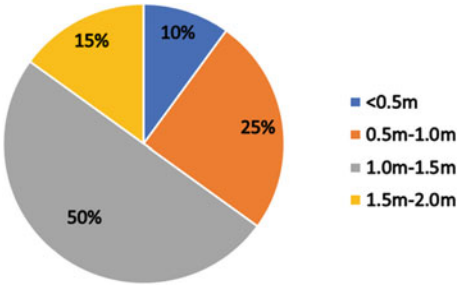

Fig. 11 Statistical graph

Through statistics of multiple projects, it can be seen that after the trenchless pipeline is laid underground, the plane divergence distance of the porous pipeline is within 0.5 m accounted for 10%, 0.5–1 m accounted for 25%, and 1–1.5 m accounted for the largest ratio is 50%, and the ratio of 1.5–2 m is 15%.

4 Conclusion

(1) Trenchless underground pipelines usually have a certain position offset or space enlargement underground, and sufficient safe space should be reserved during the construction process to prevent construction operations from damaging the pipeline.
(2) When there are many pipeline bundles in the local area, the number of detection holes should be increased if necessary to increase data reliability.
(3) When there are many trenchless pipeline holes and only one of them is detected, no matter where the measured hole is in the entire bundle of pipeline holes in the manhole, the pursuit of single-hole detection accuracy is of little practical significance.

References

1. Wang Y (2012) Study and application of detection techniques and methods of urban underground pipelines. Jilin University
2. Zhang CH(2009) Theoretical research and application practice of extra-deep underground pipeline detection. City Surv (1):89–93
3. Si YF(2009) Application of the transient Rayleigh wave in evaluating foundation reinforcement effect using com paction grouting method. Shanghai Geol 25–28+32
4. Mercer, John E(1998) Locating systems f or horizontal directional drilling-Part1. No-Dig Eng 4(5):2–4
5. Xiang LB (2016) Application of geological radar in detection of underground pipeline and case analysis. Geol Anhui 68–70
6. Zhang J (2018) Application analysis of high density resistivity method in engineering geophysical prospecting. World Nonferrous Metals 286–287
7. Liu CF, Zhang YX, Yang XD, Wu S(2016) The application of guidance instrument system in detection of urban non-metallic pipeline by the trenchless technology. Urban Geotech Invest Surv 166–169
8. Chen S, Li YQ, Zhang J, Liu Y(2017) Technical points and progress of shallow surface wave and longitudinal wave reflection exploration methods. Western Prospecting Project, pp 169–171
9. Zhang YY, Liu DJ, Li Y, Guo ZY, Wang Z (2016) Numerical simulation of surface high-precision magnetic detection of underground metal pipes. J China Univ Mining Technol 186–192

Temperature and Thermal Deformation Analysis of Pump Mechanical Seal

Gang Chen, Xianghui Liu, Mingtao Liu, Jian Dong, Jingguo Cao, and Edmund Luksch

Abstract In order to study the influence of temperature field and thermal deformation of a centrifugal pump mechanical seal, the CAD model of mechanical seal ring and ring seat is established by Solidworks. The CFD model of the seal ring is explored through Navier Stokes (N-S) equation and energy equation, and variation of the temperature field is analyzed through the FEA method. The results show that for this type of centrifugal pump, the end face temperature of the seal ring decreases gradually from the inner diameter to outer diameter, the maximum appears in the center of the seal end face. The thermal deformation at the inner diameter of the seal ring is greater than that at the outer diameter, and at the contact end face decreases along both sides of the axial direction.

Keywords Mechanical seal · Temperature field · Heat conduction · Thermal deformation

1 Introduction

In recent years, with the increase of sewage discharge around the world year by year, the urban drainage network has gradually improved. But the drainage pipeline is prone to sediment deposition, excessive sediment derived into pipeline blockage, resulting in sewage overflow and environmental pollution [1–3].

In the practical applications, centrifugal pump plays an important role in pipeline dredging. Due to seal failure and shutdown maintenance, the life of centrifugal pump mechanical seal has been paid more attentions. The high temperature of sealing ring end face will affect the stability of centrifugal pump during operation. The

G. Chen · X. Liu · M. Liu (✉) · J. Dong · J. Cao
School of Mechanical Engineering, Tianjin University of Science and Technology, Tianjin 300457, China
e-mail: liumingtao@tust.edu.cn

E. Luksch
RTi ASIA-PACIFIC PTY LTD, 1/29 Rundle Street, 5067 Kent Town, SA, Austria

X. Liu (ed.), *Proceedings of 2021 China-Europe International Conference on Pipelines and Trenchless Technology*, Lecture Notes in Civil Engineering 212,
https://doi.org/10.1007/978-981-19-4067-5_10

temperature rise may result in vaporization of liquid film between sealing face, lead to the thermal deformation of the sealing ring, and accelerate the wear sealing parts.

Large amount of the researches have been done by the scholars, Shirazi et al. [4] established a CFD numerical calculation model to predict the temperature distribution of mechanical seals, and calculated the convective heat transfer coefficients of different geometric sizes under different working conditions of seal rings, and carried out experimental verification. Merati et al. [5] obtained the Nusselt number curve of the vertical plane through fluid simulation and experimental verification. Luan et al. [6] gave the numerical solution method of N-S equation and energy equation of seal cavity in laminar flow state, calculated the temperature distribution of seal ring solid domain and seal cavity fluid domain. Doane et al. [7] combined the finite difference method with the experiment to explore the heat transfer characteristics of the balanced seal, and proposed the equation that can accurately predict the Nusselt number of the rotating parts. Calculation of Temperature Field of Sealing Face by SSTk-ω Turbulence Model in Fluent Simulation Environment, and explored the relationship between the flow field and the convective heat transfer of the outer diameter surface [8]. Zhang et al. [9] calculated the heat transfer coefficient by simulation, and studied the its influence factors, such as film thickness and inlet velocity of seal groove. The above research studies by changing some initial conditions such as the force and material of sealing ring. It is difficult to intuitively find the deformation and temperature distribution between the seal rings [10].

This paper selects the seal ring of centrifugal pump mechanical seal equipment as the research object, studies on the temperature field and thermal deformation, investigates the influence of spindle speed and cavity temperature on temperature distribution and thermal deformation of seal ring end face. It lays the foundation for the theoretical design and engineering application of mechanical seal.

2 Finite Element Analysis Model of Mechanical Seal

2.1 Calculation Model

The geometric model adopts a double end face mechanical seal of a centrifugal pump. It can be simplified as axisymmetric, the model of the moving ring assembly is shown in Fig. 1.

2.2 Control Equations

The sealing medium is water, the differential equation of liquid film fluid motion is expressed as

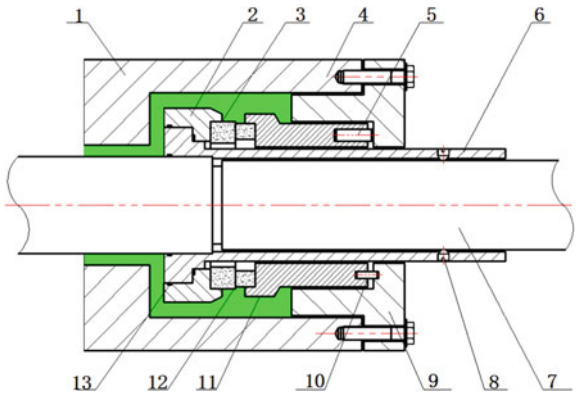

Fig. 1 Structure diagram of mechanical seal. 1-Machine Shell; 2-ush ring; 3-otating seal ring; 4-bolt and back-up plate; 5-spring; 6-axle sleeve; 7-axis; 8-driving screw; 9-gland; 10-top pin; 11-Static ring support; 12-rotating ring; 13-seal ring

$$\frac{\partial u_{\mathrm{x}}}{\partial x}+\frac{\partial u_{\mathrm{y}}}{\partial y}+\frac{\partial u_{\mathrm{z}}}{\partial z}=0 \tag{1}$$

The momentum conservation equation is N-S equation is expressed as follows

$$\rho\frac{\mathrm{d}u_{\mathrm{x}}}{\mathrm{d}t}=\rho f_{\mathrm{x}}-\frac{\partial p}{\partial x}+\frac{\partial}{\partial x}\left[\eta\left(2\frac{\partial u_{\mathrm{x}}}{\partial x}-\frac{2}{3}\mathrm{div}\bar{u}\right)\right]+\frac{\partial}{\partial y}\left[\eta\left(\frac{\partial u_{\mathrm{x}}}{\partial y}-\frac{\partial u_{\mathrm{y}}}{\partial x}\right)\right]+\frac{\partial}{\partial z}\left[\eta\left(\frac{\partial u_{\mathrm{z}}}{\partial x}-\frac{\partial u_{\mathrm{x}}}{\partial z}\right)\right] \tag{2}$$

where $div\bar{u}$ is divergence; f_{x} is a single direction coordinate axis volume component. The mass transport equations of the gas and liquid phases are expressed as [11]

$$\frac{\partial}{\partial t}\rho_{\mathrm{v}}+\frac{\partial}{\partial x_{\mathrm{i}}}\alpha\rho_{\mathrm{v}}v_{\mathrm{v}}=R_{\mathrm{e}}-R_{\mathrm{c}} \tag{3}$$

where R_e and R_c represent mass transfer between liquid and gas phases, respectively. The temperature of the heat transfer system in the working state changes only with the position. The steady-state heat balance differential equations are expressed as [9, 12]

$$k\left(\frac{\partial^2 T}{\partial x^2}+\frac{\partial^2 T}{\partial y^2}+\frac{\partial^2 T}{\partial z^2}\right)+q=0 \tag{4}$$

$$\frac{\partial}{\partial_{\mathrm{x}}}\left(\lambda_{\mathrm{xx}}\frac{\partial T}{\partial x}\right)+\frac{\partial}{\partial_{\mathrm{y}}}\left(\lambda_{\mathrm{yy}}\frac{\partial T}{\partial y}\right)+\frac{\partial}{\partial_{\mathrm{z}}}\left(\lambda_{\mathrm{zz}}\frac{\partial T}{\partial z}\right)+\dddot{q}=0 \tag{5}$$

where T is the temperature of each node of the sealing face; k is the thermal conductivity of the object. k is the heat source intensity; $\dddot{q}$ is the heat source intensity; Symbols of x, y and z are the Cartesian coordinate component.

Table 1 Material parameters of moving ring assembly

Parameters	Moving ring	Ring frame
Young's modulus *E*/Gpa	24	200
Poisson's ratio μ	0.22	0.3
Density ρ/(g·cm^3)	1.8	7.85
Specific heat capacity C_p/(J·kg^{-1}·k^{-1})	921	538
Expansion coefficient α/K^{-1}	5.16×10^{-6}	1.2×10^{-5}
Thermal conductivity λ/(W·m^{-1}·k^{-1})	8.6	60.5

2.3 Boundary Conditions

The heat source of seal system generally comes from three aspects: the heat generated by the friction of the contact face, the heat generated by the sealing medium of the sealing cavity and the stirring heat generated by the rotation of the moving ring [13, 14]. The sealing medium is water and the working temperature is 25 °C. The material of the moving ring and frame are graphite and stainless steel, respectively. The parameters of the dynamic ring assembly are as follows: the sealing medium pressure is 3.0 Mpa, the initial spindle speed is 1500 r/min, and temperature of the sealing cavity is 22 °C. The material properties of the ring and seat are shown in Table 1. In order to facilitate the calculation and simplify the model, the following assumptions are made:

a. The temperature field of sealing ring and loading of force boundary conditions are axisymmetric.
b. Ignore the heat generated by stirring.
c. Ignore leakage and heat radiation dissipation.
d. The material properties of sealing ring and sealing medium do not change with temperature.

3 Analysis on Influence Factors of Sealing Face Temperature

3.1 Temperature Distribution of Sealing Ring

The temperature distribution of the moving ring assembly is shown in Fig. 2.

The maximum of the moving ring appears at the inner diameter, the inner surface of the moving ring contacts with air, the outer surface of the moving ring contacts with the ring frame, and the heat released by the inner surface of the air flow heat transfer is less than the heat transferred by the ring frame, so the temperature is concentrated in the inner diameter, and the maximum can reach 119.4 °C.

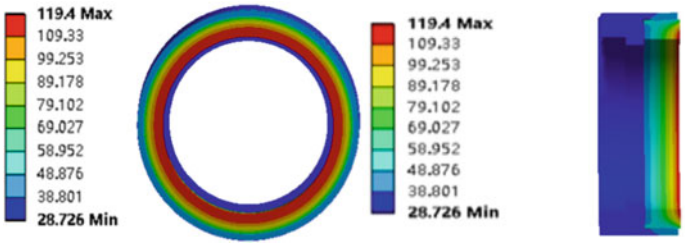

(a) Radial (b) Axial

Fig. 2 Temperature distribution of moving ring assembly

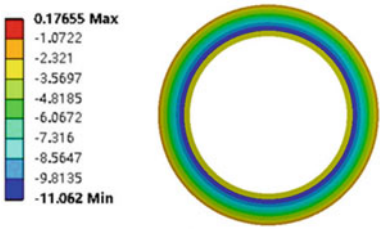

Fig. 3 Axial deformation diagram of moving ring assembly

The temperature is transferred from the end face of the moving ring to the ring frame. The minimum appears on the back of the ring frame, which is close to the ambient values. Therefore, it can be determined that the adiabatic simplification on the back of the sealing ring is reasonable.

3.2 Deformation of End Face Under Temperature Field

The axial deformation has the greatest impact on the end face deformation gap. Therefore, this paper only analyzes the deformation of the moving ring in the axial direction, as shown in Fig. 3.

The maximum deformation occurs at the inner diameter of the moving ring, and the maximum deformation is 11.0 μm, which implies the temperature is much higher than those of other positions.

The stress in the end face and radial section of the moving ring is shown in Figs. 4 and 5. The moving ring end surface expands outward from the inner diameter under the thermal expansion and contraction. The max deformation of the moving ring appears at the inner diameter.

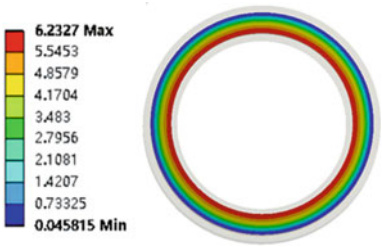

Fig. 4 Stress of moving ring end face

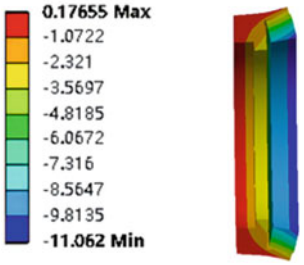

Fig. 5 Radial section of deformation of moving ring

The temperature distribution of the moving ring end face at different rotational speeds is shown in Fig. 6. The increase of rotational speed changes the temperature field distribution of the moving ring assembly, resulting in an increase in the friction force at the end face and a significant increase in the heat generated by friction. Therefore, the rotational speed is positively correlated with the temperature rise at the end face. Due to the contact between the inner diameter and the air, the heat dissipation is slow and the temperature is increased, which leads to the outward deformation of the inner diameter affected by thermal expansion. The temperature change at the outer diameter is small, so the deformation at the outer diameter is small.

3.3 Sealing Chamber Temperature

The deformation of the end face of the moving ring is calculated at the four temperatures of 7, 22, 37 and 52 °C according to the actual operating conditions. The remaining parameters remain unchanged, and the influence of the cavity temperature on the end face deformation is explored. Figure 7 shows the contact heat dissipation rate between the inner diameter of the moving ring and the air is slow, and the heat emitted by the outer diameter decreases, resulting in the accumulation of heat at the inner diameter of the moving ring, and the deformation of the inner diameter of the moving ring increases sharply.

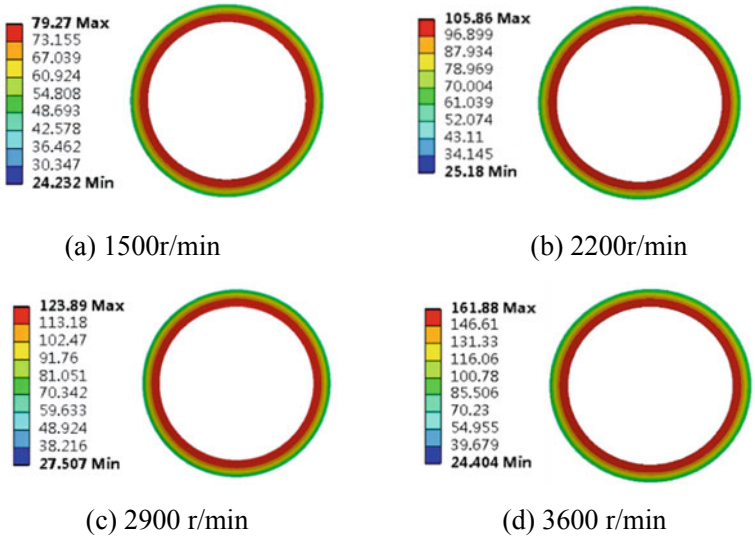

(a) 1500r/min (b) 2200r/min

(c) 2900 r/min (d) 3600 r/min

Fig. 6 Temperature diagram of end face at different speeds

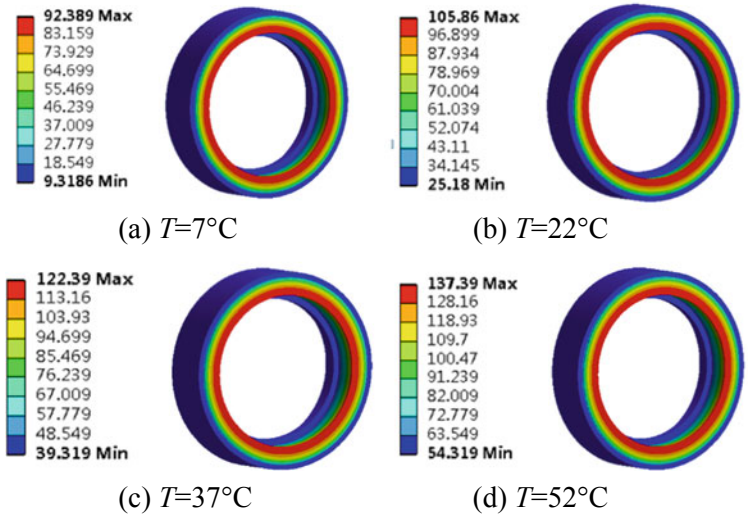

(a) T=7°C (b) T=22°C

(c) T=37°C (d) T=52°C

Fig. 7 Deformation diagram of temperature end face of different seal cavity

4 Conclusion

The temperature distribution and thermal deformation of the sealing ring end face are studied by the FEA method, and the conclusions are drawn as follows:

(1) Increasing the rotating speed of the shaft will aggravate the friction and temperature of the end face. The thermal deformation at the inner diameter is greater than that of the end surface at the outer diameter, and the thermal deformation decreases along both sides of the axial direction.
(2) The temperature rise of the ring makes the deformation of the inner diameter significantly greater than that of the outer diameter, the end temperature will rise as the speed goes up if the medium pressure unchanged.
(3) Sealing cavity temperature directly affects the ring temperature. And the deformation of the outer diameter of the moving ring is also greatly increased.

References

1. Li J (2011) Discussion on key points of reconstruction design of municipal pipe network. Chinese High-Tech Enterprise (21)
2. Wang X, Wang F (2009) Urban drainage pipeline reconstruction design points and implementation process scheme. China Municipal Eng (03)
3. Wu B (2015) Study on construction technology of municipal road drainage engineering. Shanxi Archit (14)
4. Shirazi S, Soulisa R, Lebeck A et al (1998) Fluid temperature and film coefficient prediction and measurement in mechanical face seals—numerical results. Tribol Trans 41(4):459–470
5. Parviz M, Nori AO, Robert P, Larry EJ (1999) Experimental and computational investigation of flow and thermal behavior of a mechanical seal. Tribol Trans 42(4):731–738
6. Luan Z, Khonsari MM (2009) Heat transfer correlations for laminar flows within a mechanical seal chamber. Tribol Int 42(5):770–778
7. Doane JC, Myrum TA, Beard JE (1991) An experimental-computational investigation of the heat transfer in mechanical face seals. Pergamon 34(4–5):1027–1041
8. Wang ZH, Suo SF, Huang WF, Li YJ, Wang YM (2011) Numerical study on convection heat transfer coefficient of mechanical seal. Lubr Seal 36(06):29–33
9. Zhang QZ, Wang H, Lin JS (2012) Study on convective heat transfer coefficient of spiral groove dry gas seal. Fluid Mach 40(09):20–24, 19
10. Liu JX (2020) Temperature rise analysis of friction pair interface of mechanical seal. Mach Tool Hydraulics 48(14):138–141
11. Minet C, Brunetiere N, Tournerie B (2011) A deterministic mixed lubrication model for mechanical seals. ASME J Tribol 133:042203
12. Shapiro W, Walowit JA, Jones HF (1984) Analysis of spiral-groove face seals for liquid oxygen. Tribol Trans 27(3):177–188
13. Liu Z, Liu Y, Liu XF (2007) Optimization design of main parameters for double spiral grooves face seal. Sci China (Ser E Technol Sci) (04):448–453
14. Etsion I, Burstein L (1996) A model for mechanical seals with regular microsurface structure. Tribol Trans 39(3):677–683

Construction of Pipeline and Station Integrity Management Technology System in Sulige Gas Field

Tan Jun, Guo Yongqiang, Jiang Chengyin, Li Xiaojuan, Liu Yongguo, and Meng Hailong

Abstract In view of the difficulties in the daily management of the gathering and transportation pipelines and stations in Sulige Gas Field, the integrity management method is applied, based on the five-step cycle, with the classification management as the basis, the double-high management as the core, and through the application of intelligent technologies such as optical fiber vibration and intelligent shade protection, the daily maintenance management and other measures are well supported to construct the integrity management technology system of the gathering and transportation pipelines in Sulige Gas Field. The inspection of station integrity pipelines and equipment is implemented. Through the application of risk RBI detection, equipment condition monitoring, corrosion monitoring and other technologies, the whole life cycle management system of station is formed. The establishment of pipeline and station integrity technology system is used to comprehensively guide the development of Sulige integrity management work. The pipeline failure rate is reduced year by year, and the key technical indicators are far below the requirements of the stock company. The intrinsic safety of pipeline and station is continuously improved.

Keyword Essential safety of five-step cycle intelligent technology system for management difficulties

1 Introduction

The third gas production plant is responsible for the construction and management of the surface gathering and processing system of Sulige gas field. At present, it has a gathering and processing capacity of 28 billion cubic meters per year. At present, the natural gas gathering and processing accounts for 60% of the total output of Changqing gas field. 6269 km of gathering and transportation pipelines have been built. The gathering and transportation pipeline network has a complex structure and is difficult to manage. The gathering pipeline covers five banners (counties) in two provinces, and the pipeline network density is large. Every year, there are many kinds

T. Jun (✉) · G. Yongqiang · J. Chengyin · L. Xiaojuan · L. Yongguo · M. Hailong
Gas Production Plant 3 of PetroChina Changqing Oilfield Company, Wushen 017300, Inner Mongolia, China
e-mail: 258448515@qq.com

X. Liu (ed.), *Proceedings of 2021 China-Europe International Conference on Pipelines and Trenchless Technology*, Lecture Notes in Civil Engineering 212,
https://doi.org/10.1007/978-981-19-4067-5_11

of constructions such as crossing and crossing of local new projects and gathering pipelines, and the risk of third-party damage is high. At the same time, Sulige Western Region is a water-bearing gas reservoir, and the pipeline corrosion rate is relatively high. Due to the low flow rate, high water cut, high salinity of produced water, the corrosion rate is greater than that of Suzhong block, and 18 times of corrosion of gathering and transportation pipelines all occurred in Suxi block.

There are 6 natural gas treatment plants, 31 gas gathering stations and 1 produced water reinjection station. There are mainly management difficulties such as complex process flow concealment, wide variety of equipment and facilities, high processing load and safety risk.

In view of the difficulties in pipeline and station management, in order to reduce the pipeline failure rate, integrity management is applied. Integrity management is generally recognized as a management method to improve intrinsic safety at home and abroad. At present, Shell, ExxonMobil and BP Petroleum Corporation are all in practical integrity management methods. After nearly ten years of development, China's major pipeline companies have established a sound pipeline integrity management system, supporting technologies and system platforms [1]. Integrity management refers to the identification and evaluation of risk factors faced by managers in the operation of pipelines and stations, and the continuous adoption of targeted risk mitigation measures to control risks within a reasonable and acceptable range, so that pipelines and stations are always in a controllable state, preventing and reducing accidents, and providing protection for their safe and economic operation [2]. The method of pipeline and station integrity management is from no accident to carry out integrity management to integrity evaluation and then to formulate integrity plan, so as to realize the transformation from "passive maintenance after the event" to "active prevention and control based on risk." Sulige gas field has begun to carry out integrity management since 2016. After five years of exploration and practice, the technical system of gas field integrity management has been gradually established.

2 Formation of Sulige's Integrity Management Concept

The traditional integrity management is a six-step cycle, and each unit of CNPC combines high consequence area identification and risk assessment to form a five-step cycle. It includes data collection, identification of high-consequence area and risk assessment, detection evaluation, maintenance and effectiveness evaluation. Data collection mainly combines pipeline completion data and historical data recovery to carry out data collection, collation and analysis. High consequence area identification and risk assessment comprehensively consider the surrounding safety, environment and production impact factors, carry out high consequence area identification, risk assessment and clear management focus. Through the implementation of pipeline detection and data analysis, the pipeline state is evaluated and the risk mitigation scheme is proposed. Maintenance based on risk mitigation programs, take targeted maintenance and maintenance measures. Effectiveness evaluation examines the effectiveness of integrity work.

Due to the large number of gathering and transportation pipelines in Sulige gas field, but the main risks are third-party damage and corrosion failure. The workload of routine inspection and testing is large. The classification management technology strategy is formulated. Aiming at the risk of double high identification, different detection technologies are selected, and the maintenance and management technical measures are implemented. The three-dimensional control measures of civil air defense, material defense and technical defense are constructed to ensure the safe and stable operation of the gathering and transportation system.

3 Establishment of Integrity Management Technology System for Gathering Pipeline

The integrity management technology system of Sulige gas gathering pipeline is established on the basis of five-step cycle. Through the classification of pipelines, the 'first-line case' of type I pipelines, the 'one-area case' of type II and III pipelines are compiled, and the identification of high consequence areas is carried out. Type I and II pipelines are carried out according to the identification rules, and type III pipelines are identified by regional method. The semi-quantitative evaluation is used for the risk assessment of Class I and Class II pipelines, and the qualitative risk assessment is used for Class III pipelines. The maintenance strategy is formulated through the detection and evaluation. In view of the failure risk, the pipeline defect repair, optical fiber vibration, intelligent cathodic protection transformation, and daily management are implemented to ensure the safe and stable operation of the gathering system (Fig. 1).

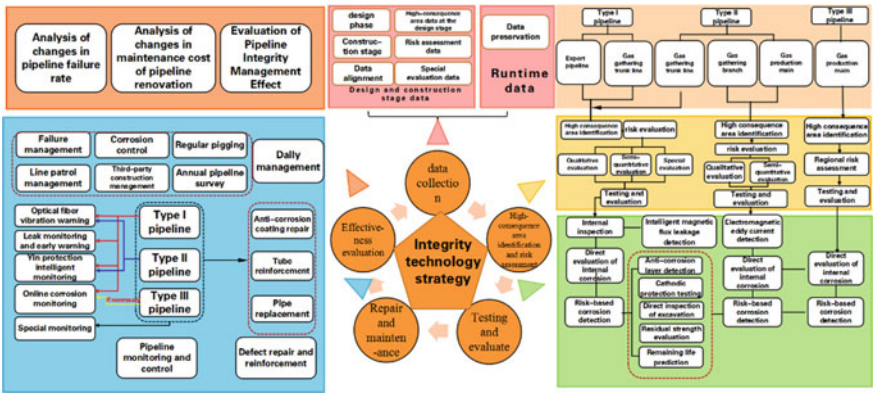

Fig. 1 Integrity management technology system of Sulige gathering pipeline

3.1 Data Collection

Outstanding operation management, failure statistics, detection and analysis of six categories of basic data acquisition, has completed the I, II pipeline operation data A5 system input, data acquisition rate of 100%.

3.2 Identification of High Consequence Areas and Risk Assessment

3.2.1 Identification of High Consequence Area

High consequence area refers to the area where pipeline leakage will endanger public safety, or cause great damage to people's property and environment. The identification procedures for high-consequence zones mainly include the four-level regions where the pipeline passes; the third-level region where the pipeline passes; if the pipe diameter is greater than or equal to 762 mm and the maximum allowable operating pressure is greater than 6.9 MPa, the affected area of the natural gas pipeline has a specific site area; if the pipe diameter is less than 273 mm and the maximum allowable operating pressure is less than 1.6 MPa, there is a specific area in the affected area of the natural gas pipeline; areas with specific locations within 200 m on both sides of other pipelines; in addition to the third and fourth grade areas, there are flammable and explosive sites such as gas stations and gas storages on both sides of the pipeline within 200 m [3].

Conducted once a year to identify nine high-consequence areas and develop six control measures, including the implementation of the system of heads of high-consequence areas; patrol cycle encryption 1 time/day; conduct pipeline corrosion inspection regularly; all defects repaired; pipeline cathodic protection potential standard; establish enterprise-local linkage mechanism.

3.2.2 Risk Assessment

Risk assessment refers to the analysis process of identifying harmful factors that adversely affect the safe operation of facilities, evaluating the possibility and consequences of accidents, synthesizing the risk of pipelines, and proposing corresponding risk control measures.

It is carried out once a year. Classes I and II pipelines adopt the semi-quantitative evaluation method to develop the risk evaluation method of Changqing gas field on the basis of Kent method. The semi-quantitative risk evaluation is to score the failure possibility of third-party damage, corrosion, manufacturing and construction defects, misoperation, and natural geological disasters, and to score the failure consequences of medium short-term harm, leakage diffusion coefficient, and affected objects, so

as to comprehensively evaluate the relative risk. Class III pipeline is evaluated by qualitative evaluation, and the failure possibility and failure consequences are qualitatively scored. Evaluation of gas gathering pipeline is mainly low risk, no high risk pipeline.

3.3 Testing Evaluation

Detection technology based on risk corrosion detection, internal corrosion direct evaluation, intelligent magnetic flux leakage has been formed.

3.3.1 External Corrosion Detection

AC current attenuation method + AC potential gradient method + dense interval potential method + ultrasonic guided wave detection form a risk-based corrosion detection method suitable for Changqing gas field. AC current decay method is used to evaluate the overall quality of the coating; alternating current potential gradient method to accurately locate the damage point location and damage relative size; the change along the pipeline-ground potential was measured by the close interval potential method to evaluate the effectiveness of pipeline cathodic protection; ultrasonic guided wave is used to detect corrosion defects inside and outside the liquid loading point of buried pipeline.

Over the years, 91 pipeline inspections/2640 km were completed. Based on the risk corrosion detection, 2421 defects were detected, mainly mechanical scratches caused by external forces, and all of them were repaired.

3.3.2 Internal Corrosion Detection

Internal corrosion direct evaluation: Gas field pipeline internal corrosion mainly through the establishment of multiphase flow prediction model to carry out direct evaluation, calculation of pipe critical dip angle, liquid holdup, corrosion rate and other parameters, clear pipeline corrosion sensitive area. Including pre-evaluation of collecting pipeline basic information and ICDA feasibility evaluation, indirect evaluation of corrosion mechanism analysis and multiphase flow simulation analysis; the excavation detection and prediction simulation were compared by the direct detection and evaluation, and the effectiveness of ICDA was evaluated and the next detection cycle was determined. Suitable for natural gas pipelines containing condensed liquid hydrocarbons or free water. Especially for small diameter gas pipeline without pigging process has obvious advantages. Over the years to carry out the collection and transportation pipeline evaluation 15/338 km, excavation verification coincidence rate of 63%.

Intelligent magnetic flux leakage internal detection: the magnetic force line along the axial direction between the tube wall is formed by the magnetic pole. Defects such as metal loss lead to changes in magnetic lines. Sensors detect and measure magnetic flux leakage to determine the location and size of defects [4]. The magnetic flux leakage detection of Su 1-L trunk line in Su 14 block was carried out, and 117 defect points were detected, which were all slight internal corrosion. The detection accuracy of the technology is more than 95%, and the detection accuracy is high. The preferred technology for internal detection can comprehensively find out the internal corrosion and defects of the pipeline, effectively evaluate the corrosion of the inner wall of the pipeline, and provide maintenance guidance for the defects of the pipeline.

Electromagnetic eddy current internal corrosion detection: In order to study the internal detection technology of small-diameter pipelines, the electromagnetic eddy current test was carried out on the gas gathering branch line (φ219 mm × 13 km) of T2 - 2 Xiagu Station in 2020, and the defect position was located by identifying the change of the induced current curve [5]. 5 defect points were detected, mileage error ±5.75 m, wall thickness error ±0.16 mm, detection accuracy 71%. It is suitable for the gathering and transportation pipelines with pigging conditions. The detection procedure is simple, the risk of sticking is small, the impact on pipeline operation is small, and the metal loss in the pipeline can be detected online.

3.4 Maintenance

3.4.1 Defect Repair

ACVG detection is used to measure the change of AC ground potential gradient in soil by using buried pipeline current measurement system (PCM) and AC ground potential difference measuring instrument (A frame) to determine the damage point and potential of protective layer. The system consists of a portable transmitter and a portable receiver. The transmitter sends a low-frequency AC signal to the pipeline, and transmits and receives the detection signal through the pipeline to obtain the strength and direction of the received current. Leakage of current at coating defects reflects the integrity of the pipeline protective covering [6]. Over the years to carry out 2391 anti-corrosion layer repair, 19 pipe reinforcement, pipe replacement 11, of which 2020 completed 66 anti-corrosion layer repair. The number of pipeline inspection defects decreased by 82%

Anticorrosive coating repair: the pipe body is mechanically scratched, and the wall thickness reduction degree is less than 10%. The anticorrosive coating is used for repair, and the viscoelastic body + PVC outer belt is used for repair, with a total of 2414 repairs.

Defect reinforcement: defect wall thickness thinning degree between 10% ~ 40% using carbon fiber reinforcement, the use of fiber material bonding resin to form a reinforcing layer, bear the internal pressure of the pipeline [7]. Construction process

fill resin + epoxy primer + carbon fiber composite material + PVC outer belt. A total of 19 reinforcements.

Pipe body replacement: pipe wall scratch serious, wall thickness thinning degree is greater than 40%, the residual strength is less than the pipeline design pressure, must replace the defective pipe. A total of 11 replacements.

According to the different types of pipeline damage points, different repair technologies are adopted to eliminate the potential safety hazard in time, reduce the protection current loss and increase the effective protection distance of pipeline cathodic protection. The good anticorrosive coating will protect the outer wall of the pipeline from corrosion.

3.4.2 Daily Management

(1) Pipeline patrol

In accordance with the 'one map, two tables, three cards, four in place and five in place' patrol working method, the implementation of pipeline '1271' classification patrol system, GPS real-time monitoring and implementation of artificial patrol track; uAV patrol once a week, the formation of artificial + GPS monitoring + UAV patrol line mode.

(2) Pipeline survey

Mainly carry out cathodic protection potential test, line cut-off valve maintenance, surrounding situation census, three piles and one card and pipeline buried depth transformation.

(3) Periodic pigging

The two-round pigging cycle of the main line of the gathering and transportation is formulated based on the factors of pigging liquid volume, operation pressure difference, corrosion and so on. According to the first round of pigging liquid volume, the encryption pigging plan is formulated, and 88,744 liquid volumes are cleared over the years. The soluble pigging is organized and implemented to prevent pipeline stuck and bypass pigging to reduce pigging and gas production.

(4) Failure management

The main failure of Sulige pipeline includes the third party construction failure accounted for 60%, corrosion failure accounted for 30%, manufacturing and construction defects 10%. Through the sampling and analysis of corrosion failure pipeline, the pipeline is due to the formation of liquid at low points. Due to the low gas flow rate and slow flow rate of the pipeline, the scale ion in the gas field produced water is high, and the local formation of 'large cathode and small anode' corrosion battery, electrochemical corrosion occurs, resulting in pipeline corrosion perforation.

3.4.3 Intelligent Control

(1) Optical fiber vibration warning of pipeline line

Technical principle: In view of the third-party damage of the pipeline, a distributed optical fiber vibration sensor is formed by using a redundant core optical fiber in the communication cable laid in the same ditch with the pipeline. When mechanical excavation, manual excavation and other events endangering the safety of the pipeline occur near the pipeline, vibration signals will be generated near the pipeline. The vibration signal transmits through the surface to the optical cable laid near the pipeline, so that the transmission characteristics of the light wave transmitted in the optical fiber change. Through intelligent identification and analysis, the dangerous events such as mechanical construction, manual excavation and natural disasters that threaten the safety of the pipeline are warned and located [8].

Application: one set of pipeline line early warning system was developed in 2020, and optical fiber vibration early warning was implemented at S6 - 1.

Effect evaluation: 86 simulation tests, system alarm delay within 30 s, positioning accuracy within 10 m, good test results, and scale application can further reduce investment costs.

(2) Cathodic protection intelligent monitoring

Cathodic protection relies on an applied current to make the protected metal a cathode, thereby reducing or eliminating metal corrosion. At present, 13 cathodic protection stations are forced current, and the cathodic protection efficiency is 100%. Cathodic protection is gradually developing towards intelligent control.

Technical principle: The intelligent cathodic protection monitoring system of pipeline consists of three parts: remote monitoring terminal, data transmission network and software system It realizes the data interconnection of the front-middle-back end of the cathodic protection system, remote transmission control and parameter adjustment, anomaly analysis and early warning, stray current interference monitoring and other functions, and realizes the comprehensive monitoring of pipeline cathodic protection [9].

Application: In 2020, 3 intelligent potentiostat are replaced, 1 set of cathodic protection monitoring system is applied, and 2/4 intelligent test piles are installed. Over the years, 20 104 trunk lines have realized remote transmission of cathodic protection potential.

Effect evaluation: By real-time monitoring the parameters of cathodic protection system, the remote management of intelligent equipment pipelines is basically realized, and the workload of maintenance personnel is greatly reduced. Through the centralized monitoring system of cathodic protection, 51 under-protected/over-protected pipelines were found in time. After adjusting the output voltage of the potentiostat, it returned to normal in time, and the effective rate of cathodic protection increased from 94.3 to 100%.

It realizes the transformation from 'finding problems—manual detection—passive processing' to 'centralized monitoring—intelligent early warning—timely processing, and forms a new mode of intelligent management of cathodic protection system.

3.5 Effectiveness Evaluation

Integrity management highlights the change of pipeline failure rate. Since 2016, the pipeline failure rate has been decreasing year by year Classes I and II pipelines have no failure, and the gathering and transportation technical indicators have reached the standard (Fig. 2).

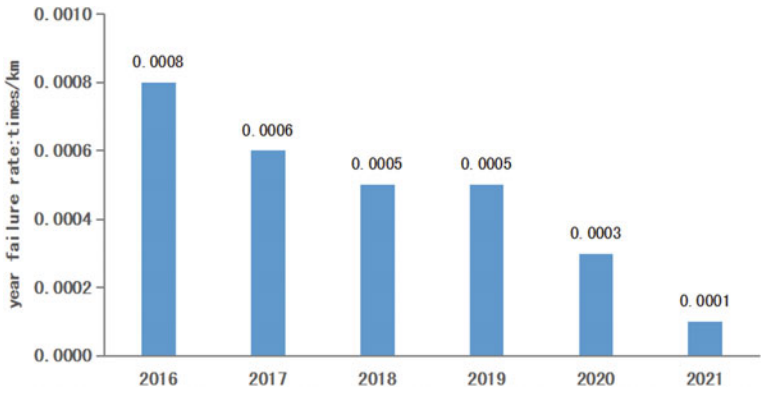

Fig. 2 Failure rate change of sulige gathering pipeline

4 Establishment of Station Integrity Management Technology System

The integrity management technology system of Sulige station is established, which is composed of pipeline equipment and process system. The pipeline and static equipment are used to carry out inspection and corrosion protection, and intelligent technologies such as corrosion monitoring and leakage monitoring are applied to perceive the operation of pipeline and equipment in advance, implement early warning of wall thickness exceeding the standard, and actively prevent pipeline and equipment failure. Dynamic equipment with compressor as the core, the construction of condition monitoring system; the SIL evaluation and maintenance test are carried out in the automatic control instrument system, and the HAZOP analysis, process maintenance and transformation, operation dynamic analysis and parameter optimization adjustment are carried out in the process system. It reflects the whole

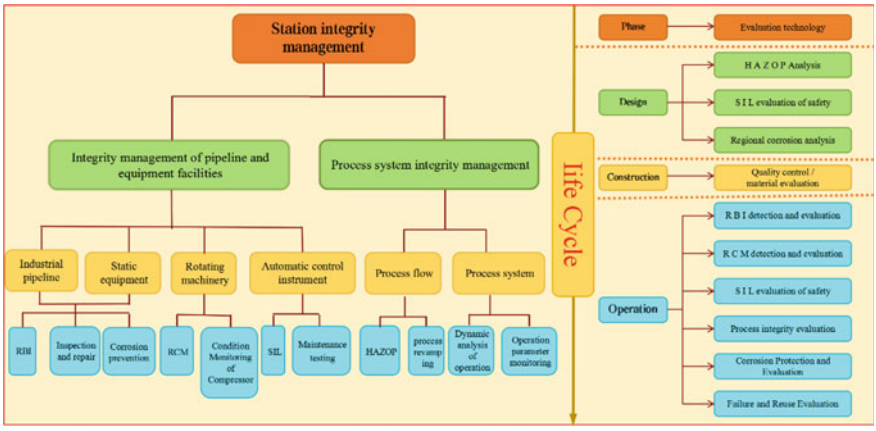

Fig. 3 Surig station integrity management technology system

life cycle management of design, construction and operation, and guides the integrity management of Sulige natural gas treatment plant, produced water treatment station and gas gathering station (Fig. 3).

4.1 Station Pipeline Detection

4.1.1 Failure Mechanism Analysis

According to the pipeline failure analysis and corrosion mechanism research of stations over the years, the pipeline corrosion causes and failure areas are clarified.

Gas gathering station: erosion corrosion is the main and CO2 corrosion is the secondary. The main failure areas are in the inlet area and the drainage system.

Treatment plant: natural gas unit erosion corrosion is given priority to, CO2corrosion is complementary; electrochemical corrosion and bacterial corrosion of liquid phase system were the main corrosion; the main failure areas are pigging area, produced water and condensate system.

4.1.2 Comprehensive Inspection of Gas Station

According to the results of pipeline failure analysis, a comprehensive inspection strategy is formulated. The comprehensive inspection includes macroscopic inspection, single line drawing, pipeline pipe wall thickness detection, weld nondestructive testing, corrosion environment investigation, direct detection of excavation, pressure strength check, stress analysis, safety accessories inspection, defect and problem disposal, safety assessment, etc.

Over the years, 19 gas gathering stations were tested and 28 defects were treated.

4.1.3 RBI Inspection of Treatment Plant

In view of the analysis results of pipeline failure mechanism and the present situation of hidden complexity, a risk-based RBI inspection strategy is formulated. Station pipeline and other static equipment use RBI risk assessment technology. According to the evaluation results, high-risk pipelines are screened. Combined with the regular inspection rules of industrial pipelines and other regulatory requirements, integrity testing and evaluation are carried out. According to the test and evaluation results, the defects are replaced or repaired, and the maintenance strategy is formulated [10].

Six natural gas treatment plants have been tested 12 times over the years, and 145 defects have been repaired (mainly surface cracks, manufacturing defects, corrosion perforation).

4.1.4 Online Corrosion Monitoring of Stations

(1) Multiphase flow model selection

According to the failure analysis results and test results of the station pipeline, the comprehensive corrosion rate (scouring corrosion + CO_2 corrosion) is introduced.

DPM model: establish gas–liquid two-phase flow field, import discrete phase model, use erosion model to calculate corrosion rate [11].

De Waard model: CO_2corrosion prediction semi-empirical formula, considering temperature, CO_2 partial pressure and other factors.

Gas gathering station: two gas gathering stations are selected for modeling respectively, in which the inlet of separator in corrosion sensitive section of natural gas pipeline is 0.07 mm/a; the sensitive section of the drainage pipeline is the first bend at the exit, and the corrosion rate is 0.08 mm/a.

Treatment plant: 9 typical pipelines of one treatment plant were selected for modeling. Among them, the corrosion sensitivity of Su-1 - S double line and pre-separator inlet pipeline was the strongest, and the predicted comprehensive corrosion rates were 0.09 and 0.07 mm/a.

(2) Online corrosion monitoring of station pipeline

According to the prediction results of station multiphase flow, combined with the pipeline detection and failure situation over the years, online corrosion detection was carried out, and ultrasonic multi-echo ultrasonic thickness measurement was applied. By calculating the time difference between the first echo and the second echo, the thickness of the metal wall was calculated as the thickness of the metal wall due to the multiple propagation inside the metal matrix, and the thickness of the overcoating was measured [12].

Nine corrosion sensitive sections were selected for ultrasonic on-line monitoring. At present, the operation has been accumulated for 7 months, and the operation effect is good. The wall thickness detection error is less than 0.05 mm. The corrosion monitoring management is changed from manual detection + passive maintenance to on-line monitoring + active prevention.

4.1.5 Station Laser Platform Methane Leakage Monitoring

Technical principle: The current of the laser is modulated by the single-chip microcomputer control circuit, so that the laser emits the laser with the required wavelength. After the laser passes through the gas monitoring area, it reaches the reflection surface and is reflected back to the laser detector. If the detected characteristic gas exists in the gas area that the laser passes through, the laser will act with the gas and be absorbed. The higher the concentration of the characteristic gas is, the greater the absorption is. The laser detector will monitor the change of the laser intensity and feedback it to the single-chip microcomputer control circuit for processing. Finally, the concentration is shown by the signal output circuit [13].

Application: In 2020, a set of T2-2 station will be installed, covering Shanggu and Xiagu gas gathering stations, with a measuring distance of 100 m.

Effect evaluation: to achieve continuous 24-h monitoring, leakage test conducted a total of 79 times, leakage occurred synchronous receiving alarm signal (0.01 s), and timely image positioning, synchronous alarm rate of 100%.

4.2 Station Static Equipment Detection

4.2.1 Static Equipment RBI

The RBI risk assessment technology is used for static equipment such as station pressure vessels. According to the evaluation results, high-risk equipment is selected. Combined with the requirements of regulations such as the “fixed pressure vessel safety technical supervision regulations”, the integrity test and evaluation are carried out. According to the test and evaluation results, the defects found are replaced or repaired, and the maintenance and maintenance strategies are formulated.

The typical problems found in the inspection mainly include: surface weld cracks, wall thickness thinning, local corrosion of anticorrosive coating, etc., and eliminate hidden dangers through maintenance, monitoring operation, replacement and other means. 2020 to carry out regular inspection of pressure vessels 245 units.

4.2.2 Corrosion Detection and Maintenance of Storage Tanks

In view of the current situation of tank operation, the continuous production detection technology is used to detect the defect signal generated by the bottom plate of the tank by installing acoustic emission sensors on the tank wall, forming a series of acoustic emission detection + tank wall and tank top ultrasonic detection technology.

Acoustic emission detection technology of tank bottom: through an elastic stress wave formed by the sudden release of strain energy inside the material, the elastic stress wave is detected, recorded and analyzed by the instrument, and then the acoustic emission source is deduced to evaluate the active defects of the tested object [14].

Under the condition of a certain liquid level, acoustic emission sensors are evenly arranged around the tank wall to detect acoustic emission signals generated by corrosion or leakage. After identification, processing, display, recording and analysis of the detection system, the corrosion status grade of the tank bottom plate is determined, and the scientific maintenance plan of the tank is formulated.

Acoustic emission testing without tank cleaning, shorten testing time, improve efficiency; less influence on the integrity of the tank; determine no corrosion and its degree, can cover the bottom of the tank.

Over the years to complete 87 steel tank inspection, detection accuracy of 90%.

4.3 Motor Equipment RCM–Condition Monitoring of Compressors

The reliability-centered maintenance technology RCM is used to test and evaluate the dynamic equipment. Through the analysis of asset failure mode and influence, the failure causes and consequences are determined, and the equipment components that need maintenance are obtained. According to the failure characteristics, the maintenance measures are formulated. In order to reduce the failure rate and maintenance cost of the unit and improve the information management level, the gas field compressor condition monitoring platform is developed to realize the function of condition assessment, fault warning and maintenance decision-making. The online monitoring of 16,133 measuring points of all compressor units is completed, and 1200 maintenance decision-making databases are formed.

4.4 SIL Evaluation of Automatic Control Instrument System

According to the <Technical Guidelines for Testing, Evaluation and Maintenance of Oil and Gas Gathering and Transportation Stations> of the Stock Company, the safety instrument device adopts the safety integrity level evaluation technology (SIL) to measure the quantitative indicators of the safety instrument system [15]. According

to the design of automatic control instrument for Surig I station, the ESD system of six natural gas treatment plants is SIL2 grade (SIL test certificate), and the PCS, FGS and supporting instrument systems are SIL A grade. SIL evaluation is mainly used in design phase.

4.5 HAZOP Analysis of Station Process

The analysis group composed of professionals analyzes the hazards and operational problems in the process, and finds a systematic method for hazard sources and operational problems by using 'guide words' to analyze various situations that deviate from normal working conditions in the process [16].

HAZOP analysis was carried out on 6 treatment plants and 8 gas gathering stations over the years, and 344 suggestions were adopted. This method is suitable for the design stage and after major process changes.

4.6 Effect Evaluation

Through the station integrity management, the failure rate of the station has decreased year by year, and the annual failure rate has decreased from 0.32 times/seat in 2016 to 0.16 times/seat at present, with a decline of 50%. At present, the failure of Sulige station is mainly concentrated in the pipeline of the gas field produced water system (Fig. 4).

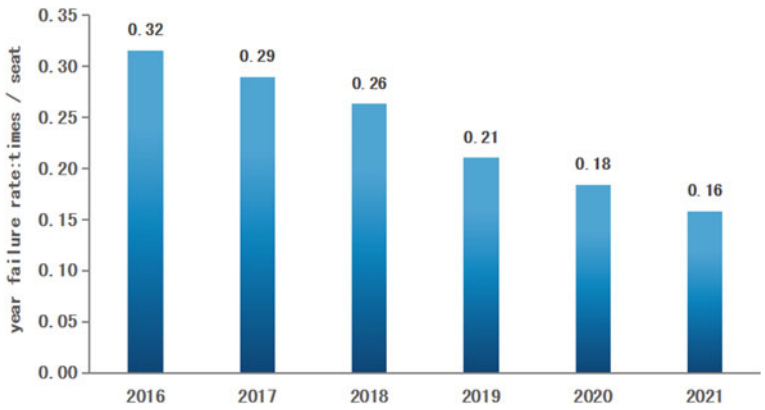

Fig. 4 Failure rate change at Surig station

5 Conclusion and Cognition

1. Based on the five-step cycle, the pipeline is integrated into the classification management, double high management, technological innovation and daily management, forming the integrity management technology system of the pipeline, guiding the integrity management of our plant to carry out comprehensively, and the key technical indicators such as pipeline failure rate are far below the requirements of the joint-stock company.
2. Integrity inspection and evaluation are carried out by station pipeline equipment, automatic control system and process operation, forming the whole life cycle integrity management technology system of the station, and the failure rate of the station decreases year by year.
3. At present, 29 key technologies of six technical series have been formed in Sulige gas field. Through the application of intelligent technologies such as optical fiber vibration, intelligent cathodic protection and online corrosion monitoring, the transformation of management mode is realized, the labor intensity is reduced, and the purpose of active prevention of pipeline failure is achieved.

References

1. Lina H, et al (2021) Construction and integration method of integrity management system for oil and gas pipelines and stations. Oil Gas Surf Eng
2. Lin T, et al (2018) Research and practice of pipeline integrity management in oil and gas fields. Oil Gas Field Ground Eng
3. Chinese National Standardization Management Committee (2015) Oil and gas pipeline integrity management specification : GB32167–2015. China Standard Press, Beijing
4. Fu X, et al (2019) Magnetic flux leakage internal detection technology for jingxi second gas pipeline and its application. Oil Gas Field Ground Eng
5. Xie C, et al (2020) Application and analysis of electromagnetic eddy current detection technology in internal detection of gas field gathering pipeline. Pipeline Technol Equip
6. Lin R, et al (2010) Combined application of ACVG and CIPS technology in corrosion evaluation of buried pipelines. Corr Prot
7. Li, et al (2013) Carbon fiber composite repair technology and application for oil and gas pipeline. Pipeline Technol Equip
8. Zhang Z, et al (2019) Application of optical fiber vibration monitoring and early warning system in oil and gas long-distance pipeline. Petrochem Technol
9. Yang T, et al (2021) Application status and prospect of cathodic protection potential intelligent acquisition system. Oil Gas Storage Transp
10. Lv Q, et al (2018) Research and application of risk-based detection methods for natural gas stations. In: Papers of 2018 national natural gas academic annual meeting
11. Liao K, et al (2020) Research progress on erosion-corrosion law of oil and gas gathering pipelines. Mater Prot
12. Xi Y, et al (2021) Online corrosion monitoring technology based on multi-channel ultrasonic echo characteristics. J Xi'an Univ Petrol (Nat Sci Ed)
13. He, et al (2021) Review of laser induced breakdown spectroscopy in gas detection. Spectrosc Spect Anal

14. Hu Z, et al (2020) Application of acoustic emission detection in risk-based inspection of atmospheric storage tanks. Nondestruct Test
15. Wang Q (2021) SIL grading and checking of SIS in service gas station. Chem Autom Instrum
16. Xu Z, et al (2019) Application of HAZOP analysis in the reconstruction and expansion project of Venezuela Oilfield. Oil Gas Field Ground Eng

Application of Nano Composite Ceramic Anti-corrosion Coiled Material in Trenchless Repair of Underground Pipeline

Shining Yuan and Guanglei Lv

Abstract With the increase of urban pipeline operation time, pipeline failure events caused by various reasons increase year by year. Experts in relevant fields at home and abroad have also successively developed different Trenchless repair technologies and equipment. Different technologies have different characteristics and are also suitable for different occasions. However, more economical, efficient and safe repair technology will become the mainstream in the future. This paper first introduces the development status of Trenchless Technology for urban pipeline, then introduces the characteristics in detail, performance indexes and construction points of light curing repair technology, and finally introduces the construction steps of different pipe diameters and the effect of using nano composite ceramic anti-corrosion coiled material.

Keywords Trenchless repair · Light curing repair technology · Nanocomposites

1 Introduction

Underground pipeline is the lifeline of a city and an extremely important urban public infrastructure. With the rapid development of urbanization in China, the number of new construction, expansion and reconstruction projects of underground pipelines has increased rapidly [1]. Before the 1980s, the pipes material were mainly concrete pipes, cast iron pipes, ceramic pipes and underground canals. Most of these pipes and canals were damaged and corroded seriously due to years of disrepair, so that ground collapse and poor drainage were common. After the 1980s, plastic drainage pipelines have been widely used in domestic water supply and drainage pipelines because of their obvious advantages such as clear weight, corrosion resistance, easy installation

S. Yuan · G. Lv (✉)
CNOOC (Tianjin) Pipeline Engineering Technology Ltd., Tianjin 300452, China
e-mail: 731735101@qq.com

G. Lv
State Key Laboratory for Heavy Oil Processing, China University of Petroleum, Qingdao 266580, China

X. Liu (ed.), *Proceedings of 2021 China-Europe International Conference on Pipelines and Trenchless Technology*, Lecture Notes in Civil Engineering 212,
https://doi.org/10.1007/978-981-19-4067-5_12

and low resistance [2]. However, in recent years, it has been found that in areas with poor geological conditions, weak strata and coastal areas, serious structural defects such as deformation and collapse occur shortly after the burial of such pipelines.

At present, the Trenchless repair technology widely used at home and abroad, mainly includes folding lining method, interleaving method, spiral winding method, in-situ curing method (CIPP), spraying repair method, stainless steel lining method, etc. [3, 4].

The continuous interleaving method is the earliest and the simplest method for Trenchless repair of buried pipelines. It had been used to repair damaged pipelines in 1940. The interpolation pipes commonly used by the continuous interleaving method include PE, GRP, PVC pipes, etc.

The folding lining method uses PE or PVC as the pipe material. Before construction, the geometric shape of PE or PVC inner lining pipe is changed in the factory or construction site to reduce its section. Then pull the deformed pipe into the original pipe, and then expand it by heating or pressurization to restore the size and shape of the original PE or PVC pipe, so as to ensure a close fit with the original pipe.

Expansion spiral winding method is a repair method in which the ribbon polyvinyl chloride (PVC) profile is spirally rotated to form a inner liner through winding machine placed at the bottom of the inspection well, and it is gradually pushed into the original pipe to form a composite pipe with the original pipe.

Thin wall stainless steel lining method is a construction method of repairing urban underground pipelines with stainless steel as lining [5, 6], and it is also a new Trenchless repair process.

In situ curing repair technology is mainly divided into thermal curing and light (UV) curing. The thermal curing process mainly includes hot water curing or steam curing. UV curing lining repair technology refers to the Trenchless repair technology that pulls the glass fiber cloth/felt hose impregnated with UV curing resin into the pipeline to make it close to the original pipeline, and then solidifies the resin through UV irradiation to form an inner lining pipe with high strength. The UV curing inner lining repair hose is composed of inner membrane, fiber resin layer, outer membrane and UV protective film from the inside to the outside. Its basic composition structure is shown in Fig. 1.

Advantages of this technology:

1) There is a close fit without grouting, and the loss of overflow area is small [7].
2) The construction speed is fast and the construction period is short.

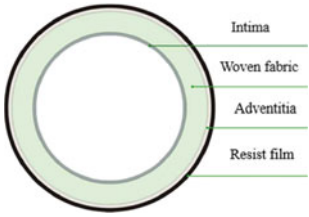

Fig. 1 Schematic diagram of typical UV curing Trenchless Pipeline Repair Technology of hose structure

3) After repair, the inner surface of the inner lining pipe is smooth and continuous without joints.
4) The curing speed is fast and the construction time is short. The maximum pulling speed of the lamp frame can reach 1 m/min. After the pipeline is repaired, it can be put into use immediately, which greatly reduces the time for pipeline plugging and water transfer.

Due to the above advantages of UV curing lining repair technology, this technology has been widely used abroad, especially in Europe. According to statistics [8], in 2004, UV curing lining accounted for 63% of Trenchless lining construction in Germany and 50% of the market in Europe. By 2012, the market share of UV curing lining construction in Germany was 72%. At present, UV curing technology has a good development prospect in Europe.

However, the problem of UV curing Trenchless Pipeline Repair Technology in China is that the UV curing hose mainly depends on foreign imports, with high cost, which is not convenient for the popularization and application of this technology. Therefore, the localization of UV curing hose materials is of great significance to solve the Trenchless UV curing lining repair technology of pipelines in China.

2 Structure and Properties of Light Cured Nanocomposite Ceramic Anti-corrosion Coil

The appearance of light curing Nanocomposite Ceramic anti-corrosion coil is soft film tape shape, and the color is generally light yellow or white. The coil is composed of outer mold, inner membrane and nano ceramic, fiber and resin paste in the middle. Its basic structure is shown in Fig. 2. The material can be quickly cured under sunlight or ultraviolet light. After curing, it forms an anti-corrosion protective sleeve layer with high strength, high adhesion and seamless sealing. The construction is simple and convenient. It can be used for heavy anti-corrosion, enhanced protection, repair and on-line repair of thermal insulation and cold insulation pipelines, storage tanks, storage tanks and reaction tanks such as petroleum and petrochemical, natural gas and organic solvents. It can also be used for Trenchless repair of underground pipelines.

Fig. 2 Light curing Nanocomposite Ceramic anti-corrosion coil

Table 1 Main performance indexes after curing

Project	Index	Project	Index
Babbitt hardness (°)	60.5	Hydrostatic burst test results (MPa)	10
Shore hardness (Shore D)	86.5	Thermal conductivity (W/m·k)	0.155
Tensile strength (MPa)	63.2	Flame retardancy (Grade)	V-0
Tensile strain at break (%)	3.4	Dielectric strength (KV/mm)	12
Bending strength (MPa)	136	Surface resistivity (Ω)	1.5×10^{14} Ω
Bending modulus (GPa)	9.84	Temperature resistance (°C)	−70–180
Compressive strength (MPa)	128	Notch sensitivity	No notch sensitivity

The light curing Nanocomposite Ceramic anti-corrosion coiled material has the advantages of light weight, simple engineering design, flexible and convenient use. It can be cut or cut into various shapes according to the needs of the project, pasted, wound and wrapped on the base course to be strengthened and protected. It can be cured by sunlight or ultraviolet lamp without adding additional curing agent and accelerator. The curing time is only 5-20 min, which can greatly shorten the construction cycle, reduce construction difficulty and labor cost. After curing, it can form an ultra-high strength, seamless and sealed anti-corrosion and fire insulation protective sleeve layer, and its mechanical properties can be comparable to most metal materials. After repair, a solid inner casing can be formed, and the single-layer casing can withstand the static pressure of 4-6 MPa, which can meet the repair requirements of general pipelines. The main performance indexes of the product as shown in Table 1.

3 Trenchless Repair Technology of Light Curing Nanocomposite Ceramic Anti-corrosion Coiled Material

3.1 Repair of Small Diameter Pipeline

According to the inner diameter of the pipeline to be repaired, it can be cut by field design. For the small diameter pipe that cannot be operated by people, it can be cut according to the pipe diameter and the length of the Trenchless pipe, rolled into a barrel, and then the material is pulled into the pipe from the convenient opening, and then one end is tied with a rope, the other end is put into the ultraviolet lamp car and inflated with an air compressor to make the coiled material close to the inner wall of the pipe, which can be electrified and solidified to form a solid inner sleeve. After curing, the excess parts at both ends can be sawed off, so as to realize the Trenchless repair of the pipeline. The construction process is shown in Fig. 3.

Fig. 3 Lining repair of small diameter pipeline

3.2 Repair Construction of Large Diameter Pipeline

For large diameter pipes that can be operated by people, people and materials can be directly pasted at the opening. After cleaning the pipeline, ventilate and dry it. After brushing (or roller coating or spraying) with the supporting light curing primer, paste the light curing Nanocomposite Ceramic anti-corrosion coiled material, press and flatten it, and then irradiate and cure it with ultraviolet lamp for 20-60 min to form a solid inner casing. The construction process includes:

1) Substrate treatment
   After cleaning the inner wall of the pipeline, ventilate and dry it. Grind the rust with sandpaper and remove the dust and impurities before construction.
2) Construction of light curing primer
   Firstly, the holes and perforations shall be smoothed with the supporting putty, and the light curing primer shall be sprayed after the putty is dry.
3) Light curing Nanocomposite Ceramic anti-corrosion coil bonding
   After spraying the light curing primer, the light curing Nanocomposite Ceramic anti-corrosion coil can be pasted for construction. When taking and cutting the coil, pay attention to block the sunlight to avoid light curing and make the material obsolete. You can also choose to cut at night when there is no sunlight radiation.

When pasting the coil, the lap length of the butt joint among sheets shall be $\geq$ 5 cm. When lapping, uncover the adhesive surface film of the overlapping long sheet, as well as the aluminum film and upper film (no less than 5 cm) in some areas of the shading treatment, lap the sheet together, cover the uncovered upper film and press

Fig. 4 Site photo of lining repair of large diameter pipeline

it tightly (roll back and forth with rollers or other tools) to make the cross-section arc of the overlapping smooth transition.

If partial curing is required, at least 5 cm non curing part shall be reserved at the edge for the construction of adjacent interfaces. Aluminum film or black tape can be used for shading treatment at the adjacent interface.

4) Light curing Nanocomposite Ceramic coiled material.
   It can be cured by irradiation with ultraviolet lamp for 20–60 min. See Fig. 4 for the construction site drawing of pipeline repair.

4 Characteristics of Trenchless Repair Technology of Light Curing Nanocomposite Ceramic Anti-corrosion Coil

- The curing is convenient and fast, the labor cost is low.
- Excellent permeability and chemical corrosion resistance.
- High temperature resistance, aging resistance, maintenance free, long service life.
- High strength, good heat shock resistance.

The construction is safe and reliable with little environmental pollution.

5 Conclusion

1) The Trenchless repair technology of insertion, lining and expansion has been relatively mature, and a lot of experience has been accumulated in the application process. However, it is greatly affected by pipe diameter, reducer, valve and flange, and is subject to many restrictions in the use process.
2) The light curing repair technology has an early origin, high technical maturity and wide application range. After combining the light curing technology with Nanocomposite ceramic materials, it can be used for Trenchless repair of urban pipelines. It has the advantages of simple process, convenient and fast construction, high strength of composite materials, strong corrosion resistance and long service life.
3) There are few application cases of light curing Nanocomposite Ceramic Repair Technology, and the construction process experience is insufficient. The large-scale promotion process needs to be further studied.

References

1. Ma B, Zhou W (2013) China's municipal pipelines: today and tomorrow. In: Pipelines conference, vol 201, pp 10–18
2. Shao W, Li T, Yao J (2018) Performance of new plastic pipe and its application in water supply and drainage engineering. Shanxi Arch 15:150–151
3. Ma B, Najafi M (2008) Development and applications of trenchless technology in China. Tunn Undergr Space Technol 23(4):476–480
4. Allouche E, Alam S, Simicevic J et al (2014) A pilot study for retrospective evaluation of cured-in-place pipe (CIPP) rehabilitation of municipal gravity sewers. Tunn Undergr Space Technol 39:82–93
5. ASTM F 1216–16 (2016) Standard Practice for Rehabilitation of Existing Pipelines and Conduits by the Inversion and Curing of a Resin-Impregnated Tube. ASTM, Philadelphia
6. Hou X Repair method of stainless steel lined pipe of locally excavated old pipeline and repair of pipeline structure. Invention patent No Zl021235192002,8 (2020)
7. Zhang H, An G, Liu T, Zhang G (2015) Application of ultraviolet light curing CIPP technology in drainage pipeline repair. Water Supply Drainage 02:103–106
8. Marsh G (2004) Composites renovate deteriorating sewers. J Reinforced Plast 48(6):20–24

Intelligent Pipeline Equipment and Pipeline Detection Technology

Research on the Node Importance Evaluation of Gas Pipeline Networks Based on Complex Networks

Chuanlu Ma, Yingbo Ji, Yan Liu, and Ruichen Zhou

Abstract As China is advancing the renewal of urban infrastructure, the renewal of urban gas pipeline networks is a must to be solved. In the renewal project of gas pipeline networks, it is not uncommon to see the failure of key nodes, which will cause the cascading failure of gas pipeline networks. Thus, it is necessary to study the key nodes of gas pipeline networks. Based on the complex network theory, the paper establishes and simplifies the topology model of the gas pipeline networks, calculates the node degree and node betweenness of the gas pipeline networks, and evaluates the importance of nodes in the complex network. It also evaluates the importance of nodes for gas supply by introducing the principle of entropy. Finally, it comprehensively explores the importance of comprehensive nodes in the complex network and the gas supply importance of nodes and identifies the key nodes in the gas pipeline networks. It provides guidance for urban renewal projects to avoid cascading failures and is of instructive significance for safety gas construction.

Keywords Gas pipeline networks · Node importance · Complex networks · Flow entropy

1 Introduction

Due to the long service period of the gas pipeline networks in some cities [1], it is necessary to renew it when China advances infrastructure renewal during its urban renewal, as it serves as one of the urban lifeline projects. However, the renewal project of the gas pipeline networks is usually accompanied by its cascading failure. Therefore, exploring which are the key nodes of the gas pipeline networks can guide its renewal.

At present, scholars have researched the road transportation network, the gas network and the subway network in cities to various extents by using the complex network theory [2–4]. For the research on the safety risk of the urban gas pipeline

C. Ma (✉) · Y. Ji · Y. Liu · R. Zhou
North China University of Technology, Beijing, China
e-mail: 1732174731@qq.com

X. Liu (ed.), *Proceedings of 2021 China-Europe International Conference on Pipelines and Trenchless Technology*, Lecture Notes in Civil Engineering 212,
https://doi.org/10.1007/978-981-19-4067-5_13

networks, some scholars proposed a risk assessment procedure when considering failure [5]. Some scholars conducted a comprehensive risk assessment for the gas pipeline networks from both internal and external perspectives [6]. Zhang Zhixia [7] evaluated the importance of nodes in the gas network based on the cascading failure and analyzed the importance of gas nodes through node deletion. Sotoodeh Hamidreza [8] considered the topological conditions of nodes in the network and the relative importance of nodes and their neighboring nodes by combining the degree ratio of a node and its neighbors. Seyed Ashkan Zarghami [9] improved the traditional betweenness centrality by adding a hydraulic-based weighting factor and compared and evaluated the measure of the three classic centralities with that of the new centrality. Ye Xue [10] introduced flow entropy to analyze the reliability of the gas transmission network.

Based on the research mentioned above, it can be found that research on the key nodes in the gas pipeline networks through the complex network method is beneficial to guide safety gas construction. However, there are still shortcomings in the current research on complex gas networks, namely, the relative importance of the medium flow of nodes is not taken into consideration when the key nodes of the gas network are analyzed. The paper analyzes the comprehensive importance of nodes by considering the index of the relative importance of the medium flow of nodes and combining it with the importance of nodes in complex networks and the gas supply importance of nodes. The analysis results show that the result of node importance evaluation is more consistent with the reality of projects when the flow entropy of nodes is taken into consideration. Therefore, the research can more accurately identify the key nodes in the gas pipeline networks so as to effectively avoid cascading failure of the gas pipeline networks by avoiding cascading failure of key nodes. The research provides guidance for safety gas construction.

2 Establishing Topology for the Gas Network

During the research, scholars usually abstract components in a complex system as nodes, and abstract the connection between components as edges, thereby abstracting and simplifying a real complex system into a complex network model.

The complex network model of the gas pipeline networks12 is a graph set $P(N, S)$ composed of a node set $N(P)$ and a pipe section set $S(P)$. In the node set $N(P)$, if node i and node j are connected, a pipe section is formed, and the pipe section set $S(P)$ is formed by many pipe sections if there is a connection between many pairs of nodes. In the complex gas pipeline networks, the number of nodes is recorded as n, and the number of pipe sections, namely the number of edges, is recorded as e to establish an undirected weightless network graph. The key nodes of the pipeline network are analyzed from the basic topology graph of the gas pipeline networks.

Generally, the urban gas pipeline networks can be simplified to reduce the complexity of the model calculation. The basic principles of simplification16 are as follows:

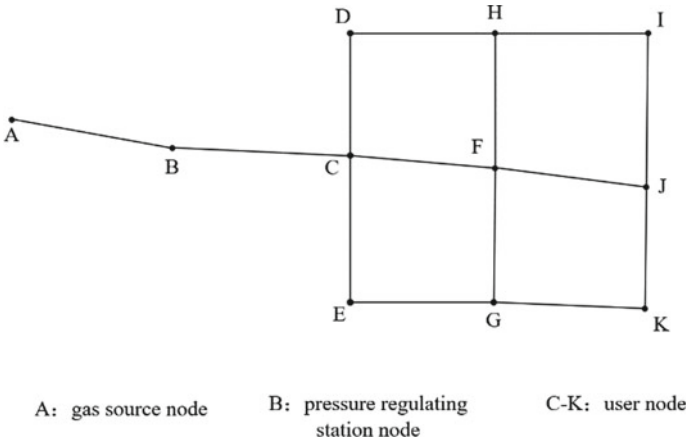

Fig. 1 Simplified topology model of general gas pipeline networks

- Regarding what to be researched, the real pipeline network is used as the basis for simplifying the topology of the gas pipeline networks in the research.
- The gas gate stations, storage and distribution stations, pressure regulating stations and users in the gas pipeline networks are abstracted as "nodes."
- To facilitate the research, a medium-pressure pipe network is selected as the pipe network.

According to the above simplification principle of the topology of the gas pipeline networks, the general gas pipeline networks can be simplified to the model shown in the figure below, wherein node A is the gas source node. The model comprises 14 pipe sections and ten user nodes (Fig. 1).

3 Analysis of the Importance of Nodes in Complex Network

3.1 Complex Network Parameters

Node Degree

The node degree K_i represents the number of connected adjacent edges of node i in the network, which can be used as one of the indicators to measure the importance of nodes in the network, as shown in formula (1).

$$K_i = \sum_{j=1}^{N} a_{ij} \tag{1}$$

wherein K_i represents the degree of node i, a_{ij} represents the edges of adjacent nodes, and N represents the number of nodes in the network.

Degree Distribution
The degree distribution refers to the ratio of nodes with a degree of k in N nodes, i.e., the probability of a node with degree k appearing in all nodes of the pipe network, which is recorded as $P(k)$. The degree distribution can reflect the macro characteristics of the network.

Node Betweenness
The betweenness defines the ratio of the shortest path number between node p and node q through target node i to the shortest path number between node p and node q in the network. It can measure the influence of nodes on the function and structure of the entire network and can be used as one of the indicators for evaluating the importance of nodes in the network.

$$B_i = \sum_{p \neq i \neq q}^{N} \frac{n_{pq}(i)}{n_{pq}} \tag{2}$$

wherein n_{pq} is the number of the shortest paths between node p and node q, and $n_{pq}(i)$ is the number of the shortest paths between node p and node q through target node i.

Clustering Coefficient
In the network, the clustering coefficient C of nodes reflects the degree of clustering of nodes. The number of nodes connected to node i is k_i, there are actually L_i edges between node i and node k_i, and there are at most $k_i(k_i - 1)/2$ edges in the network, then the clustering coefficient C_i of node i satisfies the following formula:

$$C_i = \frac{2L_i}{k_i(k_i - 1)} \tag{3}$$

3.2 The Node Importance of Complex Network

In the network with adverse events, from the perspective of deleting key nodes to destroy the network, nodes of high importance in the network can be more effectively identified through the node removal strategy of degree and betweenness the more [11]. Thus, the paper uses node degree and node betweenness as indicators to calculate node importance and rank the centrality of nodes in the gas pipeline networks so as to identify key nodes in the pipeline network.

The node degree and node betweenness are comprehensively analyzed to define the node importance index. The calculation method of node importance is shown in the following formula.

$$I_i = B_i \times K_i \tag{4}$$

wherein I_i is a metric value of the importance of node i, B_i is the betweenness of node i, and K_i is the degree of node i.

When calculating the node betweenness, the study uses the Matlab software to calculate due to the large amount of calculation of node betweenness. First, an adjacency matrix is established according to the topology graph of the simulated gas pipe network. Then the code for calculating node betweenness is written in Matlab to obtain the betweenness of each node.

Based on the above calculation results of the node degree and betweenness of the general gas pipeline networks, the gas node importance of the complex network is calculated and ranked according to formula (4) (Table 1).

When only considering the complex network structure, the five nodes of C, F, G, H, and J have relatively high node importance, and their network topology is the most complicated. Analyzing from the perspective of complex networks, the importance of these five nodes is relatively high in the network. The five nodes of A, I, K, D and E are relatively low in importance, and their network topology is the simplest. Analyzing from the perspective of complex networks, these five nodes are relatively low in importance.

Table 1 Network node importance

Node number	Degree	Betweenness	Importance value	Importance rank
A	1	0	0	8
B	2	9	18	4
C	4	21	84	1
D	2	3	6	6
E	3	3	9	5
F	4	17.33	69.32	2
G	3	6.33	18.99	3
H	3	6.33	18.99	3
I	2	1.33	2.66	7
J	3	6.33	18.99	3
K	2	1.33	2.66	7

4 Analysis of the Importance of Nodes Through Traffic Entropy

4.1 The Principles of Entropy

Information Entropy
In 1948, Claude E. Shannon [12] proposed to use information entropy to measure the random uncertainty and the amount of information of a system. The formula of information entropy is as follows:

$$S = -K \sum_{i=1}^{N} p_i \ln p \tag{5}$$

wherein K is a normal number, and p_i is a finite probability space in which events are mutually incompatible.

The Principle of Maximum Entropy
In 1957, E. T. Jaynes [13] proposed the principle of maximum entropy based on Claude E. Shannon's research, using the maximum entropy probability distribution for information inference. Normally, the selected feasible solution is the distribution with the largest entropy value under certain constraints. The principle of maximum entropy maximizes the uncertain distribution of information under unbiased probability distribution and is the only solution distribution form.

4.2 The Calculation Model of Node Flow Entropy

In the urban gas pipeline networks, the gas flow in different paths from the gas source to each node. The node flow entropy is related to the number of nodes' paths and node flow. The probability space is supposed as $\rho_i = \frac{f_i^h}{q_{io}}$., and a flow entropy formula is established by formula (6):

$$S_i = -\sum_{h=1}^{NP_i} \frac{f_i^h}{q_{i0}} \ln \frac{f_i^h}{q_{i0}} \tag{6}$$

wherein NP_i is the number of paths of node i, h represents the flow of the h th path of node i, f_i^h is the flow of the path from the gas source to node i, and q_{i0} is the gas flow of node i, so $q_{i0} = \sum_{i=1}^{NP_i} f_i^h$.

If node i has n direct upstream nodes, suppose q_{ni} is the pipe flow from node n to node i, and Q_i is the total gas flow of node i, then formula (6) can be simplified to:

$$S_i = \sum_{n \in U(i)} \left[-\frac{q_{ni}}{Q_i} \ln\left(\frac{q_{ni}}{Q_i}\right) + \frac{q_{ni}}{Q_i} S_n \right] \tag{7}$$

wherein S_i is the flow entropy of node i, and $U(i)$ is the set of upstream nodes of node i. If there are many gas source nodes in the pipe network, the upstream nodes of the gas source nodes are a total virtual source composed of all gas sources. S_n is the flow entropy of the upstream node S_n.

5 Analysis of Comprehensive Node Importance

In the gas pipeline networks, the centrality parameters of nodes in the complex network can be used to measure the invulnerability of the network structure [14], and the flow entropy of nodes can be used to measure the reliability of the pipeline network. When network invulnerability and gas supply reliability are taken into comprehensive consideration, the calculation formula of node importance is as follows:

$$I_i = S_i \times B_i \times K_i \tag{8}$$

wherein, I_i is the importance index of the node I_i, S_i is the traffic entropy of node i, B_i is the betweenness of node i, and K_i is the degree of node i.

In this study, the software of TGNET (Pipeline Studio) is used to simulate the gas pipeline networks, through which the pipe flow q_{ni} and the node flow Q_i are obtained, and the sequential method is used to solve the node flow entropy.

According to formula (8), the node importance and the rank of the node importance are calculated, and the calculation results are as follows (Table 2):

According to the calculation results, the comprehensive node importance changes when the node flow entropy is introduced. For example, node A has the least importance in the complex network when serving as a gas source node. But its node importance is the highest from the perspective of gas supply. From a practical point of view, node A should be the most important node in the network. Node B is the only downstream path node of gas source nodes, and its alternative counterpart is zero, so its importance ranks in the middle position in the complex network. But its node importance is the second from the perspective of gas supply, so its comprehensive node importance rank rises. Node J ranks in the upper-middle position in the importance of the Fu'an network. But it is the most downstream node in the network from the perspective of gas supply, so its comprehensive node importance decreases. The analysis shows that the research results are consistent with real projects.

In summary, when flow entropy is introduced to the calculation of node importance, the rank of node importance will change. When the practical significance is taken into consideration, it is found that the nodes whose importance ranks change are of great significance in the aspect of gas supply in the pipeline network. The node

Table 2 Comprehensive rank of node importance

Number	Importance values obtained through flow entropy ($1/S_i$)	Importance values in the complex network	Comprehensive importance	Rank
A	$+\infty$	0	$+\infty$	1
B	7998.5	18	143,973	2
C	5.24	84	440.57	3
D	2.27	6	13.61	8
E	2.34	9	21.09	5
F	2.51	69.32	173.86	4
G	0.98	18.99	18.59	6
H	0.96	18.99	18.27	7
I	1.16	2.66	3.10	10
J	0.54	18.99	10.20	9
K	0.87	2.66	2.31	11

importance ranking for node importance evaluation in the gas pipeline networks is more accurate when flow entropy is considered. Therefore, the gas supply significance of nodes should be considered in evaluating the importance of nodes in the gas pipeline networks.

6 Conclusion

- Based on complex network theory, the importance of nodes in the gas pipeline networks is calculated and evaluated.
- Based on the entropy principle, a calculation model for node flow entropy is established. The node flow entropy is used to evaluate the relative importance of node media flow and the gas supply importance of the gas pipe network nodes.
- A comprehensive analysis of the importance of nodes in the complex network is performed based on the complex network theory and the principle of entropy. When the node flow entropy is introduced, the evaluation of node importance is more reasonable and conforms to real projects, which has instructive significance for evaluating the importance of nodes in the gas pipeline networks.

References

1. Wang CX (2017) System dynamics simulation analysis of the leakage risk of urban gas pipelines. Fire Control Sci Technol 36(09):1287–1291 (In Chinese)

2. Xiu ZB (2020) Research on node importance and cascade failure of urban traffic complex networks. Jilin University (In Chinese)
3. Cai JM, Deng W (2019) Analysis of the complex characteristics and cascade failure robustness of the changsha metro network. J Rail Sci Eng 16(06):1587–1596 (In Chinese)
4. Chen LY, Li XJ, Yin X, Bi J (2018) Analysis method of node importance of gas pipeline networks in the complex network theory. J Chin Saf Sci 28(09):74–80 (In Chinese)
5. Tutunchi A, et al (2020) Risk assessment of an urban natural gas polyethylene piping system. J Pipeline Syst Eng Pract 11(2): 06019005
6. Han ZY (2010) Research on risk assessment method of urban gas pipeline networks. Tsinghua University (In Chinese)
7. Zhang ZX, Jiang QQ (2018) Assessment of the node importance of gas pipeline networks based on cascading failure. Fire Control Sci Technol 37(04):541–544 (In Chinese)
8. Sotoodeh H, Falahrad M (2019) Relative degree structural hole centrality, CRD-SH: a new centrality measure in complex networks. J Syst Sci Complexity 1009–6124:1559–7067
9. Zarghami SA, Gunawan I (2020) A domain-specific measure of centrality for water distribution networks. Eng Constr Archit Manag 27(2):341–355
10. Ye X, Xie Y (2016) Analysis of gas supply reliability of gas transmission network systems based on flow entropy. Liaoning Chem Ind 45(05):654–656 (In Chinese)
11. Jahanpour E, Chen X (2013) Analysis of complex network performance and heuristic node removal strategies. Commun Nonlinear Sci Numer Simul 18(12):3458–3468
12. Shannon CE (1948) A mathematical theory of communication. Bell Syst Tech J 27(3):379–428
13. Jaynes ET (1957) Information theory and statistical mechanics. Phys Rev 106(4):620–630
14. Nie T, et al (2018) Evaluation of invulnerability of scale-free networks using total information of local sub-graph. Int J Mod Phys C 29(08):1850075

Dynamic Simulation on Linepack of Long-Distance Natural Gas Pipeline

Jiale Wang, Yuguang Fan, and Lin Gao

Abstract As a low-carbon fossil energy, natural gas is the key to the transformation of the world energy consumption structure. With the development of natural gas transmission industry, it is very important to diminish the transportation difference of long-distance pipelines. However, the linepack computing plays a key role in it. In this paper, a TGNET model was established to study the influence of ambient temperature fluctuation on linepack, which is based on Jingxi natural gas pipelines. The results showed that the linepack in the long-distance natural gas pipelines is related to the ambient temperature negatively. Combined with the related theoretical knowledge, the simulation results are analyzed: the ambient temperature indirectly affects the linepack by changing the natural gas temperature in the pipelines as the heat transfer. Therefore, the conclusions in the present study are helpful to optimize the operation of gas storage and peak shaving in practical work.

Keywords Gas pipeline · Ambient temperature · Linepack · TGNET

1 Introduction

With the proposal of the goal of carbon neutralization, China's energy structure will change to a new pattern, which is dominated by new energy. As a low-carbon fossil energy with high efficiency, clean and mature development technology, natural gas can form a benign complement with new energy, that is the key to realize the transformation of the world energy consumption structure [1, 2]. The two main transportation modes of natural gas are pipeline transportation and liquefaction transportation. Pipeline transportation is considered to be the best transportation mode according to the physical property of natural gas [3]. At present, a large and complex natural gas pipeline network system has been built in China. As an important performance index to measure the natural gas pipeline transportation system, the natural gas transportation difference affects the economic interests of both sides of the metering.

J. Wang (✉) · Y. Fan · L. Gao
School of Mechanical Engineering, Xi'an Shiyou University, Xi'an 710065, China
e-mail: wang_jake01@163.com

X. Liu (ed.), *Proceedings of 2021 China-Europe International Conference on Pipelines and Trenchless Technology*, Lecture Notes in Civil Engineering 212,
https://doi.org/10.1007/978-981-19-4067-5_14

The linepack of natural gas pipeline refers to the volume of natural gas actually stored in the natural gas pipeline under the standard condition. The change in the natural gas linepack is directly involved in the calculation of transportation difference [4]. In addition, linepack can also reflect the operation of the pipeline. Control of linepack can be used to regulate the peak of gas supply and to ensure the emergency reserve capacity of the pipeline in case of emergency [5–7]. As a result, the operation of Jingxi third-line pipe network is numerically simulated by TGNET software to explore the influence of ambient temperature changing on linepack, and analyze how the ambient temperature affects the storage. It is hoped that this study can reduce the economic loss caused by transportation difference for natural gas companies and provide theoretical reference for gas storage and peak regulation.

2 Simulation Methods

The model of Jingxi third-line pipeline network is built based on the existing schematic diagram of natural gas pipeline network, with TGNET [8–10]. The basic data of natural gas product composition, gas source pressure, temperature and flow rate, compressor configuration and other parameters given by the collection station are used to improve the established model. According to relevsant standards and combined with the actual situation of natural gas pipe network operation, BWRS state equation is selected as the gas state equation used in the simulation process [11]. The calculation formula of pipeline friction is Colebrook formula, as shown in Eq. (1):

$$\sqrt{\frac{1}{f}} = -2 * lg\left(\frac{e}{3.7 * d} + \frac{2.51}{R_e * \sqrt{f}}\right) \tag{1}$$

where, f is the hydraulic friction coefficient; e is roughness of inner wall of pipeline, mm; d is the inner diameter of the tube, m; Re is the Reynolds number.

After determining the validity and accuracy of the model, dynamic scripts are established according to the numerical values of the ambient temperature of each pipe section collected at different time of the day to carry out dynamic simulation [12]. To determine whether the simulation results are correct, the following methods are used: Check the pipe storage trend curve and dynamic simulation report obtained by dynamic simulation, and observe the relationship between pipe storage and ambient temperature. Then the correctness of the simulated results are judged by the calculation formula (2) of tube stock and the relationship between ambient temperature and natural gas temperature.

$$Q_c = V\frac{P}{P_{SC}} \cdot \frac{T_{SC}}{T} \cdot \frac{Z_{SC}}{Z} \tag{2}$$

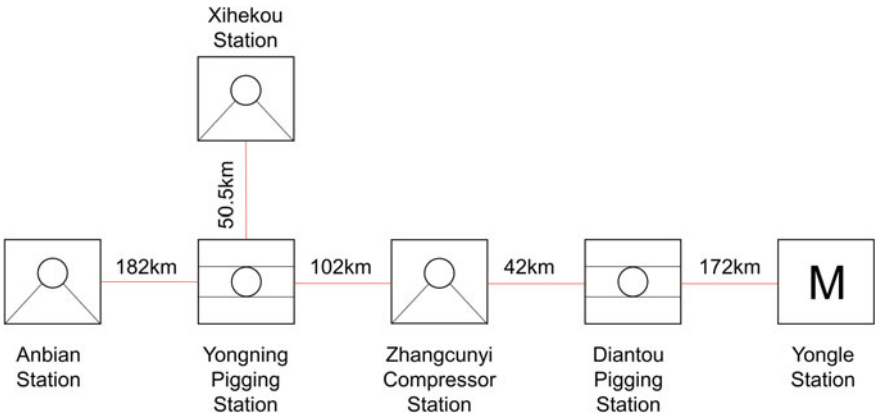

Fig. 1 Schematic diagram of Jingxi third-line pipe network

where, Q_c is the gas storage capacity of the pipeline, m^3; V is the volume of pipeline, m^3; P is the average pressure in the pipeline, MPa; P_{SC} is the standard condition pressure, MPa; T_{SC} is the standard condition temperature, °C; T is the actual average temperature in the tube; Z_{SC} is the ideal gas compression factor; Z is the actual gas compression factor.

3 Simulation Analysis

3.1 Basic Composition of Pipe Network

Based on Jingxi Third-line in Shaanxi province, the simulation analysis is carried out. The pipeline is double-gas source and single-user pipeline Fig. 1, which has the characteristics of large geographical span and seasonal variation of downstream users' gas consumption. The pipeline is connected to two primary pressure stations, two pigging stations, one compressor station, one final station and 18 valve chambers (one branch line).

The component parameters given are shown in Table 1.

3.2 Model Establishment

Large-scale natural gas pipeline network is generally multi-gas sources as the gas demand of users varies with the season and gas consumption fluctuates greatly day and night. The flow state in the pipe is affected by the upstream and downstream pressure. For such an unsteady flow system, the state of natural gas in the pipeline

Table 1 Natural gas component

	Name of the component	Molecular formula	Volume fraction of matter	
			Anbian station	Xihekou station
1	Methane	CH_4	0.930732	0.9610
2	Ethane	C_2H_6	0.040459	0.00586
3	Propane	C_3H_8	0.007435	0.00070
4	Isobutane	i-C_4H_{10}	0.001314	0.00006
5	N-butane	n-C_4H_{10}	0.001270	0.00007
6	Isopentane	i-C_5H_{12}	0.000592	0.00002
7	N-pentane	n-C_5H_{12}	0.000266	0.00001
8	Hexane	C_6H_{14}	0.000361	0.00008
9	Carbon Dioxide	CO_2	0.009346	0.0239
10	Nitrogen Gas	N_2	0.007819	0.00786
11	Hydrogen Gas	H_2	0	0.00007
12	Helium	He	0.000406	0.00037

should be restored as much as possible, and the simulation model of the natural gas pipeline network should be established.

Before establishing the model, the main components of the natural gas pipeline network system need to be simplified: the pigging station which plays the role of pigging and separation is simplified to the nodes between the pipelines; ignoring the influence of the valve chamber which is usually in the fully open state [13]. Use TGNET software to build the pipe networks model according to the above principles. The simulation model adopts the boundary conditions of flow at the supply and the pressure at the terminal. The results are shown in Fig. 2.

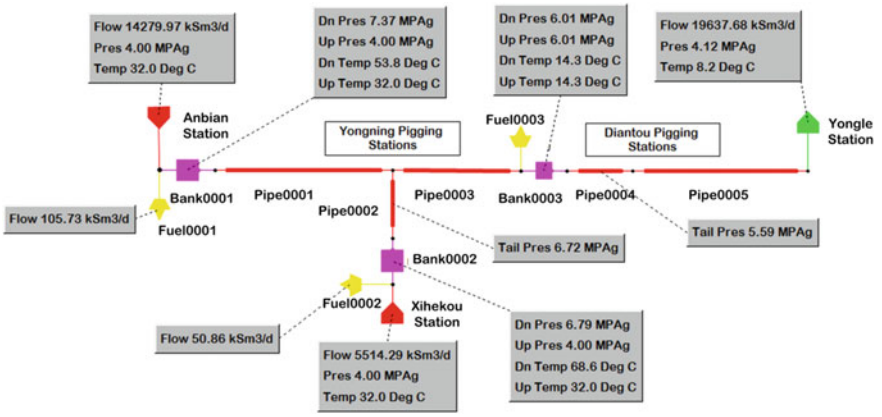

Fig. 2 Steady-state simulation results

Table 2 Comparison of design conditions and simulation parameters

Station	Parameters	Design condition/MPa	Simulation results/MPa	Absolute error/MPa	Relative error
Anbian station	Inlet pressure	4.00	4.00	–	0
	Outlet pressure	7.31	7.37	0.06	0.82%
Xihekou station	Inlet pressure	4.00	4.00	–	0
	Outlet pressure	6.80	6.79	0.01	0.15%
Zhangcunyi station	Inlet pressure	6.02	6.01	0.01	0.17%
	Outlet pressure	6.02	6.01	0.01	0.17%

Compare the simulation results with the design parameters, as shown in Table 2. It can be seen that the error between the TGNET simulation data and the design parameters is small. The absolute deviation of the pressure is less than 0.10 MPa, and the relative error is less than 2.0%.The relative error meets the requirements of engineering error, and the accuracy of the model is verified [14, 15].

3.3 Simulation Analysis of Pipe Storage with Ambient Temperature

The initial ambient temperature is used for steady state simulation to provide the initial state for dynamic simulation, and the dynamic script of ambient temperature changing with time is established.

Select the gas pipeline from Anbian station to Yongning Station and check its dynamic trend report. Figure 3 shows the simulated results of linepack changing with ambient temperature. The red curve represents ambient temperature and the blue curve represents linepack. Linepack during 0:00–7:00 is at the peak, with the lower ambient temperature; and during 14:00–20:00 the linepack is at a low point with the higher temperature. The change of linepack lags behind the change of ambient temperature.

According to Formula (2), the linepack is inversely proportional to the actual average temperature of the gas in the pipe, which is affected by environmental temperature, gas transmission volume, and gas temperature at the starting point of the pipe. Under the condition that other conditions remain unchanged, the ambient temperature affects the gas temperature in the pipeline through heat exchange with the gas transmission pipeline, and then affects the linepack. The natural gas temperature in the pipeline increases with the increase of the ambient temperature. In conclusion, there is a negative correlation between linepack and ambient temperature.

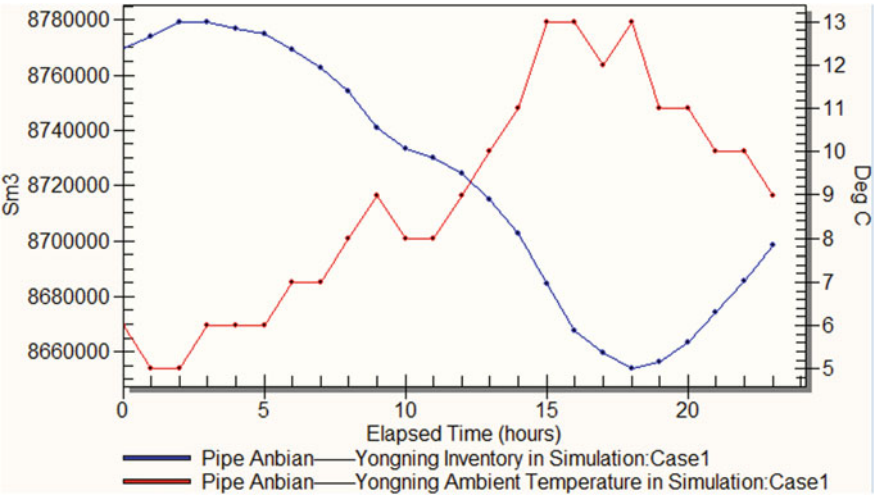

Fig. 3 Variation trends of Anbian-Yongning pipe storage with ambient temperature

4 Conclusion

In this paper, the relationship between influencing factors and linepack is studied by simulation, which provides theoretical basis for calculation of pipe storage, transportation difference control and peak regulation of gas storage. The TGNET simulation model of natural gas long-distance pipeline was established and verified, and the environmental temperature was used as a dynamic script to analyze the change of linepack. It was concluded that:

(1) The pipe network model of Jingxi Third-line was built with the flow of supply and the pressure at terminal as boundary conditions, and the accuracy of the model was verified by validity test and error analysis.
(2) The ambient temperature affects the temperature of natural gas through heat transfer, which indirectly affects the storage size of the natural gas long-distance pipeline.
(3) The storage capacity of natural gas pipeline in Jingxi pipeline is negatively correlated with the ambient temperature, which provides theoretical support for effective control of natural gas storage in long-distance pipeline.

References

1. Zhou C, Xue Q, Xiong B, Zhang G, Pan S, Jia C, Wang Y, Ma F, Sun Q, Guan C, Lin M (2021) Connotation, innovation and vision of "carbon neutral." Nat Gas Ind 41(08):46–57
2. Li L (2021) Development of natural gas industry in China: review and prospect. Nat Gas Ind 41(08):1–11

3. Li D (2021) Technical measures for energy saving and consumption reduction of long distance natural gas transmission pipeline. Clean World 37(06):85–86
4. SY/T 5922–2012 (2012) The operation regulation of gas pipeline
5. Li Y (2019) Study of measurement shortage of Shandong natural gas pipeline and control. M.A. Thesis, China University of Petroleum Shandong
6. Fan M (2017) Study on reliability calculation of Shan-Jing natural gas pipeline network system. M.A. Thesis, China University of Petroleum, Beijing
7. Cao Z (2015) Dynamic simulation on the gas storage and peak shaving of gas pipeline. Contemp Chem Ind 44(10):2349–2351
8. Ju Z (2018) Application of TGNET in natural gas pipeline construction. Oil-Gas Field Surf Eng 37(09):98–100
9. Pi Y (2019) Simulation and application of TGNET software in pipeline network running. Inner Mongolia Petrochem Ind 45(04):20–21
10. Lan Y, Zhang L, Song D, Yang S, Zhang J (2015) The discussion of gas storage and peak shaving methods between pipeline studio and SPS. Petrochem Ind Technol 22(05):22–23+131
11. GB 50251–2003 (2003) Code for design of gas transmission pipeline engineering
12. Yang S (2019) Adaptability analysis of sinopec north China natural gas pipeline network. M.A. Thesis, China University of Petroleum, Beijing
13. Wei M, Yao R (2009) Study of TGNET software in sulige gas field applicability. Petrochem Ind Appl 28(06):57–60
14. Wang W, Fu Z, Liu F, Yang Y, Huang J (2021) Numerical simulation of supply and demand forecasting of multisource and multi-user annular pipeline network. Oil Gas Storage Transp 40(10):1187–1193
15. Wu X, Li Q, Lu H, Yu S, Li L, Wang X (2019) One of forecast methods and the influential factors of naphthalene deposition in the artificial gas pipeline. J Saf Environ 19(03):909–916

Research on Smart Pipeline Network Architecture Based on Pipeline Lifecycle Integrity Management

Xixiang Zhang, Yufeng Yang, Shaohui Jia, Qiang Zhang, and Ranran Wei

Abstract With the increasing maturity of information technology, the research of oil and gas pipelines in smart pipeline networks is becoming more and more mature. At the same time, the construction of an smart pipeline network is also an important part of China's smart energy construction. The establishment of smart pipeline network systems, the use of big data analysis, cloud computing, and other advanced technologies do a good job in data mining, mobile application, comprehensive decision-making, emergency disaster prevention and other support work, which promotes the integration of pipeline management and intelligence, serving as an effective means and inevitable choice to improve the level of oil and gas pipeline management and promote the development of the industry. This paper analyzes the practical needs of China's smart pipeline network, puts forward a smart pipeline network architecture guided by the pipeline lifecycle integrity management, and discusses some problems of China's smart pipeline network.

Keywords Pipeline · Integrity · Life cycle · Smart pipeline network · Big data · Artificial intelligence

1 Introduction

Since 2016, China successively issued documents such as *Guiding Opinions on Promoting the Development of 'Internet + Smart Energy,'* etc., proposing the direction of 'Internet + smartization' for future energy exploration. Under this context, the construction of smart oil and gas pipelines began to flourish. Actually, the Sino-Russian Eastern Route (Heihe-Changling Section) constructed by PipeChina is China's first large-scale smart pipeline, in which smart pipeline technologies were adopted for the first time, linking it to the Internet technology and making a pioneering attempt [1–3].

X. Zhang (✉) · Y. Yang · S. Jia · Q. Zhang · R. Wei
North Petro China Pipeline R&D Center Affiliated to National Pipeline Network Group, National Engineering Laboratory for Pipeline Safety, Langfang 065000, Hebei, China
e-mail: zhangxx11@pipechina.com.cn

X. Liu (ed.), *Proceedings of 2021 China-Europe International Conference on Pipelines and Trenchless Technology*, Lecture Notes in Civil Engineering 212,
https://doi.org/10.1007/978-981-19-4067-5_15

2 Background and Actual Needs

2.1 Development Background of Smart Pipeline Network

In January 1998, the then-Vice President of the United States Albert Gore put forward the concept of 'digital earth' in a speech [8], applying digital technology to reproduce the earth and other fields. As time went by, the application of digital technology has gradually expanded from earth science to the areas of electricity, communications, medical care, transportation and energy. In August 2009, IBM released a report entitled *Smart Earth Prevails in China* [4–7], in which such concepts as Smart Power, Smart Medical, Smart City, Smart Transportation, Smart Supply Chain, and Smart Banks were proposed, making the perception more comprehensive, interconnection smoother, and smart thinking more thorough. In 2015, the Columbia Pipeline Company of the United States applied the smart pipeline solution [9, 10], making it have comprehensive pipeline management functions by integrating pipeline-related aspects including production, operation, risk management, equipment, etc.

In April 2011, the Ministry of Industry and Information Technology of China, together with other departments, jointly issued *Opinions on Accelerating the Deep Integration of Informatization and Industrialization*, emphasizing the importance of information technology in promoting effective services, giving the direction of informatization and industrialization, namely towards intelligence, and introducing smart technologies such as cloud computing and the Internet of Things (IoT). In March 2015, 'Internet+' and other related concepts such as cloud computing, IoT, and big data, appeared in the government work report for the first time, marking that China has entered the era of smart construction. The proposal that pipeline network system should be integrated with IoT, cloud computing, and other advanced technologies were mentioned both in the 2016 *Guiding Opinions on Promoting the Development of 'Internet + Smart Energy'* (National Energy Administration of National Development and Reform Commision [2016] No. 392) and the 2017 *Medium and Long-term Oil and Gas Pipeline Network Planning.* Many scholars in China have carried out related research accordingly [11–15].

2.2 Current Status of Pipeline Integrity Management

Pipeline integrity management is one of the crucial means to ensure the safe operation of pipelines. The United States promulgated the *Natural Gas Pipeline Safety Act* in 1968 and began the work of pipeline protection through legislation. In addition, the *Pipeline Act* of the United Kingdom and the *Special Law for Public Use of Deep Underground Space* of Japan [1] all mention the importance of protecting pipeline construction and operation processes in accordance with the law.

China's State Council issued the *Oil and Natural Gas Pipeline Protection Law of the People's Republic of China* in 2010, which clarified the legal rights and obligations when oil and natural gas pipelines intersect with the establishments of other projects, providing laws for the pipeline protection work.

By referring to integrity management experiences in other countries, China formed its own integrity management process [4] by conducting many types of research and practices. In 2015, the national standard GB 32,167–2015 *Oil and Gas Pipeline System Integrity Management Specifications* was released. Later in 2019, the ISO 19345–2019 Pipeline Integrity Management Specifications was issued, marking China's pipeline integrity management has reached the world's highest level.

2.3 Actual Needs

2.3.1 Lack of Orientation Regarding How to Explore Smart Pipe Network

The current smart pipe network architecture mostly relies on IoT technology, cloud computing, big data and other algorithms to form a relatively complete management architecture. However, to what extent this kind of architecture can promote pipeline management still lacks scientific evidence. The lack of a scientific guide for the construction of a smart pipeline network is a systematic bottleneck to be dealt with by the industry urgently.

2.3.2 Insufficient Digitization Levels of China's Pipeline Industry

At present, there are many problems in the digitalization of China's pipeline industry, including difficulty in pipeline data collection, low collection efficiency with redundant data, etc. Moreover, most of the pipeline data are still recorded manually, impairing the timeliness and accuracy of data collection.

3 Smart Pipeline Network Architecture Based on Pipeline Lifecycle Integrity Management

Onshore pipeline integrity management runs through the entire lifecycle of the pipeline, including phases such as feasibility study, design, procurement, manufacturing, transportation, storage, installment, pre-commissioning and commissioning, handover, operation, maintenance, repair, and suspense/discard. The specific processes include data management, risk evaluation, monitoring, completeness evaluation, mitigation measures, and evaluation and improvement of performance and

efficiency. According to the relevance of different functions, this paper divides the pipeline integrity management process into three links: the data acquisition link, the inspection and evaluation link, and the decision-making improvement link, as shown in Fig. 1.

In view of the above analysis, a smart pipe network architecture based on Pipeline lifecycle integrity management generally includes a state-sensing layer, a data-transmitting layer, a data-processing layer, and a decision-supporting layer. A 'terminal + cloud + big data' architecture is formed, which clarifies the functions and roles of each layer as shown in Fig. 2.

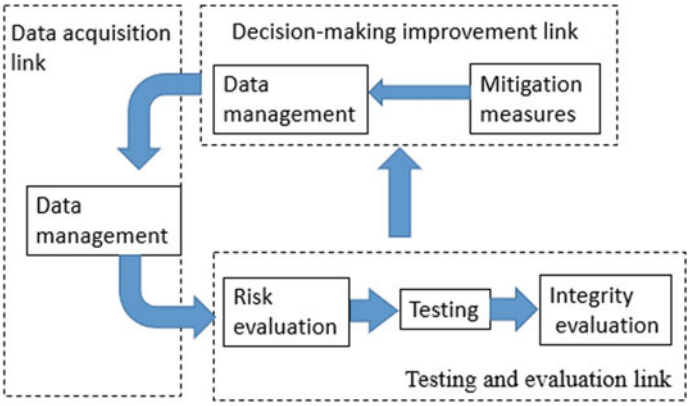

Fig. 1 Pipeline lifecycle integrity management process

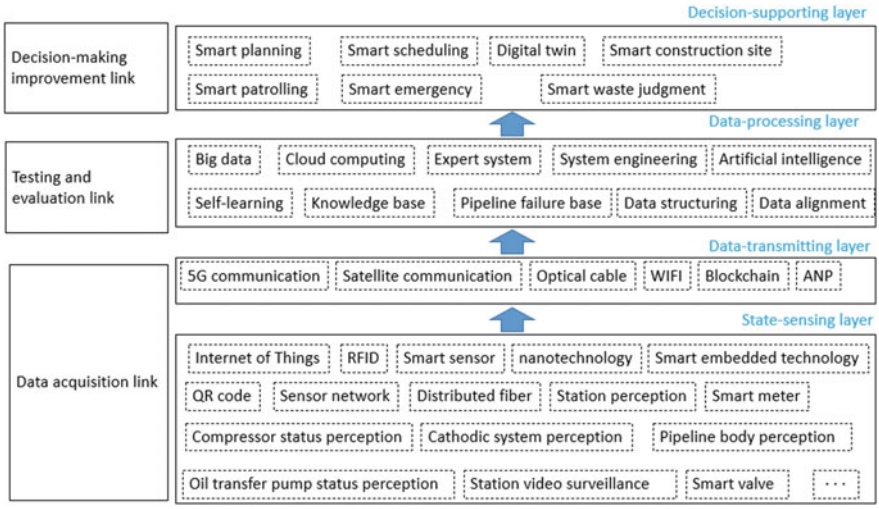

Fig. 2 Smart pipe network architecture based on pipeline lifecycle integrity management

3.1 Data Acquisition Link

The first link of pipeline lifecycle integrity management is to acquire data, which relates to the collection and transmission of pipeline-related data and involves the corresponding state-sensing layer and data transmission layer in the smart pipeline network architecture. Data management includes definition and collection of necessary data and information for pipelines and perception of data throughout the pipeline's life cycle, including phases such as feasibility study, design, procurement, manufacturing, transportation, storage, installment, pre-commissioning and commissioning, handover, operation, maintenance, repair, and suspense/discard. The state-sensing layer is to apperceive the data of the pipeline, and then the apperceived data is uploaded to the next level through the data-transmitting layer.

Data acquired for integrity management mainly comprises pipeline station data perception, pipeline body data perception, pipeline line data perception, surrounding environment data perception, and emergency data perception. At present, most of the pipeline data-collecting methods are based on 'manual collection + upload,' while some systems are based on 'automatic collection + upload,' such as pipeline system SCADA, pipeline integrity management system PIS, natural gas and pipeline system ERP, pipeline construction management system PCM and pipeline production management system PPS. Notably, the pipeline system SCADA can automatically collect some data of the pipeline, such as pressure, temperature and flow data. Besides, it can simplify the management process of the pipeline system (its valves, for example) through the remote terminal unit (RTU) and programmable logic control (PLC)). Although it has played an essential role in the pipeline industry, its functions such as smart perception and analysis need to be further strengthened.

As for station perception, the IoT technology is adopted to digitally transform pipeline station instruments to automatically sense and record the data related to conveying pressure, medium temperature, and medium flow rate, etc. Smart sensors around the compressors and pumps in the station yard are installed to monitor and record data related to temperature, noise, etc., forming a sensor network to sense their status. The valve perception is realized by installing sensors that monitor the pressure and flow rate of the medium on both sides of it to detect the jam and leakage in time automatically. Concerning the cathodic protection systems, satellite clock synchronization technology and smart sensor technology are adopted to automatically record and upload the power-off potential of equipment such as process pipelines and storage tanks in the station. Besides, laser cameras and infrared cameras are used to perform video perception on the station yard, and to record and upload real-time images. Smart inspection robots equipped with flammable gas leak detectors, temperature sensors, etc. are taken to conduct regular inspections on the station yard. Technologies such as QR code, radio frequency identification (RFID) and image recognition are adopted to grasp the real-time status of station equipment accurately, and to record and upload the corresponding data.

Pipeline body perception is realized by equipping pipeline robots with internal and external pipeline inspection devices, stress monitoring devices, and vibration

monitoring devices through nanotechnology to record the body information, such as weld defects, sheet defects, pits, fatigue, etc. Meanwhile, perations such as pipeline internal and external inspection are carried out based on the risk assessment results. In the stages of pipeline procurement, manufacturing, transportation and storage, QR code, radio frequency identification (RFID) and other technologies are adopted to collect and record in advance the pipeline-related parameters and data. Then data management is carried out for later data traceability and simulation analysis.

Pipeline line perception is realized by installing vibration warning systems and cameras in third-party construction sites to monitor and upload the vibration conditions and video images in real time. Pipeline sites that may cause a serious adverse impact on society and the environment if leakage happens are equipped with explosive gas detection devices and video surveillance devices to detect their conditions in real time and upload data accordingly. Pipeline inspection is achieved by smartly planning the inspection route through GIS and GPS technology, recording the inspection route and time of the inspector. The inspector is equipped with GPS inspection devices to automatically report such information as the pipeline coordinates and the pipeline pile, as well as alert notification if something unusual happens, which can also be conducted by using smart inspection robots. Devices to monitor temperature, pressure, and flow sensors of the pipeline, and video instruments are installed at the pipeline crossings to record its status information that is then uploaded in real time to realize real-time perception. The smart line patrol is realized by equipping drones with temperature sensors, acousto-optic sensors, remote sensing image recognition devices, etc., to record and upload the data related to the sensors. An optical fiber pipeline safety warning system is installed along the pipeline to record and upload pipeline vibration status that is taken as the data source for automatic pipeline line perception. The cathodic protection piles along the pipeline are upgraded to smart ones in order to realize automatic measurement, remote monitoring and instant upload, as well as monitor the stray current along the pipeline.

Environmental perception is realized by installing distributed optical fiber tools for monitoring soil displacement in key areas such as geo-hazard prone sites to record and upload soil displacement data that is used together with satellite remote sensing images to record, alarm and predict geological disasters around the pipeline. Sensors to detect atmospheric humidity, temperature and pH are installed along the pipeline to monitor the atmospheric corrosivity of crossing and aerial crossing of the pipeline and exposed sections. Precipitation sensors are installed in areas prone to geological disasters such as landslides and mudslides to record and upload precipitation data and monitor the situations in those areas in real time. Meanwhile, it can also perform functions such as flood prediction based on historical data. Sensors to detect soil moisture, soil pH, etc., are installed in areas with low altitudes, where rivers cross, lakes, swamps, and wetlands to monitor the degree of soil corrosion. The environmental data on the pipeline route to be laid is sensed and recorded to provide a basis for later analysis and decision-making in the feasibility and design stages.

Pipeline emergency perception is realized by establishing a pipeline emergency resource management system to record and upload real-time data related to pipeline

maintenance, emergency repair, and equipment configuration, track the distribution of staff involved in pipeline maintenance and emergency repair, and collect public emergency resources along the pipeline such as public security, medical treatment, and fire protection to have an overall perception of emergency forces along the pipeline.

Data management also involves the safe and reliable transmission of collected data, which is completed by the data-transmitting layer of the smart pipe network. The data-sensing layer records the relevant data of the pipeline and then transmits it through the data-transmitting layer by dint of different manners. Large-volume of audio, image, video, and pipeline data can be instantly transmitted and uploaded by adopting 5G technology in areas covered communication base stations. In areas not covered by communication base stations, such as sparsely populated deserts and mountainous regions, relevant data can be transmitted through mobile communication satellites. In addition, pipeline communication optical cables and WIFI where conditions permit can be used as supplementary data transmission. Technologies such as APN private networks and blockchain are used in the process of data transmission to establish encryption channels so as to encrypt data to prevent it from being invaded securely.

3.2 Testing and Evaluation

The testing and evaluation link includes three parts: risk assessment, testing, and integrity assessment. It mainly revolves around data processing and analysis based on the data obtained in the data acquisition link.

Data processing is to handle the data in a unified manner. The data collected and transmitted through the data acquisition link are various, and different data are stored in different formats. To reduce storage space and improve computing efficiency, the data is structured to form unified formats such as PIDM so as to facilitate storage and recall. Besides, although the same indicators can sometimes be obtained through different paths, there are some discrepancies in the values corresponding to those indicators. So data alignment is required, including data verification and cleaning, to ensure data continuity and integrity.

The data analysis includes risk evaluation, monitoring, integrity evaluation and various data algorithms. The risk assessment of the pipeline is carried out according to the data obtained, and the semi-quantitative risk assessment of the entire pipeline and the quantitative risk assessment of the key sections of the pipeline are carried out according to the way data is acquired and the degree of refinement. Corresponding detection methods, such as internal detection, external detection, direct evaluation and pressure test, are chosen to monitor the pipeline according to the risk assessment results of the previous step. Pipeline integrity assessment based on risk assessment results and testing results are conducted, and measures such as risk elimination, physical control, and procedural control are adopted. In the process of testing and evaluation, cloud computing is fully exploited. Based on various professional file

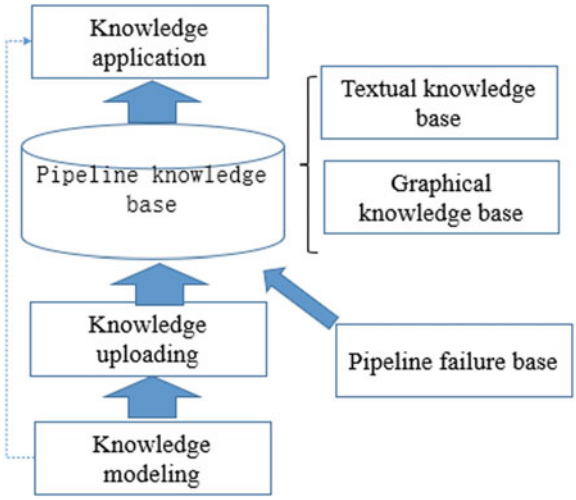

Fig. 3 Architecture of pipeline knowledge base

systems distributed on the Internet, users upload the data to be evaluated through different terminals; the system terminals on the cloud platform then perform calculation and evaluation regarding data about instrument abnormalities, valve abnormalities, station image abnormalities, internal and external detection results, image abnormalities in high-consequence areas, soil displacement, and flammable gas leakage by dint of methods such as big data, expert system, system engineering, and self-learning. At the same time, various professional knowledge is collected to form a pipeline knowledge base (as shown in Fig. 3), which includes knowledge modeling, knowledge upload, pipeline knowledge base and knowledge application. Meanwhile, the pipeline knowledge base combines with the relevant content of the pipeline failure database to form the pipeline knowledge neural network that can optimize the logical relationship between the various subjects and elements in the pipeline knowledge map. The relevant calculation and evaluation methods are continuously upgraded and optimized and the utilization and reasoning efficiency of the pipeline data are improved. Eventually, a textual knowledge base and a graph knowledge base are formed, which are then applied to improve the decision-making process.

3.3 Decision-Making Improvement Link

The decision-making improvement link includes two parts: mitigation measures, and efficiency evaluation and improvement. The results from testing and evaluation are analyzed by the advanced technologies such as cloud computing and big data in the previous step to provide pipeline operators with the best safety, efficiency, and environmental protection. The smart planning function is applied in the pipeline feasibility study phase and the design phase; the smart site function is applied in the

pipeline construction phase; the smart scheduling, inspection and emergency function is applied in the pipeline operation phase; and the smart waste judging function is applied in the pipeline suspension/discard phase. The pipeline digital twin is used to virtually map the physical quantity, object, and scale of the pipeline entity. It can be applied in the pipeline lifecycle for functions such as simulation, analysis, and prediction.

4 Conclusion

4.1 Pipeline Integrity Management Helping the Realization of Smart Pipe Network

There is an excellent industrial foundation for pipeline integrity management in China. As China launched its own ISO standard for pipeline integrity management, the integrity management in China's pipeline industry has reached the international level, which marks a milestone of China's achievement in pipeline integrity in recent years. On the one hand, the existing pipeline integrity management system can provide oriented support for the smart pipe network so that it has a direction to expand and develop, making it easier to achieve safety, efficiency and environmental protection goals. On the other hand, many indicators, processes, and mechanisms in the existing pipeline integrity management system have been established, which can provide a great convenience for the smart pipeline network, while avoiding redundant construction, saving money, and reducing the workload of the grassroots staff.

4.2 Smart Pipeline not Equivalent to Smart Pipeline Network

The function of the smart pipeline is to ensure that if certain parameters of the pipeline are abnormal, such as the pressure is lower than the critical value, or the pipeline appears to be leaking, the pipeline RTU valve will be automatically closed and an alarm is issued to complete the smart pipeline operation. If the same scenario occurs in a smart pipe network, it will analyze the cause of the abnormality based on the perceived historical data, environmental data, ontology data and through the Internet, big data, artificial intelligence, cloud computing, expert system, and system engineering. It will further determine whether there is third-party construction damage, whether stress corrosion cracking on the pipeline occurs, or whether the pipeline is broken or sheared by geological disasters, and judge whether there is a false alarm. If the valve is to be closed, we should consider the operational status of the compressor and pump, and whether it is necessary to open the bypass line and increase transmission and deployment of adjacent pipe networks to complete the smart decision-making process.

4.3 Relationship Between Smart Pipeline Network and Digital Twin

The pipeline digital twin technology and the smart pipeline network are relatively independent, which means that the former does not have to be realized through the latter, and vice versa. According to PetroChina's definition of a smart pipeline network, its basic characteristics are pipeline digitization, comprehensive perception, integration and interconnection, and decision support. As long as a pipeline network has these characteristics, even if it has not adopted digital twin technology, it can be said to be a smart pipeline network.

4.4 China's Smart Pipeline Network Boasting Greater Advantages Than that in Foreign Countries

An interconnected pipeline network has been established within the EU, but it is managed separately by operating companies set up in each country. each country, and pipeline, which makes it unable to become a whole pipeline network, and therefore cannot realize smart management. In the United States, several pipeline network companies are responsible for the operation of the national network, and there are certain defects in the national system that make it impossible to operate it in a unified manner. In Russia, the work is now focused on energy development, and progress in smart pipeline networks is relatively slow. In contrast, China's advantages existing in its political system, together with the establishment of PipeChina, make it gradually form an 'X + 1 + X' management grid, and now a nationwide, interconnected pipeline network has been formed. In addition, information technology in China has achieved obvious progress in recent years, so our country's smart pipeline network will certainly accomplish great success on a global scale.

Project Research and Application of Key Technologies for Smart Pipeline Network Construction and Operation (2019E-20), a major scientific project initiated by China National Petroleum Corporation;

Security Technology and Equipment R&D for National Oil and Gas Reserve (2017YFC0805800), a national key project funded by the Central Government.

References

1. Dong S (2020) A twenty-year review of china's oil and gas pipeline integrity management and development suggestions. Oil Gas Storage Transp (03)
2. Li J (2018) Identification of high-consequence areas and reliability study about offshore gas pipelines. Xi'an University of Architecture and Technology, Xi'an

3. Su H (2018) Research on reliability evaluation of natural gas supply pipeline network. China University of Petroleum, Beijing
4. Chen P, Feng W, Yan B (2020) How to construct integrity management system for the entire life cycle of oil and gas pipelines. Oil Gas Storage Transp 39(01):40–47
5. Jiang C (2020) Engineering management and technological innovation of the sino-russian east route natural gas pipeline. Oil Gas Storage Transp 39(02):121–129
6. Gong J, Xu B, Zhang W (2020) Thoughts on the implementation and operation of smart technology on the Sino-Russian east route natural gas pipeline. Oil Gas Storage Transp 39(02):130–139
7. Li Z, Wang J, Wang X, Dong L, Liu D, Li M, Ye Q (2017) How to construct smart pipeline system in the era of smarter energy. Oil Gas Storage Transp 36(11):1243–1250
8. Cheng W, Wang J, Wang X, Wang X (2018) Discussion on the status quo and key technologies concerning smart pipeline construction in China. Oil Forum 37(03):34–40
9. Dong S, Zhang Y, Zuo L (2021) Development status and countermeasures of domestic and foreign smart pipe networks. Oil Gas Storage Transp 40(03):249–255. https://mall.cnki.net/magazine/article/CJFD/YQCY202103002.htm
10. Accenture. Accenture and GE (2018). Accessed 20 Nov 2020, https://www.accenture.com/us-en/insights/industry-x-0/accenture-ge-alliance
11. Li B, Wang X, Xu B Sun W, Wang X, Zhao Y (2019) The status quo and intelligence trend of oil and gas pipeline operation and management at home and abroad. Oil Gas Storage Transp (03)
12. Shui B, Zhang D, Li L, Xue L, Chen G (2020) Main characteristics and construction concept concerning smart pipeline network. Oil Gas Storage Transp 39(05):500–505
13. Cai Y, Jiang H, Wang J, Wang X, Li L, Chen G, Zhang H (2019) The overall architecture and key technologies for smart pipelines. Oil Gas Storage Transp 38(02):121–129
14. Li H (2018) The status quo and development trend of smart pipeline technology. Nat Gas Oil 36(02):129–132
15. Zhang H, Cai Y, Li B, Sun W, Wang H, Yang X (2018) Key technologies for monitoring equipment conditions on smart pipeline stations. Oil Gas Storage Transp 37(08):841–849

Research on Control System of Wheeled Pipeline Robot

Minghang Jiang, Hejin Xiong, and Chenhui Fan

Abstract At present, the working environment of pipeline robot is more and more complex, and the stability of the work is higher and higher, On this basis, the control of pipeline robot is discussed from two aspects of PID controller and ADRC controller. According to the model of pipeline robot under general conditions, the transfer function is calculated. Different interference is simplified into different function expression, using Simulink module to build the system model, adding different interference, simulation experiments, respectively under the PID control and active disturbance rejection controller simulation curve, in order to analyze the anti-interference ability of the two controllers. The results show that compared with the active disturbance rejection controller, no matter in adjusting time or steady-state error, the active disturbance rejection controller has better control effect. it can reach a stable state in a shorter time, and the overshoot is smaller. At the same time, the ADRC has stronger anti-interference ability and robustness.

Keywords Wheeled robot · PID control · Active disturbance rejection control

1 Introdction

According to the moving mode of pipeline robots at home and abroad, self-driven pipeline robots include piston type, wheel type, foot type, crawling type, peristaltic type, and crawler type, which can be roughly divided into six kinds [1]. Each has its advantages and disadvantages. According to the actual situation, wheeled pipeline

M. Jiang (✉) · H. Xiong · C. Fan
College of Automation, Wuhan University of Technology, Wuhan 430070, China
e-mail: jiangminghang@whut.edu.com

H. Xiong
e-mail: xionghejin@whut.edu.com

C. Fan
e-mail: fanchenhui@whut.edu.com

X. Liu (ed.), *Proceedings of 2021 China-Europe International Conference on Pipelines and Trenchless Technology*, Lecture Notes in Civil Engineering 212,
https://doi.org/10.1007/978-981-19-4067-5_16

robot is studied because wheeled pipeline robot has the advantages of simple structure, continuous and stable walking, fast speed, high reliability and high walking efficiency, and pipeline robot can carry its own power source [2] and has autonomous walking ability. Walking in the pipeline, the uneven road surface will make the robot vibrate, thus affecting the clarity of the image, bringing interference to the whole system; In the process of avoiding obstacles, sudden changes in speed and direction will also affect the stability of the whole system. In order to improve the anti-interference performance of the system and ensure the safe and stable operation of the system, anti-interference design of the system is needed.

Now, in the field of process control and motion control, the classical PID control technology is widely used, and is still one of the most widely used control technology. PID control still has some shortcomings, the initial control force of PID controller is too large, the system response will appear large overshoot [3;] The introduction of error integral feedback in PID control will make the closed-loop system slow, easy to produce oscillation and integral saturation, which is not expected in the actual control [4]. Han Jingchen, a researcher of Chinese Academy of Sciences, has researched the ADRC technology in the late 1980s and proposed the idea of Active Disturbance rejection Controller (ADRC). Active disturbance rejection control technology is a perfect combination of classical control theory and modern control theory, which can control and adjust nonlinear uncertain objects. Observation and compensation methods are adopted to greatly improve the dynamic index of active disturbance rejection controller [5]. Active Disturbance Rejection Control (ADRC) developed in recent years has made important progress in both theoretical research and engineering application [6]. Because it does not need accurate mathematical model, and has the characteristics of strong robustness and small computation, it has also been successfully applied to multi-class control systems [7–9]. The reason why ADRC is used to resist interference is that the environment of the pipeline is completely unknown, and ADRC does not strictly depend on the accurate model of the controlled object, because the extended state observer can estimate the influence of model uncertainty or external disturbance on the system in real time [10].

2 PID Controller of Wheeled Pipeline Robot

2.1 Motion Model Analysis of Pipeline Robot

This paper takes an independent dual-drive robot as an example. It consists of two wheels, and its left and right structures are independently driven by two motors (Fig. 1).

According to the relationship between the physical quantities in the figure, the following formula can be obtained:

$$\Delta l = 0.5(v_R + v_L)\Delta t \sin \Delta\theta \tag{1}$$

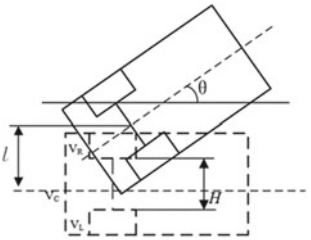

Fig. 1 Motion model of pipeline robot

$$\Delta\theta = \frac{(v_R - v_L)\Delta t}{H} \tag{2}$$

$$v_C = 0.5(v_R + v_L) \tag{3}$$

In the formula, Δl represents the distance between the midpoint of the two driving wheels of the inspection robot and the center line of the tunnel. Δt represents the time interval between two moments; V_R represents the speed of the right driving wheel; V_L represents the left driving wheel speed; θ represents the included Angle between the traveling direction of the inspection robot and the center line of the tunnel. H represents the distance between two driving wheels; V_C represents the speed of the inspection robot wheel distance from the center. Considering that the path of inspection robot is continuous in the process of movement, after Laplace transform is performed on the above equation, the relationship in the complex frequency domain is as follows:

$$\theta(\mathrm{s}) = \frac{v_R - v_L}{Hs} \tag{4}$$

$$l(s) = \frac{1}{2s}(v_R + v_L)\sin\theta = \frac{v}{s}\sin\theta \tag{5}$$

$$d(s) = \frac{v}{Hs^2}\Delta v(s) \tag{6}$$

where ΔV(s) represents the speed difference between left and right motors. The kinematic structure of the pipeline robot can be obtained from the above equation, as shown in the figure (Fig. 2):

Take the most widely used pipeline, Pipe of φ320mm—φ380mm inner diameter, The maximum working speed is $V_m = 0.2$ m/s, the maximum traction force is F = 300 N, the radius of the driving wheel is $r = 0.0025$ m, the angular velocity of the driving wheel is $\omega = 8$ rad, and the transmission ratio is $i = 15$ [11].

$K_R = K_I = K_m 2\pi r/60i$, T_m represents the time constant of the DC motor, then the relationship between the armature voltage and the linear velocity of the left and right driving wheels is:

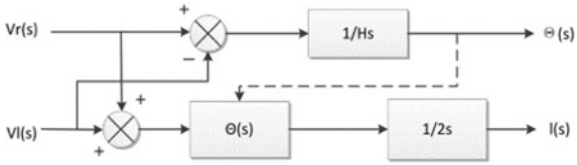

Fig. 2 Kinematic structure block diagram of pipeline robot

$$v_R(s) = \frac{K}{1 + T_m s} U_R(s) \tag{7}$$

$$v_L(s) = \frac{K}{1 + T_m s} U_L(s) \tag{8}$$

After small deviation linearization, the mathematical model of the pipeline robot can be obtained. The Laplace transform value of the armature voltage of the two motors can be represented by ΔU(s), which is written in the form of transfer function as follows:

$$G(s) = \frac{l(s)}{\Delta U(s)} = \frac{K T_m v_c}{2Hs^2(T_m s + 1)} \tag{9}$$

2.2 PID Controller Model Simulation

As can be seen from the figure, the adjustment time is about 1.5 s, the rise time is about 0.8 s, the overshoot is less than 10%, and finally reaches the stable state, basically completing the control task of PID controller (Figs. 3 and 4).

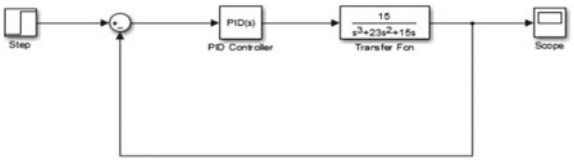

Fig. 3 PID controller model simulation block diagram

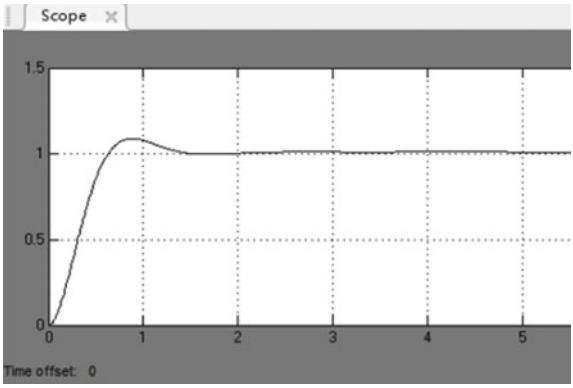

Fig. 4 PID controller model simulation curve

3 Active Disturbance Rejection Controller for Wheeled Pipeline Robot

3.1 The Basic Structure of Active Disturbance Rejection Controller

ADRC is generally composed of three parts, including arranged transition process (TD), nonlinear state error feedback (NLSEF) and extended state observer (ESO) [12] (Fig. 5).

Arranging transition process Arranging transition process can preprocess the given input value of the system. The nonlinear state error feedback can be combined with the compensation of the extended state observer and the output of the tracking differentiator to obtain a suitable input control quantity, and then realize the purpose

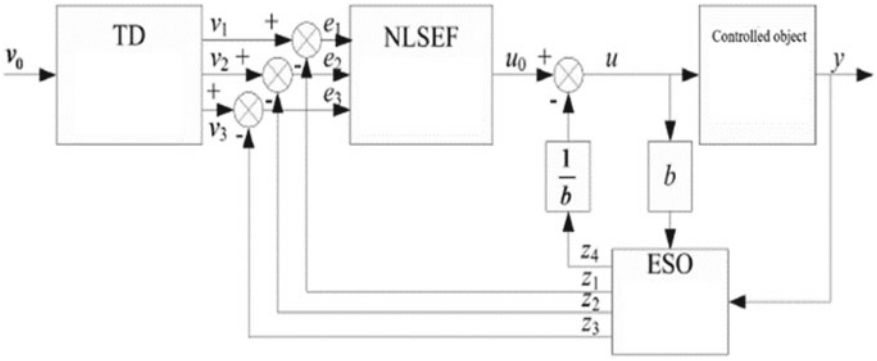

Fig. 5 Third order structure diagram of active disturbance rejection controller

of compensating the unmodeled disturbance and reducing the overshoot. The extended state observer can effectively observe and track the state variables of each order of the system as well as the combined effects of the unmodeled dynamic parts of the system and external disturbances, and estimate and compensate the unmodeled dynamics and external disturbances of the system [13].

3.2 *Active Disturbance Rejection Control Simulink Simulation Model*

Set the initial state as: velocity $V_0 = 0$, amplitude $A_0 = 0$, Angle $\boldsymbol{\theta_0} = 10°$; The steady state is velocity $V_1 = 0.2$ m/s, amplitude $A_1 = 0$ and Angle $\boldsymbol{\theta_1} = 0°$. In the ideal state, the simulation results are as follows (Figs. 6, 7, 8 and 9):

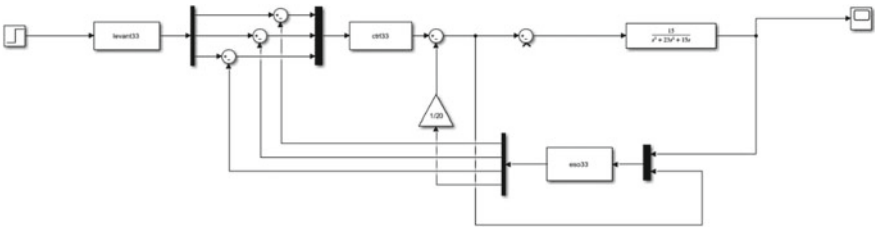

Fig. 6 Simulation model of active disturbance Rejection controller

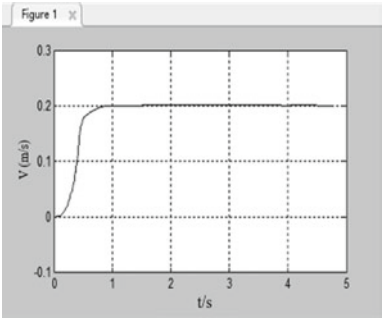

Fig. 7 ADRC speed simulation curve

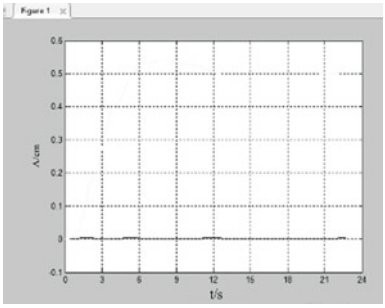

Fig. 8 ADRC amplitude simulation curve

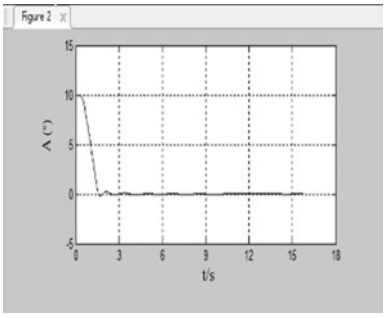

Fig. 9 ADRC Angle simulation curve

4 Analysis of Active Disturbance Rejection Control and PID Anti-interference

4.1 Velocity Anti-Interference Simulation

ADRC has a faster response speed than PID and can rise to the stable value set by the system in a shorter time. The overshoot of ADRC is smaller than that of PID, and the deviation of the system is smaller, indicating that the ADRC system has small fluctuation and strong stability. ADRC requires less stabilization time than PID, and the system can stabilize at the desired set point more quickly (Fig. 10 and Table 1).

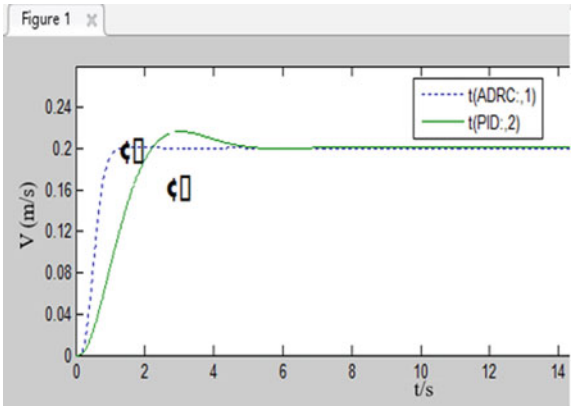

Fig. 10 ADRC and PID speed simulation curve

Table 1 ADRC and PID speed regulation comparison

Project	Rise time (s)	Stable time (s)	Overshoot amount
ADRC	1	2	0
PID	3	5	10%

4.2 Amplitude Anti-interference Simulation

The main method used for pavement smoothness is harmonic superposition method, also known as trigonometric series synthesis method, which decomposes the roughness of pavement and finally expresses it as the sum of a large number of sine or cosine functions with random phase [14].

We take an approximate triangular wave model to replace the road roughness model as the external interference of the robot system, and add the interference lasting for 4 s.

The system of PID controller fluctuates up and down with disturbance, and the amplitude reaches 0.35 cm, which takes about 10 s to stabilize. However, the system of active disturbance rejection controller fluctuates very little after being affected by disturbance and basically stays near zero value.For the random environment faced by the robot, random interference is added to the simulation model (Figs. 11 and 12).

The influence of random disturbance on PID control system is much greater than that on ADRC control system. The system using PID controller vibrates up and down along with the direction of external disturbance fluctuation, and the amplitude is more than 0.2 cm. The system using active disturbance rejection controller fluctuates very little and basically stabilizes at the same value before interference is added (Table 2).

After the ADRC is added to the pipeline robot system, the vibration of the robot caused by the unevenness of the unknown road surface is greatly reduced, the amplitude is effectively reduced, and the robot runs more smoothly.

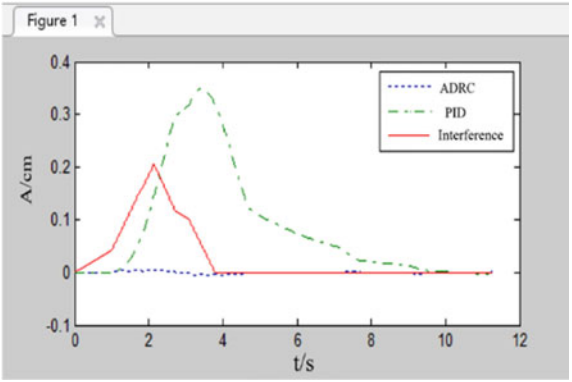

Fig. 11 ADRC and PID triangle wave amplitude simulation curve

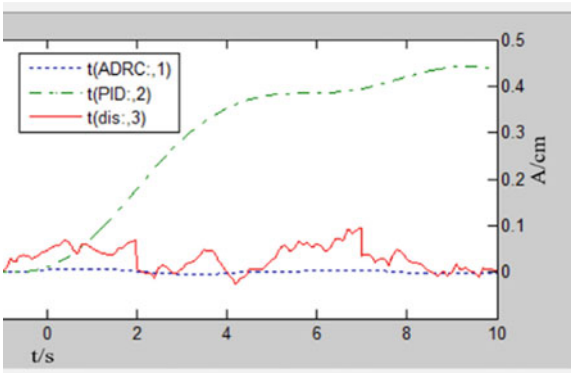

Fig. 12 ADRC and PID random disturbance amplitude simulation curve

Table 2 ADRC and PID triangular wave amplitude ratio to random interference

Project	Triangular wave interference overshoot	Random interference overshoot
ADRC	0.02	0.01
PID	0.35	0.45

4.3 Angle Anti-interference Simulation

The deviation Angle of the robot before starting is set as 10°. When the robot starts to move, the ADRC system only needs 2 s to adjust the deviation Angle to 0°, and the robot runs along the center line of the tunnel. The PID system adjusted the deviation Angle to 0° at 3 s, but the adjustment of the robot did not stop, but deviated in the opposite direction, until about 8 s, the system was stable in the direction of the tunnel center line (Fig. 13 and Table 3).

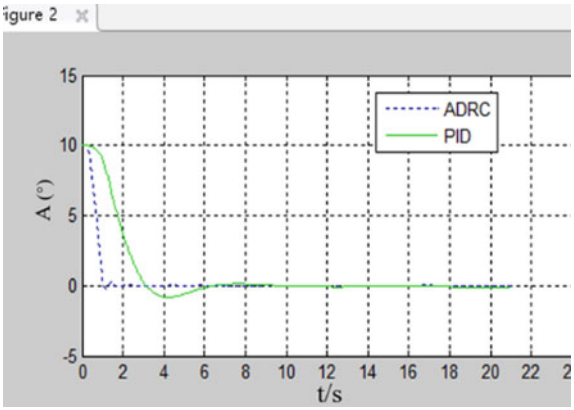

Fig. 13 Deviation Angle simulation curve of ADRC and PID

Table 3 Comparison of DEVIATION Angle between ADRC and PID

Project	Overshoot amount	Stable time (s)
ADRC	0	2
PID	10%	8

In order to verify that the ADRC system can guarantee the stable driving direction of the robot, we added a mutation signal with amplitude of 10 and pulse width of 4 s to observe the anti-jamming performance of PID and ADRC (Fig. 14).

When the external disturbance is added, the robot of ADRC system returns to the stable state within 7 s, while the robot of PID system needs 15 s to adjust to the stable state, and then needs 5 s to slowly adjust to the stable state. Under the same external disturbance, the fluctuation of ADRC system is controlled within the range of 1°,

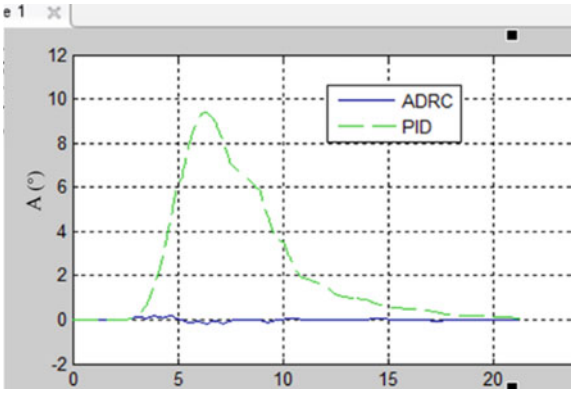

Fig. 14 ADRC and PID add the simulation curve of Angle interference

while the fluctuation of PID system is more than 9°. To sum up, the ADRC system has stronger stability and anti-interference performance in the direction of driving against the disturbance of external mutation.

5 Conclusion

In this paper, the active disturbance rejection control technology is applied to the wheeled pipeline robot. By comparing with the PID control system, the conclusions are as follows:

Compared with active disturbance rejection controller, PID controller has better control effect in adjusting time and steady-state error, and can reach stable state in shorter time and overshoot is smaller. In the simulation experiment of velocity anti-interference, amplitude anti-interference and Angle anti-interference, PID controller will go through a process of fluctuation with interference after being disturbed, while the fluctuation of active disturbance rejection controller is very small and can be ignored basically. Therefore, for the control system of pipeline robot, the anti-interference effect of active disturbance rejection controller is better than that of PID controller, which has robustness.

References

1. Gan X, Xu B, Dong S et al (2003) The development of pipeline robots is piling up. Robot Technol Appl 2003(6):5–10 (in Chinese)
2. Ou CW, Chao CJ, Chang FS, et al (2017) Design of an adjustable pipeline inspection robot with three belt driven mechanical modules. In: IEEE International Conference on Mechatronics and Automation. IEEE, pp 1989–1994
3. Su S (2011) Research on active disturbance rejection controller and its application. Jiangnan University (in Chinese)
4. Zhao F, Li H (2015) Research on PID controller improvement method. Control Eng 22(3) (in Chinese)
5. Han J (2007) Active disturbance rejection control technology. Front Sci 2007(1) (in Chinese)
6. Chen ZQ, Cheng Y, Sun MW et al (2017) Surveys on theory and engineering applications for linear active disturbance rejection control. Inf Control 46(3):257–266
7. Wang SX, Ren C, Ma SG (2017) Active disturbance rejection control with friction compensation for an omnidirectional mobile robot. Control Theory Appl 34(10):1285–1292
8. Ruan XG, Wang X, Chen ZG (2015) Modeling and active disturbance rejection control algorithm of single wheel robot. Control Decis 30(12):2253–2258
9. Guo YN, Zhang Z, Gong DW, et al (2021) Optimal active-disturbance-rejection control for propulsion of anchor-hole drillers. Sci China Inf Sci 64(4). https://doi.org/10.1007/511432-018-9815-8
10. Zhao R, Li H, Miao J, et al (2008) The formation and development of active disturbance rejection theory. In: 2008 national automation application technology academic exchange conference (in chinese)
11. Li Y, Cao J, Liao J, et al (2013) Structural design of supporting wheel type pipeline robot traction mechanism. J Beijing Inst Petrochem Technol (in chinese)

12. Han J, Zhang R (1999) Error Analysis of second order expansive Observer. J Syst Sci Math 1999(4):465–471 (in Chinese)
13. Ye G (2013) Robot joint control system based on active disturbance rejection control. Zhejiang University of Technology (in Chinese)
14. Liu N (2011) Multi-sensor Information fusion filtering and performance analysis. Zhengzhou University (in Chinese)

Numerical Analysis on Mechanical Behavior of GFDST Columns with Stainless Steel Outer Tubes

Baowen Hou, Yue Wang, Huanze Zheng, and Jia Peng

Abstract Grout-filled double skin tubular (GFDST) columns can avoid the adverse effects of steel tube corrosion on structural members and decrease the self-weight of the members to further reduce their response under earthquake action. A three-dimensional solid numerical modeling was established with a GFDST column with stainless steel outer tube as the object. The effect of the stainless steel outer tube thickness, the carbon steel inner tube width, and whether grout is filled between the tubes on the failure modes, load–displacement curves, and ultimate strength of GFDST columns with stainless steel outer tubes were analyzed based on the Finite Element Modeling (FEM). Results show that the FEM results are in good agreement with the experimental results. The failure modes of GFDST columns with stainless steel outer tubes are outward local buckling, and it can be seen from the stress nephograms that the location where buckling occurs is also the location of high stress in the member. With the increase of stainless steel outer tube thickness, the ultimate strength is increased. Increasing the carbon steel inner tube width has little effect on the ultimate strength of specimens with grout infilled and has a significant effect on the ultimate strength of specimens without grout infilled. The load versus displacement curves obtained from experiment and FEM have an initial linear stage followed by a transitional and plastic stage. Subsequently, the curves decrease slowly.

Keywords GFDST · Compressive behavior · Stub columns · Stainless steel

1 Introduction

Concrete-filled steel tube (CFST) members, combined structural members formed by filling thin-walled steel tube with concrete, have good mechanical behavior and

B. Hou · Y. Wang
CCCC Fourth Highway Engineering Co., LTD., Beijing 100124, China

H. Zheng · J. Peng (✉)
College of Architecture and Civil Engineering, Beijing University of Technology, Beijing 100124, China
e-mail: JiaPeng1469@emails.bjut.edu.cn

X. Liu (ed.), *Proceedings of 2021 China-Europe International Conference on Pipelines and Trenchless Technology*, Lecture Notes in Civil Engineering 212,
https://doi.org/10.1007/978-981-19-4067-5_17

excellent fire-resistance performance [1–3]. With the rapid development of assembled buildings, concrete-filled double skin tubular (CFDST) members have come into being, which not only facilitates construction and protects the environment, but also greatly reduces the mass of the components for transportation [4]. Zhao et al. [5] and Huang et al. [6] proposed the CFDST columns with various structural forms, CFDST columns have good development prospects due to light self-weight and high bending stiffness. Uenaka et al. [7], Han and Huang et al. [8, 9] carried out experimental tests on CFDST members, CFDST members have excellent compressive behavior, bending behavior, and torsional behavior. However, steel tubes are susceptible to corrosion when in service in actual engineering, thus affecting the normal use of members, especially in marine structures and underground structures [10].

In order to avoid the adverse effects of steel tube corrosion on structural members and decrease the self-weight of the members to further reduce their response under earthquake action. This paper proposed a grout-filled double skin tubular (GFDST) column with stainless steel outer tubes (As shown in Fig. 1), which consist of two concentric thin-walled stainless steel outer tube and carbon steel inner tube with the same height, and grout was infilled between the tubes. The use of stainless steel tube instead of carbon steel can avoid the adverse effects of corrosion on structural members, while bringing better deformability and seismic energy absorption capacity [11]. The use of grout instead of concrete can decrease the self-weight of the members to further reduce their response under earthquake action. In this paper, a FEM study on the compressive behavior of proposed GFDST columns with stainless steel outer tubes is investigated. The effect of the stainless steel outer tube thickness, the carbon steel inner tube width, and whether grout is filled between the tubes on the failure modes, load–displacement curves, and ultimate strength were evaluated. Furthermore, the FEM results were compared with the experimental results.

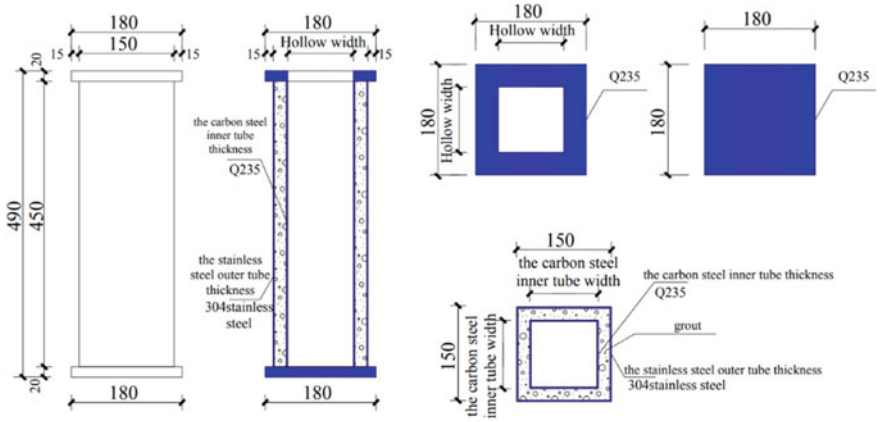

Fig. 1 GFDST columns with stainless steel outer tubes

Table 1 Design parameters for each specimen

Specimen label	B_o/mm	t_o/mm	A_o/mm^2	B_i/mm	t_i/mm	A_i/mm^2	A_c/mm^2	Hollow ratio
S3S3-50-1	150	3	1764	50	3	564	18,236	0.3472
S3S3-50-2	150	3	1764	50	3	564	0	0.3472
S2S3-50-1	150	2	1184	50	3	564	18,816	0.3425
S2S3-50-2	150	2	1184	50	3	564	0	0.3425
S4S3-50-1	150	4	2336	50	3	564	17,664	0.3521
S4S3-50-2	150	4	2336	50	3	564	0	0.3521
S3S3-100-1	150	3	1764	100	3	1164	10,736	0.6944
S3S3-100-2	150	3	1764	100	3	1164	0	0.6944
S2S3-100-1	150	2	1184	100	3	1164	11,316	0.6849
S2S3-100-2	150	2	1184	100	3	1164	0	0.6849
S4S3-100-1	150	4	2336	100	3	1164	10,164	0.7042
S4S3-100-2	150	4	2336	100	3	1164	0	0.7042

2 Experiment Overview

GFDST columns with stainless steel outer tubes from Ref. [12] were used as the numerical modeling, as shown in Fig. 1. The height of each specimen was 450 mm, the outer steel tube was made of grade 304 austenitic stainless steels, the inner steel tube was made of grade Q235 carbon steels, and grout grade is C55. Other design parameters of the specimen were shown in Fig. 1 and Table 1.

The specimen labels in Table 1 determined were determined according to following rules: (1) The first S refer to stainless steel tubes with square cross-Section (2) The following 2, 3, and 4 indicate the thickness of stainless steel outer tubes. (3) The second S refer to carbon steel tubes with square cross-Section (4) The following 3 indicates the thickness of carbon steel tubes. (5) The following 50 and 100 indicate the width of carbon steel tubes. (6) The last numbers 1 and 2 designate whether grout is filled between the carbon steel and stainless steel tubes.

3 Numerical Modeling

3.1 Model Parameters Selection

Grade 304 austenitic stainless steel was used as outer steel tube, grade Q235 carbon steel was used as inner steel tube, and grade C55 grout was used as the grout between the tubes.

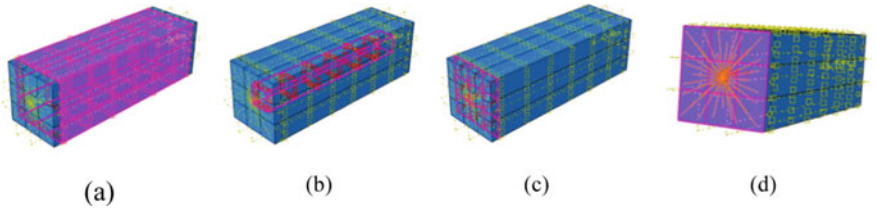

Fig. 2 Treatment of boundary conditions and contact conditions

3.2 Model Building and Meshing

According to the working characteristics of GFDST columns with stainless steel outer tubes and test setup, the end plates with the same width as stainless steel tubes, stainless steel tubes, carbon steel tubes, and the grout were selected as the numerical modeling. Because the height of columns is 450 mm and the height of specimens is 490 mm, the grid division size set at 1/15–1/10 of the height of columns is more reasonable, which is 30–45 mm.

3.3 Treatment of Boundary Conditions and Contact Conditions

The contact conditions between grout and stainless steel outer tube, between grout and carbon steel inner tube, between grout and end plates are all frictional contact (see Fig. 2(a)–(c)). The contact conditions between the steel tubes and grout include 'hard' contact in the normal direction and frictional contact in the tangential direction. By analyzing the relative sliding displacement existing between the contact surfaces and the relative relationship of the unit, a very small contact slip is used in the model, the friction coefficient of friction contact is defined as 0.3 and the shear stress limit of grout is defined as 0.15 MPa. A point system is established at the centre of each structure end, and two planes of the bottom and top surfaces are each coupled to the point at its centre (see Fig. 2(d)). The stainless steel outer tube and carbon steel inner tube are coupled to the end plates for shell and solid connection, respectively. Furthermore, to simulate the working characteristics of the specimen, a fixed restraint is applied at the bottom of the stub column.

3.4 Stress Nephogram

Figure 3 gives the stress nephograms of some specimens. The failure modes of specimens with grout infilled between the tubes are local buckling. Furthermore, it

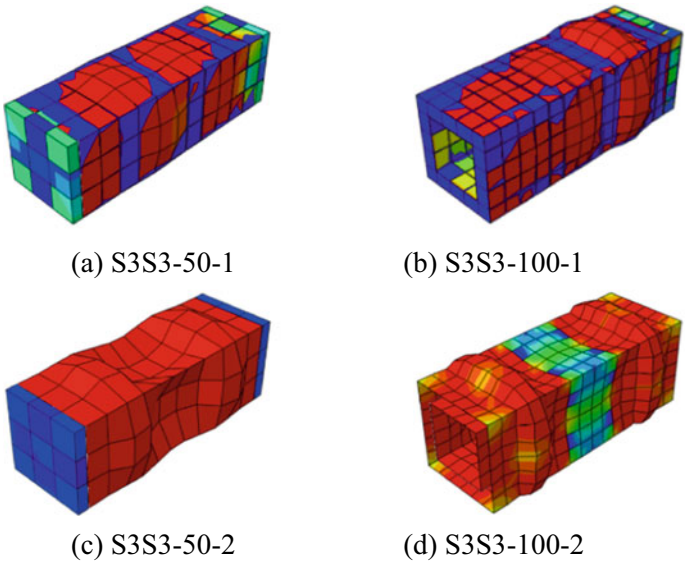

Fig. 3 Stress nephograms

can be seen from Fig. 3 that the location where buckling occurs is also the location of high stress in the member.

4 Comparison of FEM Results and Experimental Results

4.1 Ultimate Strength

Table 2 shows the comparison of FEM and experimental ultimate strengths. The FEM results are in agreement with experimental results. Increasing the thickness of stainless steel outer tubes can significantly increase the ultimate strength of specimens. Changing the width of carbon steel inner tubes has little effect on the ultimate strength of specimens with grout infilled between the tubes, but has a significant effect on the ultimate strength of specimens without grout infilled between the tubes.

Table 2 Comparison between the FEM and experimental ultimate strengths

Specimen label	Experimental ultimate strength N_{exp}/kN	FEM ultimate strength N_{FEM}/kN	N_{exp}/N_{FEM}
S2S3-50-1	1144.69	1237.9	0.92
S2S3-50-2	380.79	367.63	1.04
S2S3-100-1	973.55	1061.6	0.92
S2S3-100-2	774.64	833	0.93
S3S3-50-1	1514.85	1483.79	1.02
S3S3-50-2	606.12	661	0.92
S3S3-100-1	1503.22	1488.2	1.01
S3S3-100-2	987.04	973.132	1.01
S4S3-50-1	2149.76	2001.01	1.07
S4S3-50-2	1079.01	1025.99	1.05
S4S3-100-1	2077.71	2084.01	1.00
S4S3-100-2	1399.1	1274.24	1.10

4.2 Load–displacement Curves

Figure 4 shows the comparison between the FEM and experimental load versus displacement curves. It can be seen that the load versus displacement curves obtained from experiment and FEM have an initial linear stage followed by a transitional and plastic stage. In the experiments, the load reached the peak load when the displacement is 2–4 mm; and in the FEM results, the load reached the peak load when the displacement is 0–2 mm. Subsequently, the curves decrease slowly.

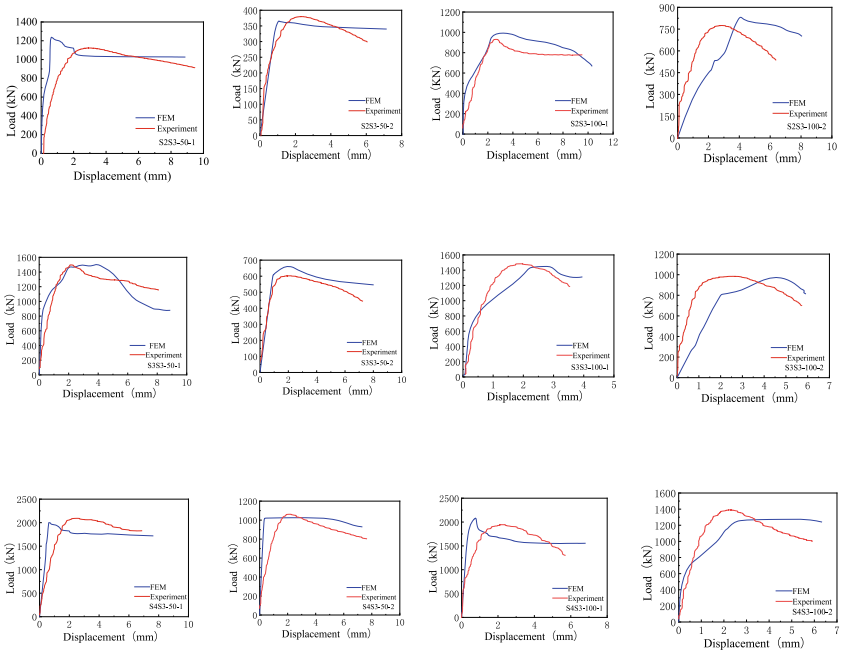

Fig. 4 Load–displacement curves

5 Conclusion

GFDST columns can avoid the adverse effects of steel tube corrosion on structural members and decrease the self-weight of the members to further reduce their response under earthquake action. This study investigated the axial compressive behavior of square GFDST columns with stainless steel outer tubes by FEM. According to the FEM results, the following conclusions can be drawn:

(1) GFDST columns exhibited excellent mechanical behaviors, and the FEM results are in agreement with the experimental results. The use of numerical modeling can predict the ultimate strength of specimens with sufficient accuracy.
(2) The failure modes of specimens with grout infilled between the tubes are local buckling. Furthermore, the location where buckling occurs is also the location of high stress in the member.
(3) Increasing the thickness of stainless steel outer tubes can significantly increase the ultimate strength. Changing the width of carbon steel inner tubes has little effect on the ultimate strength of specimens with grout infilled between the tubes, but has a significant effect on the ultimate strength of specimens without grout infilled between the tubes.

(4) The load versus displacement curves obtained from experiment and FEM have an initial linear stage followed by a transitional and plastic stage. Subsequently, the curves decrease slowly.

Acknowledgements This work was supported by a national Key R&D Program of China grant funded by the Chinese government (No. 2018YFD1100402). The support is greatly appreciated.

References

1. Wang ZB, Tao Z, Han LH et al (2017) Strength, stiffness and ductility of concrete-filled steel columns under axial compression. Eng Struct 135:209–221
2. Serras DN, Skalomenos KA, Hatzigeorgiou DE et al (2016) Modeling of circular concrete-filled steel tubes subjected to cyclic lateral loading. Structure 8:75–93
3. Han LH (2001) Fire performance of concrete filled steel tubular beam-columns. J Constr Steel Res 57(6):695–709
4. Zha XX (2011) Hollow and solid concrete-filled steel tube structures. Science Press, Beijing (In Chinese)
5. Zhao XL, Grzebieta R (2002) Strength and ductility of concrete filled double skin (SHS inner and SHS outer) tubes. Thin-Walled Struct. 40(2):199–213
6. Huang H, Han LH, Tao Z et al (2009) Analytical behaviour of concrete-filled double skin steel tubular (CFDST) stub columns. J Constr Steel Res 66(4):542–555
7. Uenaka K, Kitoh H, Sonoda K (2010) Concrete filled double skin circular stub columns under compression. Thin-Walled Struct. 48(1):19–24
8. Han LH, Huang H, Tao Z et al (2006) Concrete-filled double skin steel tubular (CFDST) beam-columns subjected to cyclic bending. Eng Struct 28(12):1698–1714
9. Huang H, Han LH, Zhao XL (2013) Investigation on concrete filled double skin steel tubes (CFDSTs) under pure torsion. J Constr Steel Res 90:221–234
10. Dewanbabee H, Das S (2013) Structural behavior of concrete steel pipes subject to axial compression and internal pressure: experimental study. J Struct Eng 139(1):57–65
11. Liao FY, Han LH, Tao Z et al (2017) Experimental behavior of concrete-filled stainless steel tubular columns under cyclic lateral loading. J Struct Eng 143(4):04016219
12. Zheng HZ (2021) Axial compressive behavior of hollow sandwich stainless steel tube concrete short column: experimental research. Beijing University, Technol

The Non-destructive Testing Technology of Reinforced Concrete Pipes Based on Ultrasonic Rebound Method

Huifang Liu, Linbing Wang, Hailu Yang, Zhoujing Ye, Pengpeng Li, Yangjun Li, and Jianfeng Li

Abstract As an important part of municipal infrastructure, the compressive strength of reinforced concrete of full-scale pipes during service cannot be obtained through conventional mechanical tests in-situ due to the complex size, working conditions and environment. The ultrasonic rebound integrated method has the characteristics of being non-destructive, rapid, accurate and convenient. This paper presents a study that uses C30 reinforced concrete full-scale pipes of different sizes, and adopts the ultrasonic rebound comprehensive method to assess the strength of the material. The results show that the ultrasonic velocity value, rebound value and compressive strength estimated value are positively correlated with the diameter of the pipes. The compressive strength value estimated by the ultrasonic rebound comprehensive method is highly correlated with the pipe size; the inner and outer surface's compressive strength conversion value of the full-scale reinforced concrete pipe are different, and the inner surface's < the outer surface's, which may infect by the ultrasonic rebound comprehensive method can be used in large-scale application in full-scale concrete pipelines.

H. Liu (✉) · L. Wang (✉) · H. Yang · Z. Ye · P. Li · Y. Li · J. Li
National Center for Materials Service Safety, University of Science and Technology, Beijing, Beijing 100083, China
e-mail: liu_hfsofia@163.com

L. Wang
e-mail: wangl@vt.edu

H. Yang
e-mail: yanghailu@ustb.edu.cn

Z. Ye
e-mail: yezhoujing@ustb.edu.cn

P. Li
e-mail: 17801051878@163.com

Y. Li
e-mail: 861145384@qq.com

J. Li
e-mail: Jianfengli@xs.ustb.edu.cn

L. Wang
Joint USTB-Virginia Laboratory on Multifunctional Materials, USTB, VA Tech, Blacksburg, VA 24061, USA

X. Liu (ed.), *Proceedings of 2021 China-Europe International Conference on Pipelines and Trenchless Technology*, Lecture Notes in Civil Engineering 212,
https://doi.org/10.1007/978-981-19-4067-5_18

Keywords Municipal infrastructure · Reinforced concrete full-scale pipelines · Non-destructive testing · The ultrasonic rebound comprehensive method

1 Introduction

With the development of urban construction and the acceleration of urbanization, the drainage pipeline network, as an important part of municipal infrastructure, shoulders the functions of collecting, transporting and discharging rainwater and sewage, and also plays an important role in preventing waterlogging in the cities [1]. Among them, reinforced concrete structure is currently the most widely used structural form in urban construction. However, due to the systematic and complex characteristics of the urban drainage pipeline network, the problems of pipe network aging and stress fatigue effects are more prominent coupled with the long history, the harsh environment, intricacies, long service time, and the majority of confluence systems. The structural resistance attenuation and damage accumulation of the drainage network are serious, which directly affects the safety of the pipeline network, and even causes major accidents, causing casualties and economic losses [2–4].

Before the 1990s, China mainly used traditional inspection techniques for drainage pipeline inspection, including visual inspection, mirror inspection, diver down-pipe inspection and mud hopper method [5]. These methods not only have a large workload and high risk, but also the test results are described and subjectively judged by the staff with different standards [6]. After the 1990s, various modern instrument detection technologies in developed countries were introduced into our country [7, 8], including closed circuit television detection systems (CCTV), sonar detection technology, pipeline periscope detection technology (QV), manhole zoom camera, laser contour scanning technology [9], infrared temperature recording and analysis technology [10], ground penetrating radar [11], ultrasonic phased array detection technology, wireless echo testing technology, electrical leak detection technology, micro deformation method [12], magnetic leakage sensing technology [13], etc. Some of these technologies use the inside and inner surface of the pipeline as the inspection object, and some use the pipeline structure as the inspection object; in addition, there are some technologies that can detect the formation conditions around the pipeline, and there is little research on the strength of the internal structure of the pipeline.

Using the ultrasonic rebound comprehensive method to measure the compressive strength of concrete pipes, the rebound value of the concrete material and the ultrasonic reflection waveform can be obtained at the same time. Compared with the rebound detection technology or the ultrasonic detection technology alone, the ultrasonic rebound comprehensive method is higher and the detection result is more accurate. We select full-scale reinforced concrete pipes with different inner diameters and wall thicknesses, and apply the comprehensive ultrasonic rebound method to full-scale in terms of pipeline compressive strength research, it is of great significance for the subsequent testing of the compressive strength of the drainage pipe

Table 1 Construction and geometrical dimensions of specimens

The inner diameter of pipe D0 (mm)	The thickness of pipe wall (mm)	The outer diameter of tube D1 (mm)	Skeletal level	Circumferential ribs				Longitudinal rib	
				Diameter (mm)	Ring inner diameter (mm)	Ring number (ring)	Pitch (mm)	diameter (mm)	Number
400	40	480	Single layer	3	429	18	55.6	5	6
500	50	600	Single layer	3	537	22.8	43.9	5	6
600	60	720	Single layer	4	644	15.5	64.3	5	6

Note Calculating the length of the reinforcement of the pipe section: per meter, in mm

network, as well as the in-depth study of the corrosion degree of the drainage pipe network, and the evaluation of the remaining life prediction of the concrete pipe structure.

2 Samples Preparation and Experiment

2.1 Experiment Materials

This paper selects ordinary portland cement with a concrete material grade of C30 and a compressive strength of 30 MP. The fine aggregate is medium-coarse sand, and the coarse aggregate particle size is 5–10 mm, which is not more than 1/3 of the wall thickness of the reinforced concrete pipe. And it is not more than 3/4 of the net spacing of the ring reinforcement, and the thickness of the inner and outer protective layer of the ring reinforcement is greater than 15 mm. The design parameters of the reinforced concrete pipeline are shown in Table 1. The concrete mixing water uses normal tap water, and the steel bars are cold-rolled ribbed steel bars. The effective length is 600 mm, and the physical map of the reinforced concrete pipe is shown in Fig. 1.

2.2 Testing Equipment

In this paper, HT225-B integrated digital rebound tester and SGT-IES-01 wireless shock echo detector are selected to detect the rebound value and ultrasonic velocity value of the full-scale pipeline respectively. The main technical indicators of the digital rebound hammer are as follows: nominal kinetic energy: 2.207 J; bounce tension spring stiffness: 785 N/m; bounce rod end spherical radius: R25; steel anvil rate setting: 80 $\pm$ 2; display screen: 3.2 in 256 $\times$ 64; online communication rate:

(a) The full size (b) The length is 600mm in different sizes

Fig. 1 Physical map of reinforced concrete pipe

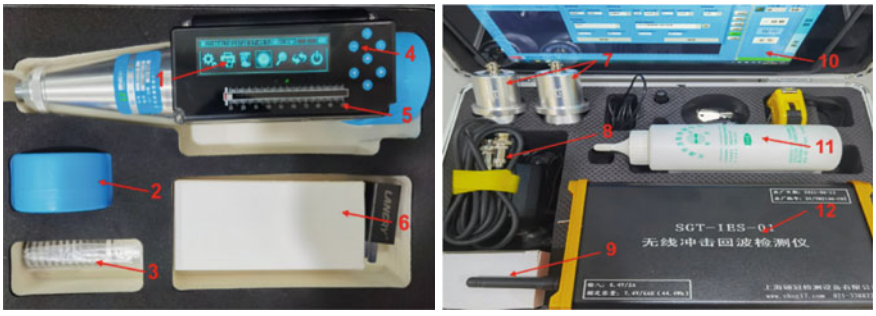

(a) Digital rebound hammer (b) Wireless impact echo detector

1 256*64 lattice 3.2 inch's LCD screen 2 Steel anvil 3 Compression spring 4 Button control area 5 Mechanical scale 6 Screwdriver box 7 Transducer 8 Accelerometer 9 Test antenna 10 Mobile PC 11 Coupling agent 12 Test host

Fig. 2 Testing equipment

115.2 kbps, as shown in Fig. 2(a). The main equipment for ultrasonic testing is SGT-IES-01 wireless shock echo detector. The main technical indicators of this equipment are: planar transducer: 50 kHz; sampling frequency: 1 MHz; transmitting voltage: 0–1000 V; sampling byte: 1 Kb; amplification gain: 50 dB; initial reading t0 when sound: 6 μs; working environment: −10–50 °C; excitation mode: manual; working time: test host ≤14 h, mobile PC ≤7 h, as shown in Fig. 2(b).

2.3 Test Program

Refer to the "T/CECS 02–2020 Ultrasonic Rebound Comprehensive Method to Detect Concrete Compressive Strength Technical Specification", in which the

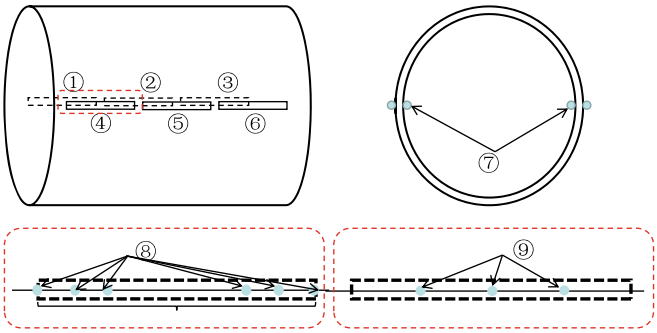

①-⑥ The distribution of rebound measurement area ⑦The distribution of countermeasure distribution points ⑧The rebound point distribution diagram ⑨The ultrasonic measurement point layout

Fig. 3 The layout of test measuring points

rebound method is divided into 2 test area lines, each of which has 3 test areas, each test area contains 16 test points, and the total of the test points is 96, the inner and outer walls are tested in pairs, a total of 192 test points (as shown in Fig. 3, ①–⑥, ⑦, ⑧); Zone line test 3 points, the total of the test points is 18 (as shown in Fig. 3, ①–⑥, ⑦, ⑨).

3 Results and Discussion

3.1 Rebound Test Results

According to the specification, 3 maximum and 3 minimum values will be excluded from the 16 rebound test values in each measurement area, and the remaining 10 effective rebound values are averaged, and each measured value is calculated according to formula (1). The rebound value of the zone is shown in Table 2.

$$R_{\mathrm{m}} = \frac{1}{10}\sum_{i=1}^{10} R_i \tag{1}$$

In the formula: R_{m} -the average rebound value of the survey area, the exact value is 0.1; R_{i}-the rebound value of the i-th point. The specific results are shown in Table 2:

Due to the test point is tested in the horizontal direction of the full-scale reinforced concrete pipe, the rebound hammer is horizontal during the measurement, so there is no need to perform angle correction and pouring surface correction. The results in Table 2 are the final results of the rebound detection of concrete full-scale pipes of various scales.

Table 2 Rebound test results of full-scale reinforced concrete pipe components

The inner diameter of pipe D0 (mm)	Survey area distribution	Representative value of concrete rebound in measurement area						
		Area 1	Area 2	Area 3	Area 4	Area 5	Area 6	Mean
400	Inner	25.2	32.1	22.2	19.8	23.2	25.4	24.65
	Outer	31.6	36.7	34.3	34.4	33.8	34.7	34.25
500	Inner	39.2	40.4	37.9	27.9	34.6	35.7	35.95
	Outer	38.1	38.8	41.4	43.4	37.8	40.4	39.98
600	Inner	41.5	44.6	40.0	32.5	32.0	33.0	37.27
	Outer	35.8	37.0	42.1	44.7	39.7	43.9	40.53

3.2 Ultrasound Test Results

The transmitting and receiving transducers are used to measure and record the sound time values of the three measuring points, and then the distance between the two transducers, which is the thickness of the reinforced concrete pipe, is used as the ultrasonic distance measurement value. After the three sound-time readings are measured, the ultrasonic velocity is calculated according to formula (2). The sound velocity calculation result is shown in Table 3.

$$\mathrm{v} = \frac{1}{3}\sum_{i=1}^{3}\frac{l_i}{t_i - t_o} \tag{2}$$

where: v—representative value of sound velocity in concrete in the measuring area, km/s; l_{i}—ultrasonic distance measurement of the i-th measuring point, mm; t_{i}—acoustic time reading of the i-th measuring point, s; t_0—sound time Initial reading, μs.

Table 3 Results of estimated strength of reinforced concrete

The inner diameter of pipe D0 (mm)	The pipe wall thickness (mm)	The ultrasonic velocity value (km/s)	The survey area distribution	The rebound value	The compressive strength conversion value (MPa)
400	40.00	2.5	Outer	24.65	7.23
			Inner	34.25	10.58
500	50.00	3.06	Outer	35.95	16.76
			Inner	39.98	18.94
600	60.00	3.83	Outer	37.27	27.36
			Inner	40.53	30.14

3.3 Analysis of Test Results

According to the conversion formula (3) of the concrete compressive strength of the unified national survey area, the conversion value of the concrete compressive strength of each survey area can be obtained, as shown in the Table3.

$$f_{cu,i}^{c} = 0.0286 v_{ai}^{1.999} R_{ai}^{1.155} \tag{3}$$

where: the $f_{cu,i}^{c}$ is the conversion value of concrete compressive strength of the i-th measuring area (MPa), accurate to 0.1 MPa; v_{ai}—the revised rebound representative value of the i-th survey area; R_{ai}—the corrected sound velocity rebound representative value of the i-th measurement area.

3.4 Analysis and Discussion

Based on the above data, we can see that the rebound test, sound velocity value, and the estimated value of ultrasonic rebound compressive strength are analyzed with full-scale pipes with different inner diameters. The rebound value is positively correlated with the inner diameter of pipe, and the internal surface rebound value is positively correlated with the full-scale pipe. The size correlation coefficient is 0.65, and the correlation coefficient between the outer surface rebound value and the full-scale pipe size is 0.63, as shown in Fig. 4(a), which is a significant correlation, which may infected by the curvature of inner and outer diameter; the correlation coefficient between the sound velocity and the full-scale pipe size of reinforced concrete is 0.98, as shown in Fig. 4(b), which is highly correlated, which may infected by the thickness and the reinforcement ratio,; the compressive strength of the internal and external surfaces of reinforced concrete is related to the full-scale pipe size through the ultrasonic rebound synthesis method, the coefficients are 1.00 and 0.99 respectively, as shown in Fig. 4(c), which are highly correlated, that is to say, the ultrasonic rebound comprehensive method can be applied to multi-scale reinforced concrete compression strength testing, and it.

4 Conclusion

Based on the results and discussions presented above, the conclusions are obtained as below:

(1) The rebound value, the ultrasonic velocity and the compressive strength estimated value of reinforced concrete pipes with different inner diameters and wall thicknesses are different. Each reinforced concrete pipe with inner diameter has a corresponding wall thickness corresponding to it, that is, reinforced concrete

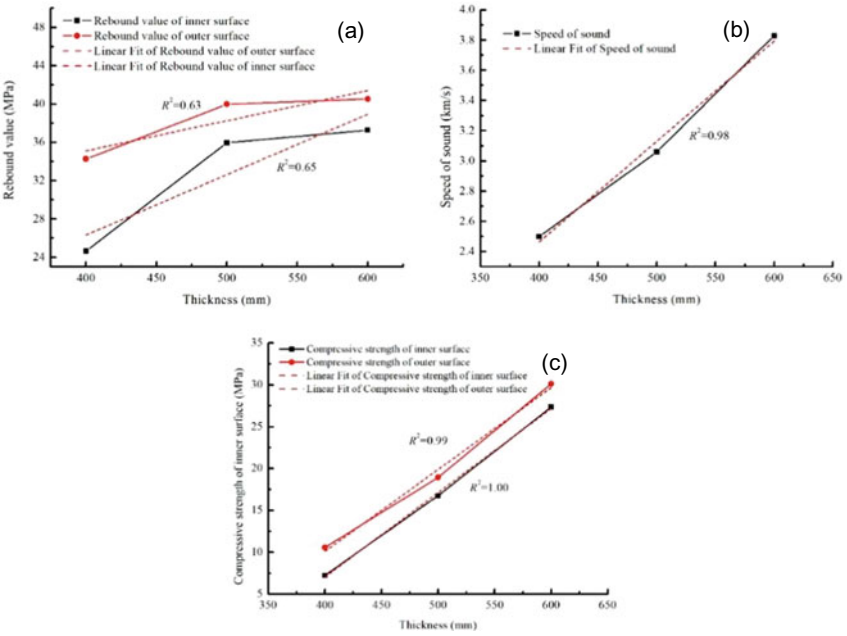

（a）The correlation graph between rebound value and pipe sizes （b）The correlation graph between the ultrasonic velocity and pipe sizes （c）The correlation diagram between estimated compressive strength and pipe sizes

Fig. 4 The correlation diagram of the rebound value, the ultrasonic velocity and the compressive strength between pipe sizes

of different sizes pipe, its pipe wall thickness and inner diameter will affect its strength.

(2) The ultrasonic rebound comprehensive method is sensitive to the size, wall thickness and reinforcement ratio of reinforced concrete full-scale pipeline segments, and be used to obtain the internal and external surface structural strength variability of the full-scale pipeline segments, to indicate the health conditions of pipelines; and the actual quality of the full-scale pipeline has no damage to the pipeline components, thereby ensuring the safety and reliability of the full-scale pipelines.

(3) Combined with actual engineering needs, the ultrasonic rebound comprehensive method technology has great application prospects in urban drainage pipeline engineering.

Acknowledgements This work was financially supported by the Beijing major science and technology projects (No. Z191100008019002).

References

1. Li L (2001) Research on planning and design of urban drainage pipeline system. Chongqing University, Chongqing
2. Changren X (2019) Research on CCTV testing and evaluation technology of taizhou drainage pipelines. Yangzhou University, Yangzhou
3. Man W, Qinghai Z (2021) Key technologies and applications of health detection for urban drainage pipe networks. Urban Survey 2021(04):158–162
4. Chengyuan Z (2021) Maintenance and management of municipal drainage network. Sci Technol Wind 2021(08):104–105
5. Heping W, Guanfeng A, Guangyong X (2014) Interpretation of technical regulations for inspection and evaluation of urban drainage pipelines (CJJ181-2012). Water Supply Drain 40(2):124–127
6. Tian L, Ruidong Z, Jun Z (2006) Development status of drainage pipeline inspection technology
7. Menfu F, Wenjun P, Kui H (2018) Drainage pipe network health status detection and assessment technical methods. Urban Surv 167(s1):90–94
8. Junling W, Yulian D, Ying L, Xianguo Z (2020) Overview of drainage pipeline inspection and defect recognition technology. Sci Technol Eng 20(33):13520–13528
9. Du W, Xu X (2017) Laser inspection method for drainage pipeline. Trenchless Technol 2017(3):53–56
10. Yan M, Gao N (2007) Modern drainage pipeline detection technology. Water Supply Drain 2007(01):110–112
11. Thums Z, Huo J, Yuxiang F (2018) A new method for evaluating the mechanical state of sewage pipes. Trenchless Technol 2018(2):118–120
12. Avci O et al (2021) A review of vibration-based damage detection in civil structures: from traditional methods to machine learning and deep learning applications. Mech Syst Signal Process 147:107077
13. Wirahadikusumah R et al (1998) Assessment technologies for sewer system rehabilitation. Autom Constr 7(4):259–270

Intelligent Identification and Diagnosis Service of Abnormality Events in the Drainage Network

Juan Xie, Ye Jun Wu, and Yu Xiang Tan

Abstract To detect and prognose drainage pipe network system failures as soon as possible, reduce the environmental, social hazards and losses, this paper proposes an intelligent identification and diagnosis software service. The service can be integrated with application, however, it provides real-time early warning and alarm notifications and auxiliary decision-making information for pipeline network maintenance personnel. It uses IoT technology perception of the water running state and combined with the hydrodynamic model to establish a complete physical map of the pipe network. It integrates weather and environmental information. Then uses data-driven models, deep machine learning, and hydrodynamic models, to recognize abnormal events, diagnose and locate fault causes, and prognose failures of pipe networks, which is a data science method.

Keywords Intelligent identification · Intelligent diagnosis · Abnormal events · Fault

1 Introduction

Firstly, with the acceleration of urbanization and increase of urban population and human activities, the operating load of the drainage pipe network system with lower design standards will increase, exceeding the system threshold. Secondly, the pipe network facilities are accidentally destroyed. Thirdly due to lags and high costs in maintenance and transformation of the pipe network system. Finally the performance degradation or function failure of the system is more and more frequent, which in turn causes urban operation safety and environmental problems.

J. Xie (✉) · Y. J. Wu · Y. X. Tan
Alibaba Cloud Intelligence Technology, Alibaba Group, Hangzhou 310000, China
e-mail: xj166841@alibaba-inc.com

Y. J. Wu
e-mail: yejun.wyj@alibaba-inc.com

Y. X. Tan
e-mail: silang.tyx@alibaba-inc.com

X. Liu (ed.), *Proceedings of 2021 China-Europe International Conference on Pipelines and Trenchless Technology*, Lecture Notes in Civil Engineering 212,
https://doi.org/10.1007/978-981-19-4067-5_19

The safety and health risk assessment of drainage system is mainly through a combination of cost-benefit and risk assessment, which explains the importance of reducing and mitigating system risks. According to the British CDM Regulations, risk assessments should be developed and reviewed at all stages of design, construction and maintenance [1]. The pilot project of the sewage pipes in Copenhagen selects high-risk areas where pipe damage will cause serious consequences for risk assessment. The method of risk assessment considers material damage, environmental impact, clean-up work and other factors to establish the probability of accidents and the severity of consequences matrix. Then the study combines risk assessment and cost-benefit analysis to provide managers with decision-making tools [2]. The literature establishes the probability of failure of the pipes (depending on the failure event set) by Bayesian model. It uses the weight of the influencing factors and the degree of influence caused by the failure to establish the severity of the consequences, and then fuzzy inference systems are used for the failure probability and the severity of the consequences to generate a risk assessment matrix to obtain the risk rank of sewage pipes, so the sewage treatment agency shall carry out repair and transformation work according to the risk rank [3]. The literature by evaluating performance such as pipe blockage, it provides references for system operation and maintenance to ensure that the system provides the required services at an acceptable cost. In addition, it uses the available data in the benchmark system of the Swedish Water and Wastewater Association to make inferences on the factors affecting blockage tendency at the overall strategic level [4]. Different failure modes of sewage network and their directly related environmental data and graphical analysis are used to estimate the severity of the consequences of pipe failure, which is used to support asset management decisions to mitigate risks, such as estimating and planning the required resources for condition inspection, renovation and maintenance of network [5].

The methods proposed above provide an important reference for systematically solving security risks. Their shortcomings are: 1) difficult to collect data (especially failure data) 2) only suitable for small-scale pilots, with large-scale manual workloads, Uneconomical 3) Lack of the ability to continuously sense the failure of the pipe network online. With the application of IoT technology in the drainage system, combined with information management and GIS technology, to build an intelligent sewage pipe network services, its functions focus on the information management of the sewage system, but analysis of issues related to safety and environment are not involved, also there is no specific research and application on intelligence [6]. Although ZHU et al. proposed that using collected sound pressure signals to calculate, through CEEMD mode decomposition combined with GG clustering algorithm to identify blockage characteristics for partial blockage of drainage pipes [7]. Jing Yan et al. proposed a wavelet transform based on the acoustic corresponding signal is adopted, and high-energy wavelet packet nodes are selected to reconstruct the signal. The feature components are extracted by methods such as approximate entropy, energy entropy, and fractal, and SVM is used for classification and recognition [8]. The research of these methods does not consider the algorithm differences caused by differences in pipe materials, pipe shapes, multiple fault couplings, etc., which

leads to the difficulty of generalization. At the same time, it does not consider the lack of fault sample data in practical applications.

This paper proposes an intelligent decision-making service for online perception, discovery, location, and prognostic of pipe network abnormalities, fault, and even failures. Through adaptive self-learning methods, with the longer of running time, the increase of data volume and the enrichment of samples, the correct rate of alarms is continuously improved, and false alarms are reduced, it provides an end-to-end data scientific method of predictive or condition-based maintenance decision for maintenance personnel.

2 Requirements

The failure modes of pipes can be divided into structural and hydraulic failures. Combining the maintenance or modification costs caused by the failures, the negative social and environmental impacts, and the frequency of failures, this paper studies the hydraulic failure modes, see Table 1 below. The abnormal state of the pipe network is classified into three categories. From the performance degradation line, it can be divided into abnormalities, fault and failures. Listed in Table 1, there are 4 failure modes, corresponding to two functional requirements: Intelligent event and intelligent diagnosis; the purpose of intelligent event is to identify abnormalities in time and give an alarm; the purpose of intelligent diagnosis is to confirm whether it is a fault based on the abnormal alarm, and locate the fault location or area, and further predict the severity of the fault or the time required for complete failure in the future based on the history and current state. The performance constraints corresponding to these functions often involve the constraints proposed by the business side. For example, the maintenance standards stipulate that the degree of pipeline blockage reaches 1/5 of the inner diameter of the pipe or the height of the pipeline, and the dredging must be carried out, which also determines that the siltation alarm must be issued before this constraint. The goal of the intelligent identification and diagnosis service of abnormal events in the drainage network proposed in this paper is to observe the precursors of performance degradation, or to detect the abnormal state earlier or in time, and deal with the failure before causing loss.

Term description

1) Abnormality refers to an unknown abnormal state.
2) Fault is defined as a known or repeatable abnormal state.
3) Failure refers to an abnormal state in which the performance of a component is degraded so that the component cannot provide the expected function.

Table 1 Pipe failure mode and corresponding requirement description

Failure mode	Pipe network Type	Consequence	Function requirement	Constraint (From customer)
Blockage	Sewage and rainwater pipe network	Reduced drainage capacity, overflow to roads and public areas	Intelligent events: Timely identification of abnormalities and early warning Intelligent diagnosis: 1) diagnose the abnormality, and identify and confirm the fault and its severity 2) locate the location or area of the faulty pipeline 3) prognostics is to prognose the severity of the failure or the time required for complete failure in the future based on the history and current state	1. Early warning or warning threshold 2. Acceptable event or prognostic time deviation range (the earliest time to advance, the latest time not to exceed). Acceptable value deviation range 3. Acceptable range of the fault location area 4. Time constraints for diagnose fault sources
Leakage	Sewage pipe network	Ground subsidence, ground voids, sewage into groundwater, etc., etc		
Overflow	Sewage and rainwater pipe network	Affect roads and public areas		
Inflow and infiltration	Sewage pipe network	Reduce sewage concentration and increase sewage treatment energy consumption		

3 Methodology

3.1 Function Framework

We consider these factors: 1) The drainage network has the characteristics of network complexity, input and environmental uncertainty, and there are often multiple mixed faults; 2) In addition to the noise error of the measurement principle itself, the current real-time online monitoring equipment also have noise errors caused by media interference; 3) The parameter uncertainty of the hydrodynamic model leads to the limited accuracy of the model; which bring challenges to the validity of the data and fault identification and diagnosis. The solution of this paper is to obtain basic data through the combination of monitoring equipment and hydrodynamic models, ignore the interference caused by uncertainty, pay attention to the change law and trend of time series data, and establish a pattern recognition and diagnosis mechanism on this basis for different failure modes. The service architecture shown in Fig. 1 below. Its main functions and operating mechanisms are as follows:

1) Sensing layer: Its communication method can be NB, 4G, Lora, etc. It connects sensor devices such as level gauges, flow meters, rain gauges, etc., which are

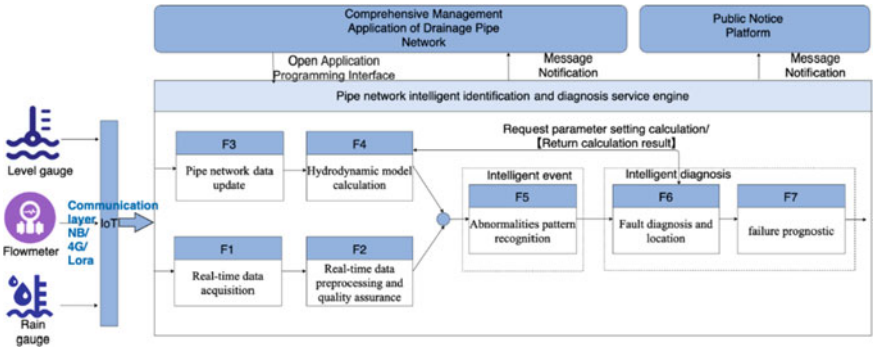

Fig. 1 Service top-level function map

distributed in different geographical locations of the pipeline network through IoT, to obtain the real-time liquid level, flow rate, and flow rate of the pipeline network, rainfall and other information.

Engine functional layer:

F1 Real-time data acquisition: Device data is transmitted to the cloud through the IoT layer, and the service engine uses real-time streaming data processing to receive device data messages. Compared with traditional polling and query data, it increases the management of the data time dimension, including device-side events (sampling) time and server processing time ensure real-time data acquisition. At the same time, the acquired data is classified and stored to facilitate subsequent data processing and pattern recognition.

F2 Real-time data preprocessing and quality assurance: Due to the quality of the sensor and comparatively hard environment, the quality of the time series data collected by the sensor is uneven. Common problems include the data type and unit collected by different sensors are not uniform, the collection frequency is not uniform, data loss, duplication, abnormality, etc. This function is mainly to ensure that the follow-up pattern recognition and diagnosis provide available data sets. There are mainly three aspects such as processing: 1) real-time data cleaning 2) sensor failure detection and alarm 3) data quality evaluation.

F3 Pipe network data update: The pipe network is modified or replaced during the operation process, so it leads to deviations between the recorded data of the pipe network and actual. A dynamic update mechanism for the pipeline network data is necessary. After the user modifies the data through the terminal, the automatic detection mechanism updates the service engine database and update the hydrodynamic model.

F4 Hydrodynamic model calculation: The reason for introducing hydrodynamic model calculation is cost and effect considerations. If each node of the pipe network deploy sensor. About 3000 nodes with a length of 100 km cost 200 million [9], this cost exceeds the acceptable budget range. Constructing a hydrodynamic model, on the one hand, realizes an online model to obtain the hydraulic state of each node

and each pipeline, and find anomalies by comparing the predicted value with the monitored value, on the other hand, it can be used to simulate faults with different parameter settings to obtain hypothetical faults. The method is also used to infer and locate the fault pipeline.

F5 Abnormalities pattern recognition: Based on the preprocessed monitoring time series data and hydrodynamic model output time series data, this paper uses data-driven algorithms such as unsupervised learning and supervised learning to identify abnormalities and obtain intelligent events. There are two sources of feature recognition: 1) Trend change or sudden change based on historical monitoring data; 2) Comparison trend change between monitoring data and the output of the hydrodynamic model. In practical applications, if the modeling accuracy of the hydrodynamic model does not meet the requirements, the case 1) is preferred.

F6 Fault diagnosis and location: After F5, the server 1) Identify the timing characteristics of related monitoring points through data-driven algorithms to confirm the fault, 2) Set different faults through the hydrodynamic model to simulate, compare the simulation results with the monitoring data to locate fault 3) Use the knowledge base method to establish a fault diagnosis knowledge map for the pipe network, including a decision model between features, faults, causes, and suggestions, for further troubleshooting and confirmation of faults, and making decisions information.

F7 failure prognose: The function model the fault process based on the features extracted from historical data, use data-driven algorithms or hydrodynamic models to prognose the time from fault to failure, or prognose the severity of the failure for specified time in future.

Application layer: The service engine can be integrated with applications software such as comprehensive management. The application layer can be informed intelligent event information by the event notification mechanism, and obtain diagnosis and prognostics related auxiliary decision-making information by calling open service interface. At the same time, the service engine can report event information to the public software platform through the message mechanism, which is convenient for the public to avoid dangerous areas.

3.2 Detailed Description

Data Pre-processing and Quality Assurance

Poor data quality will result in low algorithm accuracy. In the failure scenarios studied in this paper, the real-time requirements of the data are inconsistent, and there are higher requirements for the validity of the data. Therefore, before intelligent detection and diagnosis, a complete guarantee system is needed to ensure the quality of basic monitoring data.

Data abnormalities can be divided into repairable and unrepairable situations. Real-time online pre-processing deal with this kind of situations that can be repaired, such as data duplication, small amount of data loss or beyond the boundary, disorder in a certain time range, etc. The use of traditional data polling methods brings processing

complexity and delays, while scenarios such as overflow and sudden blockage require timely and accurate judgments, which depend on the real-time of data cleaning. Therefore, the data stream processer is introduced, and the operation of data cleaning is integrated into processor as an operator. The cleaning process mainly includes out-of-order data sorting, de-duplication filtering, delayed data filtering, outlier filtering, resampling and so on. Outliers are values that are far away from other observations or are inconsistent with other observations, and may cause the system to issue false alarms. It may be caused by disturbances or data collection errors. It will cause regularized noise in subsequent machine learning algorithms, and feature filtering must be performed. Firstly, the commonly used method is to predict based on the sliding average method of the time window, KNN, the kernel function smoothing method [10], etc., relative to the lag of the sliding average method, the estimation of KNN is not smooth, and the kernel function smoothing method is similar to weighted moving average method of Kernel, except that the boundary has a deviation, the effect is better. The kernel function usually uses a Gaussian kernel. Secondly, then combined with the PCI interval to determine whether it is out of bounds [11], as shown in the formula (1) (2),$\overline{v}_{t_i}$ is the predicted value, smoothing window length h_w, $t_{\alpha/2,2k-1}$ represents the student distribution with 2 k–1 degrees of freedom, and s is the standard deviation of the model residual, 2 k is the window size.

$$\overline{v}_{t_i} = \frac{\sum_{j=1}^{2k} Kernel\left(\frac{t_i - t_j}{h_w}\right) * v_{t_i}}{\sum_{j=1}^{2k} Kernel\left(\frac{t_i - t_j}{h_w}\right)} \tag{1}$$

$$PCI = \overline{v}_{t_i} \pm t_{\alpha/2,2k-1} \times s\sqrt{1 + 1/2k} \tag{2}$$

Sensor fault detection generate an alarm that must be issued when the sensor device no longer sends valid data or the valid data does not meet the available standards, and promptly notify maintenance personnel for maintenance. Faults include: The sensor is offline, the sensor exceeds the device range extreme value and the slope is abnormal.

Data quality assessment, through the analysis of the characteristics of time series data and business scenario requirements, selects the five dimensions of effectiveness, completeness, accuracy, timeliness, and accuracy and their corresponding indicators to measure the quality of the collected data:

Validity refers to the data collected is valid and can be used by the upper system. Its measurement indicators include beyond the boundary, abnormal rate of change, repetition, disorder, etc.

Completeness means that the collected data is complete, without partial or complete loss. The metrics include missing sampling time, missing sampling values, and missing sampling data (both time and value).

Precision refers to whether the granularity of sampled data meets business requirements. It includes two aspects of accuracy. One is the accuracy of the sampling value, and the other is the accuracy of the sampling frequency.

Timeliness measures whether the sampled data can be reported to the system in time. The collected data that cannot be reported in time has an adverse consequence on the real-time of the system's decision-making.

Accuracy refers to the unreasonable data, such as the mismatch between the flow rate and the liquid level value, and the abnormal temperature value.

Abnormalities Pattern Recognition and Fault Diagnosis Location

These two functions are the core of intelligent events and diagnosis. They are the process of discovering the abnormality, dynamically confirming whether it belongs to a certain kind of fault, and locating fault. Whether it is the process of discovering abnormalities or confirming faults, it is based on physical principle judgment or feature recognition. Different failure or failure modes, extract features based on hydraulic characterization, and choose different algorithms, including complex event rule processing, unsupervised learning algorithms, supervised deep learning algorithms, etc. Figure 2 below takes the blockage failure mode identification and diagnosis as an example to illustrate its principle and process.

Abnormalities Pattern Recognition

As mentioned above, an abnormality is a kind of suspected failure. Because some system failures may have happened suddenly and have serious consequence, so the abnormality recognition is sometimes time-critical. By the professional knowledge and experience analysis of consultants, a more accurate failure mode and causes analysis can usually be obtained, but the disadvantage exists lag analysis in many cases and suitable for small-scale pilot projects. According to the current status of digitalization of the pipe network system, there are not enough fault samples, and it is unrealistic to manually mark a large amount of data through expert experience. The

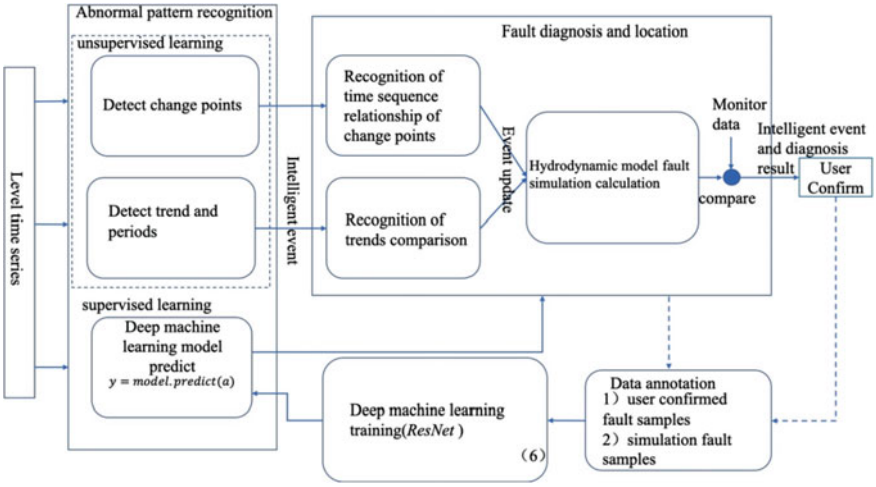

Fig. 2 Schematic diagram of blockage failure pattern recognition and diagnosis

method used in this article is to combine unsupervised learning algorithms and supervised learning algorithms. Unsupervised learning recognizes abnormalities from a large amount of data, and combines diagnosis and manual confirmation methods to accumulate fault samples; supervised learning realizes by combines accumulation samples from unsupervised learning and fault samples simulated by hydrodynamic models for deep learning training models, relatively as far as unsupervised learning algorithms, the accuracy of supervised learning algorithms is higher when there are enough marking samples.

As shown in Fig. 2, the blockage is taken as an example. Using an unsupervised learning algorithm, two blocking modes are studied: One is sudden pipeline blockage, the other is long-term accumulation of silt or other materials. Emergencies are found by detecting change points, dividing different liquid level sub-time series, calculating the loss function c, and comparing the signal difference $d(y_{a..t}, y_{t..b})$ of the subsequences to find the change point when it is greater than the given penalty value. The change point detection is shown in the formula (3). Long-term blockage through historical data for a long time, using the principle of time-series decomposition to decompose the inflow component caused by trends τ_t, cycles and seasons $S_{i,t}$, other rainwater and other factors r_t, as shown in the formula (4), to detect the liquid level trend to determine whether it is rising or not, the timing decomposition algorithm can be optimized using STL, Robust Periods and other algorithms [12–14]. These unsupervised algorithms are based on the laws and trend changes of the historical data of a single monitoring node to identify, mainly to ensure the timeliness of abnormality discovery, without considering that the pipe network is a network time-varying system and system relevance, and the accuracy is limited.

$$\mathrm{d}\left(\mathrm{y}_{\mathrm{a..t}}, \mathrm{y}_{\mathrm{t..b}}\right) = \mathrm{c}\left(\mathrm{y}_{\mathrm{a..b}}\right) - \mathrm{c}\left(\mathrm{y}_{\mathrm{a..t}}\right) - \mathrm{c}\left(\mathrm{y}_{\mathrm{t..b}}\right)(1 \le \mathrm{a} < \mathrm{t} < \mathrm{b} < \mathrm{T}) \tag{3}$$

$$\mathrm{y}_{\mathrm{t}} = \tau_{\mathrm{t}} + \sum\nolimits_{\mathrm{i}=1}^{\mathrm{m}} \mathrm{S}_{\mathrm{i,t}} + \mathrm{r}_{\mathrm{t}}\ \mathrm{t} = 0, 1, \ldots \mathrm{N} - 1 \tag{4}$$

$$\mathrm{a}^{\mathrm{l}+1} = \mathrm{Activate}\left(\mathrm{w}^{\mathrm{l}+1}\mathrm{a}^{\mathrm{l}} + \mathrm{b}^{\mathrm{l}+1}\right) \tag{5}$$

$$\mathrm{a}' = \mathrm{w}^{\mathrm{l}+2}\mathrm{Activate}\left(\mathrm{w}^{\mathrm{l}+1}\mathrm{a}^{\mathrm{l}+1} + \mathrm{b}^{\mathrm{l}+1}\right) + \mathrm{b}^{\mathrm{l}+2} \tag{6}$$

$$\mathrm{a}^{\mathrm{s}} = \mathrm{Soft} - \mathrm{Thresholding}\left(\mathrm{a}', \alpha\right) \tag{7}$$

$$\mathrm{a}^{\mathrm{l}+2} = \mathrm{a}^{\mathrm{s}} + \mathrm{F}\left(\mathrm{a}^{\mathrm{l}}\right) \tag{8}$$

$$\frac{\partial \mathrm{A}}{\partial \mathrm{t}} + \frac{\partial \mathrm{Q}}{\partial x} = 0 \tag{9}$$

$$\frac{\partial \mathrm{Q}}{\partial \mathrm{t}} + \frac{\partial\left(\mathrm{Q}^2/\mathrm{A}\right)}{\partial \mathrm{x}} + \mathrm{gA}\frac{\partial \mathrm{H}}{\partial \mathrm{x}} + \mathrm{gAS}_{\mathrm{f}} = 0 \tag{10}$$

The training of deep learning model is a way to improve the recognition performance in the later stage. The training of the model is based on the samples generated by the fault simulation of the hydrodynamic model and the samples confirmed and marked by the user. These samples are two-dimensional samples composed of the trend comparison of the time series data of the upstream and downstream monitoring node and the corresponding simulation data, rather than the comparison of the previous single monitoring node. The classification training is carried out according to the physical characteristics of the upstream and downstream nodes and different blockage degrees. The formula (5)(6)(7)(8) in Fig. 2 represents the deep residual shrinkage network model Resnet [15]. W and b are the weight vector and the bias vector. a^l, a^{l+1}, a', a^{l+2} are the input of the network, the output of the first hidden layer, the second hidden layer, and the output, respectively. a^s is output of Soft-Thresholding which purpose is to flexibly set the feature value interval, to reduce the noise of time series data, and to deal with the uncertainty disturbance in the pipeline network. $F\left(a^l\right)$ is the residual item added to CNN, the purpose is to reduce the sample feature loss in the multi-layer training process. Compared with the traditional deep learning model, the ability to learn features is stronger. The model adopts an online update training mode. As the number of samples increases, the accuracy increases. After the training meets the loss and cross-validation performance evaluation, it is automatically updated to the online model to predict and identify the blockage fault classification.

Fault Diagnosis and Location

After receiving the abnormality event, server engine starts the fault diagnosis. The diagnosis result will follow the hydraulic process time series of the relevant monitoring point to meet the diagnosis requirements, and the final diagnosis result will be obtained. If the abnormality cannot be confirmed as a fault, the event will be cancelled and fed back to the abnormality identification model, which is used for subsequent improvement. If the fault is confirmed, the hydrodynamic model is started to perform fault simulation calculation for fault location.

Regarding the confirmation method of fault diagnosis, feature recognition and confirmation are performed based on more dimensional data. The methods can be divided into: classification and recognition based on deep learning, asynchronous timing correlation determination based on DTW, and empirical threshold determination. Take blockage as an example. Sudden blockage is confirmed by the sequence of the rise of the upstream and downstream monitoring nodes, which is different from the sudden increase due to the sudden large flow of upstream; Long-term blockage is confirmed that the upstream trend is rising and the downstream trend is not rising.

Fault location further enhances the credibility of fault confirmation, using the method of hydrodynamic model inference, as shown in the hydrodynamic model simulation calculation module in Fig. 2, formula (9)(10) is the quality and momentum of the unsteady free surface flow of the pipe or conduit equation. After the fault is confirmed, the scope of the fault is obtained, and the different fault degree of each pipe (see Fig. 2 Set pipe bottom filled depth Y_{btm} to different value) is assumed in the hydrodynamic model within the scope, the model calculation is performed, and the likelihood of the model output and the monitoring data is compared to determine

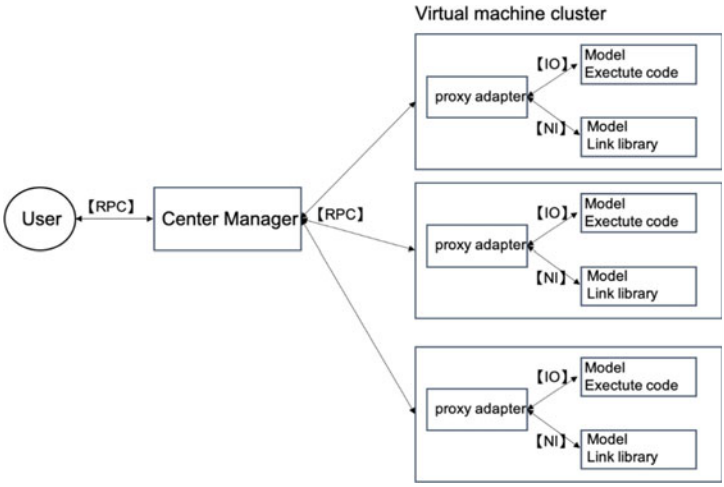

Fig. 3 Cloud model architecture diagram

whether the assumption is correct, then get the specific location of the fault. The time required for fault location is also determined by the fault simulation time of the model. The fault simulation calculation involves batch plan calculation. In order to improve calculation efficiency and control costs, the cloud is used to select idle or low-load virtual machine clusters, and the intelligent algorithm scheduling model plan is used distributed parallel computing improves computing efficiency. As shown in Fig. 3, the proxy adapter can interact with different model forms through IO or local interface.

Performance Metrics

Performance evaluation is actually a paradox. The evaluation can only be done after the failure event occurs after the user has confirmed it. It is impossible to damage the pipe or artificially create a blockage for verification. If the server before online, the performance evaluation can be based on historical fault data or simulated faults.

The performance indicators of smart events can use accuracy and recall to evaluate different algorithms or models. F1 Score is a comprehensive evaluation of accuracy and recall. The higher the value, the better the performance. For multi-class event evaluation, micro F1 Score can be used, as shown in formula (11)(12)(13).

$$precision_{mi} = \frac{\sum_{i=0}^{n} TP_i}{\sum_{i=0}^{n} TP_i + \sum_{i=0}^{n} FP_i} \tag{11}$$

$$recall_{mi} = \frac{\sum_{i=0}^{n} TP_i}{\sum_{i=0}^{n} TP_i + \sum_{i=0}^{n} FN_i} \tag{12}$$

$$micro\,F1 = 2 * \frac{precision_{mi} * recall_{mi}}{precision_{mi} + recall_{mi}} \tag{13}$$

The performance of intelligent diagnostic location is firstly whether the scope of location is accurate, which can be located to a few pipes or a certain pipe; secondly, the time required for location, involving batch calculation of hydrodynamic models, that is the time from the generation of intelligent events to the output of diagnosis results. For example, the time from the occurrence of the suspected blockage event to the specific blockage pipe location is t. Time t is restricted by the emergency treatment time limit of the business department, and must be much smaller than this limit, and the diagnosis and location will become practical significance.

The basic information of failure prognostics and the uncertainty in the future determine that the quantification of prognostics confidence is essential. The reference α-λ index represents accuracy, precision, timeliness and prognostics confidence [16]. These indicators are derived from system performance, cost, and schedule. This article will not elaborate on them.

4 Experimental Results and Analysis

The pilot area of a project covers an urban area of approximately 10 km^2, the length of the sewage pipe network is approximately 110 km, the deployment of sensors: 45 level gauges, the deployment density is 2 to 3 km, and the intelligent service engine is online for 6 months. For blockage events, as shown in two different abnormal scenarios in Chapter 3.2.1, the corresponding time series characteristic curve and recognition effect are shown in Figs. 4 and 5. First, the time series decomposition is carried out on the water level historical data collected by the water level gauge installed in the pipe diameter of 0.5 m to obtain the trend component trend, seasonal and periodic, and rainwater inflow component residual component, from the trend component, it can be seen that there is an overall upward trend from January to June, which is consistent with the actual situation of 50% pipe diameter siltation in June. Second, the change point detection corresponding to the sudden change of liquid level, the black dotted line is the predicted change point position, which is consistent with the actual situation. The statistical data of the accuracy of suspected blockage abnormal events are shown in Table 2 below. At present, the recall rate cannot be obtained.

After the intelligent event, the diagnosis location will be started. The diagnosis range of the pipe network is determined by the number of pipes between the two monitoring points. The number of pipes is 25, and the number of model solutions is 250. Currently, it is assumed that only a single pipe is blocked. Performance results: 1) The diagnostic location range obtained is two pipes, one of which is a real blocked pipe and the other is a non-blocked pipe. 2) Diagnosis and positioning time. The cloud cluster has elastic scalability of computing resources. You can select the corresponding resource configuration according to the performance requirements. For example, the diagnosis location requirements are completed within 15 min after the event occurs, then the computing performance is that 250 solutions is computed within 15 min. Table 3 below uses the test performance of the server on the cloud, and

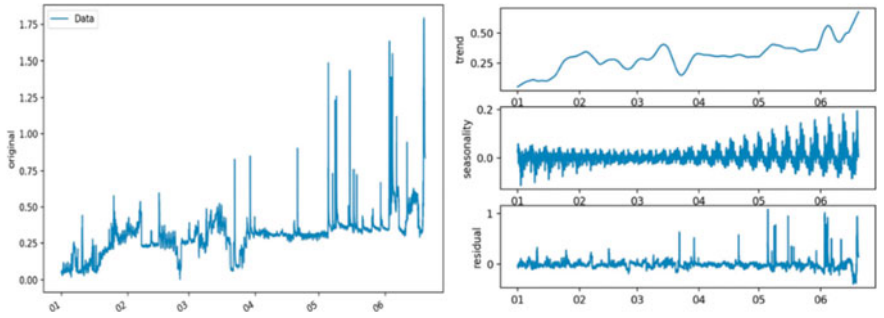

Fig. 4 Decomposition diagram of liquid level sequence corresponding to long-term blockage

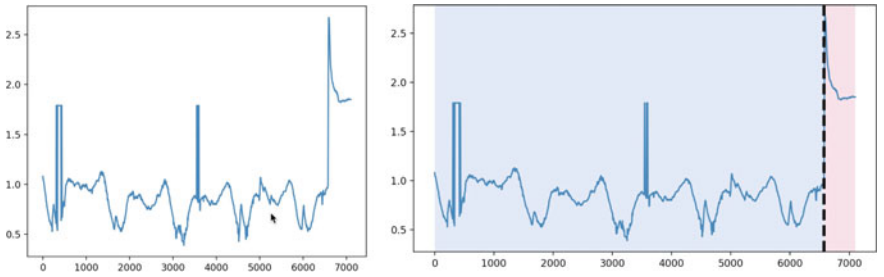

Fig. 5 Change point detection diagram of suspected sudden blockage

Table 2 Performance statistics of unsupervised learning algorithm for blockage events

Sub item	Value
Number of events	16
TP	12
FP	4
Precision	0.75

the calculation time of the solution represents the time for diagnosis location. The test data can be seen from Table 3, 20 server machines on the cloud, the calculation time is 11–12 min, which is basically consistent with the theory, which proves the advantages of distributed parallel computing for batch computing.

Table 3 The calculation performance of the simulations corresponding to the diagnosis location

Number of simulation solutions (scale)	Resource allocation on the Alibaba Cloud (C: CPU Cores, G: Memory unit GB)	Computing time
1	8C16G	70–90 S
250	20*8C16G	11–2 min

Table 4 Simulation data sample set corresponding to blockage fault

Blockage type	Severity description	Sample set (number of time series)
L1	The degree of blockage is 0–25% of the pipe diameter, normal	30,000
L2	The degree of blockage is 25–50% of the pipe diameter, and the severity level is 1	30,000
L3	The degree of blockage is 50–75% of the pipe diameter, and the severity level is 2	30,000
L4	The degree of blockage is 75–100% of the pipe diameter, and the severity level is 3	30,000

Solve the problem of F1 Score and low accuracy of smart events. In view of the insufficient fault feature data confirmed by online users, the training data mainly comes from the features extracted from the hydrodynamic model simulation fault, provided that the overall accuracy of the hydrodynamic model can reach 70%, the overall accuracy is estimated by using all monitoring node data and corresponding simulation data for likelihood estimation. The sewage pipe network model is selected to simulate the severity of different blockages of a certain pipe, and the time series corresponding to the upstream and downstream monitoring nodes are selected as the sample set. The sample set is shown in the following Table 4. The sample set is derived from the model simulation results of different input settings, which include: Different sewage discharge regular sequences, rainwater inflow, and different siltation degrees.

The sample set is taken from the time series of the upstream and downstream nodes where placed monitoring equipment of the simulated blockage pipe. The sample sampling frequency is 2 min, and the sample window is fixed at 6 h. The sample is normalized, and an example of selecting 4 classifications is shown in Fig. 6 below. L1–L4 samples correspond to L1–L4 blockage type in Table 4. The yellow represents the downstream node, and the blue dashed line represents the upstream node.

Divide the sample set, 10% as the test set, and 90% as the training set. Two different deep learning models are used to train 4 types of feature data, and the test performance is evaluated through micro F1 Score. After 500 epochs of training, the performance evaluation results are shown in Table 5 below. It can be seen that the performance of the Resnet method has improved nearly 0.2.

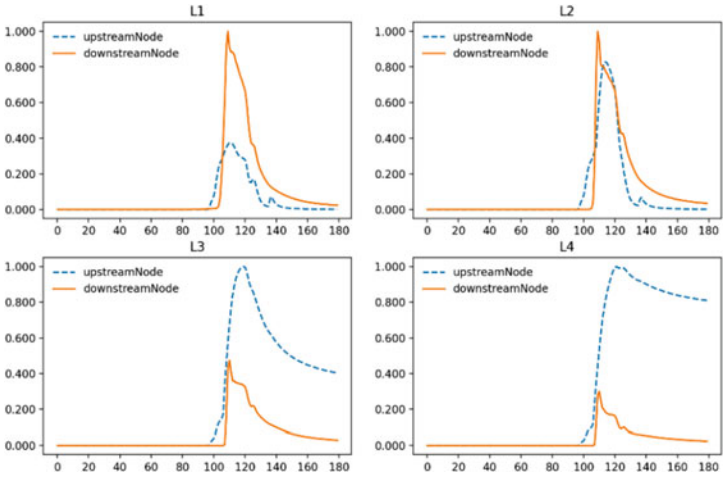

Fig. 6 Schematic diagram of blockage classification characteristic curve

Table 5 Performance statistics of deep learning algorithm for blockage events

Algorithm	CNN	Resnet
Micro precision	0.91	0.93
Micro recall	0.58	0.89
Micro F1	0.708	0.909

5 Conclusion

The paper proposes intelligent identification and diagnosis services for the hydraulic failure modes such as blockage, leakage, inflow and infiltration, overflow of the drainage pipe network, and takes blockage as an example to explain the process and algorithms of pattern recognition and diagnosis. The performance of intelligent event recognition and diagnosis is evaluated using real pipe network fault samples and hydrodynamic model simulation fault samples, and the results show the rationality and feasibility of the method. Insufficiency, the online performance evaluation of the deep learning model needs to be performed after the sample is enough, which can only be proved from the simulation that it has better performance than the unsupervised learning algorithm. At present, the research focuses on data processing, fault identification and diagnosis and location. For fault prognostics, in addition to the application of hydrodynamic model for overflow prognostics, we will develop the prognostics of other faults. The research scope of this paper belongs to the prognostic maintenance of pipe networks. It has not covered the prognostics pipe life, asset management, and business applications. Its goal is to improve the performance indicators of fault identification, diagnosis, and prognostics and integrate by upper application software.

Acknowledgements The model fault simulation method for diagnosis location in this work was proposed by experts from the partner China Water Resources and Hydropower Science Research Institute.

References

1. CIRIA RP992 The SuDS Manual Update Paper RP992/17 November 2013
2. Risk assessment of sewer systems NOVATECH 2007
3. Anbari MJ, Tabesh M, Roozbahani A (2017) Risk assessment model to prioritize sewer pipes inspection in wastewater collection networks. J Environ Manage 190:91e101
4. Okwori E, Viklander M, Hedström A Performance assessment of Swedish sewer pipe networks using pipe blockage and other associated performance indicators. H2Open J 3(1)
5. Lee J, Park CY, Baek S, Han SH, Yun S (2021) Risk-based prioritization of sewer pipe inspection from infrastructure asset management perspective. Sustainability 13:7213
6. Liu Y, Zhang W, Cui X, Zhang G, Hang G, Wang G (2014) City pipe network intelligent service based on GIS and Internet of Things. In: 2014 7th international conference on intelligent computation technology and automation
7. Zhu X, Feng Z, Huang G (2018) Blocking detection of underground drainage pipe based on CEEMD and GG clustering. In: The 30th Chinese control and decision conference (2018 CCDC)
8. Yan J, Feng Z, Wu J, Ma J (2017) Research on identifying drainage pipeline blockage based on multi-feature fusion. In: 2017 29th Chinese control and decision conference (CCDC)
9. Guo X Quantification and case study of the online monitoring scheme of drainage pipe network. Beijing Qinghuan Smart Water Technology Co., Beijing
10. Wand M, Jones M(1995) Kernel Smoothing: Monographs of Statistics and Applied Probability. Chapman & Hall, London
11. Yu Y, Zhu Y, Li S, Wan D Time series outlier detection based on sliding window prediction. Math Probl Eng
12. Wen Q, He K, Sun L, Zhang Y, Ke M, Xu H (2021) RobustPeriod: time-frequency mining for robust multiple periodicities detection. In: SIGMOD 2021
13. Cleveland RB, Cleveland WS, McRae JE, Terpenning I (1990) STL: a seasonal-trend decomposition procedure based on loess. J Official Stat 6(1):3–73
14. Taylor SJ, Letham B (2017) Forecasting at Scale. PeerJ Preprints, 27 September 2017
15. Zhao M, Zhong S, Fu X, Tang B, Pecht M (2020) Deep residual shrinkage networks for fault diagnosis. IEEE Trans Ind Inform 16(7)
16. Abhinav Saxena R, Roychoudhury I, Celaya JR Requirements flowdown for prognostics and health management. American Institute of Aeronautics and Astronautics

Analysis of Construction Technology and Soil Settlement Law for In-Situ Break-and-Replace of Pipelines

Minghao Su, Yu Gan, Shaohui Yu, Yang Li, and Peng Cheng

Abstract In order to solve the problem of renewing the whole structure of the old pipeline, this paper proposes a new construction method for mechanized non-excavation pipelines in-situ break-and-replace method (PBR). In order to analyse the law of soil deformation caused by PBR construction, combined with the specific pipeline renewal project, a model was established through finite element software to simulate the pipeline renewal construction. The results show that with the advancement of the pipeline renewal construction, the displacement of the soil is mainly concentrated around the jacking surface, and the maximum settlement is 3.04 mm, which meets the requirements of the specification. During the pipeline renewal construction process, the surface settlement curve showed a quasi-normal distribution, and the impact range was mainly about 3D before and after the advancement.

Keywords PBR · Construction simulation · Settlement

1 Introduction

In recent years, various municipal pipelines in the shallow underground space in the core area of the city have been corroded and aging, and the problems that they are on the verge of or even exceeding their design life have become prominent. The problems of pipeline misalignment, leakage, damage, and foreign matter intrusion are high occurrences, such as sewage overflow, water pollution, and water pollution. Urban heavy rain and waterlogging, lake "black water", pipe bursts, road collapse and other problems and the root causes of accidents, the urban pipe network system is close to the period of comprehensive renewal [1–3].

With the progress of the times, it has become more difficult to meet the many requirements of urban core areas with the use of open-cut method to update and repair pipelines. In recent years, trenchless technology has gradually matured and

M. Su · Y. Gan (✉) · S. Yu · Y. Li · P. Cheng
Underground Space Research and Design Institute, China Railway Engineering Equipment Group Co., Ltd., Henan 450016 Zhengzhou, China
e-mail: creggy@126.com

X. Liu (ed.), *Proceedings of 2021 China-Europe International Conference on Pipelines and Trenchless Technology*, Lecture Notes in Civil Engineering 212,
https://doi.org/10.1007/978-981-19-4067-5_20

has begun to be widely accepted by people [4–7]. Among them, the PBR construction method uses pipeline boring equipment to destroy the old pipeline in situ, and at the same time replace the new pipeline by jacking, so as to realize the replacement of the entire pipeline structure.

In-situ removal and renewal of pipelines are mostly characterized by complex surrounding environments and sensitive to deformation of buildings (structures) and underground pipelines [8, 9]. How to more accurately assess the impact of pipeline renewal construction on surrounding strata and environment One of the most important links in the application of this technology [10]. At present, there are many researches on the characteristics of ground settlement caused by shield tunneling and pipe jacking construction, and there are few analyses on the law of soil deformation caused by pipeline in-situ breaking and renewal construction.

Therefore, this article relies on the specific pipeline renewal construction project, based on PLAXIS 3D finite element software to analyze and study the surface settlement deformation law caused by the pipeline renewal construction, and verify the feasibility and applicability of PBR on this basis, and provide reference for related projects.

2 Engineering Applications

2.1 Project Overview

The original pipeline before the renewal of the project section is composed of 3 sections and 2 inspection wells (Fig. 1), each section is about 20 m in length, with a total length of 60 m, and the buried depth of the pipeline is 3 m. The soil layer is mainly silt sand. The pipeline is DN1000 prefabricated reinforced concrete socket type tertiary pipe. Section 1 is a sand-gravel foundation, Sect. 2 is a plain concrete foundation, and Sect. 3 is a staggered working condition, and the staggered heights are 200, 400, and 600 mm respectively. The updated pipeline is a DN1200 flexible type B steel socket prefabricated reinforced concrete tertiary pipe (Fig. 2).

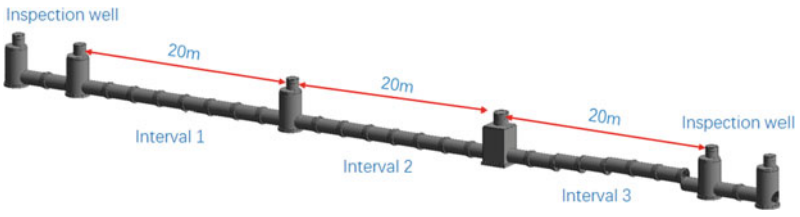

Fig. 1 The pipeline before the update

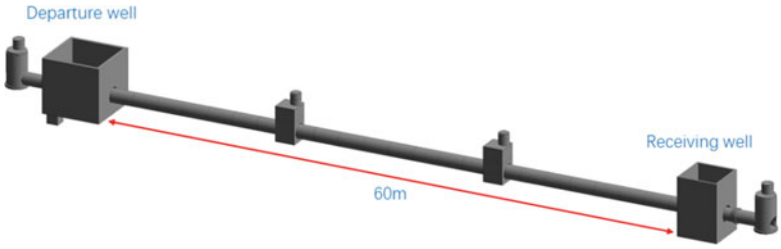

Fig. 2 The updated pipeline

2.2 The Key Technology of Construction

The main steps for the construction of the pipeline breaking and renewal construction method are: Work well construction, equipment installation, equipment initiation, broken pipe excavation (pipe section installation), and equipment reception. Pipeline breaking construction is different from ordinary stratum tunneling construction. The equipment is facing the breaking up of existing structures and tunneling construction. It not only needs to cut old pipelines, but also pass through intermediate inspection wells. The control of construction tunneling parameters, attitude control, and surface deformation control require high requirements. The key points in the construction of pipeline demolition and renewal are:

(1) Tunneling parameter control. The working conditions of the pipeline renewal and excavation are more complicated. There are both reinforced concrete pipes and sandy soil layers. The tunnel face is soft and hard, which is a composite soil layer. Reasonable control of the relationship between thrust, tunneling speed and rotational speed can ensure the size and length of the fragments and fragments of steel and concrete, thereby reducing the risk of pipe blockage in the mud-water circulation. Through the collection of the removed slag, it was found that the removed concrete slag can be controlled below 10 mm, and the steel bar accounted for a larger proportion of about 5 cm. At the same time, the chopped old pipe sealing tape was also collected (Figs. 3, 4 and 5).

(2) Line attitude control. During the tunneling process, when the pipe section is cut close to the interface, the remaining length of the pipe section becomes less, and it is easy to cause a sudden change in the direction line during the tunneling

Fig. 3 Drain the slag

Fig. 4 Drain the rebar

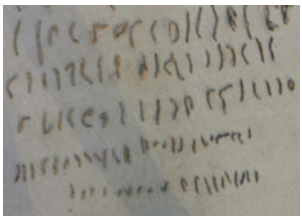

Fig. 5 Drain the apron

process. In addition, the test section interval 3 is set to the working condition of the staggered platform, and the influence of eccentric cutting on the tunneling line It's also very big. The control of the line attitude during tunneling is the key. It should also be noted that the test section project involves two inspection wells, and the equipment needs to be pushed through the well by air, and the equipment line must be controlled below 3 cm to ensure a smooth crossing.

(3) Surface deformation control. The equipment adopts mud-water balance to control the stability of the tunneling surface, but the tunneling surface of the equipment is small and the soil is sandy, which belongs to poor geology that is difficult to control. In addition, the condition of both soft and hard soil layers requires special attention to changes in the ground surface. Pipeline renewal construction During this period, attention should be paid to strengthening the surface monitoring during tunneling, and the tunnelling parameters and control strategies should be adjusted in time through changes in settlement.

3 Modeling

In order to further analyze the feasibility and applicability of the PBR method. PLAXIS 3D finite element software was used to carry out the numerical simulation of Sect. 1 of the project to analyze the impact of pipeline construction on ground settlement.

The model was established based on the pipe section shape and the symmetry of the surrounding environment, which only included half of the pipe. Combined with the actual situation and the distribution of soil layers, the size of the model is set to $10 \times 20 \times 17.4$ m (x × y × z). The model is divided into 44,052 nodes and 26,668 units.

For the simulation of the on-site construction process, the renewal of the pipeline starts from the entrance of the tunnel and the renewal of the tunnel is carried out along the direction shown in Fig. 6. The length of the pipe section is 2.5 m, then every 2.5 m in the simulation process is a jacking, and the jacking stops at a position of 20 m. As shown in Fig. 7, the focus of the pipeline renewal construction process simulation is to freeze the old pipe and the soil with a thickness of 0.1 m around the pipe, and install the new pipe as the pipe jacking equipment advances. Among them, the interaction between the pipe jacking equipment, the new pipe and the soil is defined as the interface unit. The top surface of the model adopts a free interface, the bottom of the model restricts the three-way displacement, and the remaining surfaces only restrict the normal displacement.

The material parameters required for this model are shown in Table 1. Among them, the soil constitutive model adopts the Moore Coulomb model; the pipe segment adopts the solid element simulation, and the linear elastic model is selected; the roadheader uses the plate element to simulate.

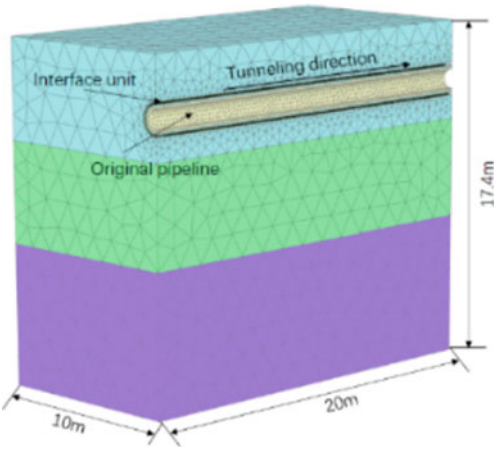

Fig. 6 Model network partition

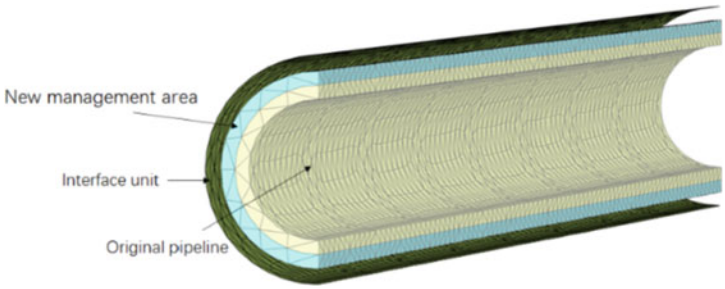

Fig. 7 Pipeline network division

Table 1 Material parameters

Material name	γ/(kN/m^2)	E/Mpa	c/kpa	φ/(°)	v	d/m
Silt	19.5	11	5	27.5	0.3	5.76
Clay	19.2	12	18	21	0.35	4.68
Granite	19	15.3	25	25	0.28	11.84
Pipe segment	25	20,000	/	/	0.2	0.1
Pipeline Boring Equipment	120	23,000	/	/	0.2	0.03

4 Analysis of Calculation Results

4.1 Analysis of the Law of Soil Settlement

The soil displacement during the pipeline renewal construction process is shown in Fig. 8. It can be found that as the pipeline renewal construction progresses, the soil displacement is mainly concentrated around the jacking surface. Figure 9 shows the distribution of plastic points after the construction. It can be found that the plastic points are mainly concentrated at the junction of the pipe joints.

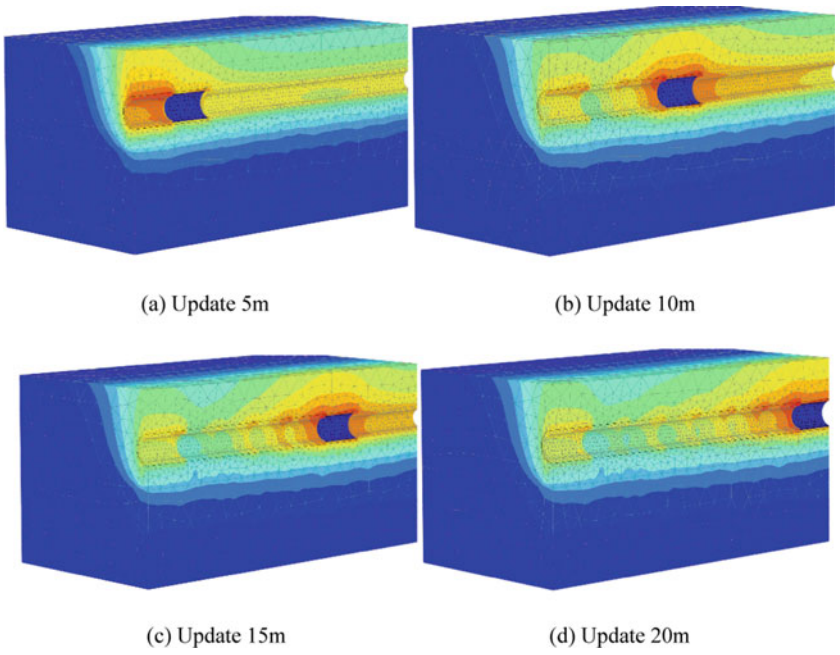

Fig. 8 Displacement cloud diagram during construction

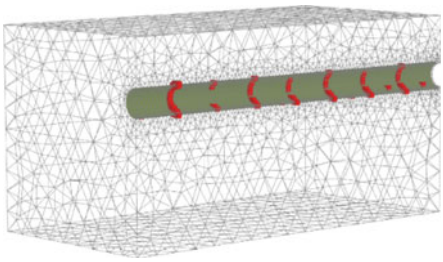

Fig. 9 Plastic point distribution

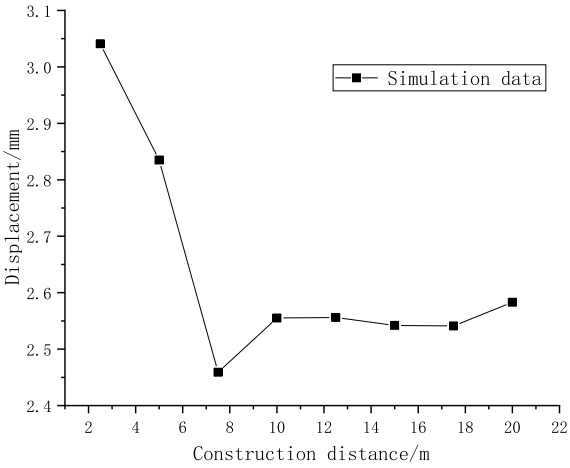

Fig. 10 Maximum displacement of soil during construction

Figure 10 shows the maximum displacement of the soil at different construction stages. During the entire construction phase, the soil settlement was the largest during the initial construction, with the maximum value being 3.04 mm. As the jacking distance increases, the settlement tends to stabilize.

4.2 Analysis on the Law of Surface Subsidence

Figure 11 shows the settlement of the ground at different horizontal distances above the center of the pipeline. Figure 12 shows the relationship between the pipeline renewal construction distance and the ground settlement. It can be seen from Fig. 11 that the settlement curve is a quasi-normal distribution, and this distribution becomes more and more obvious as the construction progresses. Except for the first, second and last construction phases, the relationship between horizontal displacement and ground settlement in the remaining phases all showed a trend of first decreasing, then increasing to the peak and then decreasing. The first and second stages are different because they are at the beginning of the construction stage, so the settlement is the

largest near the origin, and it decreases with the increase of the distance. In the last construction phase, the opposite is true. The place where the distance is farthest has the largest settlement, and the general law is the same. The surface settlement was the largest during the initial construction, with the maximum value being 2.11 mm. As the jacking distance increases, the settlement tends to stabilize. The surface settlement at the middle position increases first and then decreases with the increase of the construction distance. The settlement at the initial position and the end point is the largest when the construction is at this position.

It can be seen from Fig. 12 that during the jacking process, the surface settlement decreases as the horizontal distance from the pipe axis increases, showing a normal

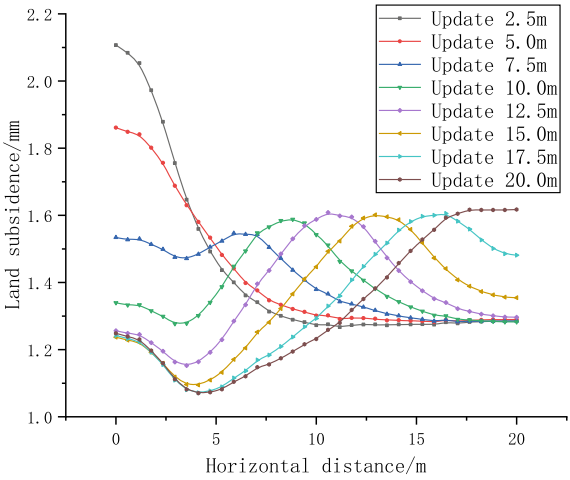

Fig. 11 Settlement at different horizontal distances

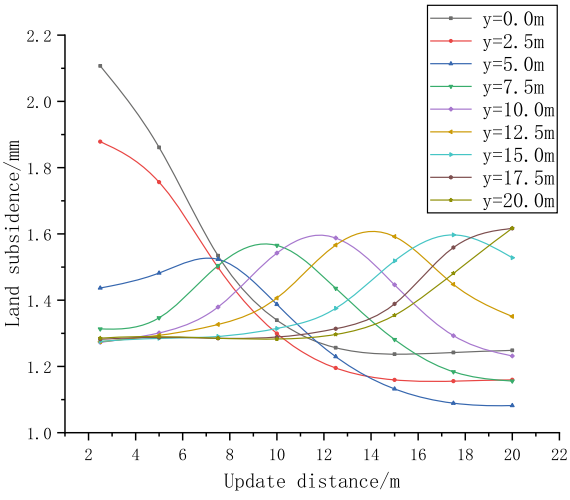

Fig. 12 Settlement at different construction distances

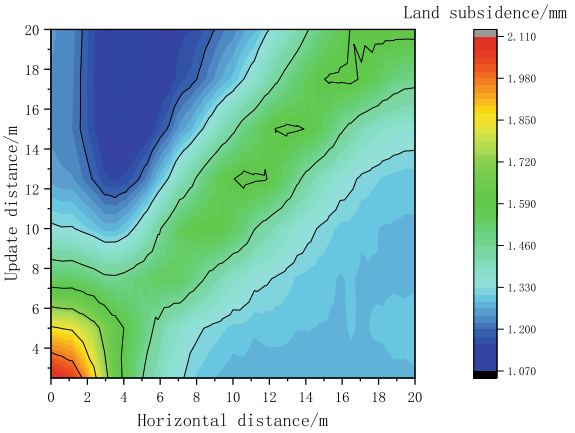

Fig. 13 The relationship between construction distance, horizontal distance and settlement

distribution; as the distance from the jacking surface increases, the surface settlement value becomes smaller and smaller. Basically, the attenuation is large in y = 3D (pipe section length). After 3D, the surface settlement tends to be stable as a whole. From this, it can be inferred that the surface settlement value of each cross section must also tend to one value after different advancing surfaces. As the distance from the propulsion surface increases, this value gradually decreases, but the difference is not significant, indicating that the impact of the pipeline renewal construction on the surface deformation is mainly in the 3D range before and after the propulsion.

In order to more intuitively show the relationship between the construction distance, the different horizontal distances from the ground surface and the ground settlement, a cloud diagram is drawn as shown in Fig. 13. It can be found that the settlement of the ground surface gradually decreases from the center of the jacking axis to the two sides. With the jacking axis as the center, the settlements on both sides are symmetrically distributed. It shows that during the renewal and tunneling of the pipeline, the surface settlement at the location of the tunneling machine is the largest, which conforms to the rules of on-site construction.

5 Conclusion

This paper analyzes the soil deformation laws caused by PBR construction through finite element software for specific pipeline renewal construction projects. The main conclusions are as follows:

(1) The PBR method can realize the in-situ renewal of the existing and old pipelines when the new pipeline location is difficult to plan. After the old pipelines are crushed in-situ to discharge the slag, the construction can be simultaneously jacked in the in-situ.

(2) With the advancement of pipeline renewal construction, the displacement of the soil is mainly concentrated around the jacking surface, and the maximum settlement is 3.04 mm, which meets the requirements of the specification. After the construction, the plastic points are mainly concentrated at the junction of the pipe joints.
(3) During the pipeline renewal construction process, the surface settlement curve showed a quasi-normal distribution, and as the construction progressed, this distribution became more and more obvious. The influence of the pipeline renewal construction on the surface deformation was mainly in the 3D range before and after the advancement.

References

1. Tang J, Zhang Y, Mei X (2019) Methods and measures for improving the quality and efficiency of urban drainage systems. Water Supply Drainage 55(04):30–38
2. Ma B, Zeng C, Yang C (2007) Investigation and analysis of the status quo of urban underground lifeline projects in China. China Society for Trenchless Technology. 2007. Trenchless Technology Conference Papers Album. China Society for Trenchless Technology: Trenchless Technology Magazine, vol 5
3. Zhang P, Shen H, Ma B (2010) Research on the evaluation technology of municipal pipelines. China Society for Trenchless Technology. In: Proceedings of the 2010 Trenchless Technology Conference. China Society for Trenchless Technology: Trenchless Technology Journal, vol 6
4. Tong H, Wu X (2009) Laboratory study of disaccharide organio compound drilling fluid for trenchless technology. In: ICPTT 2009: proceedings international conference on pipelines and trenchless technology, Shanghai
5. Yan C (2010) Current status and prospects of my country's trenchless industry. Prospect Eng (Rock Soil Drill Tunneling Eng) 10:5660
6. Zhang G, Ma C (2007) Technical comparative analysis of similar processes in current domestic trenchless lining technology. Trenchless Technol 2–3:127–130
7. Ren F, Yuan B, Zhu Y, Liu C (2003) Application of trenchless technology in urban pipeline engineering. J Guangdong Univ Technol 2:6064
8. Zhang P, Ma B, Zeng C et al (2016) Key techniques for the largest curved pipe jacking roof to date: A case study of Gongbei tunnel. Tunnelling Undergr Space Technol 59:134–145
9. Shi P, Yu C, Pan J et al (2017) Research on the jacking force of the large-diameter curved tube curtain of Gongbei Tunnel. Chin J Rock Mech Eng 36(9):2251–2259
10. Chen X, Zhang P, Ding S et al (2015) Estimation and measurement analysis of jacking force of large-diameter three-dimensional curve pipe jacking. Rock Soil Mech 36(S1):547-552.2

An Experimental Study on the Acoustic Emission Response of Reinforced Concrete Pipe Under Diametrical Load

PengPeng Li, Jian Feng Li, YaJian Wang, ZhouJing Ye, HuiFang Liu, SongLi Yang, and LinBing Wang

Abstract In this study, mechanical loading tests and acoustic emission (AE) monitoring were conducted for reinforced concrete pipe segments, and the AE response of the whole process of segment failure is explored. The results of test show that the AE signal is correlated with the change of load, and the accumulated ringing count of AE signal can effectively characterize the failure characteristics of reinforced concrete pipe segments. Based on the energy and cumulative ringing count of AE signals, the damage process of the pipe segment under load is divided into four stages: in the compaction stage, the AE energy and cumulative ringing count are small; in the linear elastic stage, the AE energy and cumulative ringing count increase steadily; in the crack extension stage, the AE cumulative ringing count increases suddenly when the load fluctuates; in the residual strength stage, the growth rate of AE energy and cumulative ringing count decreases. The full-scale pipes and segment specimens have the same variation trend of load curve and spectrum range of AE signal. Therefore, the segment mechanical loading test can be used as an effective method to study the local loading stress distribution of full-scale pipe.

Keywords Reinforced concrete pipe segment · Mechanical loading · Acoustic emission · Time–frequency analysis

1 Introduction

Reinforced concrete pipes are mainly used in urban construction, agricultural water conservancy projects, factories, ports, and mines. The most widely used are underground drainage pipes. As the lifeline of the city, urban pipeline network undertakes

P. Li · J. F. Li · Y. Wang · Z. Ye · H. Liu · S. Yang
National Center for Materials Service Safety, University of Science and Technology Beijing, Beijing 100083, China

L. Wang (✉)
Joint USTB-Virginia Laboratory on Multifunctional, Materials, USTB, Beijing 100083, China
e-mail: wangl@vt.edu

Virginia Tech, Blacksburg, VA 24061, USA

X. Liu (ed.), *Proceedings of 2021 China-Europe International Conference on Pipelines and Trenchless Technology*, Lecture Notes in Civil Engineering 212,
https://doi.org/10.1007/978-981-19-4067-5_21

the function of transporting water, gas and other materials and energy. Due to the imperfect design of drainage pipes at the early stage of construction and the lack of systematic maintenance at the later stage, underground pipeline networks in China have started to face problems such as corrosion and damage in recent years [1, 2]. The study and monitoring of the service performance of drainage pipes have gradually become the focus of many scholars' research.

In the study of mechanical properties and corrosion of pipes, Huang Wenchun [3] et al. established a load model for buried drainage pipes under vibration load and uniform load with reinforced concrete pipes, FRP pipes and HDPE pipes, and the results of the study showed that the vertical displacement of all three types of pipes decreased continuously when the burial depth increased within a certain range; Liao Daocheng [4] et al. studied the effect of steel reinforcement configuration on the structural performance of reinforced concrete pipes by establishing a finite element analysis model for direct buried pipes in trenches. The effect of reinforcement configuration on the structural performance of reinforced concrete pipes was investigated by Abdul-Aziz Younis [5] et al. who verified the strength parameters of the finite element prediction model using full-scale pipe tests and numerical simulations; reinforcement corrosion under the conditions of drainage pipe scaling will further promote concrete corrosion and cracking [6]; Fouad T. Al Rikabi [7] et al. evaluated the performance of thin-walled concrete pipes made of synthetic fiber materials by cyclic loading experiments using parameters such as load, deflection, stiffness, crack extension and crack width as evaluation indicators, and the results showed that the new concrete pipes have significantly enhanced strength while keeping the deflection essentially constant.

In the monitoring of reinforced concrete pipelines, the AE detection technique was first applied to the monitoring of concrete structures by Rusch [8] in 1959. Reza Goldaran [9, 10] conducted accelerated corrosion experiments and internal loading and unloading damage detection of pipelines by internal hydraulic loading of pipelines. The results showed that various damages at any stage of the pipeline life cycle would generate AE signals, and the damage sources could be identified and classified using AE; Mohammad Pour-Ghaz [11] et al. used electrical sensing, magnetic sensing, and AE to monitor the structural damage evolution during pressure loading of different pipe sections of concrete pipelines. The damage process of concrete pipes with pipe segments was divided into three stages based on the monitoring results.

The service environment of urban drainage pipes is particularly harsh and complex among all types of pipeline systems, and they are subject to long-term decline in strength due to the combined effects of road traffic loading, soil acid and alkali corrosion and rainwater erosion, etc. Once cracks and corrosion damage occur during service, they can cause sewage leakage, soil and water pollution and road collapse, bringing serious economic losses and casualties.

AE is defined as the elastic energy released from materials which are undergoing deformation. Also it can be defined as "the transient elastic waves which are generated by the rapid release of energy from localized sources within a material" [12]. The rapid release of elastic energy, the AE event, propagates through the structure to

arrive at the structure surface where a piezoelectric transducer is mounted. These transducers detect the displacement of the surface at different locations and convert it into a usable electric signal. By analysis the resultant waveform in terms of feature data such as amplitude, energy and time of arrival, the severity and location of the AE source can be assessed.

At present, there are relatively few studies on nondestructive monitoring of reinforced concrete pipes, and it is important to investigate the characteristic indexes that can effectively characterize the strength of reinforced concrete pipes for the maintenance and service monitoring of reinforced concrete pipes. In this paper, by collecting the AE signals during the loading process of the pipe segment, we aim to use the time domain evolution law and frequency domain characteristics of the AE signals in different damage stages of the pipe to realize the risk monitoring and early warning of the damage of the pipe, which is of great significance to ensure the long-term stable operation of the urban drainage network system.

2 Experimental Methods

2.1 Experimental System

The experimental system is composed of two parts: the pipe piece loading system and the data acquisition system. The loading system as shown in the figure below consists of specimen loading device, MTS microcomputer-controlled electro-hydraulic servo pressure tester and main control computer, which has a maximum load of 10 kN. The data acquisition system consists of four parts: AE sensor, amplifier, collector and host computer. This experiment adopts DS5 full information AE analyzer from Beijing Soft Island Times Technology Co., Ltd. which can realize multi-channel, high acquisition frequency and full waveform data acquisition simultaneously.

2.2 Preparation of Pipe Specimens

Due to the strict requirements of equipment for full-scale pipeline experiments, and due to the scale effect of tiny crack expansion and formation is extremely slow to observe, and the AE signal generated by large-scale pipeline experiments is severely attenuated. The previous numerical simulation study [13, 14] of the pipeline shows that the buried pipeline is under the action of the surrounding pressure at the top 1/4 arc of the pipeline section bending moment is 0, the loading process of the pipe section is only subject to axial force. Based on this, this paper simulates the pipeline loading experiment by using the pipe piece specimen on the basis of reducing the cross-sectional stress distribution of the buried pipeline in service, simplifying the experimental setup and steps. The top 1/4 arc of reinforced concrete pipe with inner

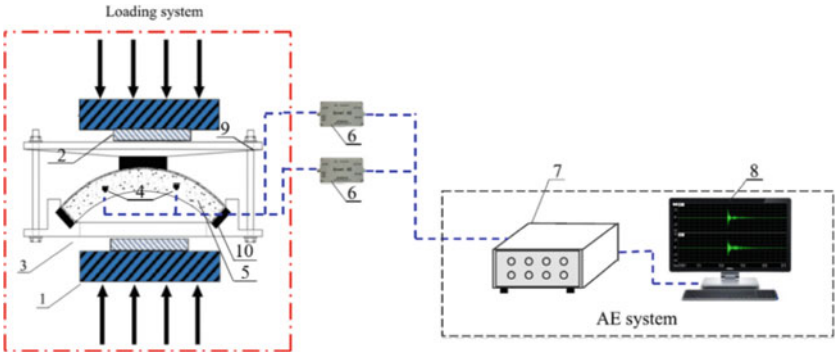

Fig. 1 Mechanical loading experiment system of reinforced concrete segment. 1-compression testing machine; 2-gasket; 3-experimental fixture; 4-AE probe; 5-concrete sample; 6-signal amplifier; 7-AE data acquisition instrument; 8-AE data analysis system; 9-bolt; 10-rubber pad

diameter of 300 and length of 150 mm was selected as the specimen, and the integrity of the structure and strength of the specimen was ensured during the cutting process, as shown in Fig. 1.

2.3 Experimental Methods

The amplification of the AE preamplifier was adjusted to 20 dB, and the AE sensor was fixed on the side of the specimen by the sensor clamping device, and the coupling agent was filled between the surface of the specimen and the AE sensor to ensure good contact of the sensor. The experiment adopts the displacement-controlled loading method, and the loading rate is 0.5 mm/s. The experiment first adjusts the position of the indenter to apply 100 N pre-stress to ensure the full contact between the indenter and the upper platen, and then ensures that the data of each channel of the AE collector are accepted normally and starts the preset experimental program of the press and the data saving function of the AE collector at the same time. Signal for full waveform data acquisition (Table 1 and Fig. 2).

Table 1 Reinforced concrete pipe parameters

Inner diameter	Thickness	Outer diameter	Skeleton layer position	Circumferential reinforcement bars				Longitudinal reinforcement	
				Diameter	Inner diameter	Number of rings	Pitch	Diameter	Quantity
300	30	360	Single	3	321	13.3	75	5	6

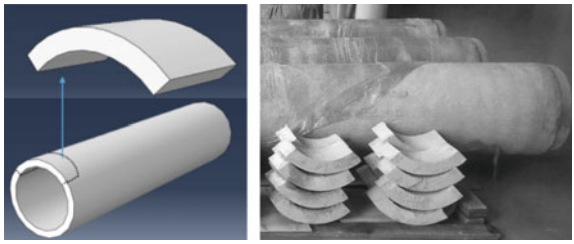

Fig. 2 Cutting pipe segment and experimental setup

3 Experimental Results and Analysis

In this paper, a total of three sets of pipe segment loading experiments were conducted, and the results of a typical pipe segment loading experiment were analyzed by a set of space limitation (Fig. 3).

3.1 Time Domain Analysis

Due to the limitation of space, one group of experimental results are selected for analysis. Figure 4 shows the curve of AE energy and stress-time relationship in the process of reinforced concrete pipe segment failure under load. emission) energy and stress-time relationship in the process of reinforced concrete pipe segment failure under load. the concrete sample can produce AE signals in the process of loading failure, and the change of AE energy has a direct relationship with the deformation In order to analyze AE energy variation law of concrete in the process of loading failure, the failure process is divided into four stages [11]: compaction stage (A stage, stress level 0–20%), linear elastic stage (B stage, stress level 20–60%), crack development damage stage (C stage, stress level 60–110%), and residual strength stage (D stage, over peak stress level).

In the compaction stage (A stage), the original pores and cracks of the sample are compacted and closed under load. When the sample gradually changes from compaction stage to linear elastic stage (B stage) under load, new cracks germinate,

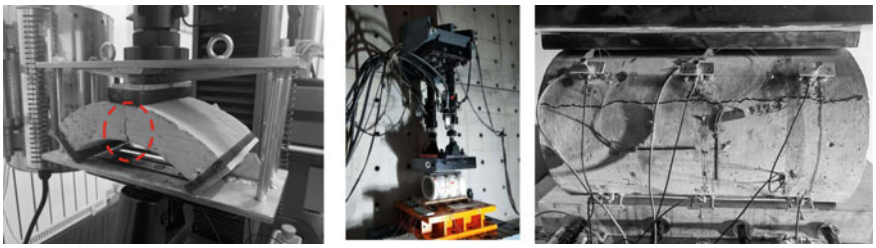

Fig. 3 Pipe segment and pipe damage under load

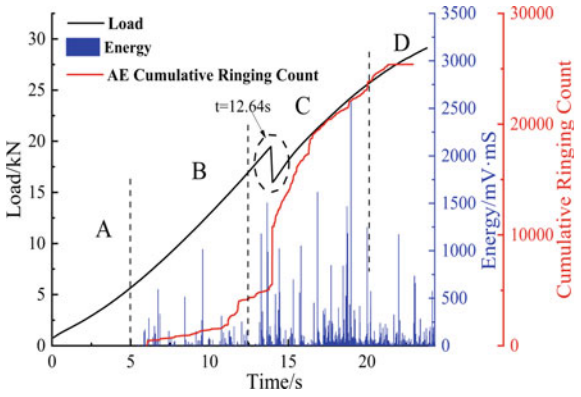

Fig. 4 Sample loading curve and AE signal energy

When the sample gradually changes from compaction stage to linear elastic stage (B stage) under load, new cracks germinate, a large number of cracks expand stably, and irreversible deformation appears, and the AE energy showed an increasing trend with a slow speed. When the load reaches the crack development damage stage (C stage), a large number of cracks inside the sample rapidly expand, cross, and gather, leading to the formation of macroscopic through cracks. At this time, the stress peak has been reached, violent friction has occurred between particles, and After the formation of a large number of macroscopic failure of the sample, After the formation of a large number of macroscopic failure of the sample, the sample enters into the residual strength stage (D stage) at which time due to the support role of the internal steel skeleton samples still have a Under the effect of the load, cracks are further generated, but the number of cracks and the rate of their generation At this stage, the rate of load increase slows down simultaneously due to the loading of the steel skeleton samples. At this stage, the rate of load increase slows down simultaneously due to the loading of the steel skeleton.

Figure 5 shows the comparison of the loading curves of the full-scale pipe and pipe piece specimens with the same material ratio, the maximum load is 20 kn when the main damage occurs in both, and the load changes in the same trend during the whole loading process. Cracks; C stage, the specimen's load curve is close to linear growth, reaching the maximum load when the specimen occurs the main damage, cracks through the surface of the specimen, after the load falls back quickly, the load drops to a certain level due to the support of the internal reinforcement structure of the specimen, the load again began to slowly climb, at this time there are still a small amount of crack development and expansion; into the D stage, the specimen is mainly internal reinforcement structure bearing pressure, the load The curve tends to be smooth, and the growth rate decreases again. Due to the existence of restraint on both sides during the loading process of the pipe piece, the load continues to grow and sing over the maximum damage load after the main damage occurs, while there is no binding force on both sides after the damage of the full-scale pipe occurs, and the load level will not exceed its maximum damage load after the main damage occurs. In summary, the damage mechanism and load change trend of the mechanical

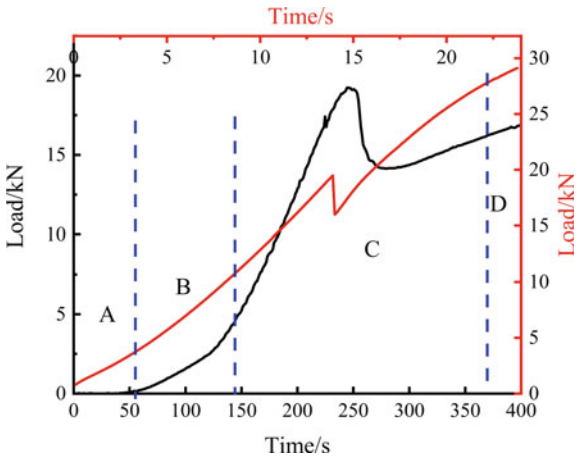

Fig. 5 Comparison of full-scale pipe and pipe segment loading curves

loading process of full-scale pipe and pipe segment are the same, which indicates that the mechanical loading of pipe segment can simulate and replace the actual loading of full-scale pipe to a certain extent.

3.2 Frequency Domain Analysis

In the following, the AE waveforms of the full-scale pipe and the pipe segment are selected for analysis when the damage occurs during the loading process.

The spectral range of AE signal of pipe segment and full-scale pipe is similar, both are 0–127 Hz, the main frequency of AE signal of pipe segment is 7.17 Hz, the main frequency of AE signal of pipe is 44.2 Hz, compared with the AE signal of pipe segment, the spectral components of AE signal of pipe are more complex, and contain the main frequency components of AE signal of pipe segment. Since the generation of AE signal is related to the material and damage form of the specimen, it can be inferred that the internal loaded damage type of the full-scale pipe is richer and the damage intensity is greater compared with the pipe segment loading damage process, and the pipe segment loading process can reflect the local loaded damage of the full-scale pipe, which is beneficial to the specific analysis of the single influencing factors of the damage of the full-scale pipe (Figs. 6, 7, 8 and 9).

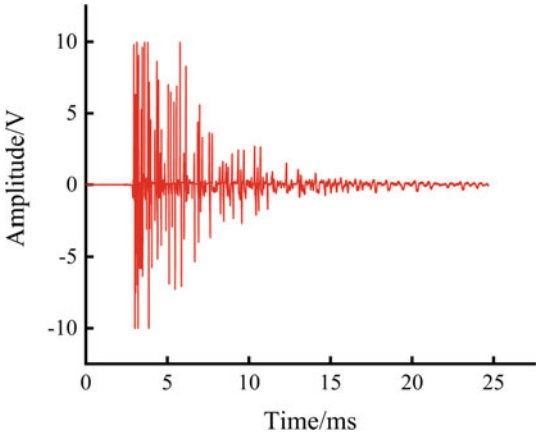

Fig. 6 AE waveform of pipe segment

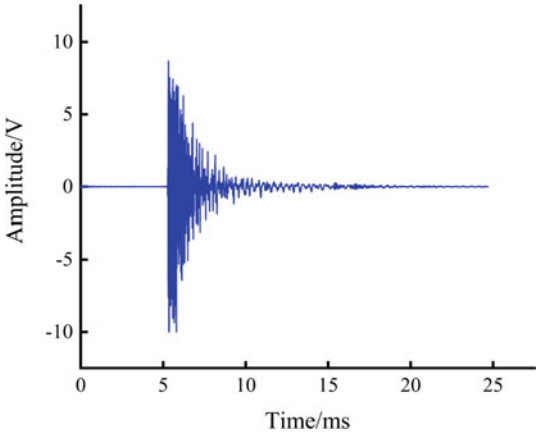

Fig. 7 AE waveform of pipe

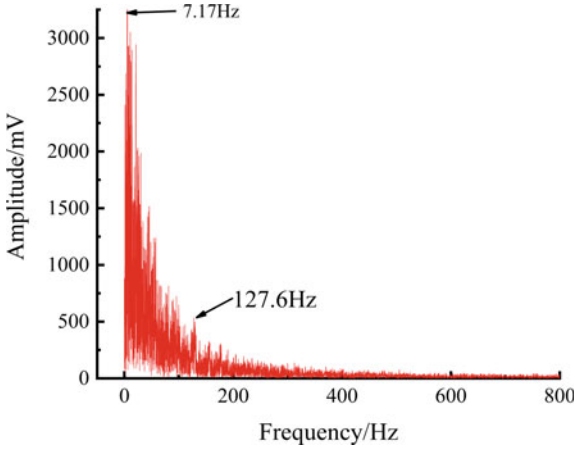

Fig. 8 AE spectrum of pipe segment

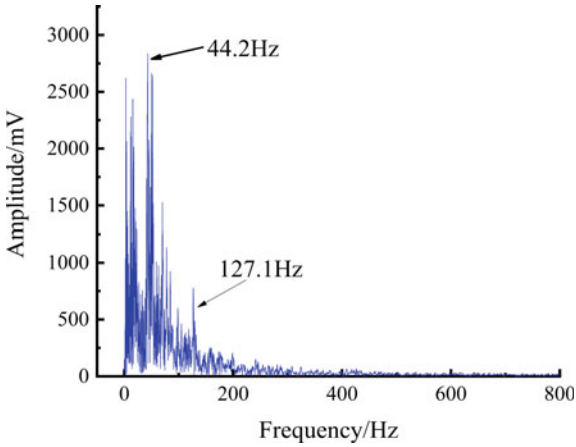

Fig. 9 AE spectrum of pipe

4 Conclusion

The present study was developed by using the AE for monitoring and identification of damage in reinforced concrete full-scale pipes and pipe segments. In order to simplify the experimental setup and improve the signal acquisition effect, the loading experiment of reinforced concrete pipe segment was designed. The signals of mechanical and AE were collected synchronously to analyze the AE response during the damage of the pipe segment. The results of the current study are summarized as follows:

(1) The AE signal during the loading of the pipe segment is load dependent. In the compaction stage, the specimens are less loaded and almost no AE signal is generated. In the linear elastic stage, the loading curve of the specimen grows linearly, the AE energy level generally increases, and the cumulative AE ringing count gradually increases, showing a small rising trend. In the crack development and damage stage, the load reaches the peak load and then decreases rapidly, macroscopic through cracks are formed, the AE energy level increases further, and the cumulative ringing count increases abruptly when the load fluctuates. In the stage of residual strength, the deformation of the internal reinforcement load of the specimen mainly occurs, the loading curve of the specimen increases slowly, the gradual weakening of AE energy, and the growth rate of AE cumulative ringing count decreases.

(2) In the process of damage of pipe piece under load, the trend of change of cumulative ringing count is the same as the trend of change of specimen under load, and the cumulative ringing count increases abruptly when the main damage of specimen occurs, so the growth rate of cumulative ringing count of AE can be used as the evaluation index of damage degree of specimen.

(3) The loading tests of full-scale concrete pipes and pipe segments show that both have the same damage mechanism and loading process, and the mechanical

loading test of pipe segments can be used as an effective method to study the local loading stress distribution of full-scale pipes.

(4) Compared with that of pipe segment, the AE signal spectrum components in the loading process of full-scale pipes are richer, the signal main frequency is higher, and the damage activities are more complex. However, the spectral range of both is the same, which further proves that the mechanical loading experiments of pipe segment and full-scale pipe are subjected to the same damage mechanism.

Acknowledgements This work was financially supported by the Beijing major science and technology projects (No. Z191100008019002).

References

1. Li R (2016) Evaluation and influence factors of urban sewage pipe inspection. Tsinghua University
2. Liu C, An X (2008) Thesis writing guide. China Standard Publishing House, Beijing (5,6)
3. Huang WC, Zhu WF (2021) Analysis of the effect of buried drainage pipes based on the action of vehicle loads. Eng Constr 35(01):6–9
4. Liao D, Huang L, Zhong W, Ma X (2021) Simulation analysis of soil pressure at the top of direct buried reinforced concrete pipe in trench. Municipal Technol 39(08):120–124
5. Younis AA, Shehata A, Ramadan A et al (2021) Modeling structural behavior of reinforced-concrete pipe with single, double and triple cage reinforcement. Eng Struct 240(112374):1–21
6. Song Y, Wightman E, Kulandaivelu J et al (2020) Rebar corrosion and its interaction with concrete degradation in reinforced concrete sewers. Water Res 182:115961
7. Rikabi FA, Sargand SM, Kurdziel J (2019) Evaluation of synthetic fiber reinforced concrete pipe performance using three-edge bearing test. J Test Eval 47(2):942–958
8. Rusch H (1959) Physical problems in the testing of concrete. Zem Kalk Gips 12(1):1–9
9. Goldaran R, Turer A, Ozlutas K (2020) Identification of corrosion in a prestressed concrete pipe utilizing acoustic emission technique. Constr Build Mater 242
10. Goldaran R, Turer A (2020) Application of acoustic emission for damage classification and assessment of corrosion in pre-stressed concrete pipes. Measurement
11. Pour-Ghaz M, Kim J, Nadukuru SS, O'Connor SM, Michalowski RL, Bradshaw AS, Green RA, Lynch JP, Poursaee A, Jason Weiss W (2011) Using electrical, magnetic and acoustic sensors to detect damage in segmental concrete pipes subjected to permanent ground displacement. Cem Concr Compos 33(7):749–762
12. Miller RK, Hill EVK, Moore PO (2005) Non-destructive testing handbook, acoustic emission testing, USA, vol 6
13. Zou J Computational model of TBM tunnel pipe segment based on finite element analysis. J Jiangxi Univ Technol
14. Guo W, Feng K, Su A, He C, Xiao M (2021) Study on the effect of surrounding pressure on the mechanical properties of staggered seam assembled pipe lining structure. Chinese J Highways 1–11. http://kns.cnki.net/kcms/detail/61.1313.U.20210622.1045.002.html

Feasibility Analysis of Pipeline In-Situ Break-and-Replace Method

Minghao Su, Shaohui Yu, and Yu Gan

Abstract At present, the more popular trenchless pipeline repair technology mainly adopts the method of strengthening the inner wall. However, in the case of serious pipeline damage or need to increase the water capacity, there is no better equipment and technology to choose from. This paper develops a new construction method for renewing the entire pipeline structure to meet the above-mentioned engineering needs. This construction method uses a tunnel boring machine to destroy and update the pipeline in situ, and can realize the expansion of the pipeline. In addition, pipeline renewal construction can still be carried out under the condition of normal pipeline operation and continuous flow. This paper verifies the feasibility of the construction method and the new equipment through field tests.

Keywords Trenchless · Pipeline update · Mechanization

1 Introduction

With the aging of urban infrastructure, many pipelines were damaged and corroded seriously, and even caused the collapse of the road surface, causing many accidents. Taking drainage pipes as an example, the pipes cannot operate healthily, the pipes are blocked, and the pipes are disconnected, which will also cause sewage and rainwater to not be collected and discharged normally, causing urban waterlogging and water pollution [1]. The key to the urban drainage system is the health of the pipeline. The traditional excavation method can no longer meet the current social development. Therefore, scholars at home and abroad have carried out a lot of research on trenchless technology.

Zhu Bo and Zhang Yonggao [2] analyzed the deformation characteristics of the liner after trenchless repair based on the theoretical solution, and provided the design and application plan of the liner. Mao Hua [3] et al. compared and analyzed the

M. Su (✉) · S. Yu · Y. Gan
Underground Space Research and Design Institute, China Railway Engineering Equipment Group Co., Ltd., Zhengzhou 450016, Henan, China
e-mail: 43960626@qq.com

X. Liu (ed.), *Proceedings of 2021 China-Europe International Conference on Pipelines and Trenchless Technology*, Lecture Notes in Civil Engineering 212,
https://doi.org/10.1007/978-981-19-4067-5_22

trenchless repair technology of river crossing pipelines based on the effects of three trenchless repair methods based on indoor model tests.

With the deepening of research, the in-situ curing method has been widely used in practical engineering. The in-situ curing method uses overturning or pulling to implant the resin-impregnated hose into the original pipeline and then cure it, and then form the pipeline lining [4, 5]. Feng Haixia [6] combined field tests and engineering examples to verify the applicability of UV-CIPP curing repair technology. Brown et al. [7] used the method of three-dimensional finite element modeling to analyze the influence of the structural stiffness of the CIPP liner pipe on the tensile stress in the limit state.

According to the defects of Guangzhou drainage pipelines and the engineering characteristics of Guangzhou area, An Guanfeng et al. [8] introduced the spiral winding method for pipeline repair. Wang Gang [9] took a specific non-excavation repair project as an example to analyze the principles, construction points, control points, and technical advantages of the mechanical spiral wound pipeline trenchless repair technology with water.

Compared with other pipeline repair methods, the broken pipe method has the advantages of less interference on the ground and lower construction cost. The most representative one is the pipe crushing method [10], which uses a mechanical expansion head as the main equipment to crush or split the original pipe, and then pull into the new pipe. The broken pipe method is currently mainly suitable for small-diameter brittle pipes, and most of the existing application cases are concentrated around 300 mm in diameter [11, 12].

At present, the pipeline repair technology of CIPP, spiral mechanism winding method and other methods are emerging in many areas. However, the stiffness of the CIPP ring is not enough to repair large pipe diameters. The spiral mechanism winding method can repair larger pipes than CIPP, but it will cause greater section loss after repair. In addition, if the pipeline is damaged to a certain extent, for example, the outline of the pipeline has been severely deformed, and both CIPP and winding methods will not be able to repair the pipeline normally. The broken pipe method also relies heavily on the surrounding soil conditions in terms of expansion scale [13], and the presence of pipe fragments in the soil will cause more adverse effects [14, 15].

Through innovations in construction methods and equipment, mechanized non-excavation methods are used to achieve in-situ renewal, expansion and renewal of old pipelines, and to reduce the pipeline interruption time during the construction process as much as possible. This method makes up for the shortcomings and deficiencies of the current pipeline repair and replacement technology, and provides more options for the pipeline network update.

2 Development of Equipment

As shown in Fig. 1, the roadheader used for pipeline renewal is manufactured by China Railway Engineering Equipment Group Co., Ltd. The total length of the main machine of the equipment is 2685 mm, the main machine weight is 10t, and the excavation diameter is 1480 mm. It can be used for the in-situ renewal project of replacing the DN1000 precast reinforced concrete pipe with DN1200. The pipeline renewal roadheader is composed of an excavation system, a shield body, a drive system, a mud-water circulation system, an electrical system, a hydraulic system, and a guiding system.

2.1 Development of the Cutter Head System

The core technology of the pipeline renewal roadheader lies in the development of the cutter head. In order to test the working performance of the cutter head, prefabricated reinforced concrete pipes. The strength test results of concrete and steel bars are shown in Tables 1 and 2. After 28 days of curing, the strength of the concrete can reach more than 50 MPa, and the steel bars are cold-rolled ribbed steel bars with a yield strength of up to 500 MPa.

Before determining the design of the cutter head, the researchers tested the cutting of the reinforced concrete prefabricated pipe by the cutter head. The test device and test process are shown in Figs. 2 and 3. The test device is composed of a bracket, a hydraulic cylinder, and a torque loader. The bracket is used to fix the pipeline, the hydraulic cylinder is used to simulate the tunneling speed, and the torque loader can control the speed of the cutter head. After the test, collect concrete slag and steel bar fragments. The cutter head is finally designed as a composite cutter head, equipped with hobs, cutters, and fishtail knives. By observing the situation of broken concrete slag and broken steel bars in the pipe cutting test, the R&D personnel believed that the engineering requirements were met.

Fig. 1 Pipeline renewal roadheader

Table 1 Concrete strength test results

Curing time/d	Specimen specifications/mm	Load/kN	Strength/MPa
3	100 × 100	388.2	37.3
		391.5	
		397.4	
28	100 × 100	588.9	54.4
		562.7	
		568.5	

Table 2 Rebar strength test results

Diameter /mm	Section/mm^2	Lower-yield strength/Mpa	Tensile strength/Mpa	Elongati-on after breaking/%
5	19.6	520	600	14.8

Fig. 2 Pipe cutting test

Fig. 3 Test process

2.2 Equipment Performance Parameters

The pipeline renewal roadheader is a mud-water balance type, the maximum thrust is 4800 KN, the maximum advancing speed is 60 mm/min, the correction angle is 1.5°, the front shield specification (diameter × length) is 1460 × 1293, and the tail shield specification (diameter × length) is 1460 × 1000, the shield structure is hinged. The drive consists of 3 frequency conversion motors. The maximum torque of the cutter head is 128 kN·m, the maximum speed of the cutter head is 7.5 r/min, the pipe diameter of the inlet and discharge pump is 80 mm, the discharge flow is 43 m3/h, and the total installed power of the equipment is 150 kW.

3 Construction Plan

3.1 Construction Process

The new construction method of pipe in-situ destruction is to use the tunnel roadheader to break the old pipe, and use the cylinder of the starting well to push the new pipe synchronously. In addition to cutting the reinforced concrete pipe, the cutter head of the tunnel boring machine also cuts the soil around the pipe. The slag discharge system mainly discharges the slag and soil of reinforced concrete. During the construction process, the pressure on the face of the tunnel will be kept stable through mud-water circulation to ensure that the ground will not settle or swell. During the construction of the equipment, a sealing device is installed about 2 m before the excavation, and the sealing device isolates the sewage from the face of the tunnel. Sewage flows through the shield through the reserved hole in the center of the cutter head, and diverts the sewage to the next non-construction section through the pump in the launch well, so that the sewage pipe runs normally during the equipment excavation process and does not affect the function of the sewage pipe. This function can effectively reduce the impact of construction on operating pipelines.

The main construction steps are as follows:

1. Construction of starting well and receiving well. The starting well and receiving well can be set up according to the actual situation of the project, new working wells can be built, and larger old inspection chamber can be used as working wells after transformation. The size of the working well can be about 3.5 to 4.5 m in width and 5 m in length. According to the geology, jacking distance and thrust size, Larsen steel sheet piles can be selected as working wells, or reinforced concrete prefabricated caisson can be selected as working wells.
2. Installation of equipment. As shown in Fig. 4., after the equipment arrives, the branch is installed underground. Generally speaking, the equipment host is relatively small. The front shield, middle shield and tail shield can be assembled in

Fig. 4 Equipment installation

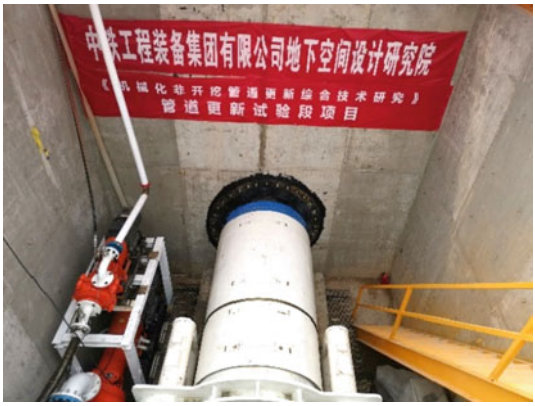

Fig. 5 Device origination

the project. What needs to be installed on site is the launching platform, jacking system, electrical system and muddy water Circulatory system.

3. Debugging originated. As shown in Fig. 5., after the system is qualified and the tunnel door is broken, the equipment can begin to excavate.
4. Interval construction. Excavate the old pipeline to remove the reinforced concrete residue. After completing a length, install the next section of the pipeline and continue the tunneling.
5. The equipment receives. As shown in Fig. 6, after the entire section is completed, the equipment enters the receiving well. After removing the pipes and cables, the equipment is recovered. The pipeline update task is completed.

3.2 Inspection Chamber Construction

The inspection chamber is an important node of the pipeline network system. Many branch pipes are connected, the elevation changes, and personnel are required to set

Fig. 6 Device receiving

up inspection chamber. Generally, one inspection chamber will be set at about 20–50 m. Sectional pipeline renewal inevitably has to pass the inspection chamber, and how the pipeline passes through the inspection chamber needs to be paid attention to. Regarding the renewal construction of inspection chamber, there are two main schemes proposed in this paper. As shown in Figs. 7 and 8, one is to construct the inspection chamber before the completion of the pipeline update, and the other is to construct the inspection chamber after the completion of the pipeline update. The inspection chamber is constructed before the pipeline update is completed, and a door opening of sufficient size needs to be reserved. At the same time, the font of the equipment should be kept accurate when entering and exiting the inspection chamber to prevent the equipment from damaging the inspection chamber. The inspection chamber is constructed after the pipeline update is completed. It is necessary to cut the upper part of the newly laid pipeline, sink the new inspection chamber to a predetermined elevation, and handle the interface between the pipeline and the inspection chamber. Two techniques were tested in this experiment, and both techniques can handle the inspection chamber well.

Fig. 7 Well before pipe

Fig. 8 Pipe before well

4 Engineering Test

4.1 Project Overview

The test section project is located in Zhengzhou, China. The original pipeline before the test section update is composed of 3 sections and 2 inspection chambers. The length of each section is about 20 m, the total length is 60 m, and the buried depth of the pipeline is 3 m. The soil layer is mainly silt, and the waterless layer. The pipe has an inner diameter of 1 m and an outer diameter of 1.2 m. The pipe is a prefabricated reinforced concrete socket pipe with a concrete strength of about 50 MPa. The steel bars are cold drawn ribbed steel bars with a yield strength of 500 MPa and a steel bar diameter of 5 mm. Section 1 of the test section is a sand-gravel foundation, Sect. 2 is a plain concrete foundation, and Sect. 3 is a staggered working condition. The staggered heights are 200, 400, and 600 mm, respectively.

The updated pipeline is a flexible type B steel socketed prefabricated reinforced concrete pipeline with an inner diameter of 1.2 m and an outer diameter of 1.44 m. The working wells at both ends of the construction section adopt a reinforced concrete structure. The size of the starting well is 5 × 5 m, and the receiving well is 3.5 × 3.5 m. The two detection wells in the middle are reinforced concrete structures with a concrete designation of 30 MPa, and the size of the well chambers is 1.6 × 1.6 m.

4.2 Analysis of Broken Pipes

By setting reasonable excavation parameters, the reinforced concrete pipe can be better broken. According to the slag collected in the project, the rotation speed should be higher, and should be kept at 2.5r/-3.5r/min. The thrust and the advancing speed are not easy to be too fast. Keep the penetration less than the knife height, and keep the steel bar as much as possible. The concrete is fully ground. In this way, the broken slag and broken steel bars that enter the mud water circulation pipeline

Fig. 9 Discharge 10 mm slag

after passing through the secondary crushing system are small and can be discharged more smoothly, so that pipe blockage and pump blockage are not prone to occur.

As shown in Figs. 9 and 10, the slag collected in the project is mainly about 10 mm and less than 3 mm. The length of the steel bars discharged through the pipeline is mainly below 5 cm, and larger steel bars often cause blockage, as shown in Fig. 11. The length of the steel bar that was manually taken out was about 10 cm, which blocked the position of the water inlet of the centrifugal pump.

Fig. 10 Discharge 3 mm slag

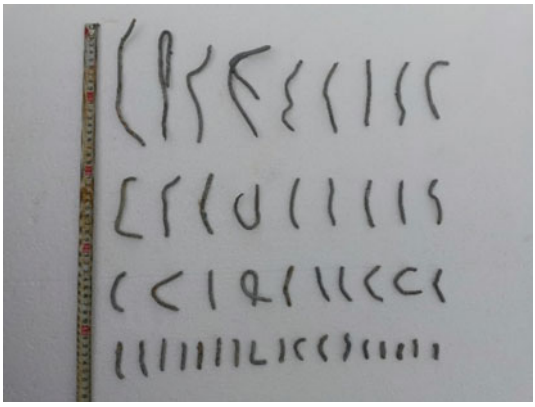

Fig. 11 Discharge the rebar

In the particle gradation composition of the concrete slag, the larger weight ratio of the pieces is less than 30 cm. It should be noted that because the secondary crushing device was not considered during the test, the diameter of the pieces will be larger, but the main diameter is still Less than 10 cm. Therefore, the crushing of concrete by the cutter head is feasible. Experimental observations found that the steel bars were also cut, and the cut length was generally about 10 cm.

5 Conclusion

This paper introduces the main technical characteristics and construction methods of the pipeline in-situ destruction and renewal technology, introduces the pipeline renewal roadheader and describes the situation of the pipeline renewal test project. Through the research and application of the pipeline in-situ breaking and renewal construction method, the following conclusions are obtained: the pipe renewal roadheader has passed the cutter head test and engineering application, which verifies the feasibility of the roadheader to break the high-strength pipe structure and the cutting condition of the reinforced concrete by the cutter head Preferably, it can meet the requirements of mud-water circulation slag discharge. The concrete slag particles collected in engineering practice are mainly below 10 mm. The pipeline renewal test also tested the process of handling intermediate inspection chambers through two methods: “well first and then pipe” and “pipe first and well”. The test proved that the two methods can well complete the update of the inspection chamber. It should be pointed out that the current cutter head design cannot complete the cutting of steel pipes. The subsequent cutting technologies for water supply, heat, gas and other metal pipes require further research.

References

1. Tang J, Zhang Y, Mei X (2019) Methods and measures for improving the quality and efficiency of urban drainage systems. Water Supply Drain 55(04):30–38
2. Zhu B, Zhang Y (2004) Calculation method for repairing underground pipeline with liner. China Water Wastewater (11):29–31
3. Mao H, Zheng J, Hong Y, Peng Y (2005) Discussion on internal repair technology of large-scale river crossing gas pipeline. J Oil Gas Technol (J Jianghan Pet Inst) (S1):295–296+10
4. Ma B (2014) Trenchless Pipeline Repair and Renewal Technology. People’s Communications Press, Beijing
5. Ma B (2008) Trenchless Engineering. People’s Communications Press, Beijing
6. Feng H (2014) CIPP ultraviolet curing repair technology used in the repair of sewage pipes. China Water Wastewater 30(16):136–138
7. Brown MJP, Moore ID, Fam A (2014) Performance of a cured-in-place pressure pipe liner passing through a pipe section without structural integrity. Tunn Undergr Space Technol 42:87–95
8. An G, Wang H, Liu T, Zhang H (2014) Inspection and non-excavation repair technology of drainage pipelines in Guangzhou. Water Supply Drain 50(01):97–101

9. Wang G, Wang Z (2018) Application case of non-excavation water-carrying repair technology for mechanical spiral wound pipes. China Water Wastewater 34(06):120–122
10. Zang C, Dong Y, Li B (2013) Discussion on some technical issues in the renewal of drainage pipes by pipe expansion method. Water Supply Drain 49(08):110–113
11. Zhang Y (2011) Application of pipe cracking construction technology in the process of gas pipeline reformation. City Gas (04):11–15
12. Dong J, Wang X, Cheng X (2003) The first successful application of pipe splitting method to replace old pipes in China. City Gas (12):11–13
13. Jin X (2007) Analysis of pipe expansion under different soil conditions. China Society for Trenchless Technology. 2007 Trenchless Technology Conference Papers Special. China Trenchless Technology Association (China Society for Trenchless Technology): Trenchless Technology Magazine, p 4
14. Shuhong W, Baosong M (2006) Analysis of environmental influence factors of pipe blasting method construction. China Society for Trenchless Technology. 2006 Trenchless Technology Conference Papers Special. China Trenchless Technology China Society for Trenchless Technology: Trenchless Technology Magazine, p 3
15. Tao W (2019) Research on construction technology of urban pipe network static fracturing pipe method and its impact on surrounding environment. Chongqing Jiaotong University

Preinstallation and Construction Technology of Pipeline of Whole Lifting Steel Grid Roof

Guangjun Li, Tianfang Mo, Ningbo Xu, Weixiong Zhang, Hanwen Lu, and Deyuan Deng

Abstract The pipeline installation technology of the overall lifting steel grid roof is incorporated into the work before lifting, and the pipeline load is taken into account in the lifting design. While ensuring that the lifting work of the steel grid is not affected, the installation mode of mechanical and electrical pipelines is convenient, which greatly reduces the difficulty of pipeline installation and reduces the investment of most of the overhead measures. This technology has been implemented in the hangar hall construction division of the project, and remarkable results have been achieved through research and practical application in the implementation process.

Keywords Steel mesh frame · Overall lifting · Pipeline preinstallation · Construction technology

1 Introduction

In large factories, maintenance hangar, pavilions and other large span steel roof construction, often using steel space frame integral lifting technology, but after rack ascension, most of the mechanical and electrical lines still need to use scaffolding or mobile crane and truck and other large machinery for high altitude installation, this method installation progress is slow, high degree of risk. So the pipeline preinstallation technology of the whole lifting steel grid roof arises at the historic moment. In the project, key construction technologies such as overall assembly of steel roof, overall hoisting point arrangement, hoisting device selection, hoisting support design,

D. Deng
China Construction Steel Engineering Co. Ltd., Shenzhen 518052, Guangdong, China

G. Li · T. Mo · N. Xu · W. Zhang
China Construction Fourth Engineering Division Corp. Ltd., Guangzhou 510430, Guangdong, China

China Construction 4th Engineering Bureau 6th Corp. Limited, Hefei 230011, Anhui, China

H. Lu (✉)
Foshan University, Foshan 518054, Guangdong, China
e-mail: luhanwen@fosu.edu.cn

X. Liu (ed.), *Proceedings of 2021 China-Europe International Conference on Pipelines and Trenchless Technology*, Lecture Notes in Civil Engineering 212,
https://doi.org/10.1007/978-981-19-4067-5_23

temporary strengthening of structure and system transformation were designed and studied, and the overall lifting installation scheme was determined [1]. Ji Dongling [2] introduced the key points of construction such as assembly, welding and lifting in steel grid construction, as well as the core technologies that need to be paid attention to during the overall upgrading. Du Qi et al. [3] verified the reliability and correctness of the application of the combination technology of prestressed steel tie rod and long-span grid truss by comparing and analyzing the whole process simulation, construction calculation results and construction measured data of the construction method. With the help of information technology software, it is of great importance to formulate economic, safe and efficient construction schemes and management measures in the construction of steel grid roof of large indoor sports stadiums [4]. Due to the large span of the aircraft maintenance hangar structure and the high total height of the building, the construction method of ground assembly and overall lifting is mostly adopted. Therefore, the safety protection of the network truss (truss) is of great importance in the process of ground assembly, overall lifting and upper air closing [5]. According to the different floors where the grid is located, it should be reasonably divided and promoted into different blocks. After cumulative promotion across the layers, it should install the filling rods between the grid frames of different blocks and lift them to the design elevation after assembling as a whole. This construction method reduces the erection height of the grid structure, has the advantages of simple construction, high safety, saving measures and greatly improving the construction efficiency of the grid structure [6]. The main frame structure of the project has been completed, the large crane can not enter the inner field for hoisting, and the high and low stands below the projection of the grid can not be assembled as a whole. According to the special working conditions of the project, the construction technology of "cumulative outward expansion and overall lifting" is adopted to place and lift the steel grid, which has achieved good social and economic benefits [7].

In this project, the technology is to pre-install water, electricity, fire and other pipelines before the overall lifting of the steel grid. Before the pipeline is installed to the lifting work, the design of the lifting will consider the line load. In order to promote the work of the space steel frame, at the same time, the installation of mechanical and electrical pipelines is convenient, which greatly reduces the difficulty of pipeline installation and reduces the cost of most of the above measures.

2 Technical Characteristics

Load transformation analysis: In steel rack overall design and calculation of different pipeline system load of quasi similar force, respectively, in the steel space frame, load analysis of integrated together, and then consider this part of the load caused by the whole steel space frame deflection change and deformation degree, to detail simulation of point and deformation of the ascension, through an arch of methods such as the best form to confirm the steel rack ground assembly.

Preinstalled disconnect: increase in mechanical and electrical piping preinstallation deepen design reasonable cut-off point, to prevent the steel space frame of pipeline damage caused by deformation of the overall process of ascension, disconnect position can use telescopic bracket, line to have long methods such as deformation, also can wait after completion of the ascent and unloading steel rack is made of stainless steel threaded compensator device to connect.

Virtual Installation: Using BIM technology to the mechanical and electrical line in steel rack virtual installation, mechanical and electrical pipeline installation itself collision test, with space truss model combined with the overall ascension, to adjust the position of the collision conflict, then the stress analysis, determine the installation position of pipeline is the most reasonable, the guarantee and the premise of meet the design requirements, pipeline installation to minimize the impact on steel rack.

Precise assembly: The main mechanical and electrical dry lines are placed in the way of precise positioning of the total station and the measurement network during the ground assembly of the steel grid. The steel grid and pipelines are assembled by point-to-point connection, and the pipelines are laid accurately according to the assembling position of the steel grid on the ground.

3 Operating Points

BIM technology is used to simulate the ground assembly construction of the grid, and the assembly sequence is determined from the middle to both sides. This assembly sequence can facilitate the backward construction of large equipment such as truck cranes from the middle of the site to the outside. Considering the influence of overall lifting and other loads, the ground assembly of steel grid needs to conduct pre-arch design. The main measures to control the arch are to adopt the method of fixing welded joints with round tube support, to control the assembly position by adjusting the position of round tube support, and to control the value of pre-arch by controlling the height of round tube support (Fig. 1).

Fig. 1 Welded ball joint support

BIM technology is adopted to conduct grid pipeline modeling first, arrange each system in the grid, conduct pipeline collision test, and make corresponding adjustments according to the test results. The load of electrical system, fire control system, siphon rainwater and other pipeline systems are analyzed respectively. The pipeline load is converted into different positions of the force applied on the steel grid, and the influence of the load on the steel grid members is calculated. If the impact is too large, corresponding measures shall be taken.

To each force point of pipeline system layout, then each system integrated to a steel rack, a comprehensive stress analysis and simulation of deformation in the process of ascension, find out the stress is concentrated in a large area of deformation or bar is easy to damage, stress and deformation in order to ensure that the steel rack comply with the design requirements, using a certain method to load adjustment. The load placed in the middle of the rod can be adjusted to the end node position of the rod, such as the fire main pipe from the middle of the rod to the end of the span; it is also possible to replace the large size rod with small section rod to reduce deflection. If the overall deflection of the steel grid in a certain area is too large, the pre-arch value can be increased by increasing the height of node support when the steel grid is assembled on the ground. If the load is too concentrated, the pipeline load can be spread out, so that the steel grid rod uniform force, such as the sprinkler system each rain area in the middle of the top solid ball connected to the grid for the main fixed fulcrum, the use of steel structure roof purlin as the fulcrum, in the node or across the middle position of the guide bracket. In this way, the pipeline load can be homogenized to the maximum and the deflection of the grid can be reduced.

Considering that the steel grid will be deformed in the process of lifting, which will lead to the damage of the installed pipelines such as bending, pulling and dislocation, corresponding measures should be adopted to prevent the pipeline quality problems caused by the deformation of the steel grid in the construction of pipeline floor assembly (Fig. 2).

For the problem that the lifting deformation of the steel grid may lead to the displacement damage of the pipeline support, adjustable support can be adopted or

Fig. 2 Stainless steel thread compensator

expansion joints can be added to the support. The support in the large deformation position of the steel grid can be temporarily fixed, which can be adjusted and fixed after the lifting of the steel grid to ensure the installation quality of the pipeline.

4 Overall Lifting and Monitoring of Steel Grid

The stability of steel grid lifting process can reduce the influence of lifting deformation on pipeline installation quality. Through the observation and monitoring of grid structure, lifting facilities and lifting equipment system in the trial lifting process, it is confirmed that it conforms to the calculation and design conditions of simulated working conditions to ensure the safety of the lifting process. The lifting process requires professional lifting control and the data from one of the truss monitoring points are shown in the table below. The monitoring data can be adjusted for lifting truss installation according to existing specifications (Table 1).

Based on the reaction force value of each lifting point calculated by computer simulation, the steel structure unit of the grid is loaded in stages (trial lifting), and the pressure of the hydraulic lifting system at each lifting point should be gradually increased in stages, which are 20, 40, 60 and 80% respectively. Under the condition that there is no abnormality in each part, the load can be continued to 90, 95 and 100% until the steel structure of the grid frame is completely separated from the assembled tire rack.

In the process of graded loading, after each step of graded loading, it should be suspended and checked, for example, the deformation of structure and grid structure before and after loading, as well as the stability of column support structure. If all is well, proceed to the next step of hierarchical loading.

When the structure is about to leave the assembled tire rack under hierarchical loading, there may be different points off the ground at different time. At this time,

Table 1 Truss monitoring

Monitoring position	Reflector position	Initial data		Truss data		Deformation value (mm)
Truss monitoring point	Beam	X	0.195	X	0.193	−2
		Y	1.013	Y	1.018	5
		Z	32.785	Z	32.789	4
	A# column	X	−0.769	X	−0.766	3
		Y	0.490	Y	0.493	3
		Z	25.798	Z	25.796	−2
	B# column	X	4.226	X	4.223	−3
		Y	1.143	Y	1.145	2
		Z	26.332	Z	26.33	−2

the lifting speed should be reduced, and the lifting condition of each point should be closely observed, and "single point moving" lifting should be done when necessary. Ensure the grid steel structure off the ground smoothly, all points synchronized.

About 100 mm after the grid structure unit leaves the assembled tire rack, the hydraulic lifting system is used to lock the equipment and stay in the air for more than 12 h for a comprehensive inspection (including the lifting point structure, bearing system and lifting equipment, etc.), and the inspection results shall be reported to the site headquarters in written form. All checks are normal, and then formal promotion.

The relative height difference of each lifting point is calculated by detecting the distance from the ground of each lifting point with measuring instrument. Through the hydraulic lifting system equipment to adjust the height of each lifting point, so that the structure to reach the horizontal posture.

Reset the displacement sensor with the adjusted height of each lifting point as the new starting position. During the overall lifting process of the structure, maintain this attitude until it is lifted near the design elevation.

In the process of overall lifting construction, the main factors affecting the lifting speed of components are the length of hydraulic tubing and the number of pump stations. According to the equipment configuration of the scheme, the overall lifting degree is about 10 m/hour, and the speed is slowed down in the early stage of lifting.

5 Conclusion

In the overall lifting scheme of steel structure grid, the first overall lifting to 10 m is carried out for the second steel structure roofing rod repair process. After the completion of rod repair, the overall lifting to the design elevation is welded in place. If mechanical and electrical installation works are involved in the installation of the steel structure of the roof when it is raised to 10 m for the first time, the operation height of mechanical and electrical installation is relatively reasonable. However, there are conflicts in the installation space of aerial vehicles, and the interpenetration construction of different majors is of low efficiency, so only steel pipe scaffolding can be used as the operation platform. The total built-up area is basically the whole area of the main pipeline in the hangar hall, with a total of 33,853.3 m^2. The maximum setting height is 18 m, and the minimum setting height is 10 m after the first lifting of the grid. That is, the average height of steel pipe scaffolding is 14 m.

With the adoption of pipeline floor assembly technology, the main pipeline is installed before the first lifting, and the overall lifting can be carried out as planned, so mechanical and electrical installation can be inserted in the steel structure floor assembly construction. The main pipeline is installed before the first lift. The operating height of the installation is 2–8 m, and the average setting height is 5 m. The process insertion time is advanced, and the installation period can be increased to two months. At the same time, the measure cost of operating frame is reduced and the cost is reduced.

The application of the pipeline preinstallation technology of the whole elevated steel grid roof in the main construction project of Kaisa Jinshawan Snow Square has greatly reduced the input of high measure cost caused by the pipeline installation at high altitude and achieved remarkable results. The efficiency of pipeline installation in the construction process is greatly improved, reducing the use of high-altitude construction machinery and equipment, and greatly increasing the safety. It has good comprehensive benefits. During the construction process, the efficiency of pipeline installation is greatly improved, reducing the use of large operation equipment such as truck crane and ascending vehicle, and greatly increasing the safety. It has good comprehensive benefit and can be popularized and applied.

References

1. Jinrong C et al (2021) Research on integral lifting and installation scheme design of large-span steel roof. Struct Constr 43(08):1485–1488
2. Dongling J et al (2021) Overall improvement technology and simulation research of steel mesh frame structure. Sci Technol Innov 05:144–145
3. Du Q et al (2021) Whole lifting technology of prestressing steel tie rod and large span net frame. Constr Technol 50(02):107–111
4. Ke P et al (2020) Construction technology and management of large indoor stadium roof steel grid. Constr Econ 41(S2):170–173
5. Hu H et al (2021) Construction safety protection technology of extra large steel space grid. Struct Constr 43(08):1479–1481
6. Zhang N et al (2021) Cross-story hoisting construction technology of large-span and long-cantilever roof grid. Constr Technol 50(08):114–116
7. Li X et al (2017) Construction technology of cumulative outward extension and integral lift" for large-span latticed steel. Struct Constr 39(12):1764–1766

Research on Filling Technology of Long Distance Pipeline Casing

Hongbo Wang, Kunfeng Zhu, Anjun Teng, Shouye Cheng, and Dongyang Geng

Abstract When buried pipelines cross railways and highways, casing protection is generally used to protect the main pipe from external dynamic loads or soil pressure. The casing pipe is generally steel pipe or reinforced concrete pipe. An insulating support is set between the casing pipe and the main pipe, and both ends of the casing pipe are sealed to prevent water or soil from entering. This hollow structure will affect the cathodic protection of the pipeline. Because the sufficient condition of pipeline cathodic protection is: there is a continuous conductive medium along the pipeline, and good electrical isolation is maintained between the pipeline and other buried metal structures. The annular gap between the casing and the main pipe destroys this continuity, and the cathodic protection current on the main line does not work on the main pipe in the casing. Therefore, the main pipe of the casing section is prone to corrosion problems. In order to avoid corrosion of the pipe in the casing, one method is to install a sacrificial anode on the main pipe in the casing to form a small system combining anti-corrosion layer and cathodic protection to provide additional protection current to avoid pipeline corrosion. Another method is to fill the casing with sealing (or conductive) materials, and use these materials to isolate corrosive media (or allow cathodic protection current to pass) to alleviate corrosion.

H. Wang · K. Zhu · A. Teng
Langfang Headquarters, China Petroleum Pipeline Engineering Corporation, Langfang 065099, China
e-mail: wanghongbo@cppe.com.cn

K. Zhu
e-mail: zhukunfeng@cppe.com.cn

A. Teng
e-mail: tengaijun@cppe.com.cn

D. Geng (✉)
School of Urban Geology and Engineering Langfang Headquarters, Hebei GEO University, Shijiazhuang 050031, China
e-mail: gengdongyang@cppe.com.cn

S. Cheng
Drilling Technology Company of Beijing China Coal Mine Engineering Co., Ltd., Beijing 100028, China
e-mail: chengshouye@cppe.com.cn

X. Liu (ed.), *Proceedings of 2021 China-Europe International Conference on Pipelines and Trenchless Technology*, Lecture Notes in Civil Engineering 212,
https://doi.org/10.1007/978-981-19-4067-5_24

This article mainly introduces the technical research of injecting the filling medium into the casing.

Keywords Long-distance pipeline · Casing · Internal filling technology

1 Introduction

Reinforced concrete casing is generally used as protection for crossing highways and railways in China. According to the "Code for Design of Oil and Gas Main Pipe Crossing Engineering", "When casing is used to cross highways and railways, the inner diameter of the casing should be more than 300 mm greater than the outer diameter of the main pipe [1]. When the casing is constructed with artificial pipe jacking, the inner diameter of the casing should not be less than 1 m." This regulation requires a large gap between the casing and the main pipe. Therefore, it is very meaningful to fill the casing. According to the requirements of "Oil and Gas Pipeline and Railway Intersection Engineering Technology and Management Regulations": Jacking casing should be filled with casing when crossing the railway [2]. The filling can be made of sand or mud and other materials, and there is no need to install two side plugging and detection pipes. The protective culvert should be filled with no inspection well after filling. When the space in the culvert is not filled, inspection wells should be set up at both ends of the culvert, and the inspection wells should have closed facilities [3]. According to the requirements of the "Code for Design of Oil and Gas Pipeline Crossing Engineering": when the casing or culvert is filled with fine soil to bury the crossing pipe section, there is no need to set up a leak detection pipe and plugging at both ends [4].

2 Concrete Casing Treatment Method

At present, the current project has two methods for the treatment of concrete casing (see Fig. 1): the first is to use red bricks, asphalt hemp wire to block, and to increase the exhaust pipe; the second is to blow sand or inject cement into the casing after the plugging. mortar. The first method of using bituminous hemp wire to block and increase the φ75 exhaust pipe was almost a conventional design before 2013.

In addition to the lack of tightness in the sealing, this method also requires the design of wire mesh on the exhaust pipes at both ends. Fences and gates prevent third parties from damaging the exhaust pipe [5]. The second method is to jack the casing to cross the highway by filling the casing after plugging [6]. The filling can be made of materials such as sand or mortar, and there is no need to set up a leak detection tube. Conduct mortar ratio test on site before construction to select appropriate ratio and materials. The grouting adopts rubber hose or hard plastic pipe.

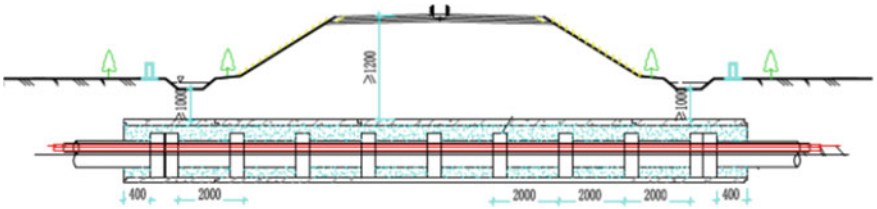

Fig. 1 Blocking diagram on both sides of concrete casing

Before grouting, both ends of the casing are plugged with brickwork (the end of the pipe is blocked by brick Mu10 and cement mortar M7.5), and the grouting pipe is placed on the top of the casing (can be Use pipe clamps to fix) and extend into the middle or far end of the casing; after the slurry is stirred, use a grouting pump to drive into the hose and transport it to the center of the pipe for grouting, and stop when the slurry overflows the grouting port at the end of the casing After the mortar is consolidated, observe the filling degree of the space in the casing. If it reaches 85% or more, the grouting is completed, otherwise, a second grouting is required until the requirements are met. See Fig. 2 for on-site casing cement mortar filling.

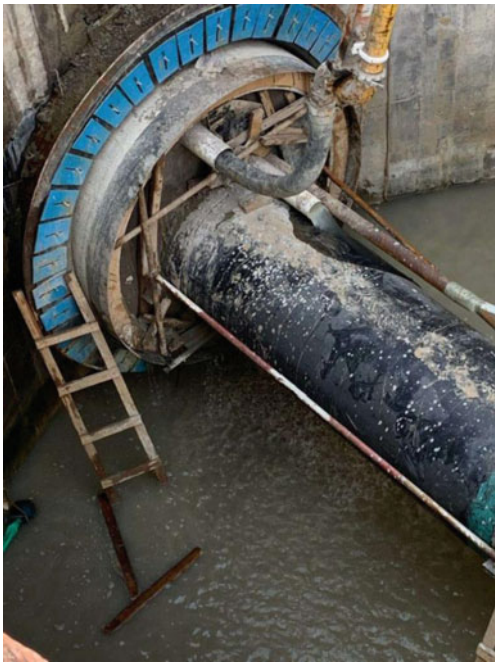

Fig. 2 Cement mortar injection into casing on site

3 The Problem of Concrete Casing

Although the concrete casing has gradually become a filling scheme, there are still many problems:

(1) The requirements for filling materials in the specification are difficult to achieve on site The "Code for Design of Oil and Gas Pipeline Crossing Engineering" requires that casing or culvert space only requires filling of fine soil. The requirements are too simple and are contrary to the commonly used sand blowing and cement mortar. The next step is to modify the specification.
(2) The specification does not clearly require the filling degree The "Code for Design of Oil and Gas Pipeline Crossing Engineering" requires that when the casing or culvert is filled with fine soil to bury the crossing pipe section, there is no need to set up leak detection pipes and plugging at both ends. The literal understanding is that there is no strict requirement on the filling degree, as long as the pipeline is buried.
(3) The construction of sand blowing is difficult, and the quality is not guaranteed The sand-blowing process has certain feasibility for filling short-distance casings with a length of less than 20 m. It is too difficult to blow sand after the distance is too long, and the quality is not well controlled, and there are not many applications. The on-site sand blowing is shown in Fig. 3.
(4) The mortar has poor fluidity and the filling rate cannot be guaranteed Support blocks and optical cable protection sleeves are generally installed in the sleeve, which will hinder the flow of the filling medium to a certain extent. The mortar filling design scheme is generally to arrange the grouting pipe in the middle of the casing, so that it cannot guarantee smooth filling of the casing. At present, there is no case of on-site mortar filling.

Fig. 3 On-site sand blowing

4 New Composite Mud Filling Technology and Scheme

Foreign roads and railways generally use steel casing pipes, and the annular gap between casing pipes and main pipes is small, so the amount of anti-corrosion filler injected is small and the cost is low. In China, reinforced concrete casings are commonly used in crossings, and casings are generally relatively large. At present, the domestic design documents require the filling of cement mortar or sand in the annulus between the casing and the main pipe. The existing problems have been introduced previously and will not be repeated here.

The new composite mud filling technology is proposed on the basis of the research on the filling technology of raise-drilling inclined wells, and many small-diameter casing grouting tests have also been carried out. The picture of grouting is shown in Fig. 4.

There are several technical problems that need to be solved for the filling in the concrete casing: fluidity, conductivity, volume shrinkage and strength. The new composite filler mainly uses cement, bentonite and cheap fly ash as the main materials, and achieves the following technical parameters and performance through a certain ratio:

(1) Liquidity For road and railway crossing casings are almost horizontal, the filling medium must be very special. The pipe jacking length is generally within 150 m. It should be ensured that the filling has good fluidity during the pipe filling process, which can be measured with a Mars funnel, and the flow time should not exceed 120 s. By adding bentonite to the filling to enhance the fluidity of the composite mud, it can meet the requirements of having good fluidity under different working conditions.

Fig. 4 Photos of field test

(2) Conductivity Bentonite itself is a clay-like substance mainly composed of montmorillonite with a layered structure, which has the characteristics of low resistivity, good water retention and stability. The added bentonite is mainly low-priced calcium-based bentonite. By adjusting the ratio, the soil resistivity after the consolidation of the filling is greater than 10 Ω · cm and less than 200 Ω · cm.
(3) Volume shrinkage rate The most direct manifestation of the volume shrinkage rate is the water separation rate, which is an indicator reflecting the stability of the slurry. In order to ensure the flow of mud, the amount of water added should be much larger than the amount of water used for complete hydration. The on-site water consumption is generally about 50% of the cement weight to make the mud fluidity good. After the slurry has solidified, excess water will separate out and rise to the top of the slurry. The separated water is free water with high salinity, which can penetrate into the formation and cause serious pollution to the production layer. Therefore, the water loss of the mud should be reduced as much as possible by adding a treatment agent. Adding bentonite to the mud can improve the dispersion of the mud and the degree of hydration and flocculation, so that the particles are not easy to settle, thereby reducing the water separation rate of the slurry and the drying shrinkage rate. The water separation rate of single-liquid cement slurry is usually about 15%, while the water separation rate of cement slurry with bentonite can be reduced to less than 5%.
(4) Strength A certain strength of the filling medium can effectively restrain the pipeline buried in it, but it is also disadvantageous if the strength of the filling medium is too high. Therefore, the compressive strength of the composite mud to be filled must not be greater than 0.5 MPa (28 d). For the strength test, test pieces can be made from newly produced new filling materials, and the uniaxial compressive strength of the test pieces can be measured. The difference between the new composite mud filling technology and the previous technology is that the two sections of the casing are no longer plugged during grouting. The pipe jacking pit is fully utilized and geotextile bags (filled with sand or soil) are used to enclose both ends of the casing. Out of the grouting port. The geobags are stacked in steps above the top surface of the concrete casing. The backfill of the work pit behind the platform should be compacted in layers, with a compaction degree of not less than 0.85. When grouting, it is better to grouting at the high point of the grouting port. If the distance is long, you can reserve the grouting pipe to the middle of the casing.

5 Precautions for Filling of New Composite Mud

The negative buoyancy calculation should be checked before grouting. After the pipeline is in place, the pressure test head can be used to inject water to the counterweight; the filling slurry should be prepared with special bentonite for grouting. Na-bentonite or calcium-based bentonite can be used, but hydrogen-based bentonite

(activated clay, fuller's earth) and organic bentonite are not allowed. The water for pulping should be clean water. The calcium ion content in the water should be less than 100 mg/L, the chlorine content should be less than 100 ppm, and the pH value should be between 6.5 and 9.5. When the temperature is below zero and the slurry freezes, no grouting construction shall be carried out.

6 Conclusion

The liquid level on both sides of the grouting shall be at least 0.3 m higher than the top of the casing, and the distance between the liquid level and the ground shall not be less than 1 m. After 24 h, if the liquid level is lower than the top of the casing, grout supplementation is required. After the grout is basically solidified, turn the geotextile to cover the grouting surface and backfill the original soil. In filling, if the groundwater is abundant and there is water in the operation pit, there are sump pits on both sides to use water pumps to pump water in time to ensure that there is no water during the grouting process.

References

1. O'brien RM (2007) A caution regarding rules of thumb for variance inflflation factors. Qual Quant 41(5):673–690
2. Peck WA, Lee MF (2008) Application of the Q-System to Australian underground mines. In: Proceedings of the International Workshop on Rock Mass Classifification in Underground Mines, U.S Department of Health and Human Services CDC/NIOSH Offiffiffice of Mine Safety and Health Services, pp 129.140
3. Shaterpour Mamaghani A, Erdogan T, Engin D, Bilgin N (2016) Evaluation of the performance of a raise boring machine in Pb-Zn underground mine, Balya, Turkey. In: World Tunnel Congress, San Francisco, USA
4. Shaterpour-Mamaghani A, Bilgin N (2016) Some contributions on the estimation ofperformance and operational parameters of raise borers—a case study in Kure Copper mine Turkey. Tunn Undergr Space Technol 54:37–48
5. Shaterpour-Mamaghani A, Bilgin N, Balci C, Avunduk E, Polat C (2016) Predicting performance of raise boring machines by using empirical models. Rock Mech Rock Eng 49(8):3377–3385
6. Shaterpour-Mamaghani A, Copur H (2017) Factors affffecting the selection and performance of raise boring machines (RBMs) and case studies from Turkey. In: 26th International Symposium on Mine Planning & Equipment Selection Conference, Luleå, Sweden, pp 153–161. (ISBN: 978-91-7583-935-6)